Spring 5-31-1990

Experimental evaluation of process zone deformation in concrete

Cherng-Maou Meng
New Jersey Institute of Technology

EXPERIMENTAL EVALUATION

OF

PROCESS ZONE DEFORMATION

IN CONCRETE

BY

CHERNG-MAOU MENG

Thesis submitted to the faculty of the graduate school of the New Jersey Institute of Technology in partial fullfillment of the requirements for the degree of Master of Science in Civil Engineering

1990

APPROVAL OF THESIS

Title of Thesis : Experimental Evaluation of
Process Zone Deformation
In Concrete

Name of Candidate : Cherng-Maou Meng
Master of Science in Civil
Engineering , 1990

Thesis and Abstract approved by :

Date

Farhad Ansari, Ph.D.
Associate Professor
Department of Civil and Environmental Engineering

Date

Signature of other Member
of the Thesis Committee

VITA

Name : Cherng-Maou Meng

Degree & Date : Master of Science in Civil Engineering 1990

Secondary education : Tsi-Shiu High School

Collegiate Institute	Date	Degree	Date Graduated
Tamkang University	1982-1986	B.S. Civil Eng.	June , 1986
New Jersey Institute of Technology	1988-1990	M.S. Civil Eng.	May , 1990

Major : Structure Engineering

Position Held :

1989-1990 : Teaching Assistant at NJIT , NJ

1990-Present : Junior Structure Engineer , Formosa Plastics CO. USA , NJ U.S.A.

ABSTRACT

Title of thesis : Experimental Evaluation of Process Zone Deformation in Concrete

Name: Cherng-Maou Meng

Master of Science in Civil Engineering

Thesis directed by : Dr. Farhad Ansari

Concrete structures are often subjected to a variety of loading conditions. Under ultimate load design , concrete structures can resist these loads without evident deformation. However , under service , tension cracks will develop and depending on their location , they may impair load carrying capacity.

It is generally believed that microcrack development is preceeded by formation of a relatively long microcracked region. A large number of studies have indicated that due to formation of this process zone (microcracked zone) , Linear

Elastic Fracture Mechanics (LEFM) principles are not applicable to concrete. However , a number of nonlinear models can be developed if the length of this zone can be determined. Determination of process zone length is a difficult experimental problem , mainly due to difficulties involved in accurate detection of microcracks during loading in a typical experiment. Furthermore , as some recent studies indicate , surface microcracks progress further than their internal counterparts. Determination of internal deformations and microcracks are even more challenging than the mere surface flaw detection mentioned earlier. Survey of technical literature indicate , inexistence of an accurate internal deformation measuring technique for concrete.

In the present study , a new technique is developed for measurement of internal deformation in cementitious composites. main emphasis is given to the development of the technique , and measurement of deformations in the process zone. Results from experiments on compact tension , and three point bend specimen are presented.

Blank Page

ACKNOWLEDGEMENTS

The author wishes to acknowledge the help of the following persons who contributed to this research in a variety of ways :

To Dr. Farhad Ansari , my graduate advisor , for his valuable guidance throughout the entire project.

To Mr. Quij Chen , for his help in doing fiber optics.

TABLE OF CONTENTS

LIST OF TABLE

LIST OF FIGURES

Figure   Page

CHAPTER I Introduction and Research Objectives

Formation and growth of microcracks play an important role in the performance of plain , reinforced , and prestressed concrete. For instance , cracking of concrete in tension is a significant factor contributing to the non-liner behavior of reinforced concrete. Therefore , logical design concepts ought to be based on realistic theoretical models that take crack formation and propagation into account. Recent advances in fracture mechanics and application of numerical methods have given possibilities for the establishment of realistic models for concrete fracture[1-2]. It is recognized that fracture toughness of concrete can not be evaluated using linear elastic fracture mechanics unless proper modifications are applied. Studies on the fracture behavior of concrete reveal some fracture characteristics that differ from those normally observed in metallic materials[3-6]. Among these characteristics is the existence of a microcracking zone or process zone at the tip of an advancing crack. Since the process zone is believed to be relatively large in concrete , calculation of fracture parameters should include the effects of this zone. Lack of data on the experimentally observed zone of microcracking , the COD-crack growth relationship , and the inelastic behavior has forced the investigators to make assumptions pertaining to process zone. The determination of the fracture process zone in concrete is a difficult experimental problem , because the resulting deformation is strongly localized.The extent of the crack tip at the crack front and the location for the tip of the advancing microcrack that forms that zone is almost impossible to detect.

Dugale-Barrenblatt model[7-8] for modeling metal fracture in the presence of large scale yielding has been extensively applied to concrete treating the fracture process zone as the strip yield zone[9-10]. Assumptions regarding the crack length and crack opening resistance of the fracture process zone were all different in above-mentioned models. Bazant[11] developed a nonlinear fracture concept , modeling the fracture process zone extension through nonlinear programming. In another report[10] , double clip-on gage technique was used to infer the location of the process zone in crack-line wedge-loaded double cantilever beams. In a simplified model proposed by Jenq and Shah a closing pressure of zero was assumed as a starting value in the interactive solution that adjusted the effective crack length to yield the value of CMOD from the experiments.

Inconsistency of results reported by many investigators and comparison of their approach in order to model fracture behavior of concrete suggest the nonlinear effects associated with crack propagation in concrete as the major source of inconsistency. Values reported in the technical literature for fracture toughness vary widely even for essentially similar materials depending on the size of the test specimen[3,11-13]. The primary reason for the discrepancy in the reported values is the effect of microcracking zone or fracture process zone ahead of the crack tip. Microcracking zone is also responsible for the slow crack growth in concrete. One impractical way to evaluate a size independent fracture toughness for concrete is to test very large specimen so that the uncracked portion of the segment in front of the crack is much larger than the fracture process zone.The alternative approach would be to test practical size specimen and develop an experimental technique such that information regarding the localized displacement field in front of the moving crack and the extent of microcracks can be determined. Once this information is acquired , then the effect of fracture process zone can be introduced in the numerical modeling with the least number of simplified assumption.

Based on above considerations , the main objective of the research reported here is to develop an experimental technique for direct full field measurement of internal deformations and microcrack widths in the process zone of concrete specimen.

CHAPTER II EXPERIMENTAL PROGRAM

II.1 Experimental Investigation

Microcracking is the essential aspect of the fracture process zone in concrete , therefore , there is a need for a testing technique that would be accurate enough to detect and measure the displacement associated with microcracks. Moreover , it is very important to make internal measurement of the deformation associated with microcracking in order to distinguish in between the structural and nonstructural development of microcracks , such as the surface microcracks developed due to shrinkage at the hydration stage.

II.2 Methodology

Transmission of light through optical fibers can be explained by the Snell's law and the concept of total internal reflection. According to Fig.1 , when light travels from the fiber core that has a high refractive index into the cladding with a lower index , the lightwave totally reflects back into the core. This is true , provided that the diameter of the core is chosen so as to force the lightwave to propagate according to a certain critical angle of incidence. However , if the fiber is stretched or bent at any point along it's length , the change in the angle of incidence will cause some of the light to escape out through

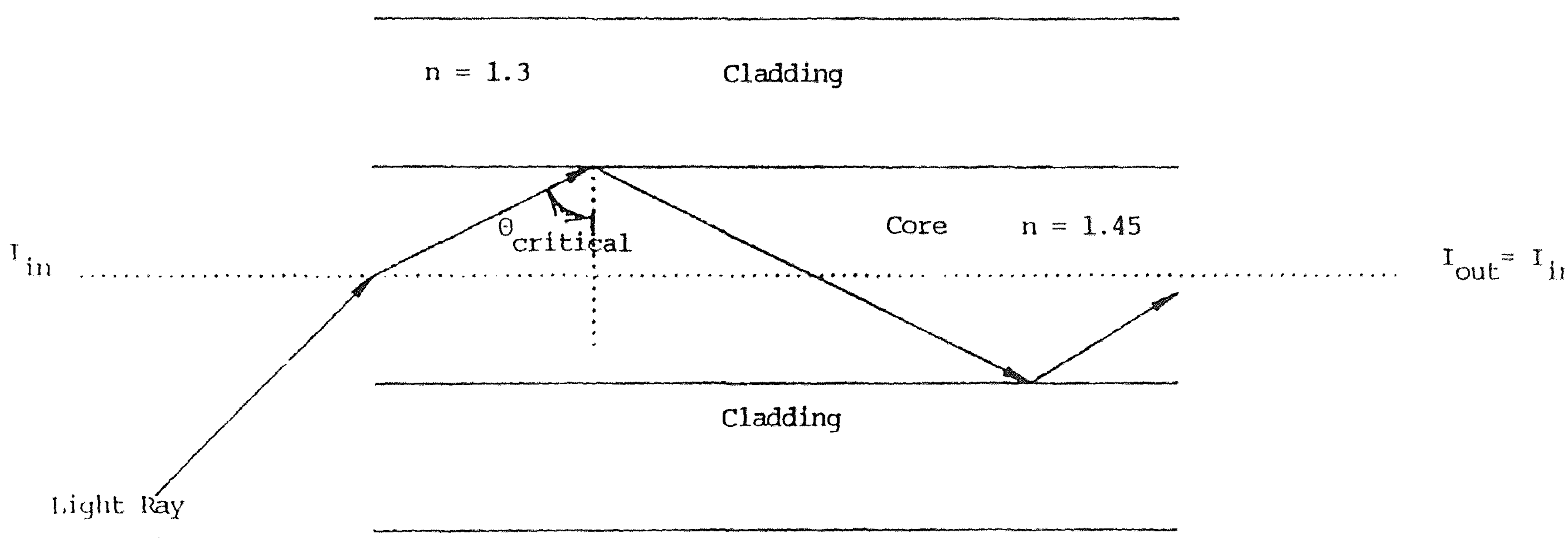

Fig.1 Basis for light transmission in optical fibers.

the cladding (Fig.2). The intensity of light at the output end of the fiber will decrease due to this loss , and it can be directly related to the amount of deformation if properly calibrated. Employing light intensity loss sensors in structural applications is simple since these sensors make use of modulation schemes which perturb the fiber itself , so that the fiber is both the transmission medium and the transducer. In other words , a thin optical fiber is all that is needed for embedment within a concrete member.

II.3 Fiber Optic Crack Opening Displacement (COD)Gage

Practical application of fiber optics to displacement measurements , particularly to COD measurements in concrete require special arrangement for placement of the optical fiber within the concrete , as well as attainment of sufficient sensitivity in measurements. The arrangement shown in Fig.3 provides optimum configuration of the fiber optics for COD measurements. It also satisfies the sensitivity requirements as bending of an optical fiber will result in increased light intensity loss through mode coupling. In other words , the microbending of an optical fiber , steepens the angle of light incidence at the core-cladding interface which in turn brings about increased light intensity loss.

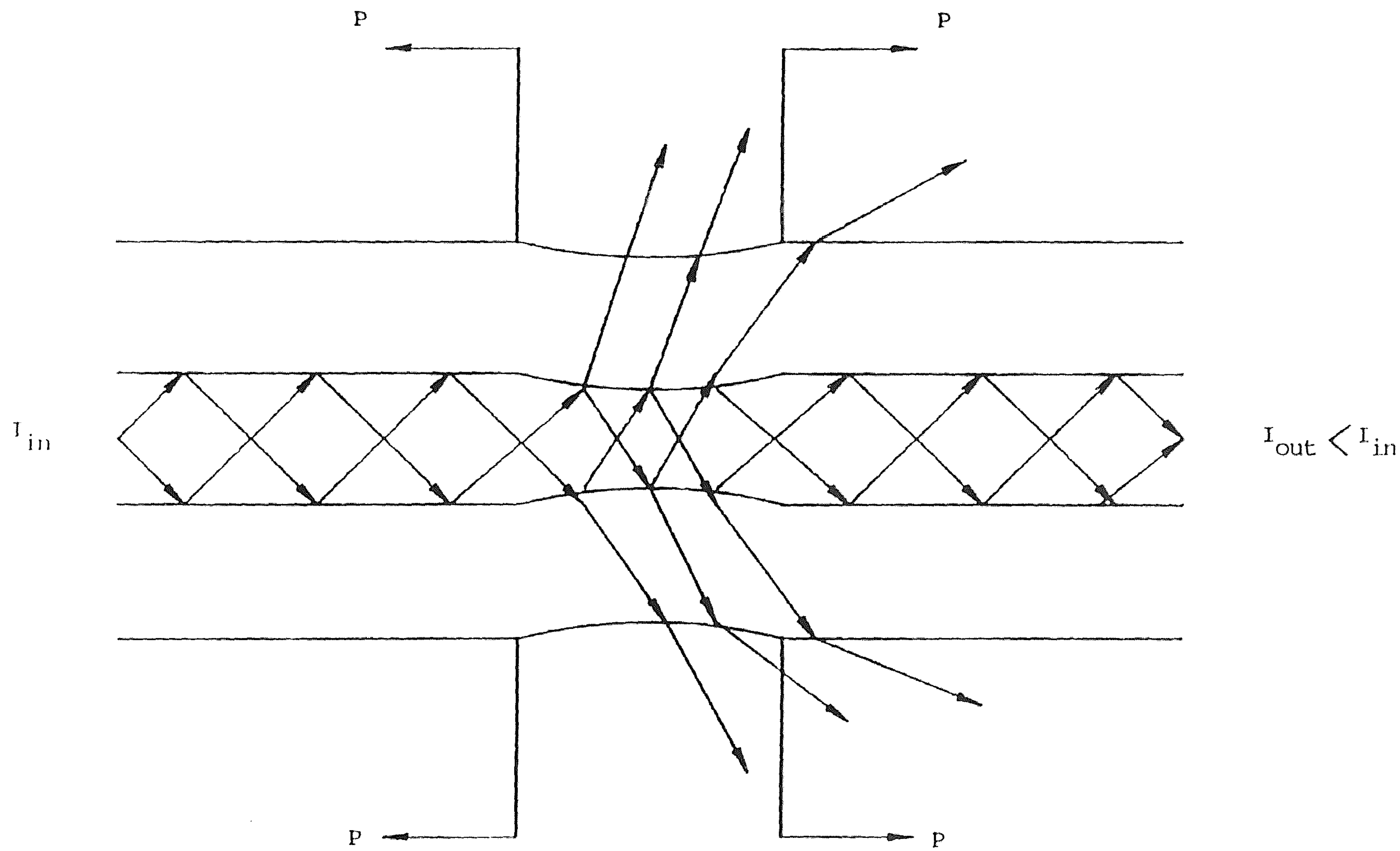

Fig. 2 Light loss in the optical fiber due to deformation.

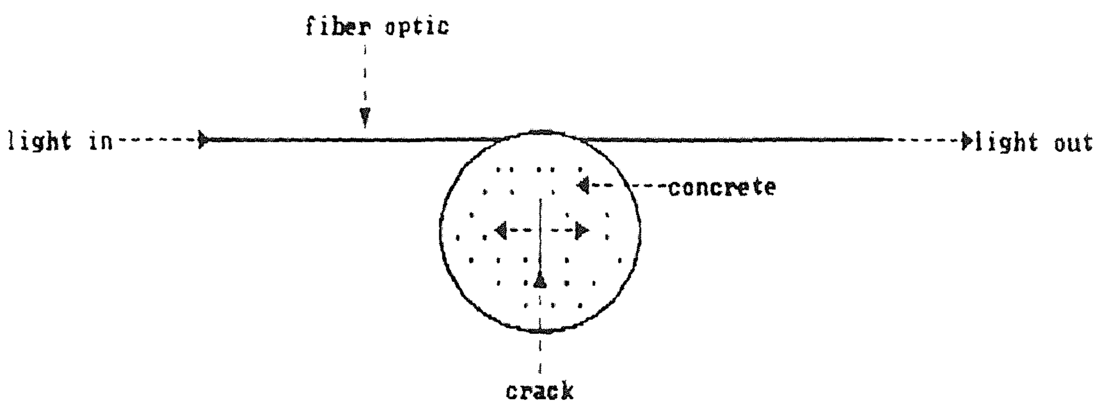

Fig.3 Plan View of Fiber Optic COD Gage

II.4 Instrumentation and Calibration

Progress of the microcracking zone was monitored by using four fiber optic COD sensors within the uncracked ligament for which details will be given in a later section. Experiments were performed in a closed loop mechanical testing machine so as to provide the capability of monitoring the descending branch of load-displacement relationship. Details in regard to various instrumentation techniques in performing the experiments , and acquiring pertinent data are given in the following subsections.

II.4.1 Sensor Intrumentation and Calibration

Instrumentation , specific to the operation of the fiber optic sensor are outlined in Fig.4. A 25 mW Helium-Neon laser source provide the input light source. At the coupler stage , light is divided into four equal divisions for use with four sensors. As explained earlier , in a particular sensor , the light output will decrease in proportion to the amount of displacement. This output is detected by a photodiode that in turn is amplified at the amplifier stage. At this point , data is converted to digital signals through a multichannel data acquisition board , and is transferred to a microcomputer.

Conversion of light intensity data (in Volts) to appropriate displacement values ,i.e. in milli-inch units ,

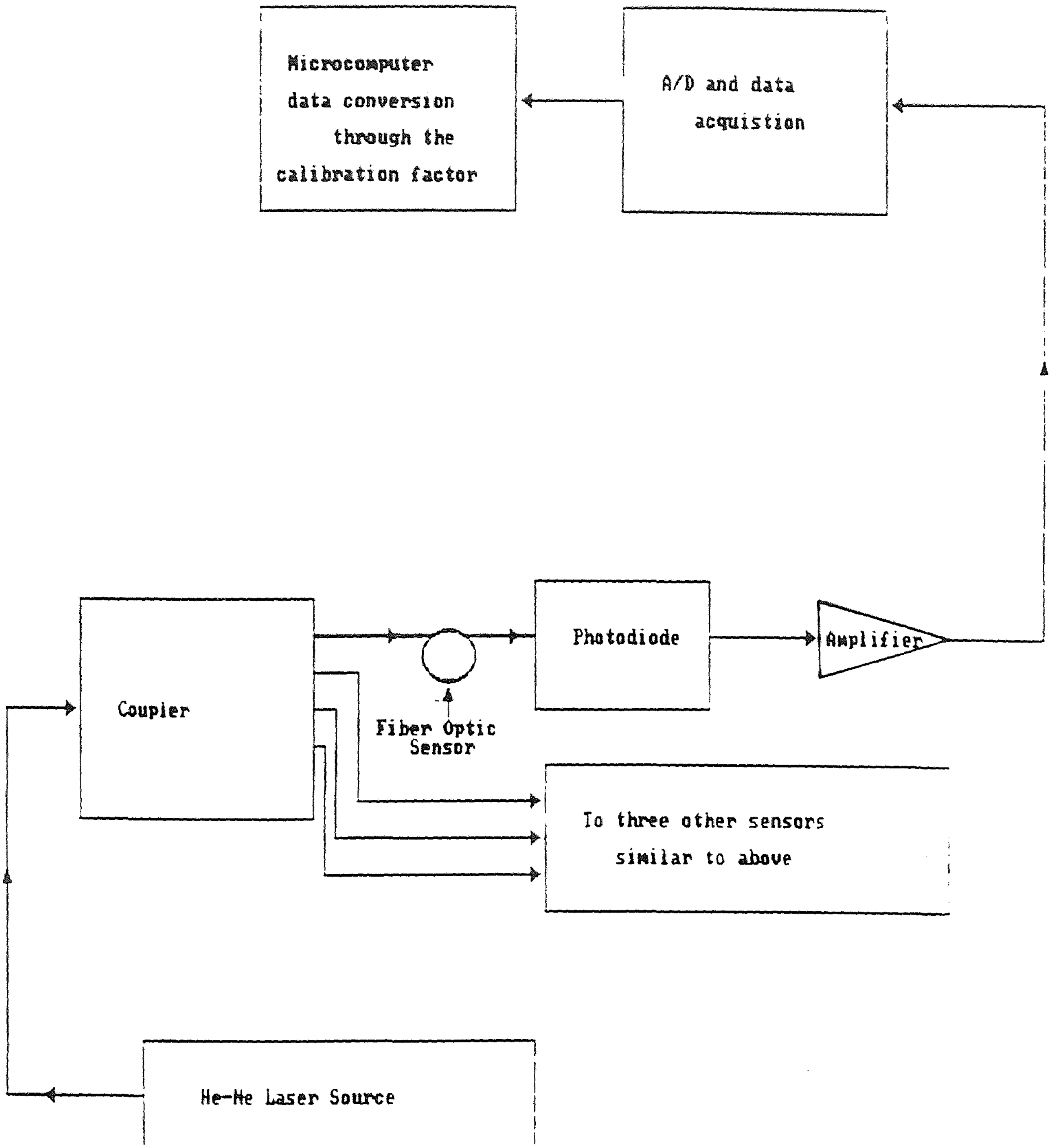

Fig.4 Block diagram of Fiber Optic Sensor operations

is accomplished through calibration. A calibration instrument is specifically designed for the fiber optic sensor (Fig.5). Calibration of the sensor is performed according to the following steps :

1) Fiber optic is wrapped around a disjoining cylinder whose diameter is 1.25 inchs (Fig.5). A groove is provided on the cylinder so as to facilitate fastening of the fiber optic into a perfect circle of 1.25 diameter. This is an important stage in the procedure , since variations in diameter result in inaccurate calibrations.
2) Stretch the fiber in a straight position by the motorized positioner. Hold it in position by an adhesive tape.
3) Use an epoxy to glue the fiber to the disjoining cylinder.
4) Once the epoxy is hardened (after 60 minutes) , apply another half inch of cement paste on top of the epoxy to insure perfect bonding.
5) Once cement is hardened (after 24 hours) , the fiber ends are connected to the laser source and the photodiode.
6) Amplifier's output is adjusted to six volts , and the output sensitivity is checked.
7) LVDT's core is adjusted to a halfway position.
8) Data acquisition rate is set at twenty Hertz for a period of ten seconds , and the computer is initialized.
9) At this point , the motorized positioner is turned on to separate the disjoining cylinder , and as a result , create loss in the intensity of input light due to

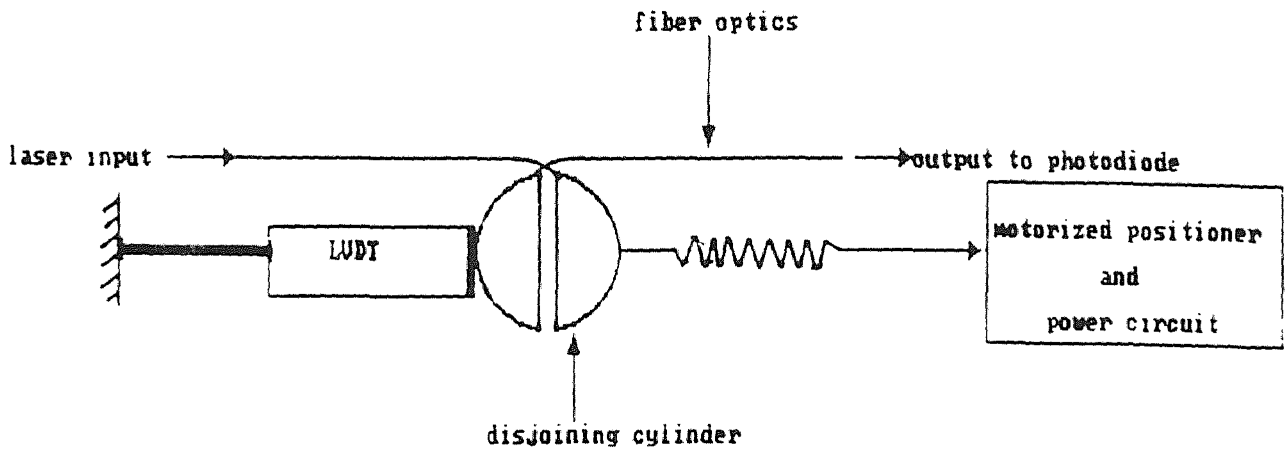

Fig.5 Plan View of The Calibration Instrument

separation of the cylinder halves.

10) By design , the LVDT core and the two halves of the cylinder displace identically , and therefore the light intensity loss measurements can be directly related to the opening of the cylinder halves.

Calibration results obtained in this way are automatically stored in the microcomputer via the data acquisition system. each of the four sensors were calibrated individually , and results are shown in Fig.6 thru Fig.21. A calibration constant relating the loss in the intensity of light to the displacement for each of the sensors can be obtained from the slope of Figs.8 , 12 , 16 , and 20. The calibration constants calculated in this way are : 34.4575volts/in. , 50.6821volts/in. , 75.43volts/in. , and 67.245volts/in. for channel 1 thru 4 respectively.

II.4.2 Closed Loop testing and Data acquisition

It is essential to study the prepeak response as well as post peak softening behavior of concrete. Therefore , specimen were tested in a screw-driven microcomputer-based closed loop testing system. An Apple II microcomputer was employed in generating testing program signals (Fig.22). The system is capable of controlling the movement of optical components as well as providing closed-loop feedback control for loading of specimen so as to maintain a constant rate of increase in the deformation of specimens. details regarding

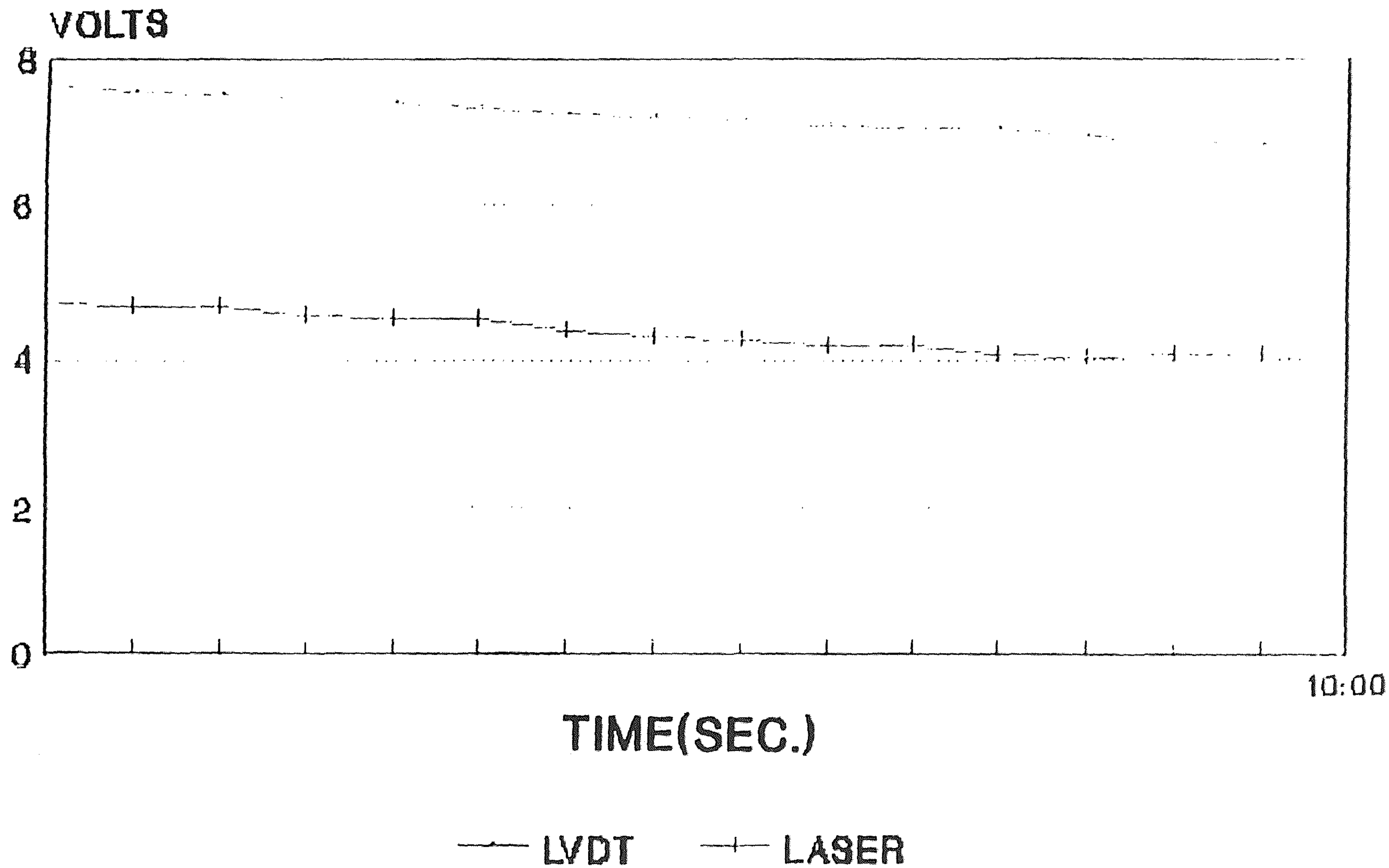

Fig.6 Calibration data for channel#1

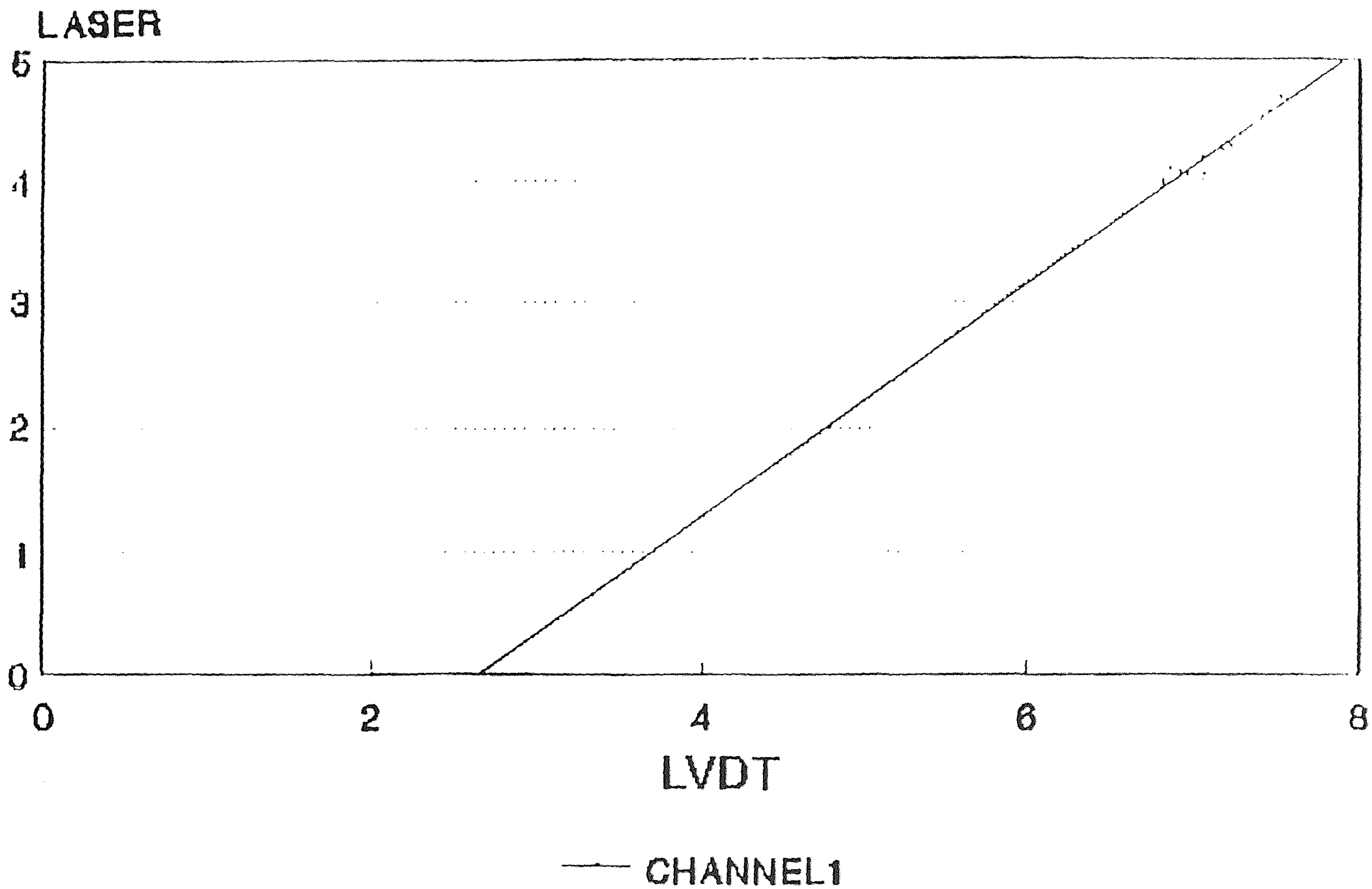

Fig.7 Light Inten. loss vs. LVDT for CH1

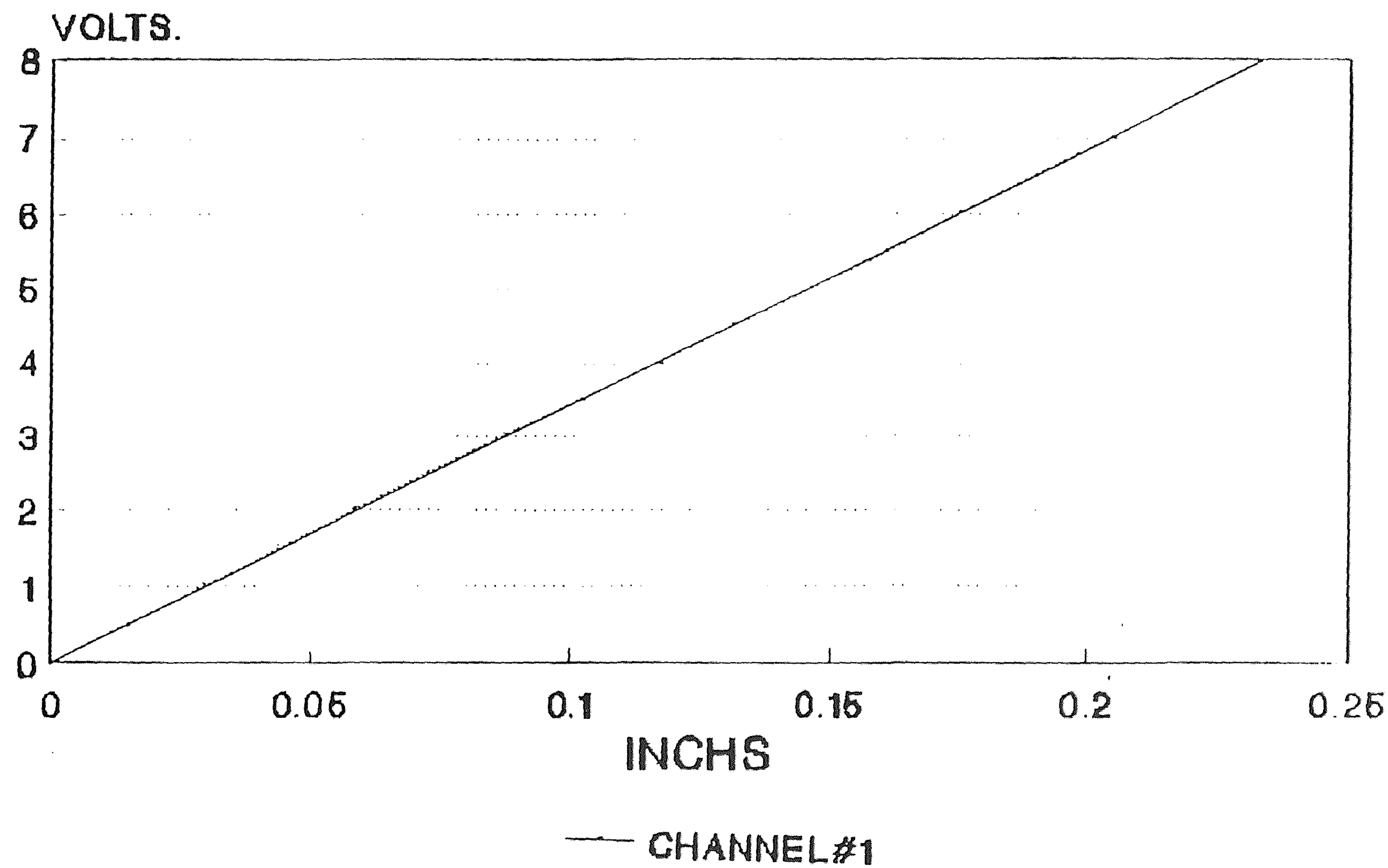

Fig.8 Light Inten. loss vs. dis. for CH1

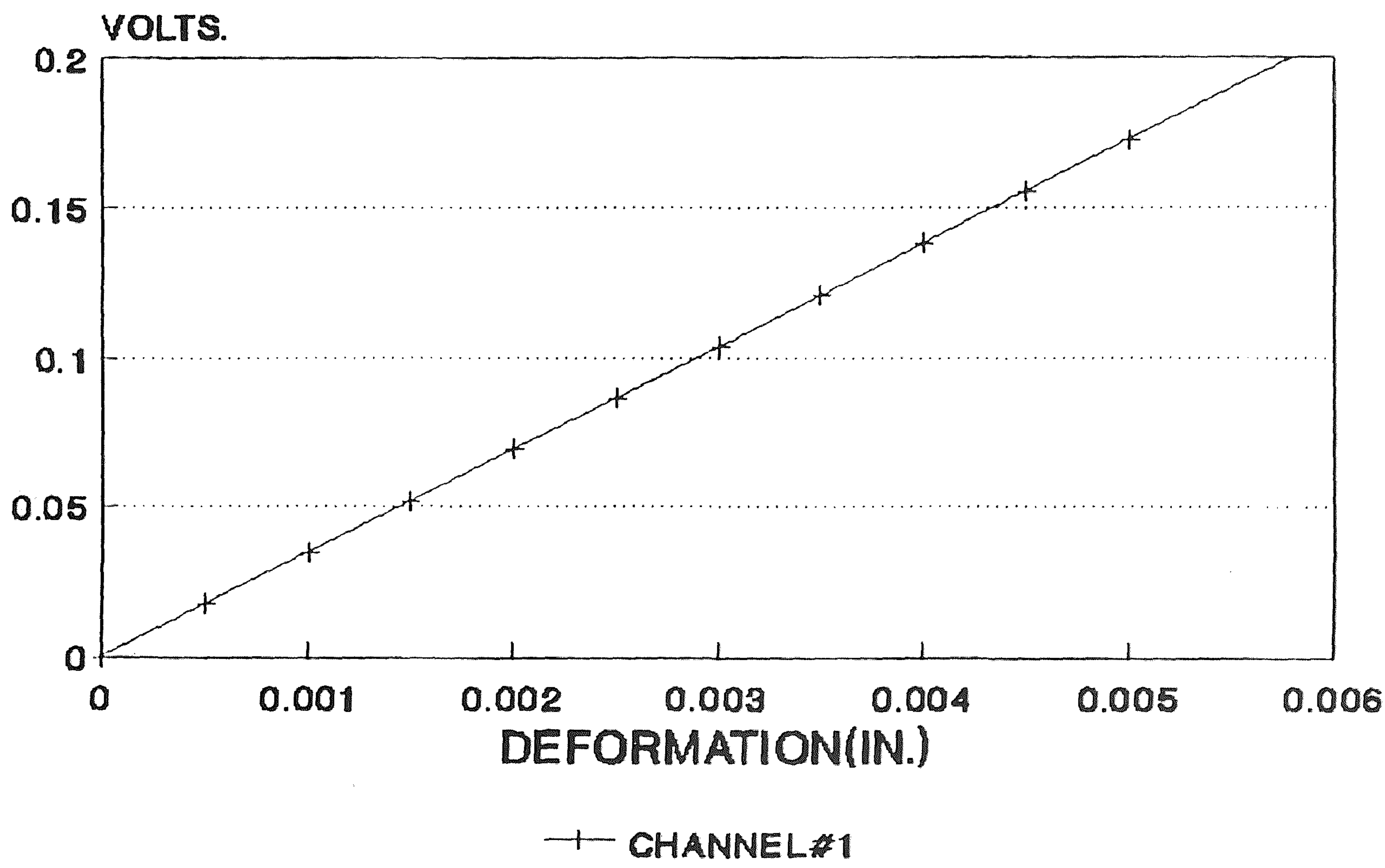

Fig.9 Lower range cali. curve for CH.1

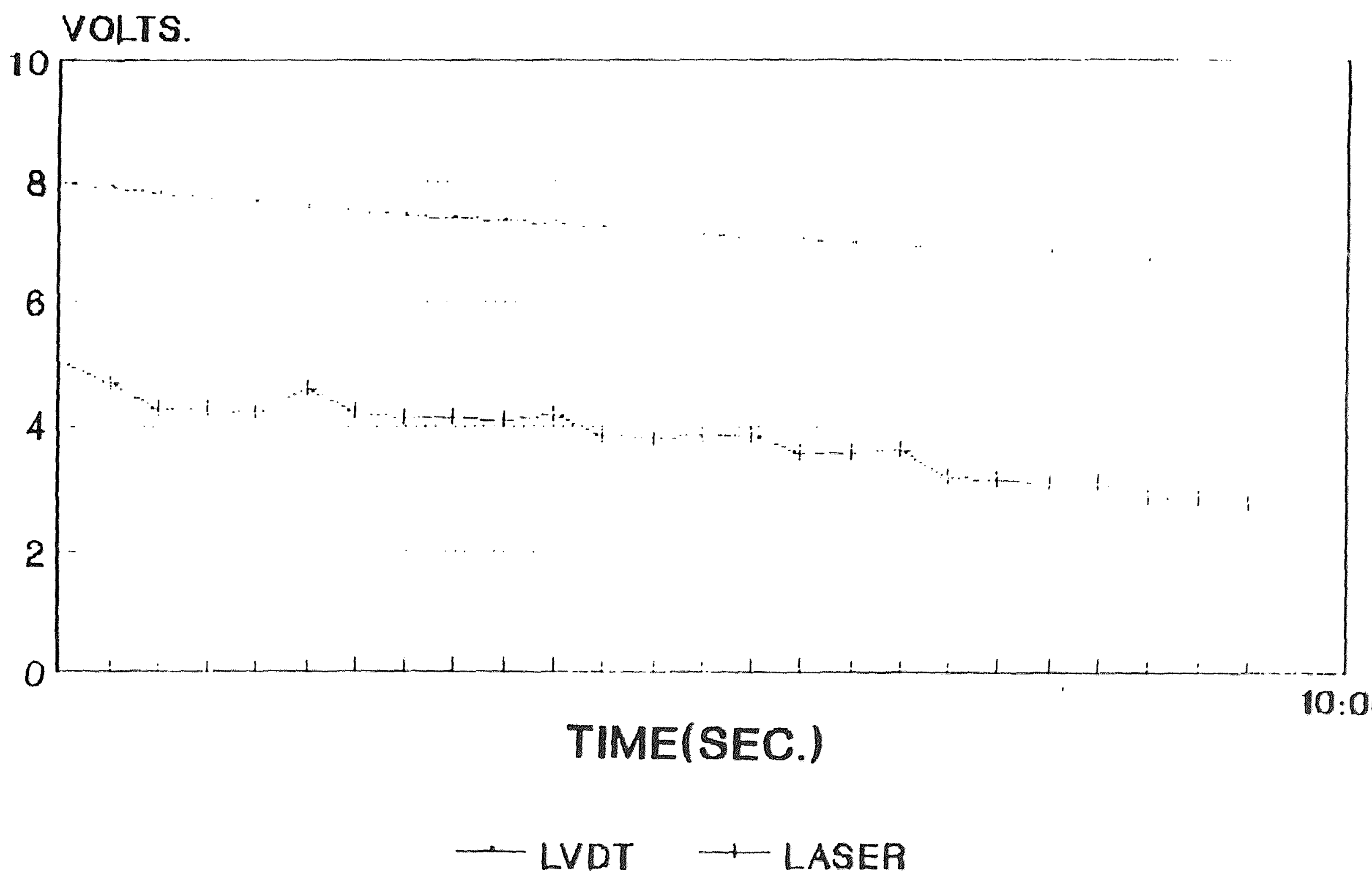

Fig.10 Calibration data for channel#2

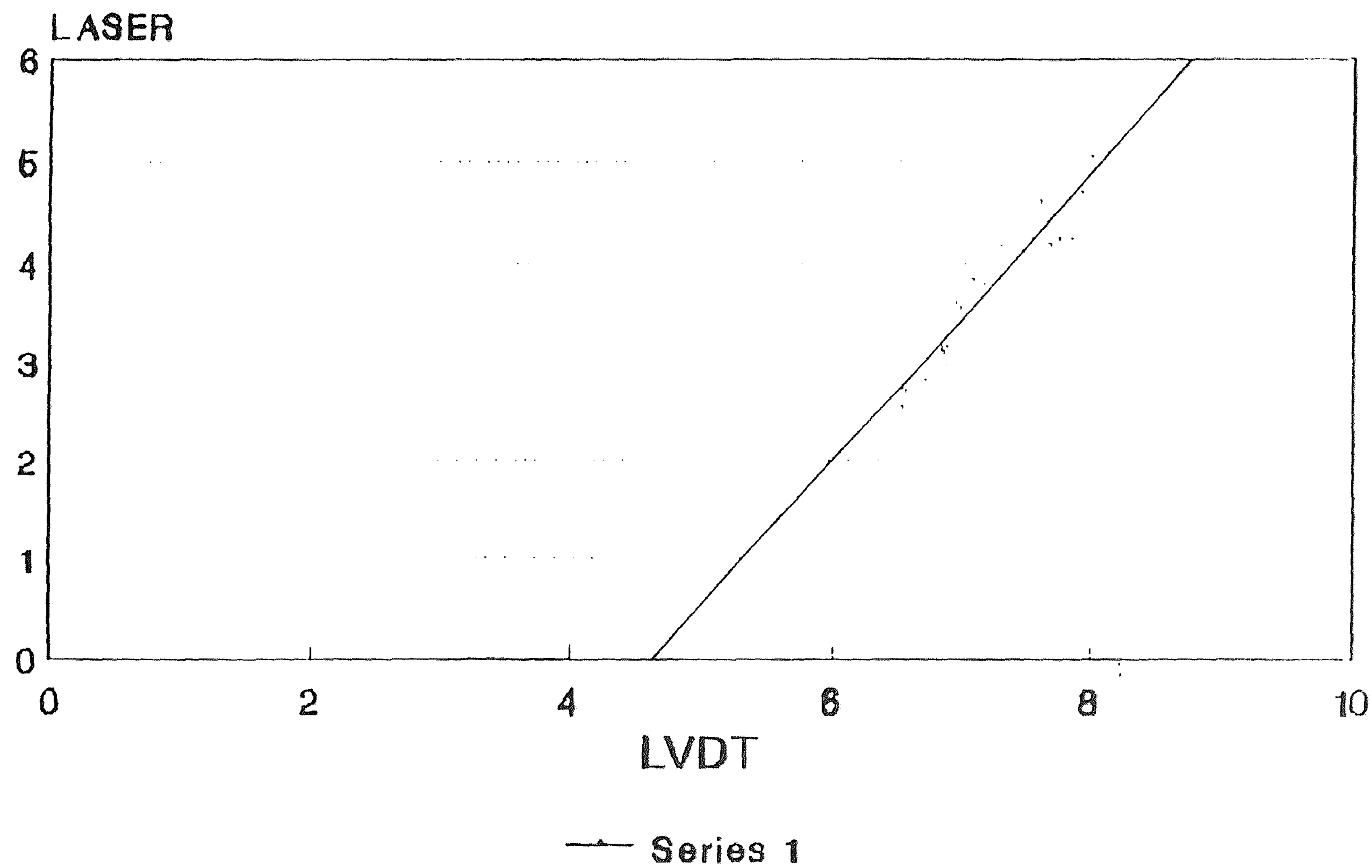

Fig.11 Light Inten. loss vs. LVDT forCH2

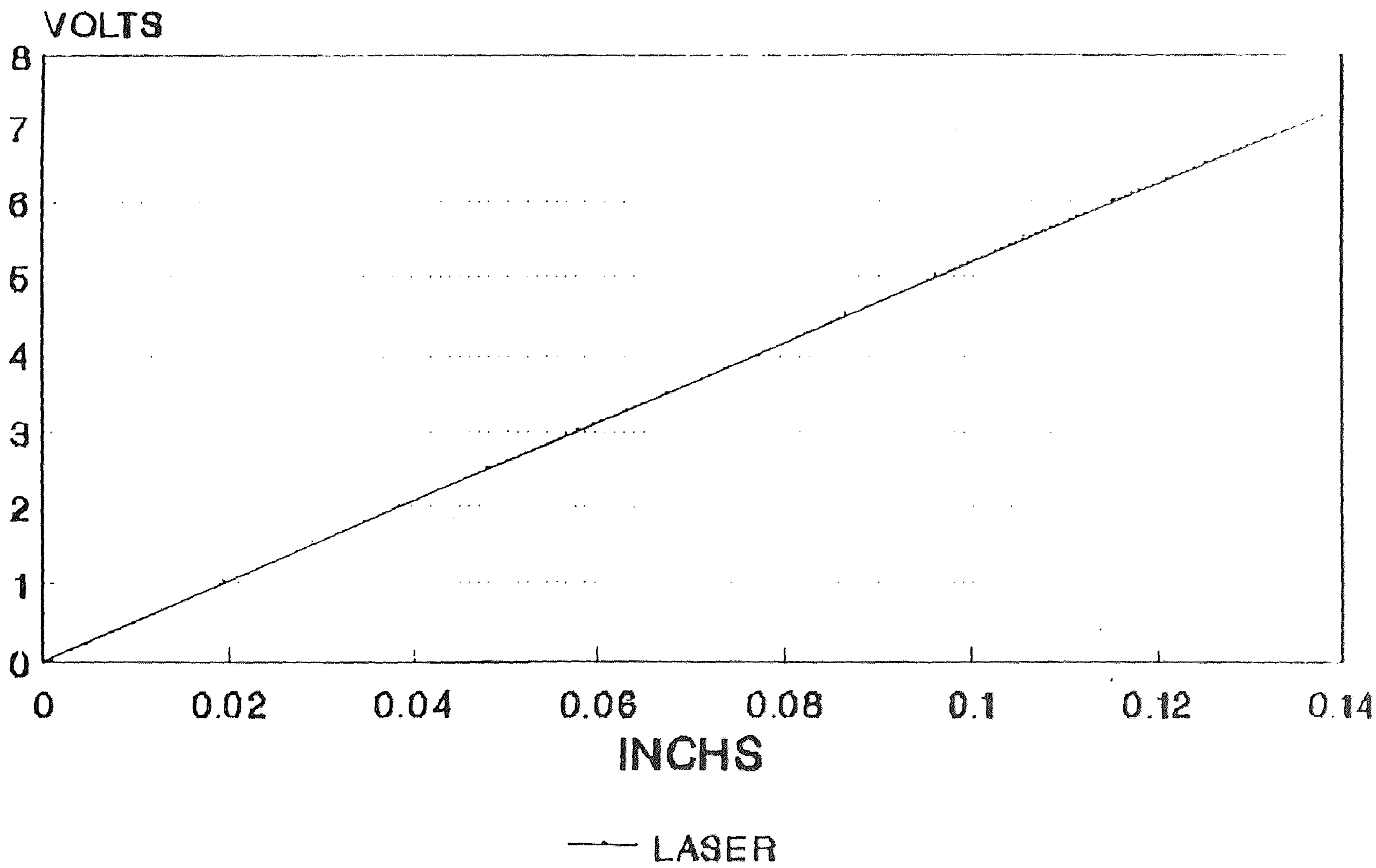

Fig.12 Light Inten. loss vs. dis. forCH2

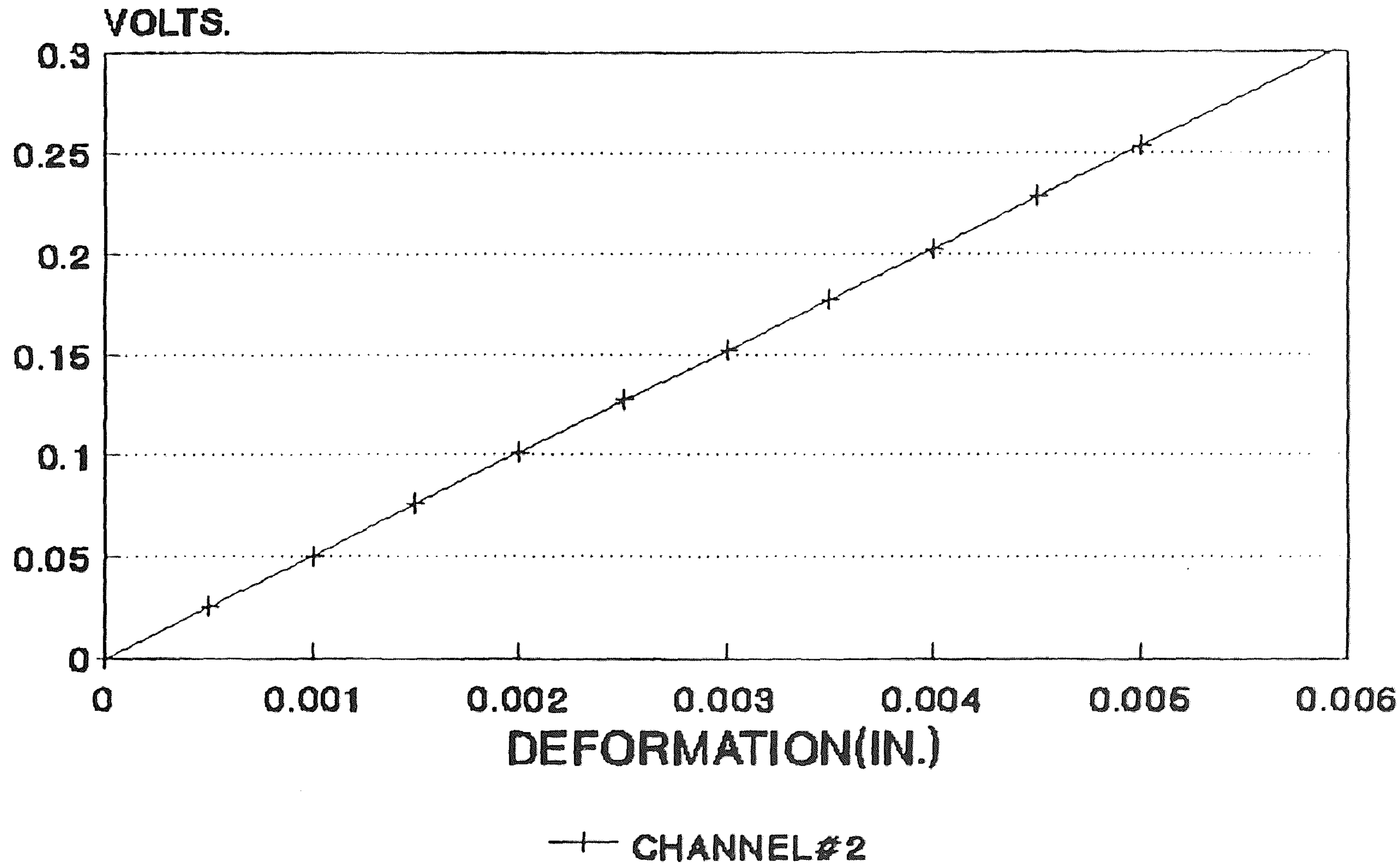

Fig.13 Lower range cali. curve for CH.2

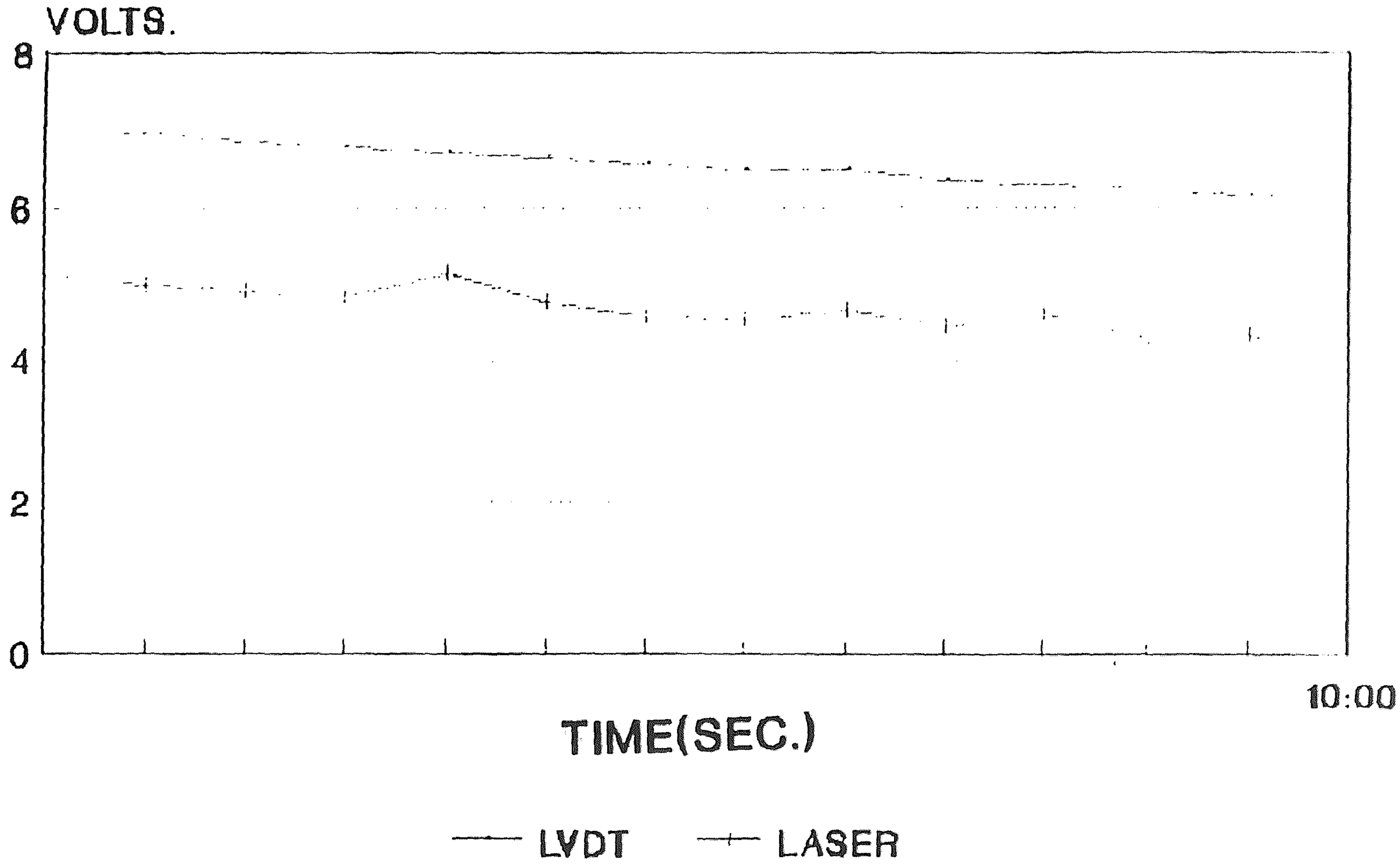

Fig.14 Calibration data for channel#3

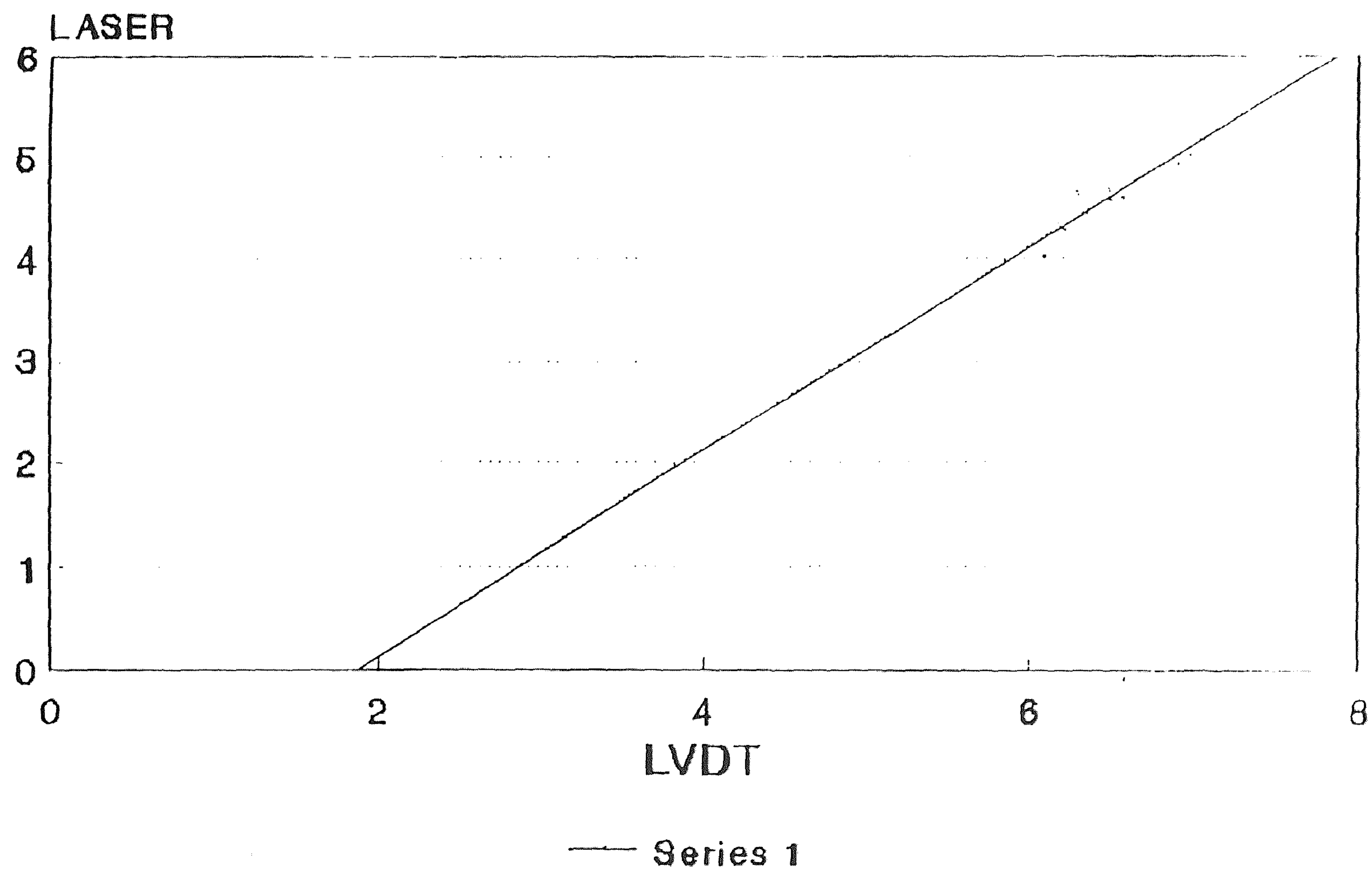

Fig.15 Light Inten. loss vs. LVDT forCH3

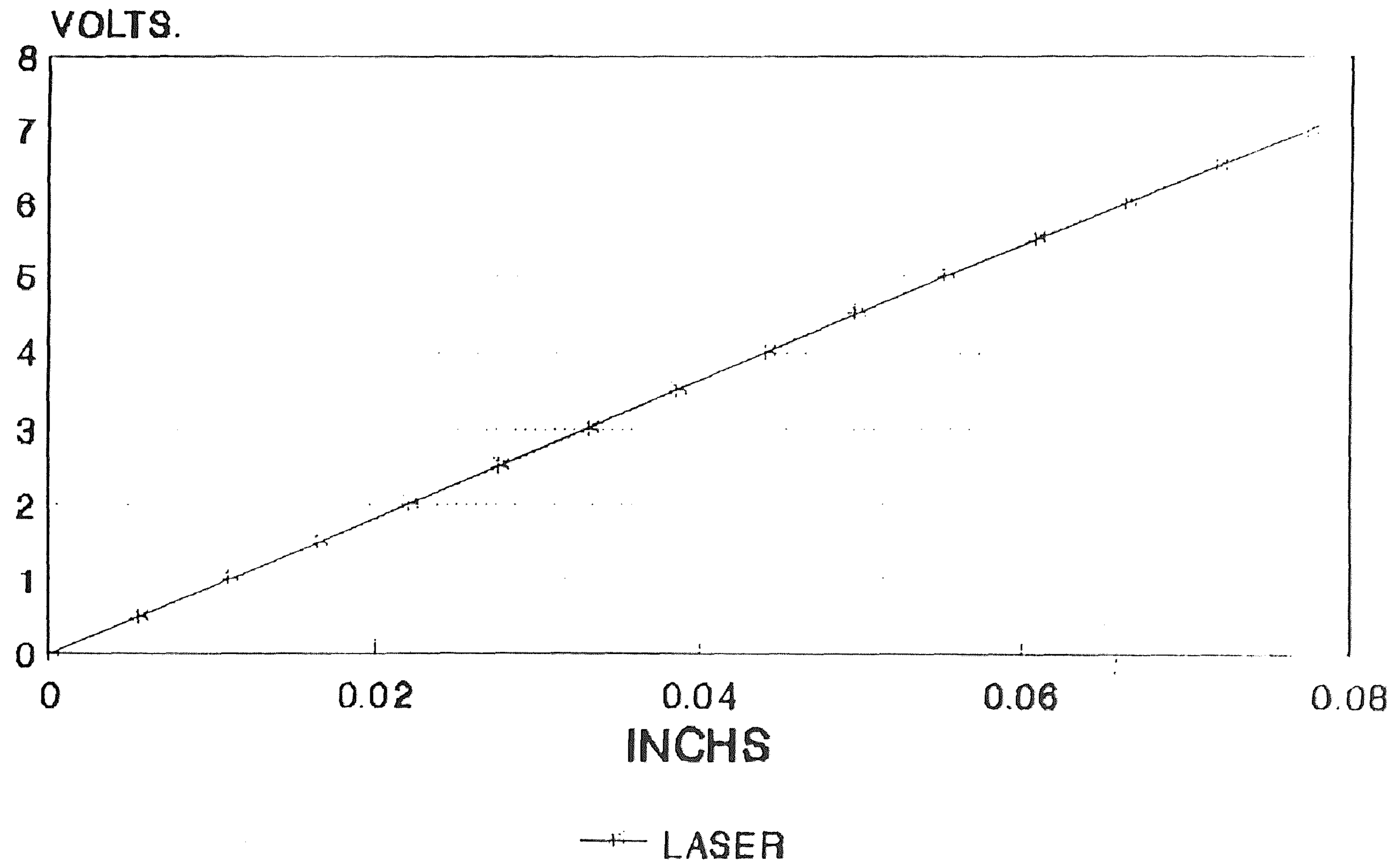

Fig.16 Light Inten. loss vs. dis. forCH3

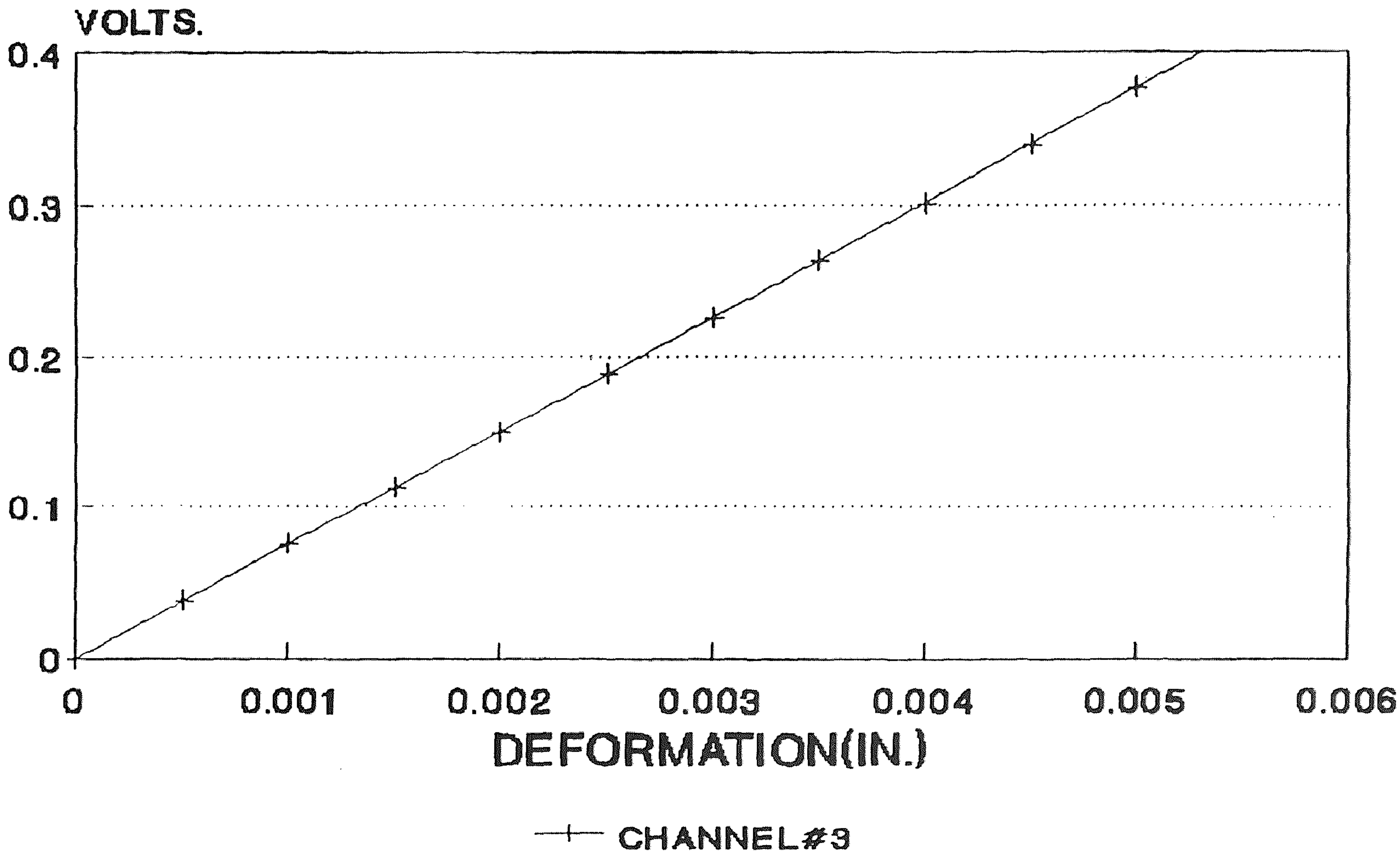

Fig.17 Lower range cali. curve for CH.3

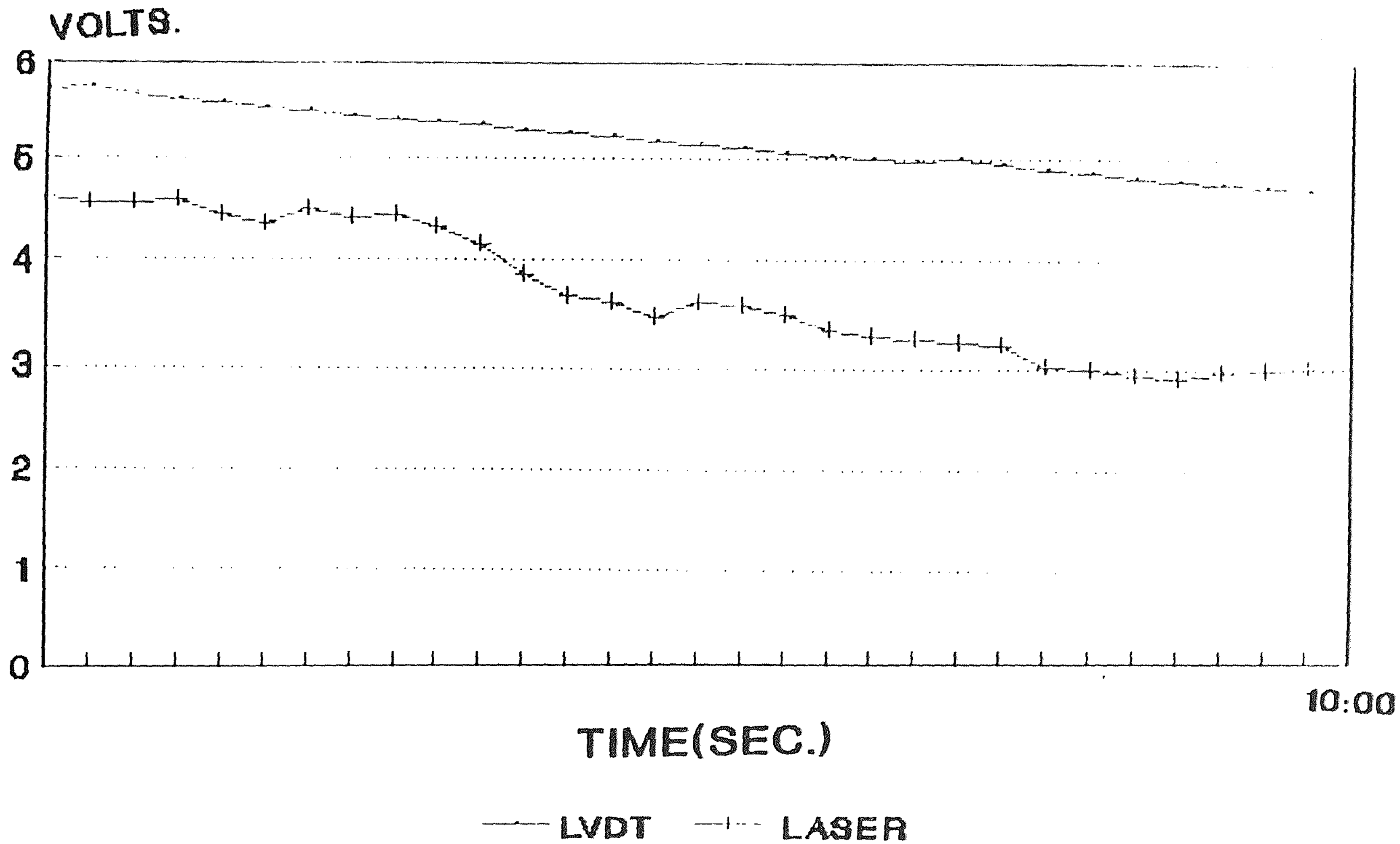

Fig.18 Calibration data for channel#4

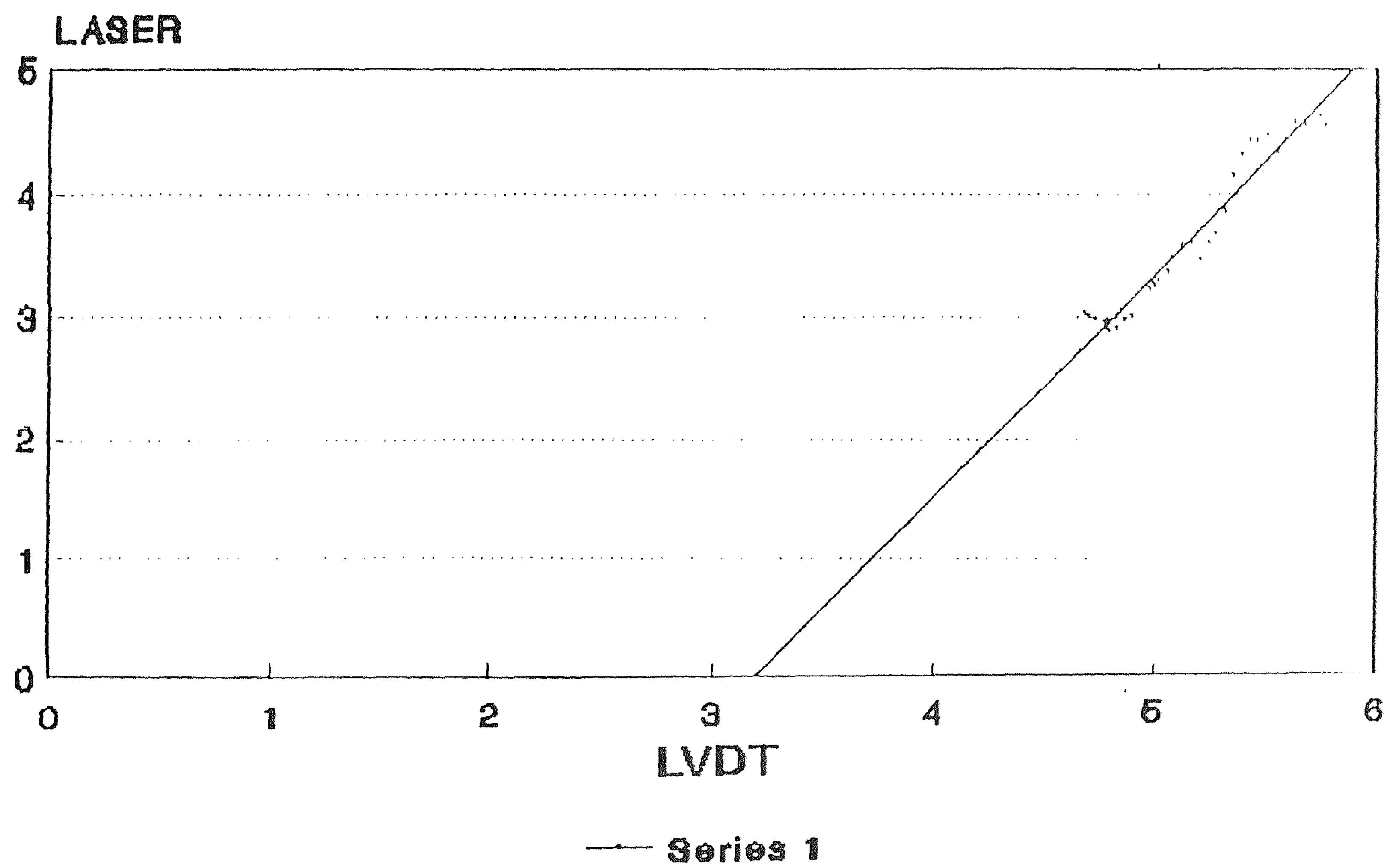

Fig.19 Light Inten. loss vs. LVDT forCH4

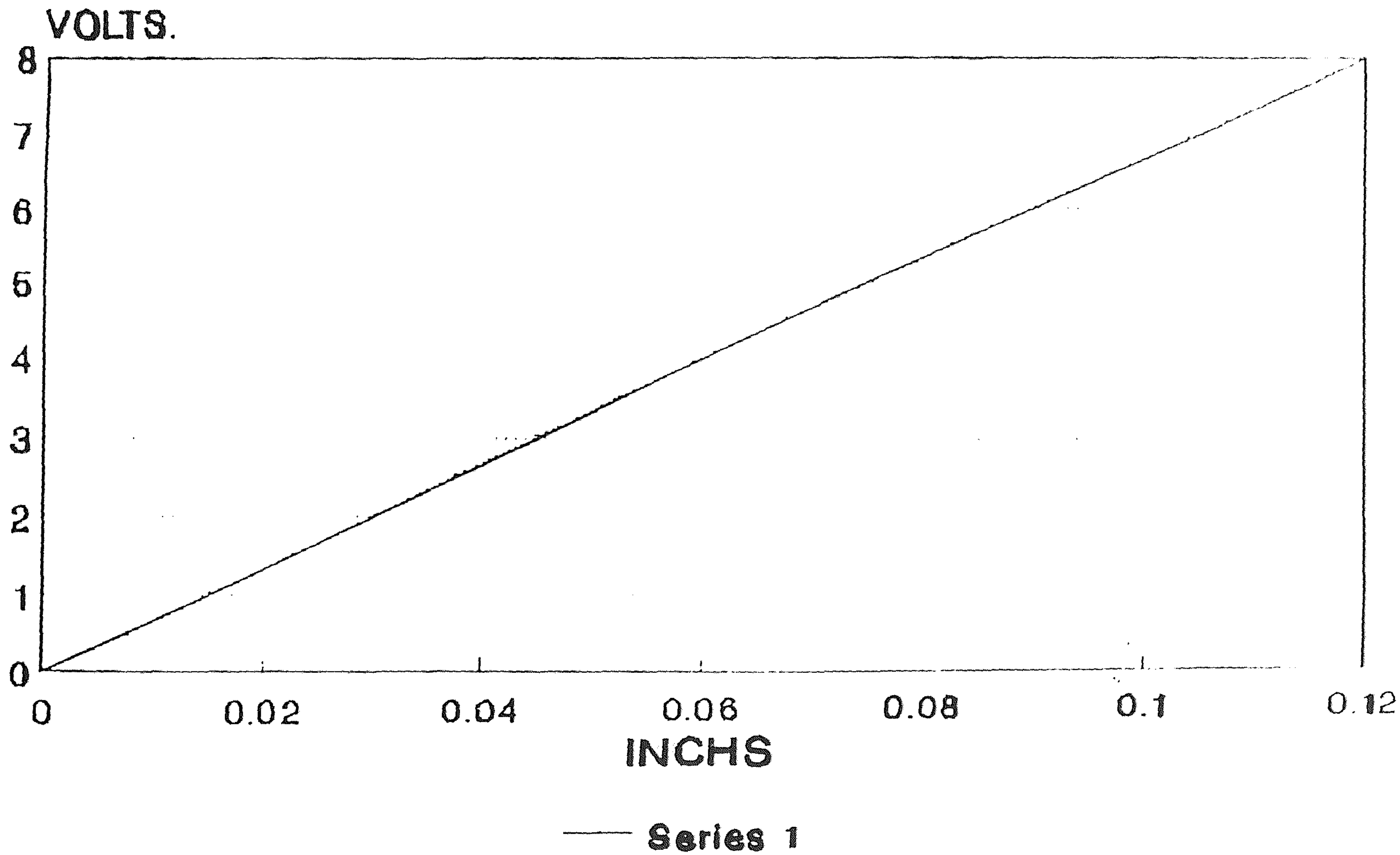

Fig.20 Light Inten. loss vs. dis. for CH_4

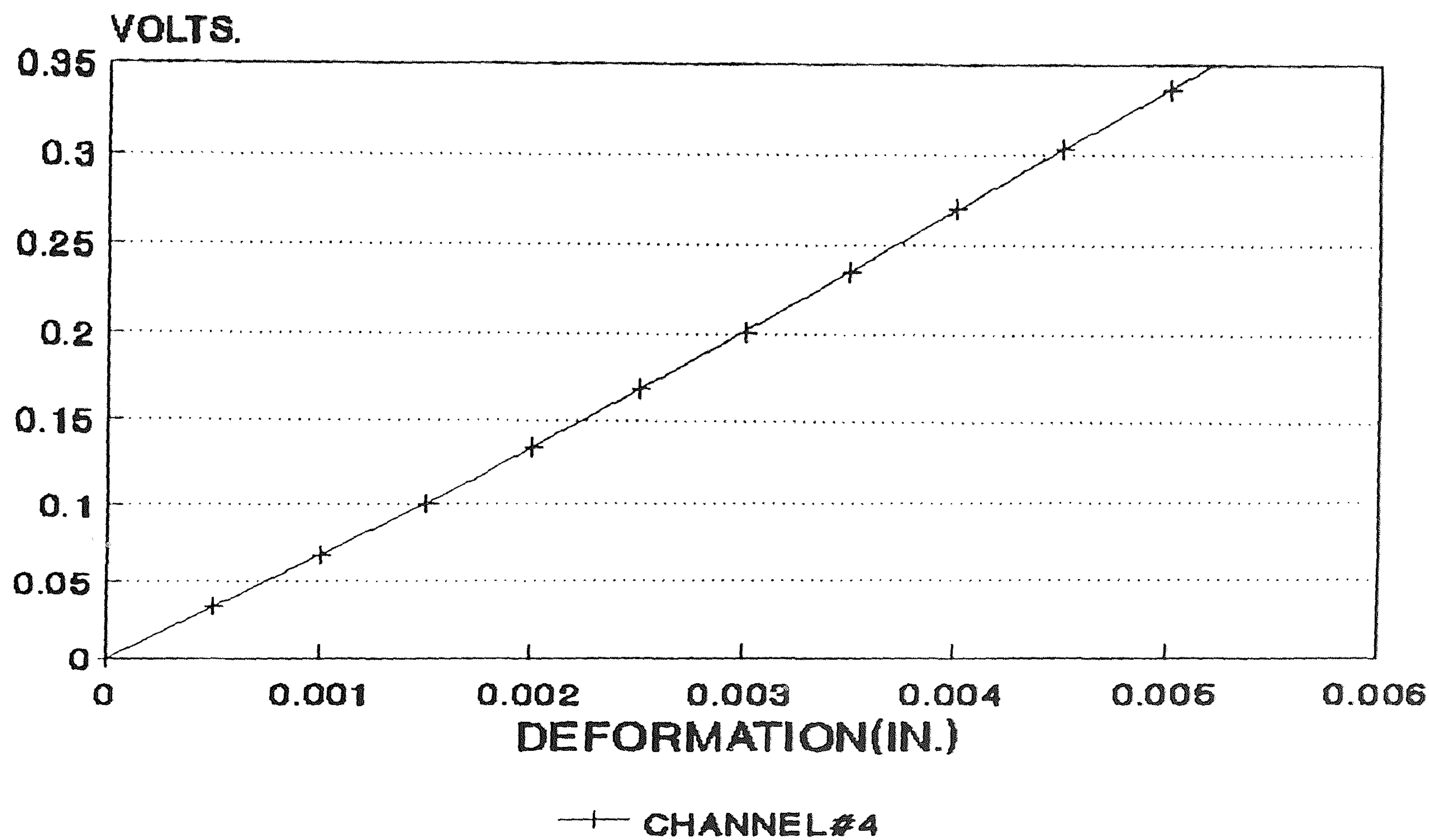

Fig.21 Lower range cali. curve for CH.4

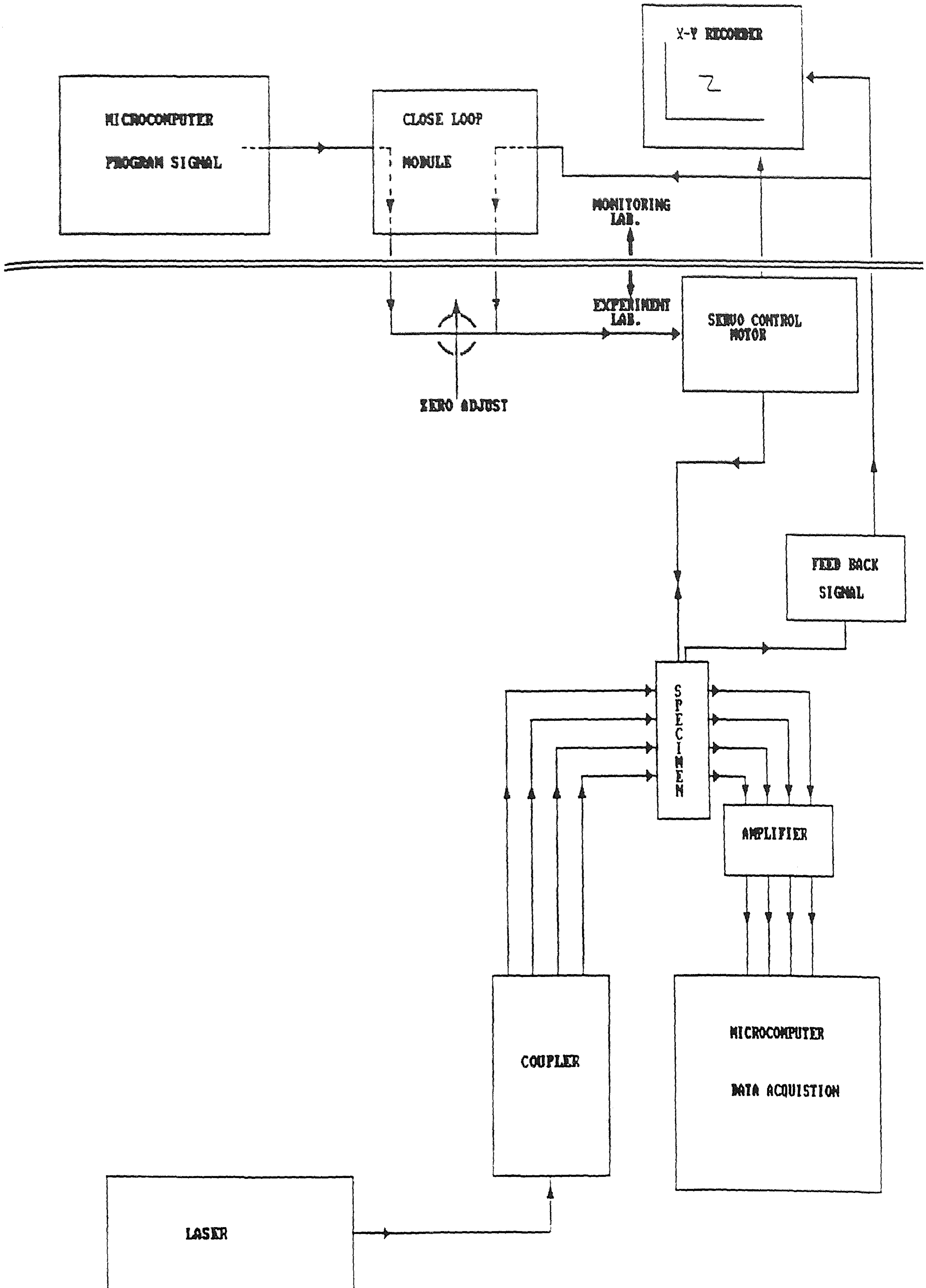
X-Y RECORDER
MICROCOMPUTER
PROGRAM SIGNAL
CLOSE LOOP
MODULE
MONITORING
LAB.
EXPERIMENT
LAB.
SERVO CONTROL
MOTOR
ZERO ADJUST
FEED BACK
SIGNAL
SPECIMEN
AMPLIFIER
COUPLER
MICROCOMPUTER
DATA ACQUISTION
LASER

the design and fabrication of the system are given elsewhere[14]. Feedback signal for loading was provided by an LVDT at the precast notch mouth. In other words , for both the three point bend and the compact tension specimen , COD was used as a feedback signal. A second LVDT was employed for measuring the Load Point Deformation. Calibration data for these LVDT's are given as :

<u>LVDT for COD measurements : 1 inch = 33.87 volts.</u>

<u>LVDT for LPD measurements : 1 inch = 35.7 volts.</u>

As mentioned earlier , four optical sensors were embeded in each specimen through equal division of laser light source by a coupler as shown in Fig.22. A data acquisition program , DASH-16 was modified by BASIC programming and employed for data handling from seven channels. Data acquisition channels included , load , two LVDT's , and four fiber optic sensors. Program modification was performed through a BASIC program , MENG.BAS , that will be given in detail in the Appendix. Sampling rate was set at 20 HZ , for 25 minutes. a total of 30,000 data points were acquired per specimen.

II.5 Details of test specimen

A mix proportion of 1:2:2:0.55 , by weight of cement : sand : gravel : water was employed. Type III portland cement conforming to ASTM c 150 , ASTM NO.2 grade river sand passing through sieve NO.8 , maximum coarse aggregate size passing 0.375 inch (9.5mm) and retained on NO.4 sieve was used. Specimen were cast in plexiglass molds. Freshly cast specimens were left at room temperature for 24 hours. They were then demolded and air-dried before testing. Average age of specimen at testing time ranged between 21 to 30 days. Specimen geometry and location of sensors are shown in Fig.23.1 and 23.2. Fig.23.3 and Fig.23.4 depict the compact tension and the three point bend specimen with associated optical setup in the loading frame respectively.

II.6 Experimental procedure

Beams were tested under three point load and Compact Tension specimen were tested under direct tension in a testing frame on a vibration isolated table. Experiments were monitored from an adjacent room employing a microcomputer as discussed earlier. Following are steps taken during testing :

1, Load "MCCLSS" program into microcomputer(Apple II) , which is a program for closed-loop system.

2, Place the specimen into the load machine very carefully , and connect the laser to the corresponding channels , and then connect the other ends of the fiber sensor to the amplifier.

3, Turn on the microcomputer (IBM) for data acquisition. Load "LABTECH" , data acquisition software for checking

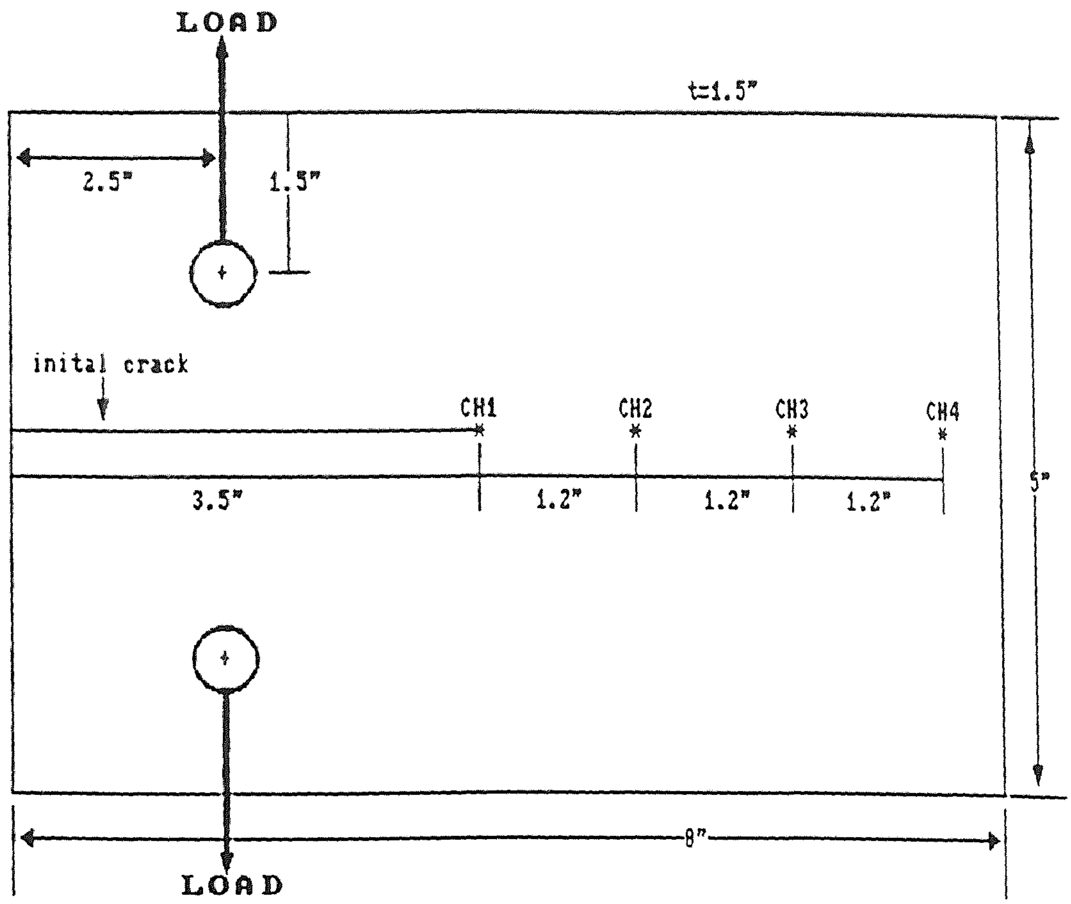

Fig.23.1 Compact tension specimen and location of sensors

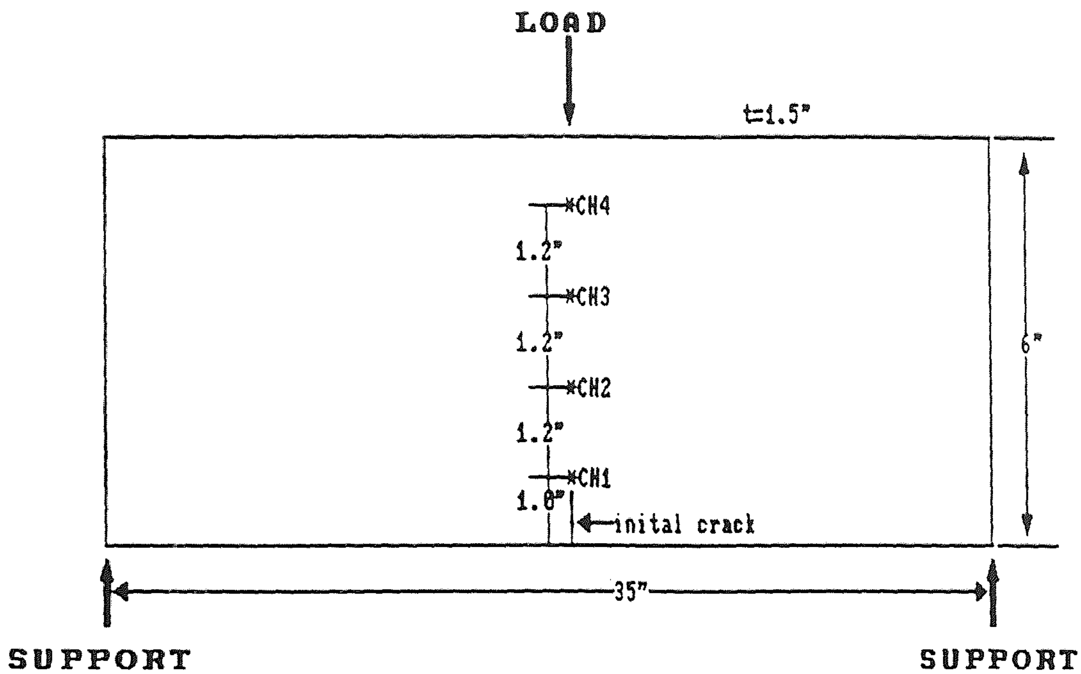

Fig.23.2 Three point bend specimen and location of sensors

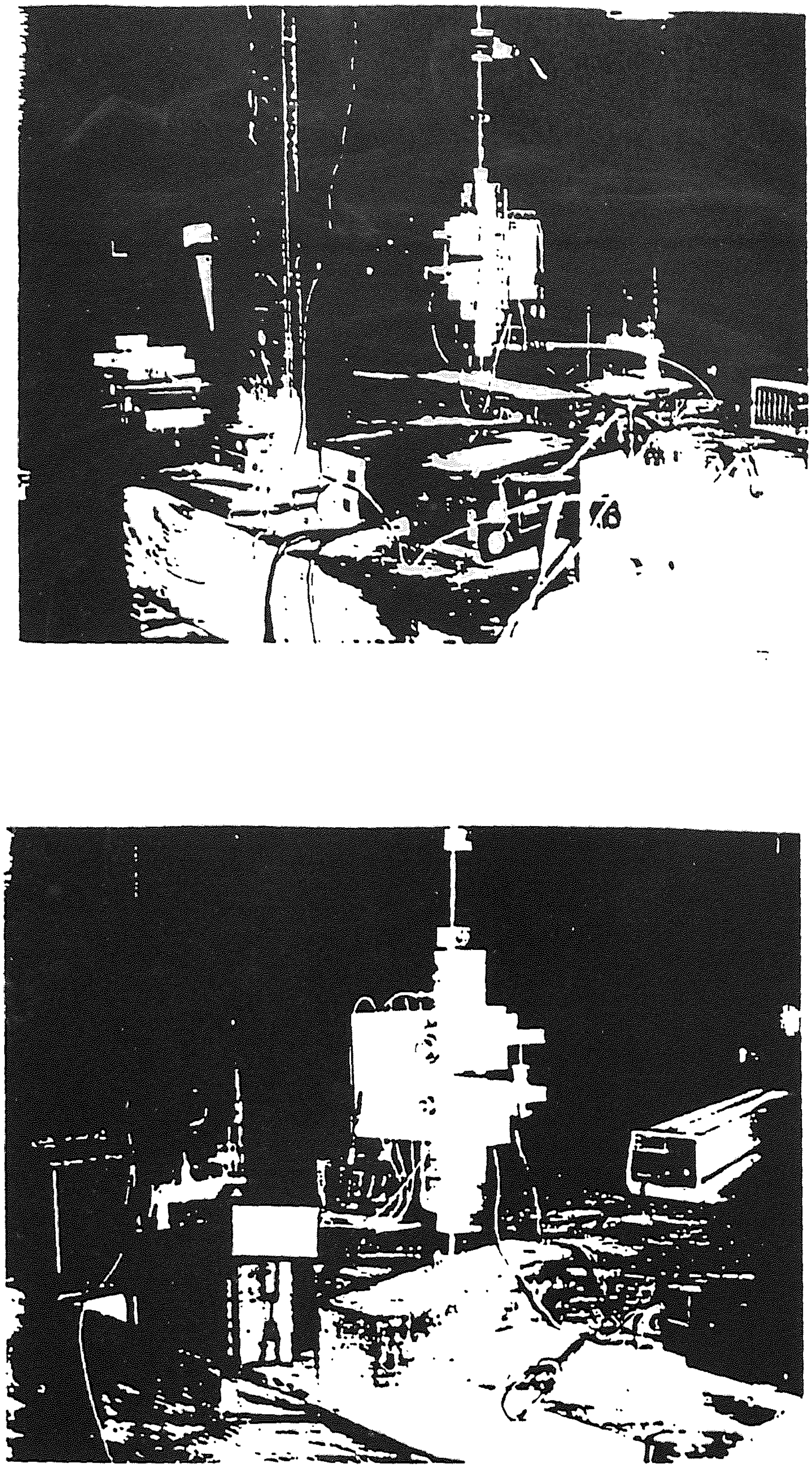

Fig.23.3 Compact tension specimen in the loading fram

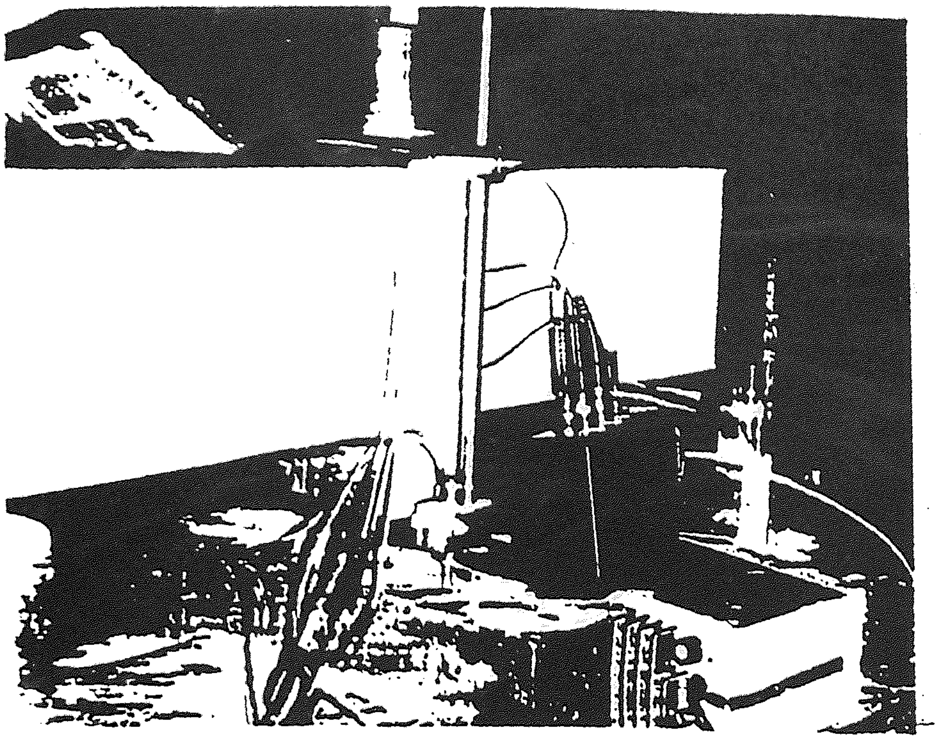

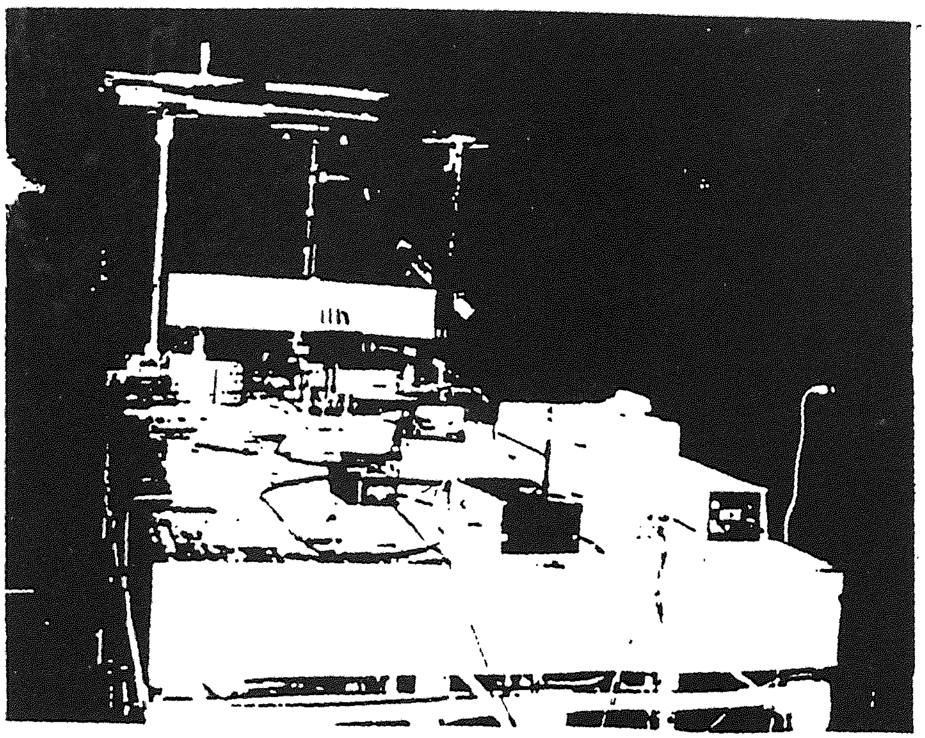

Fig.23.4 Three point bend specimen in the loading frame and the optical setup

proper operation of all the channels.

4, Load "DASH-16" and "MENG.BAS" into micro-computer for data acquisition .

5, Following steps are required for zero adjustment of the closed-loop testing system :

   (a), Loosen the drive belt in order not to damage the specimen.

   (b), Adjust the LVDT at the crack mouth for zero adjustment.

   (c), Adjust the load controlling switch so as to get the exact zero point on the specimen.

6, Use "MCCLSS" to set all the required parameters into the program in order to operate the testing system.(While doing compact tension specimen use an exposure time of 0.09 min. , for BEAM tests use 0.2 min..)

7, Run "MENG.BAS" in the IBM microcomputer for data acquisition.

8, After the test turn off all system.

CHAPTER III Analysis and Results

This chapter presents experimental results , their analysis and a discussion of observed trend. As shown in Table 1, sixteen concrete specimens were tested. Seven specimens were tested under tension and the rest were tested under three point load.

Experimental data acquired by the computer , representing load , load point displacement , COD , and the four sensor outputs are given in direct data acquisition voltage units in Figs.24 thru 87.

These figures represent raw experimental data. Program CHAN.FOR , DEF.FOR , and TOT.FOR that are explained in detailed in the Appendix and the HARVARD GRAPHICS software were employed to convert the raw data into corresponding load , COD , LVDT , and deformation values.

Load versus corresponding COD , LPD , and internal deformations are shown in Figs.88 thru 99.

Experimental results indicated that specimen F2 , F8 , F11 , F12 , F19D , F28A , M1A , and M1B showed consistent results , whereas , the rest of the specimen did not provide good results. These bad results were due to either deficiencies in the specimen such as damages due to precast notch , or fracture of the compact tension arms prior to the completion of tests. Experimental data indicates that in

Table I Specimen types and designations

CONCRETE SPECIMEN		
NUMBER	NAME	TYPE
1	J31	CT
2	F2	CT
3	F3#2	CT
4	F8	CT
5	F10	CT
6	F11	CT
7	F12	CT
8	F19A	BEAM
9	F19B	BEAM
10	F19C	BEAM
11	F19D	BEAM
12	F28A	BEAM
13	F28B	BEAM
14	F28C	BEAM
15	M1A	BEAM
16	M1B	BEAM

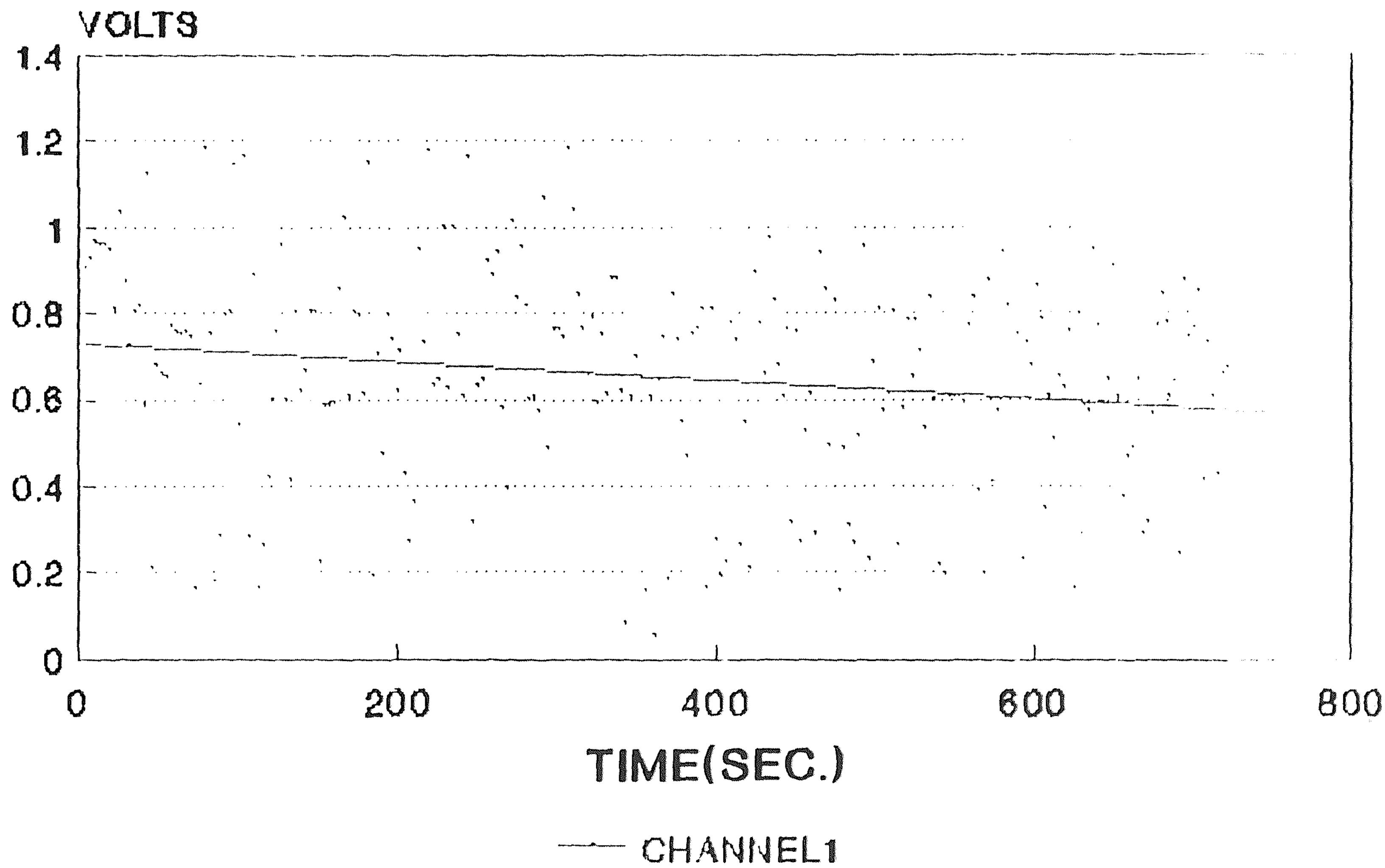

Fig.24 Internal deformation for J31

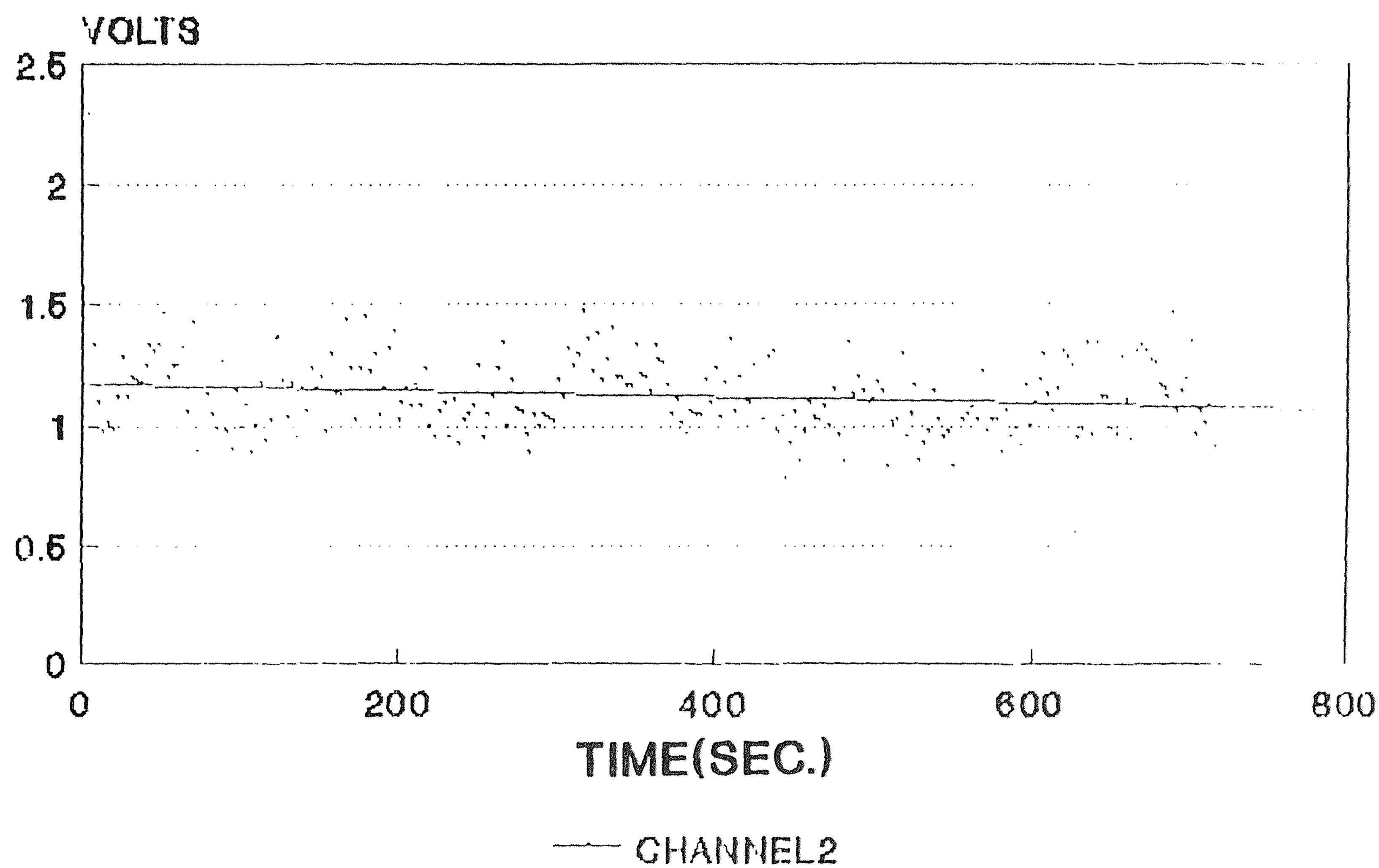

Fig.25 Internal deformation data for. J31

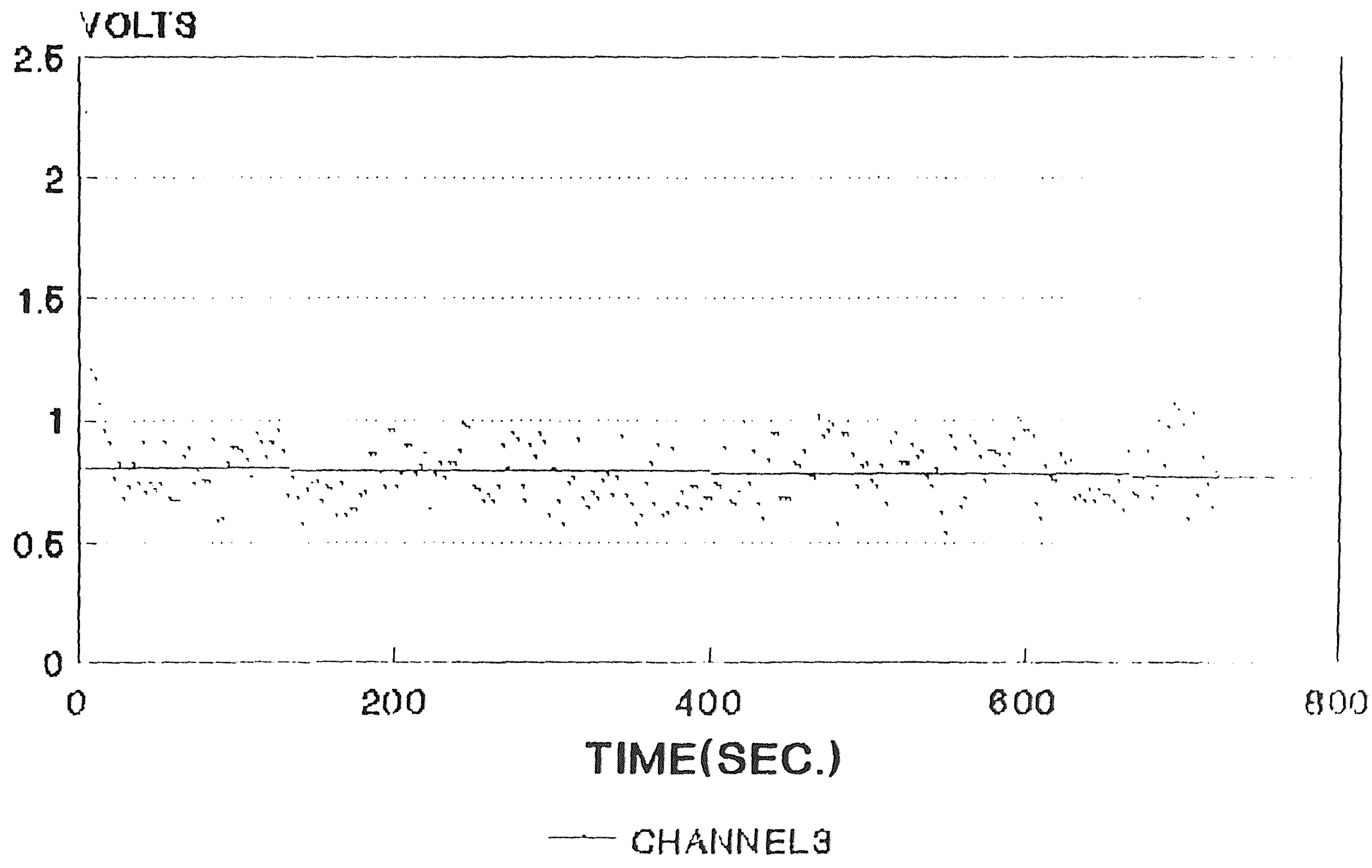

Fig.26 Internal deformation data for J31

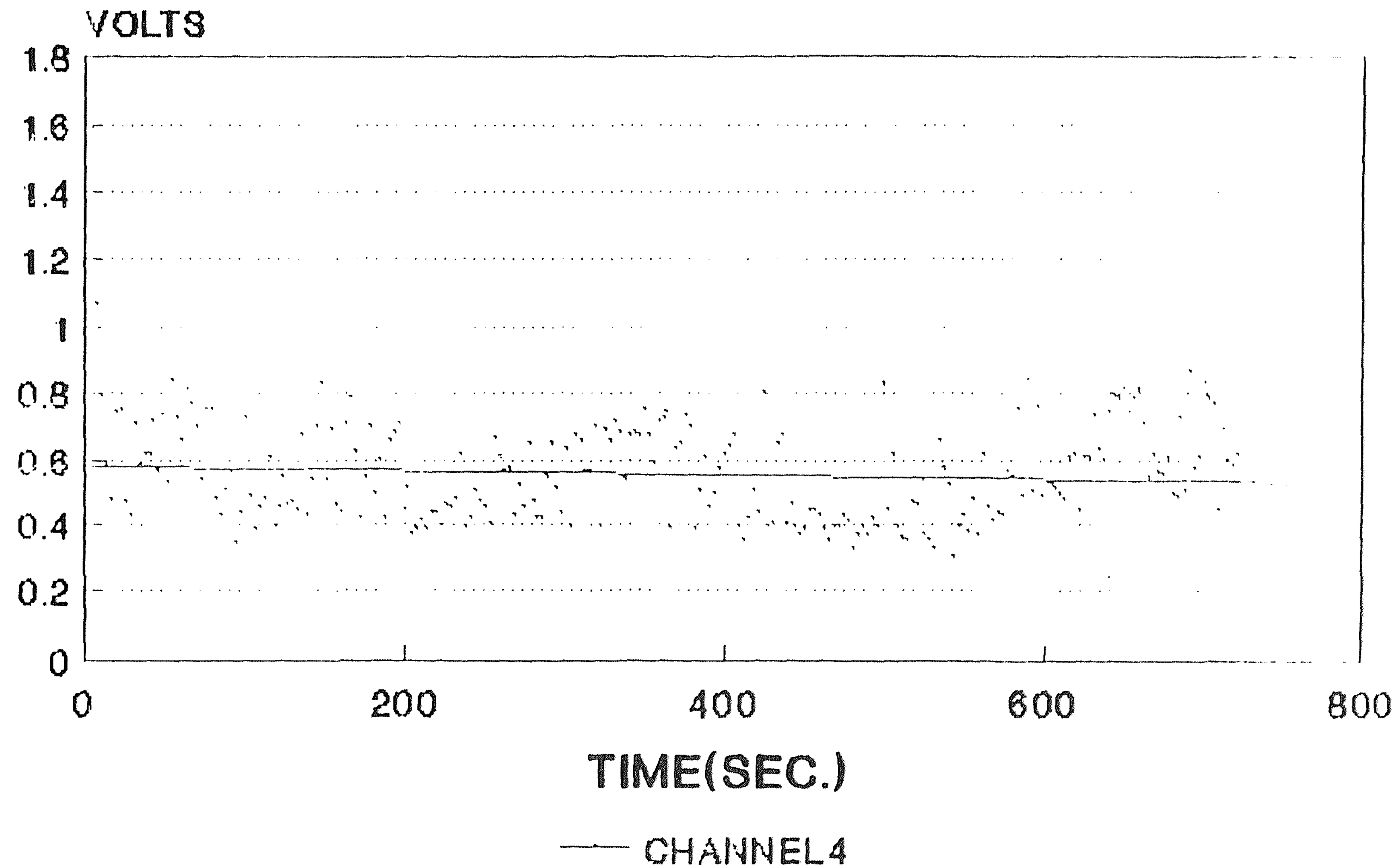

Fig.27 Internal deformation data f J31

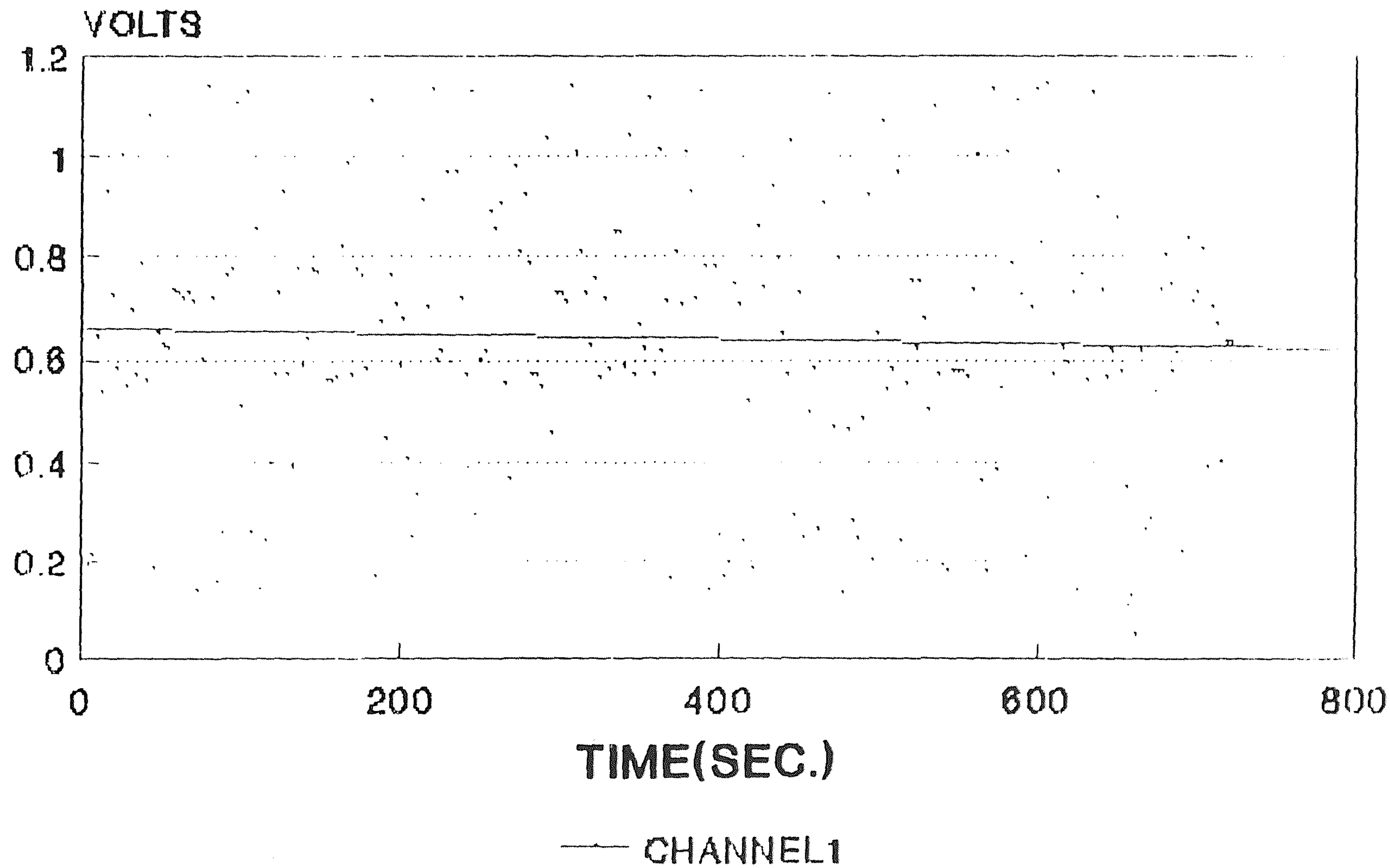

Fig.28 Internal deformation data for F2

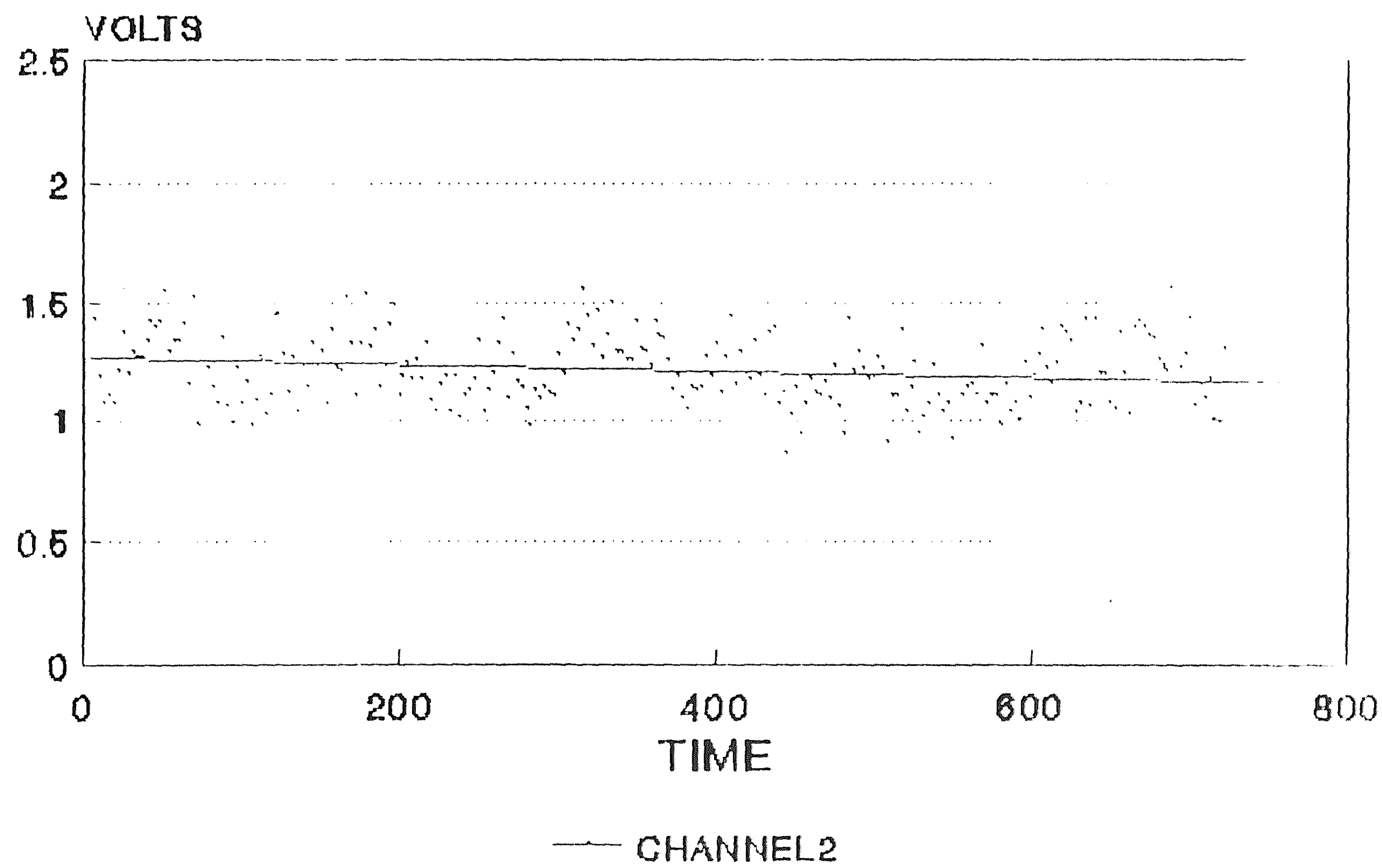

Fig.29 Internal deformation data for F2

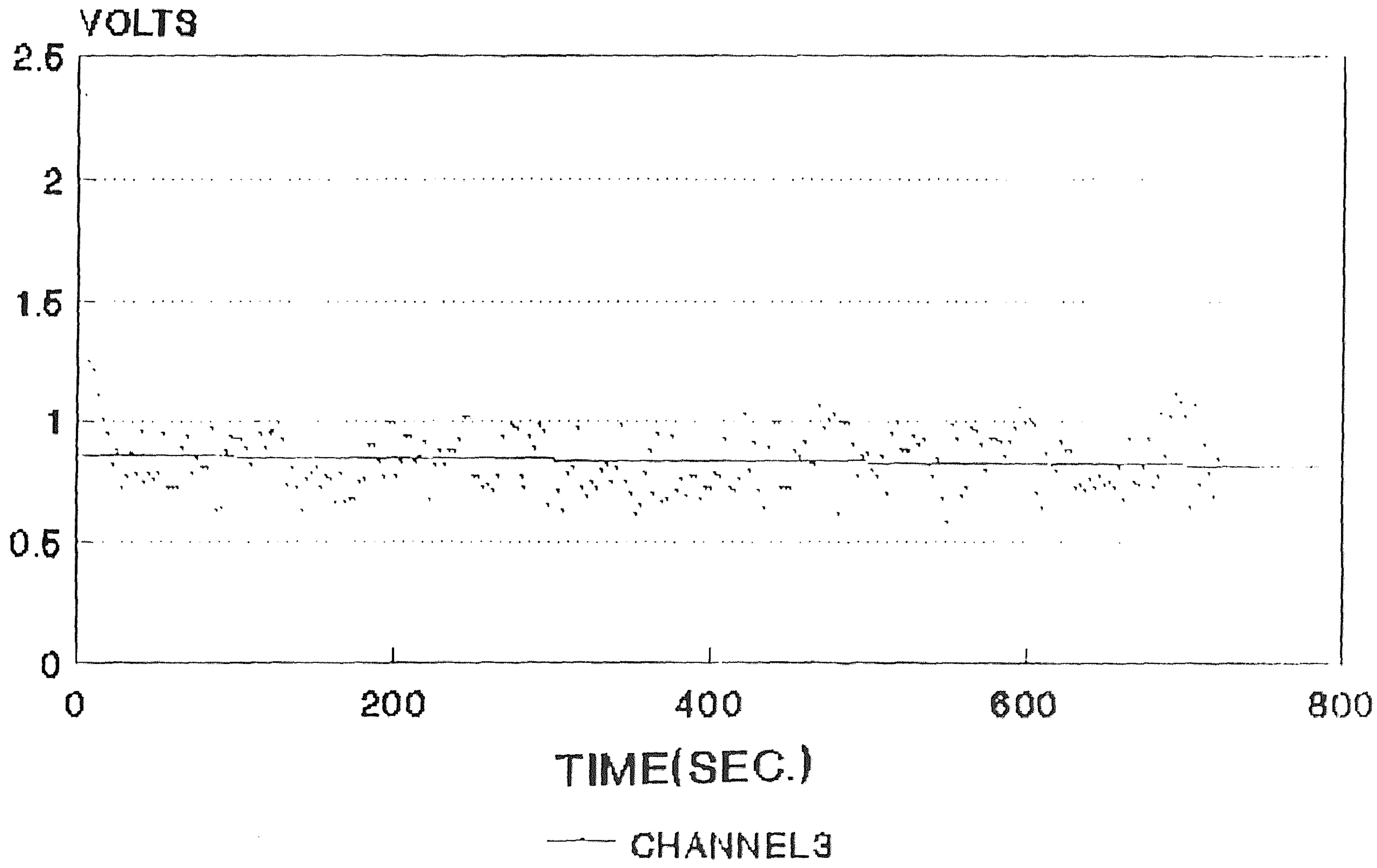

Fig.30 Internal deformation data for F2

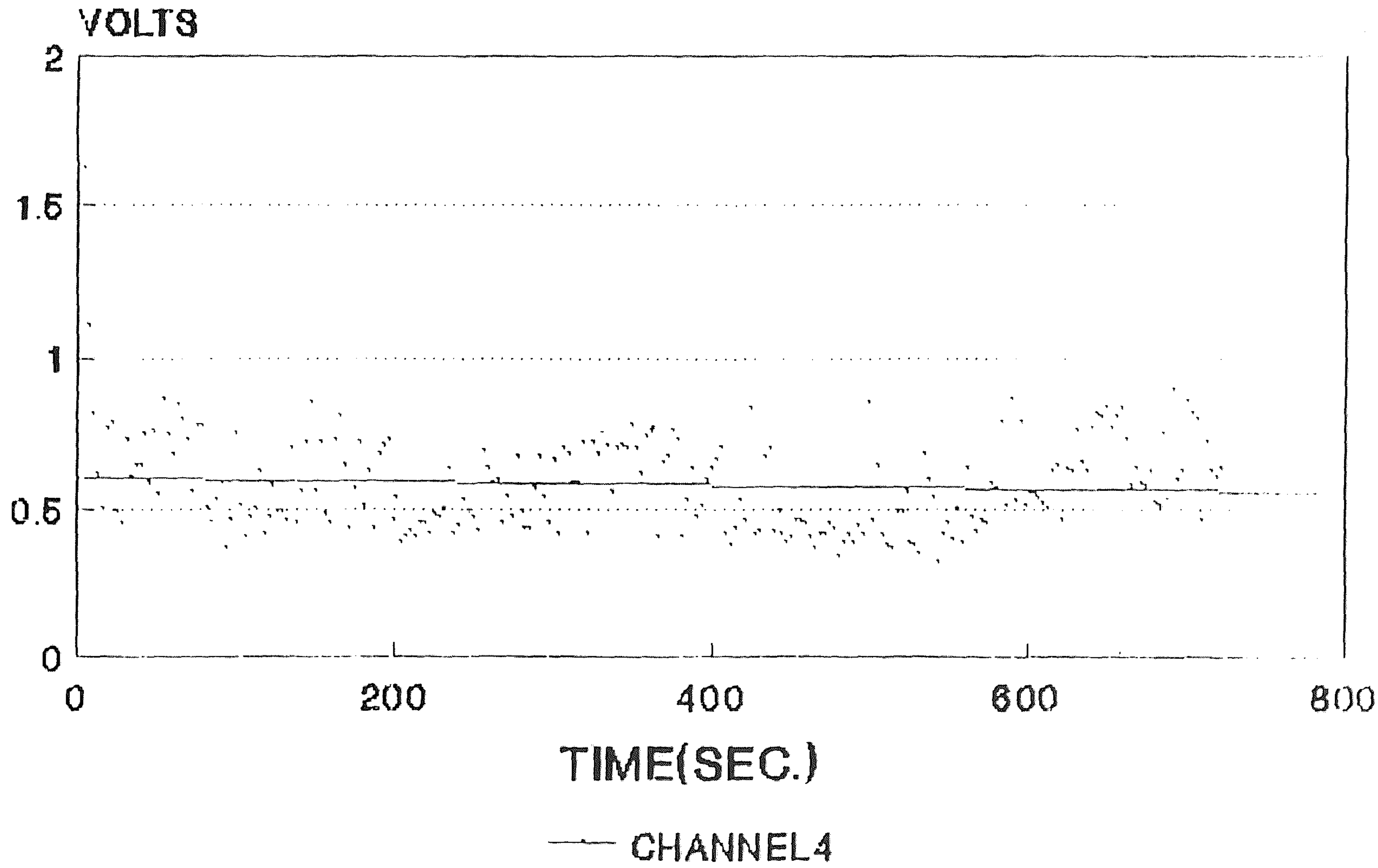

Fig.31 Internal deformation data for F2

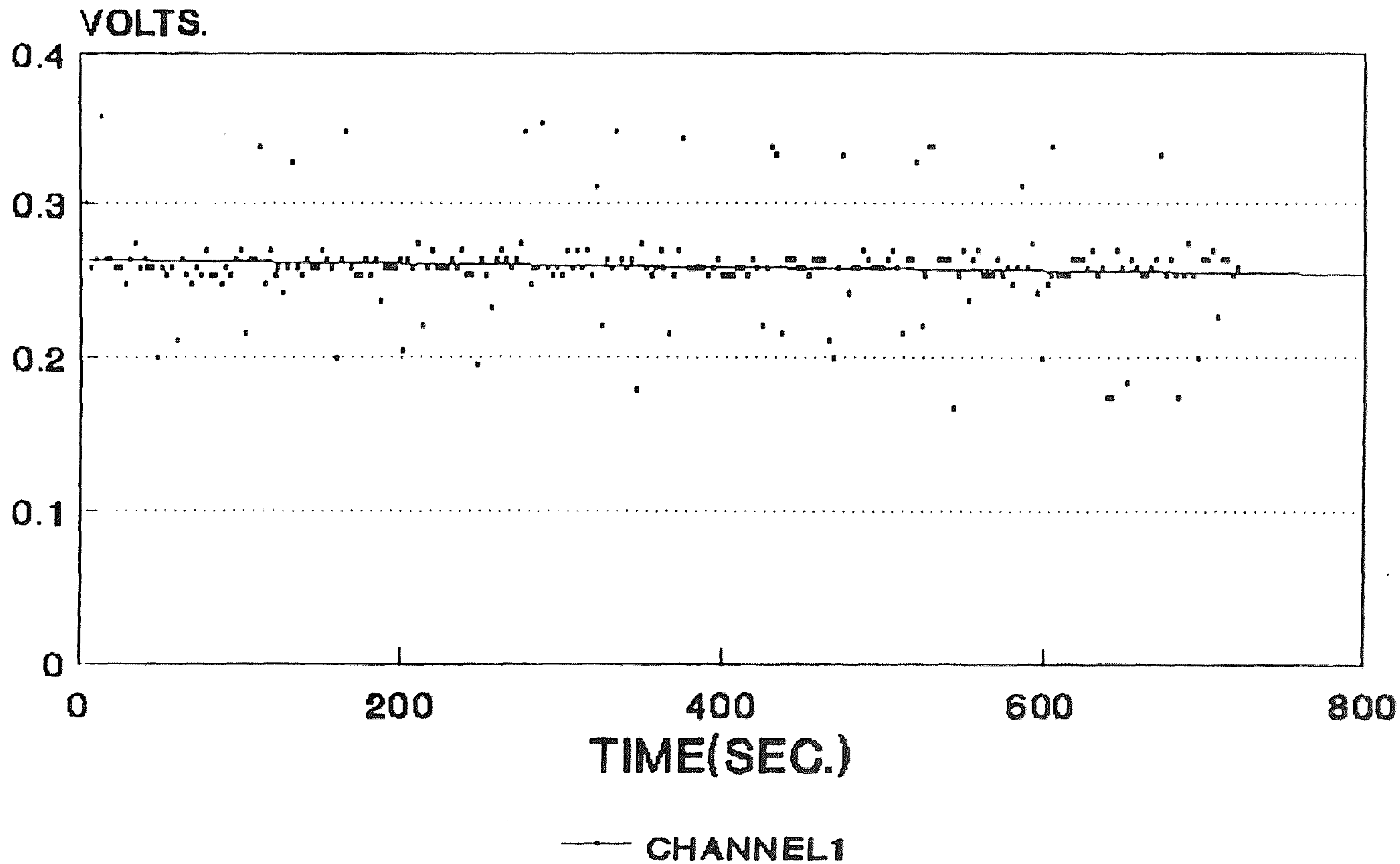

Fig.32 Internal deformation data forF3#2

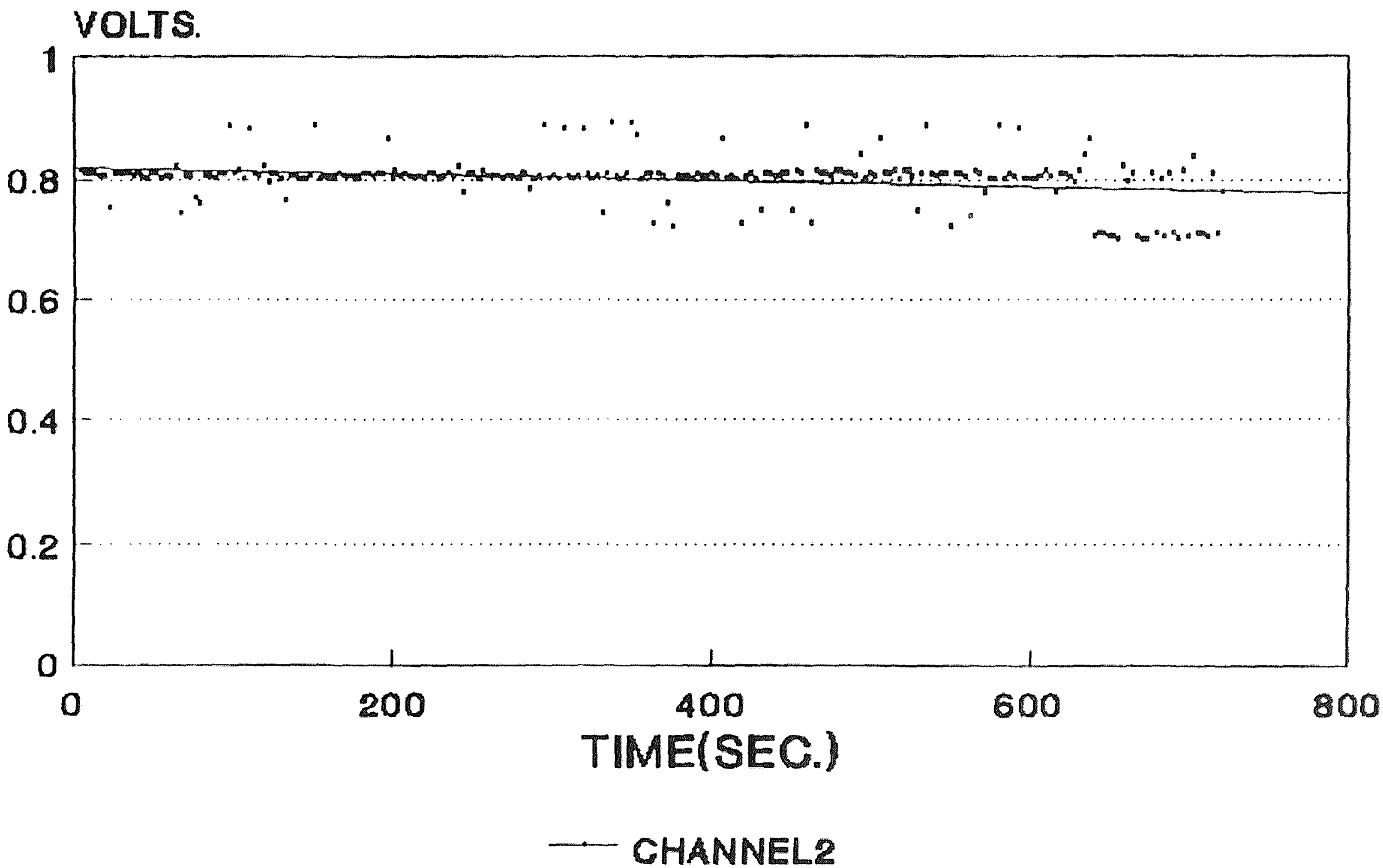

Fig.33 Internal deformation data forF3#2

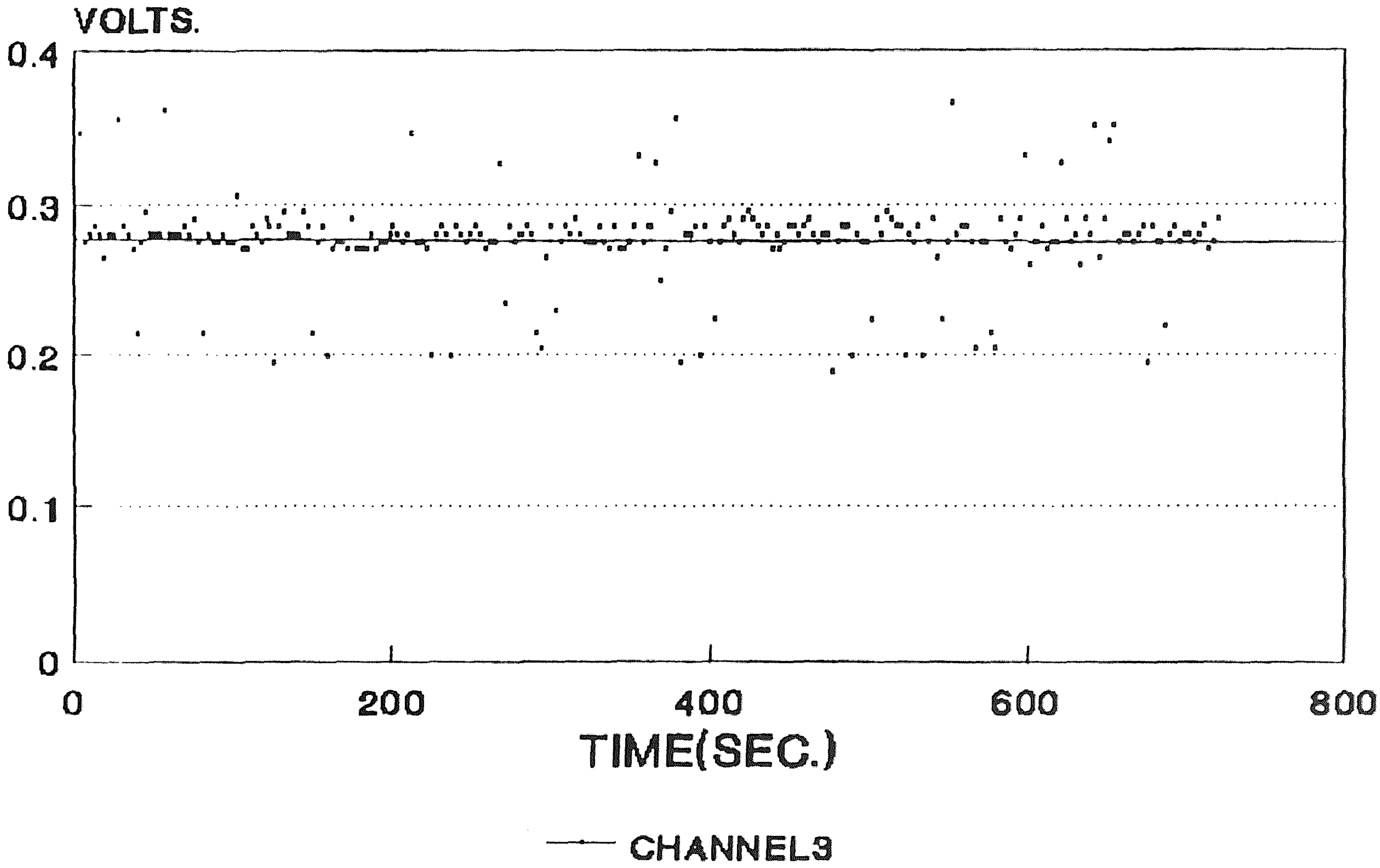

Fig.34 Internal deformation data forF3#2

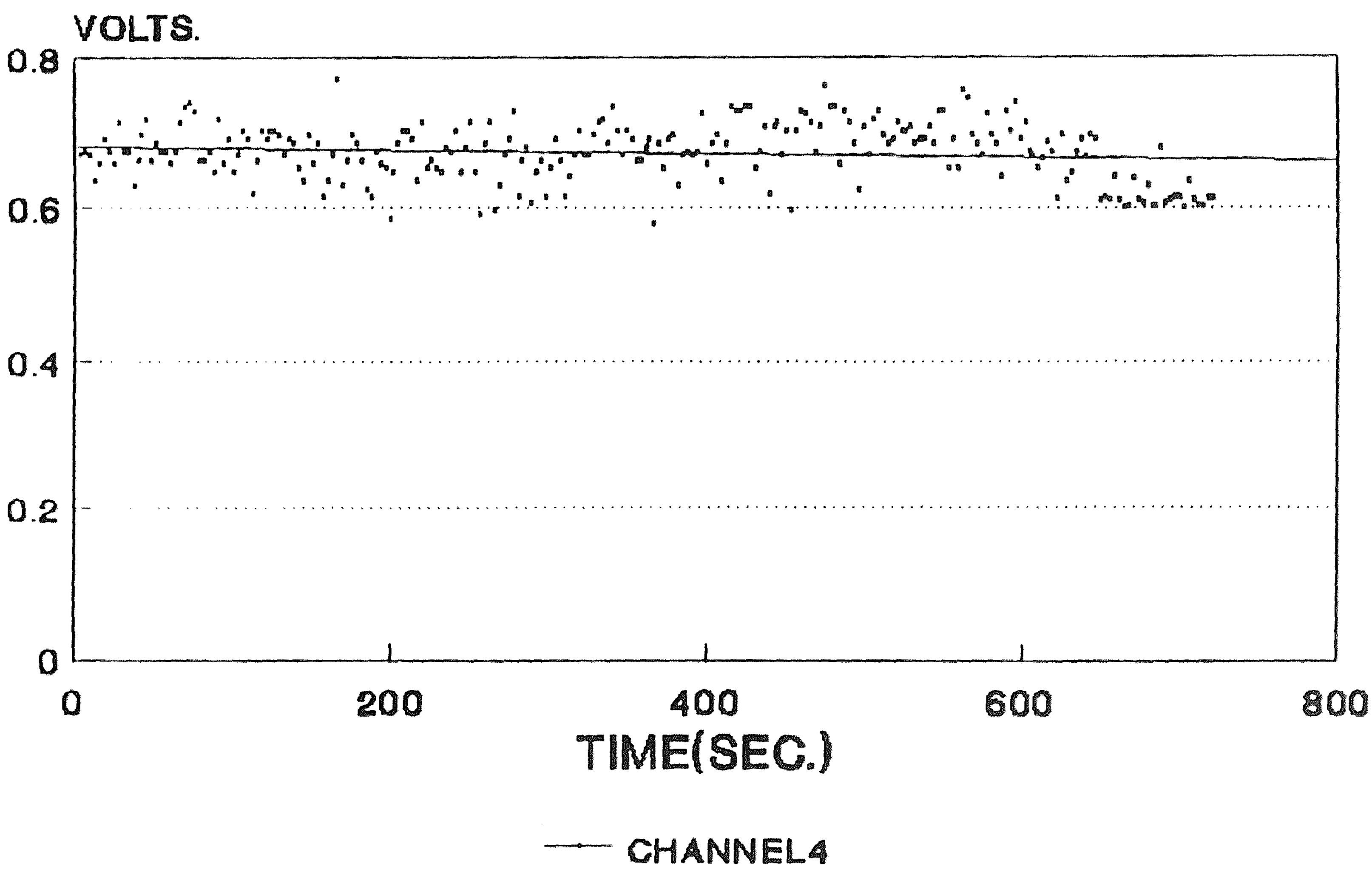

lg.35 Internal deformation data forF3#2

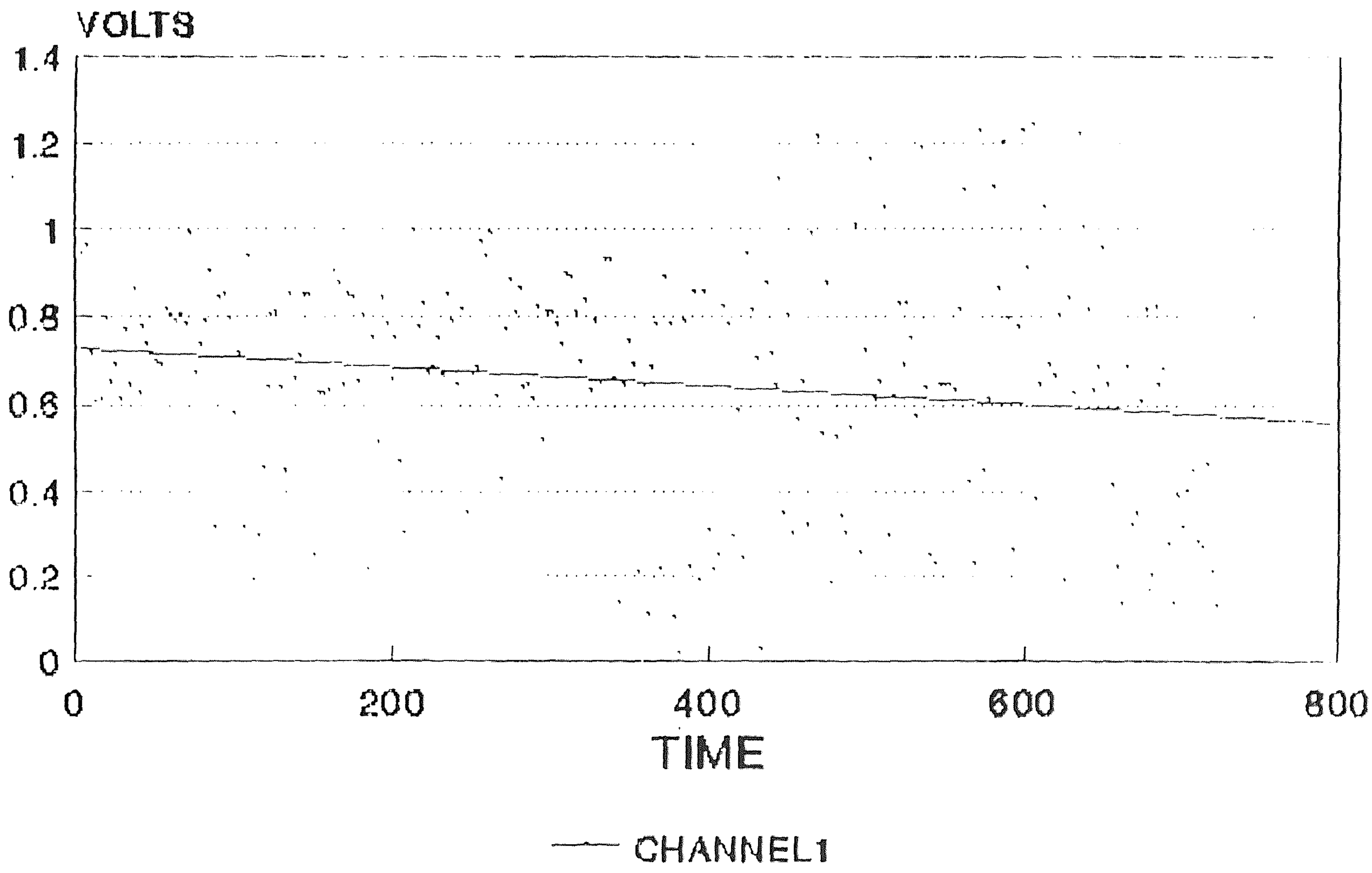

Fig.36 Internal deformation data for F8

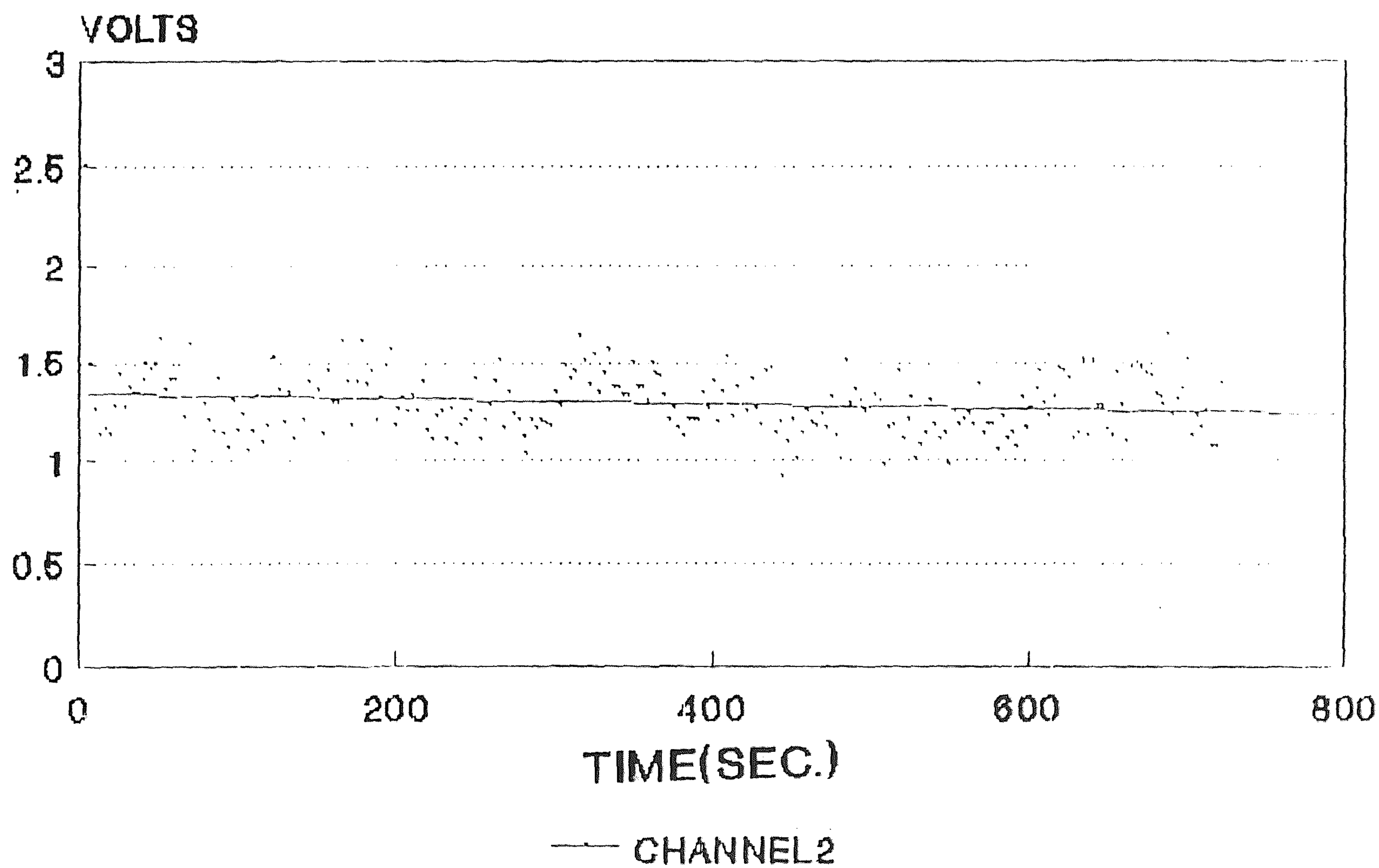

Fig.37 Internal deformation data for F8

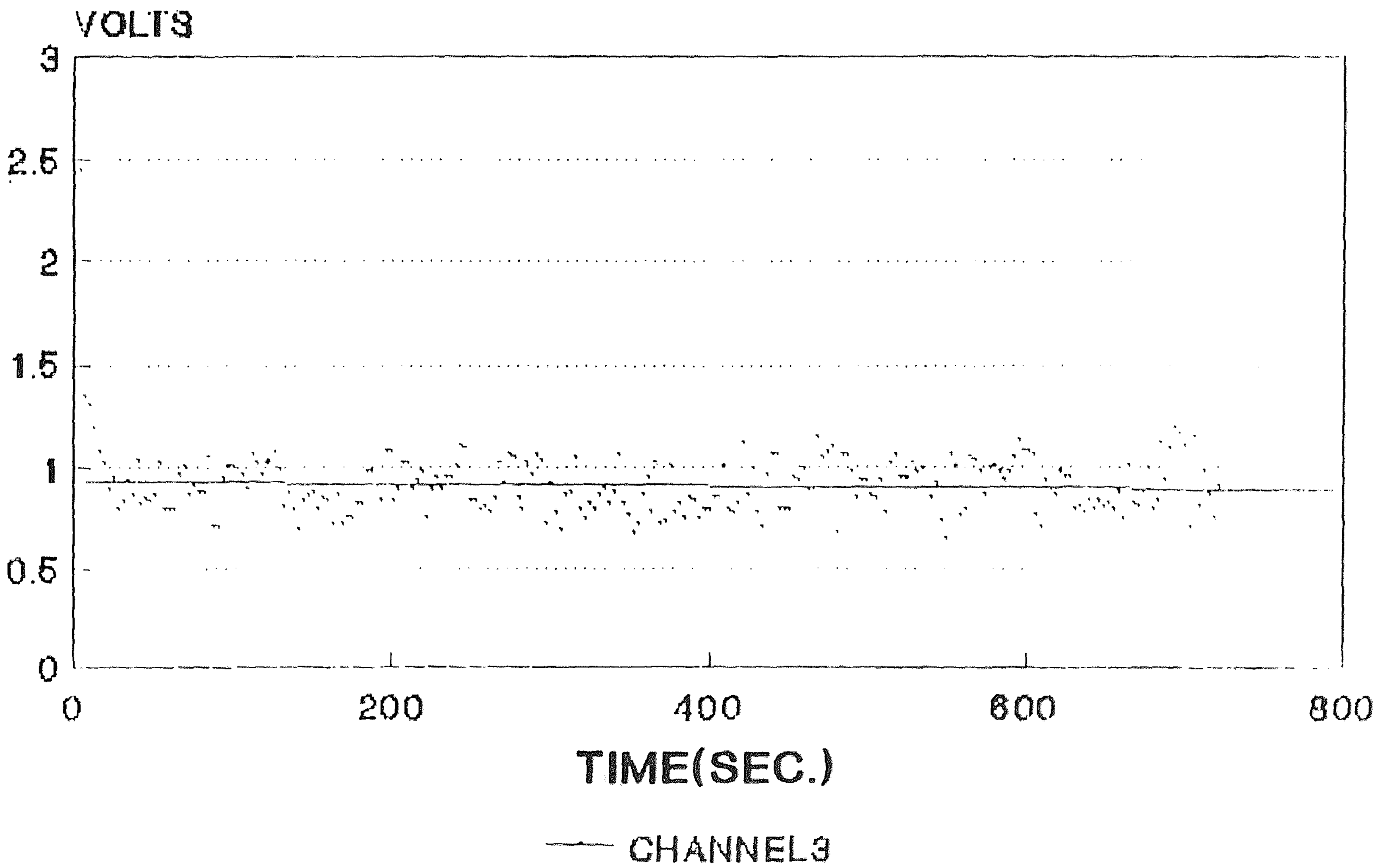

Fig.38 Internal deformation data for F8

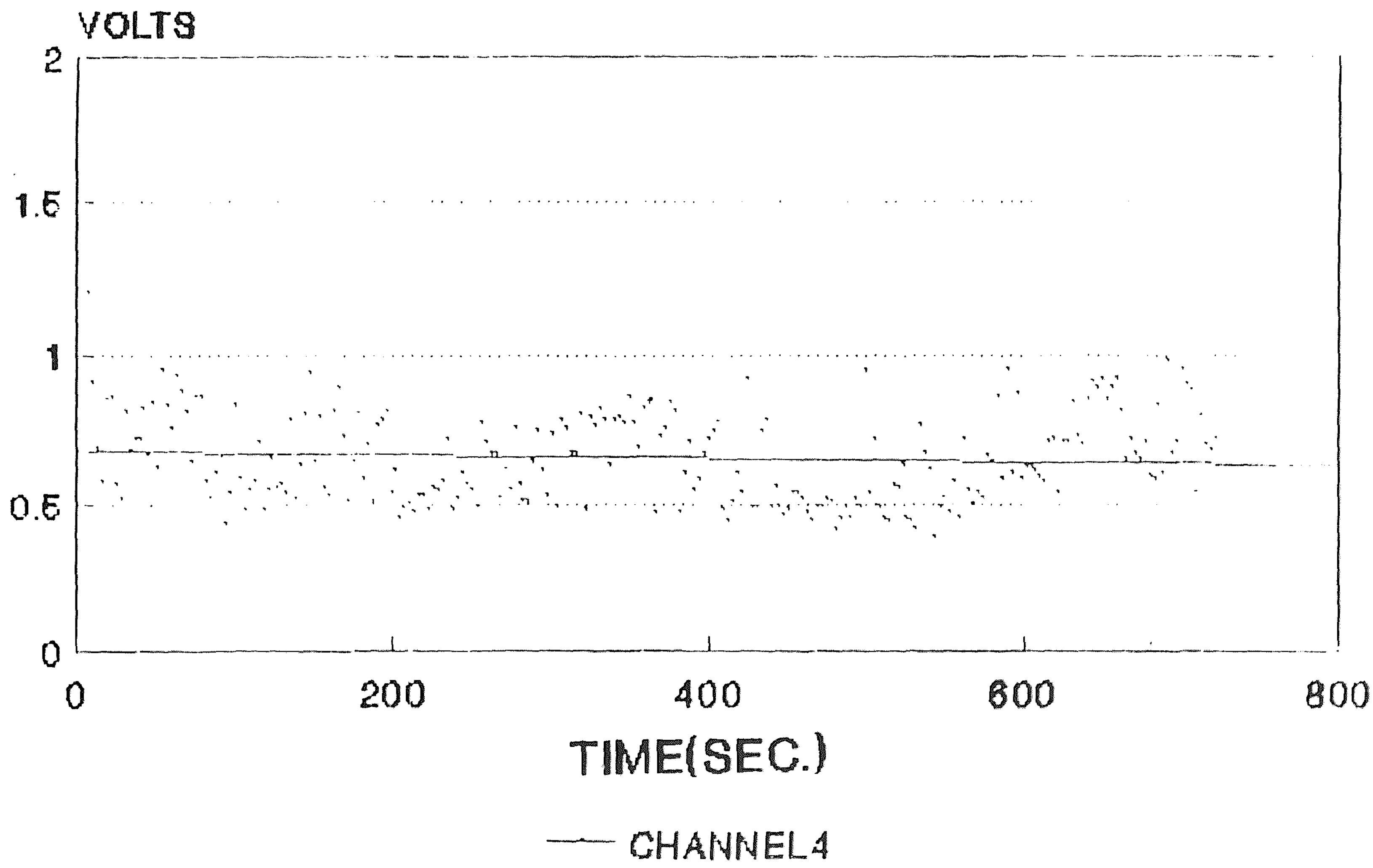

Fig.39 Internal deformation data for F8

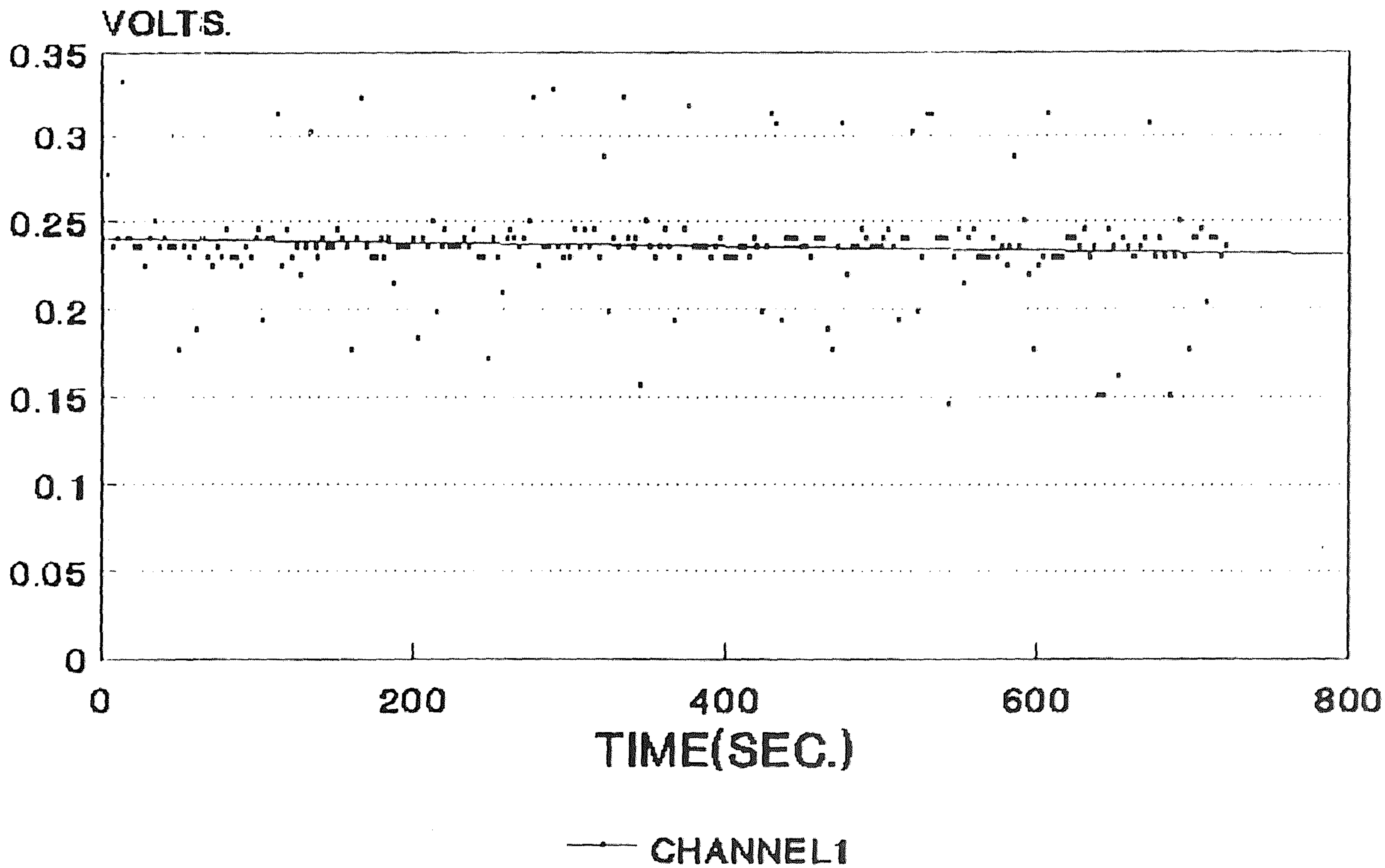

Fig.40 Internal deformation data for F10

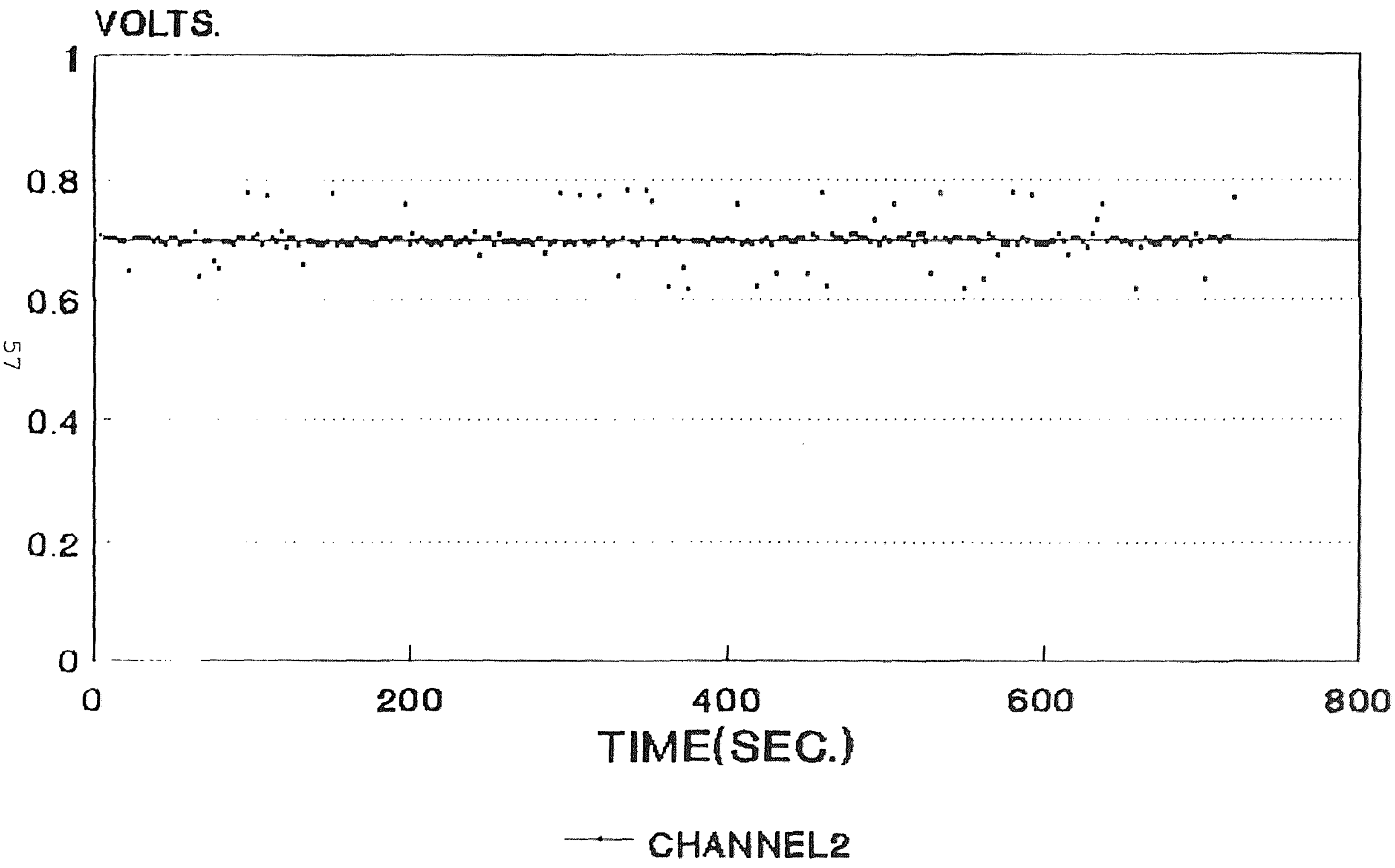

g.41 Internal deformation data for F10

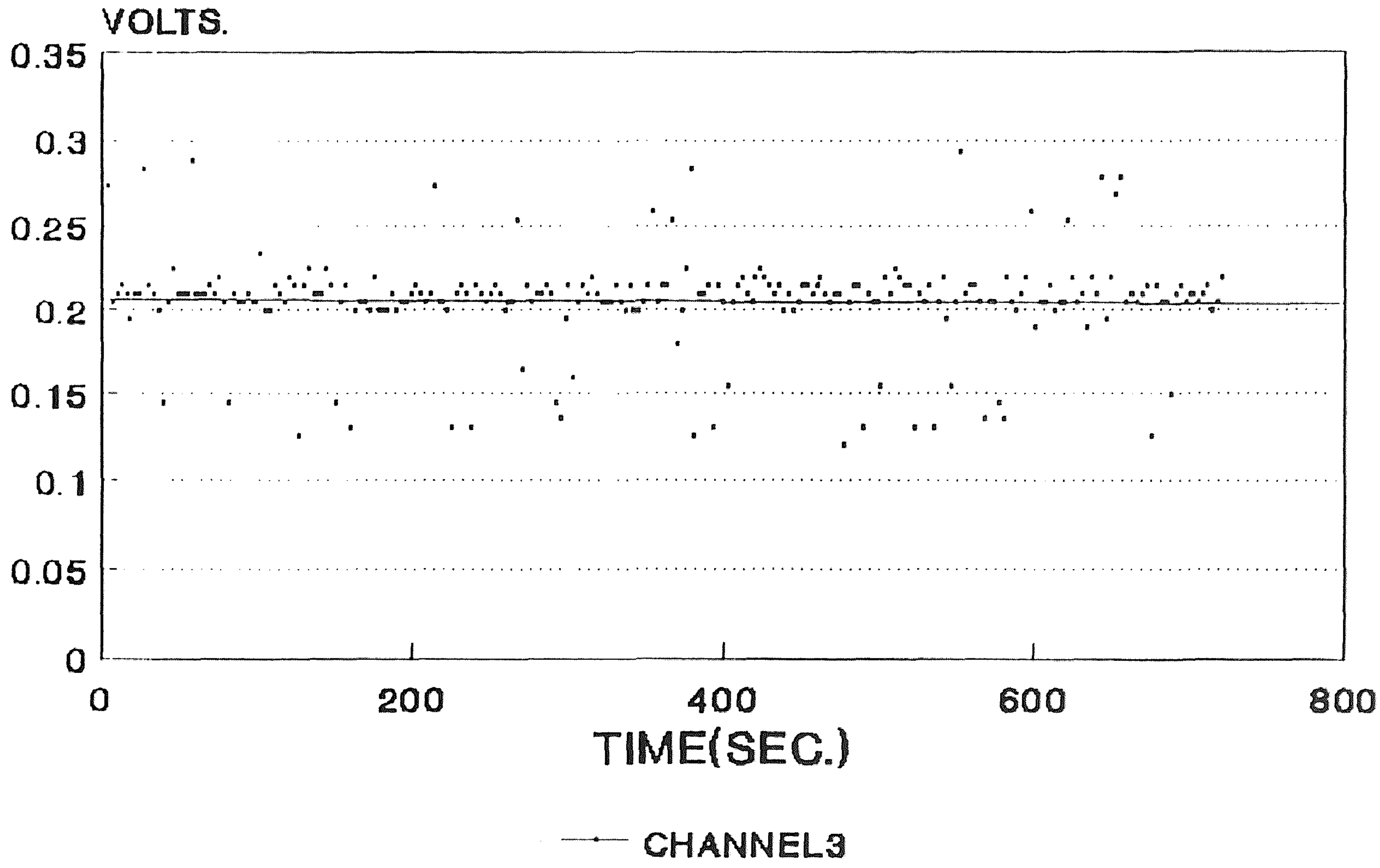

Fig.42 Internal deformation data for F10

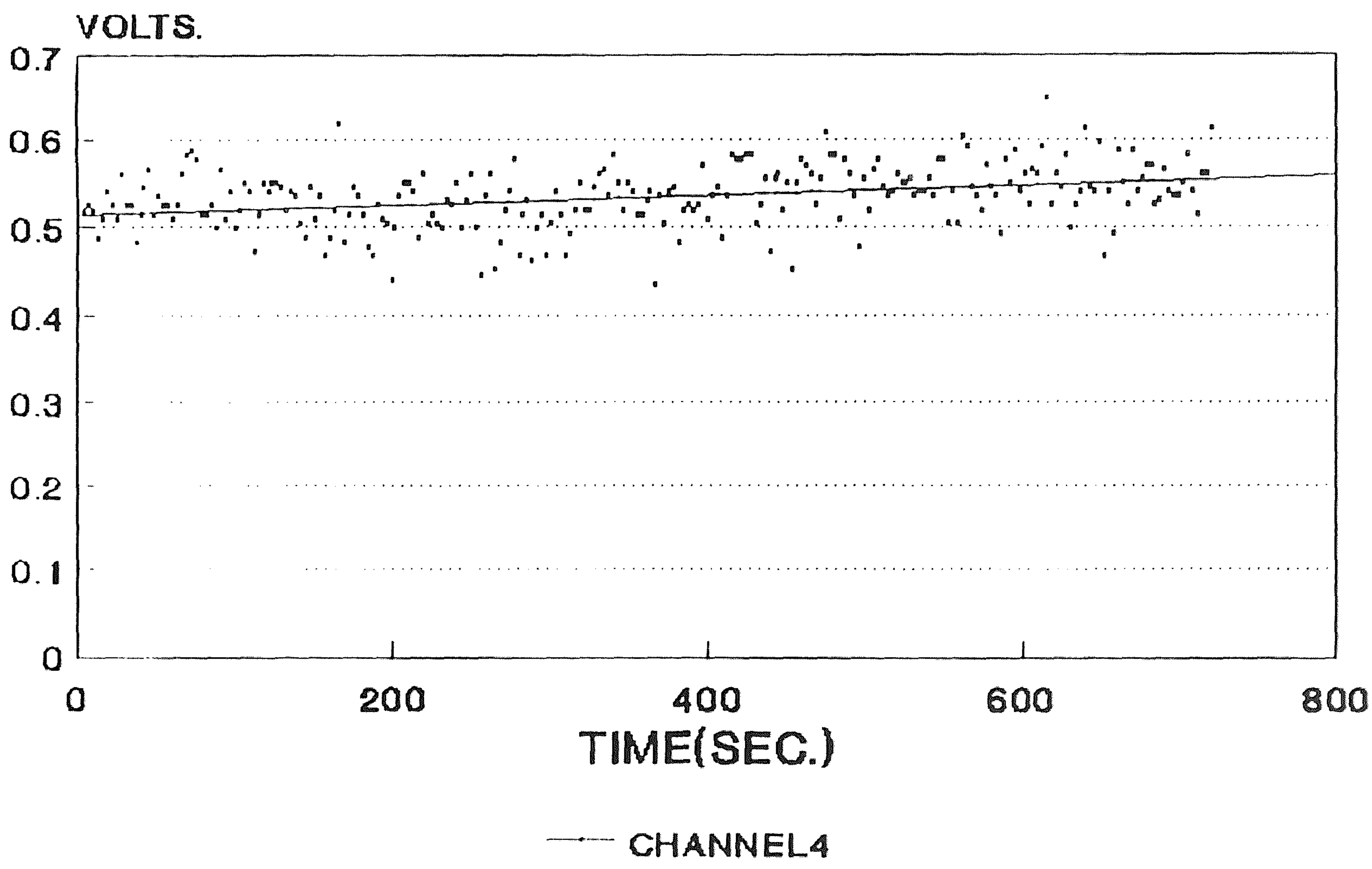

Ig.43 internal deformation data for F10

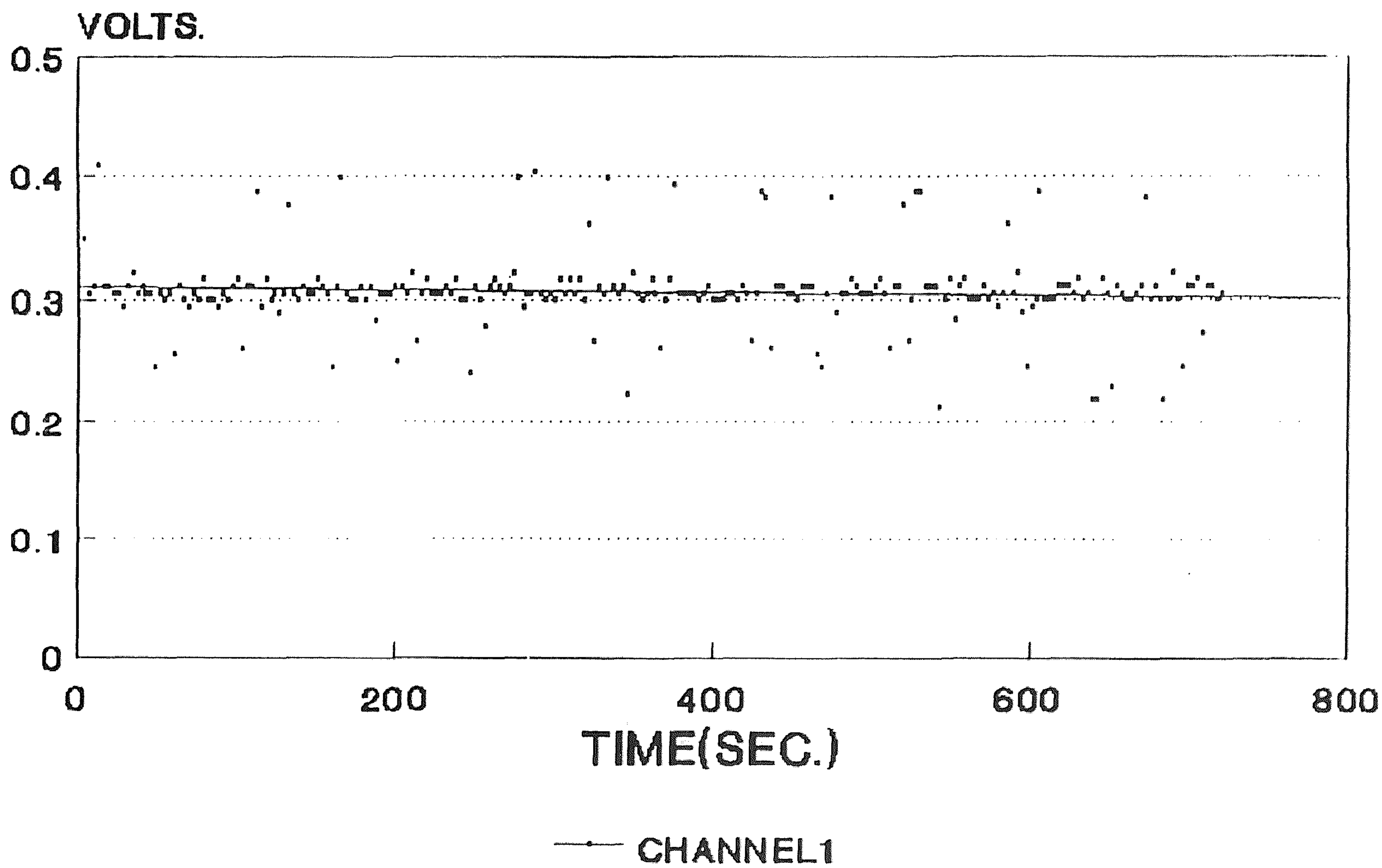

Fig.44 Internal deformation data for F11

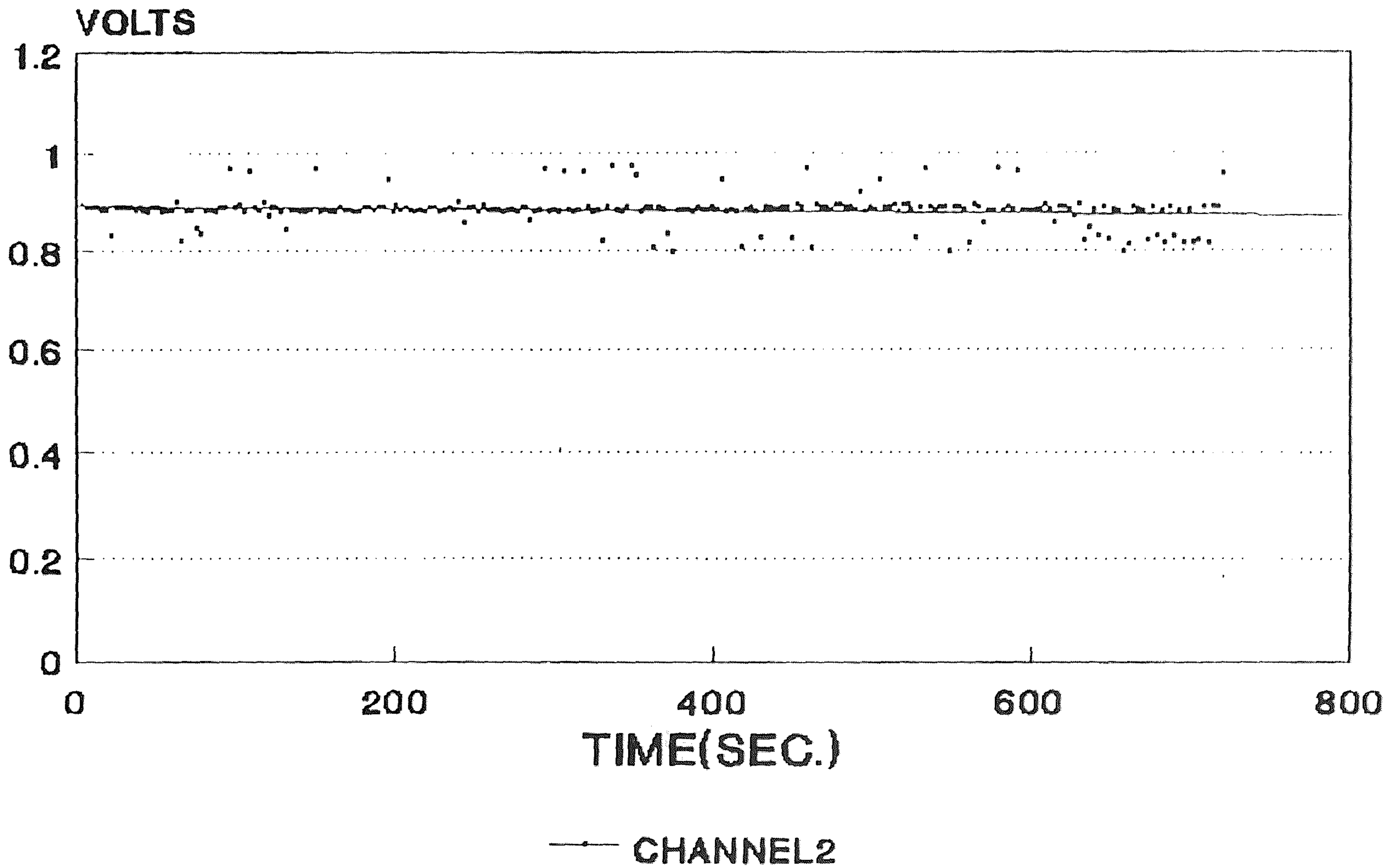

Fig.45 Internal deformation data for F1.

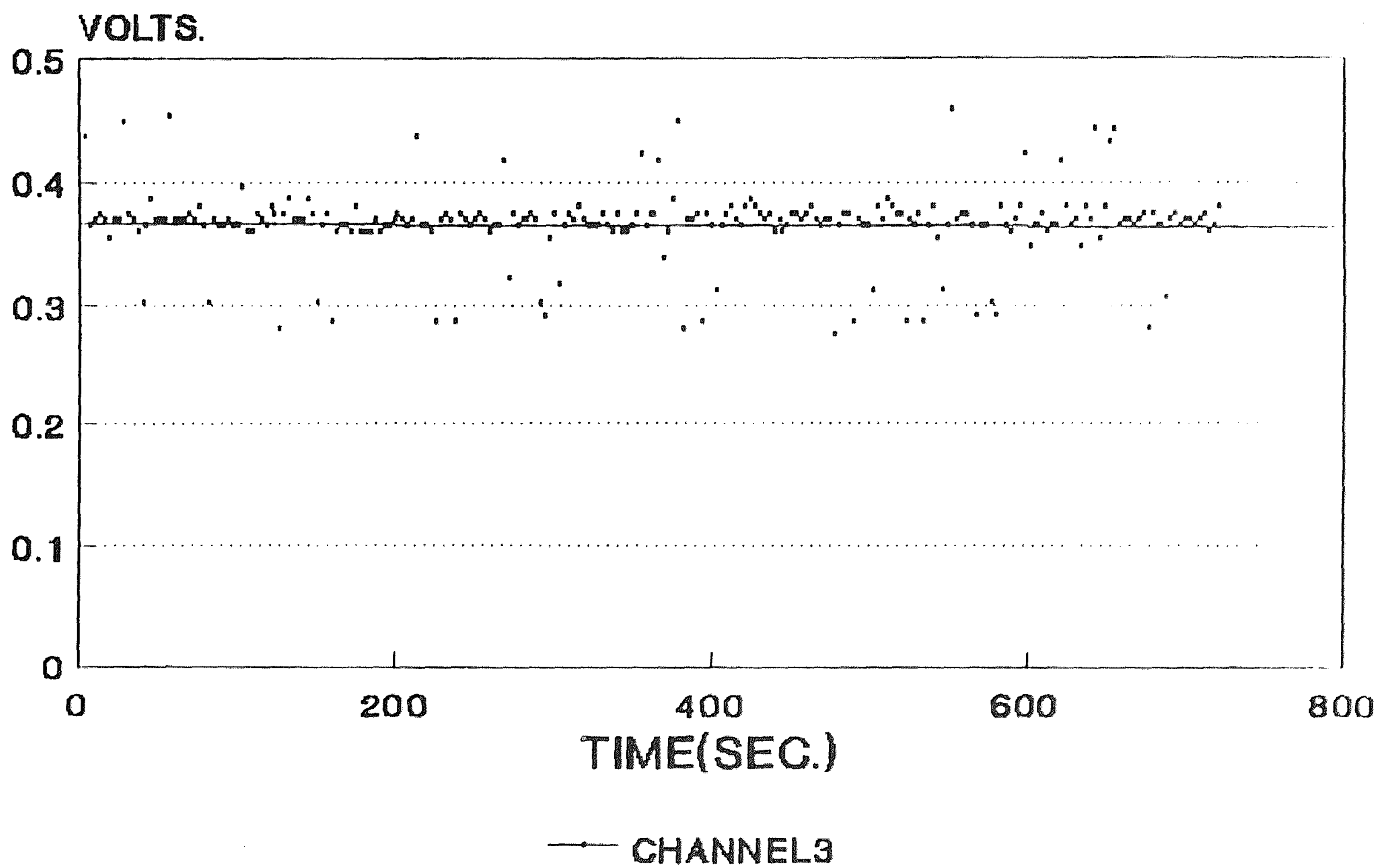

Fig.46 Internal deformation data for F11

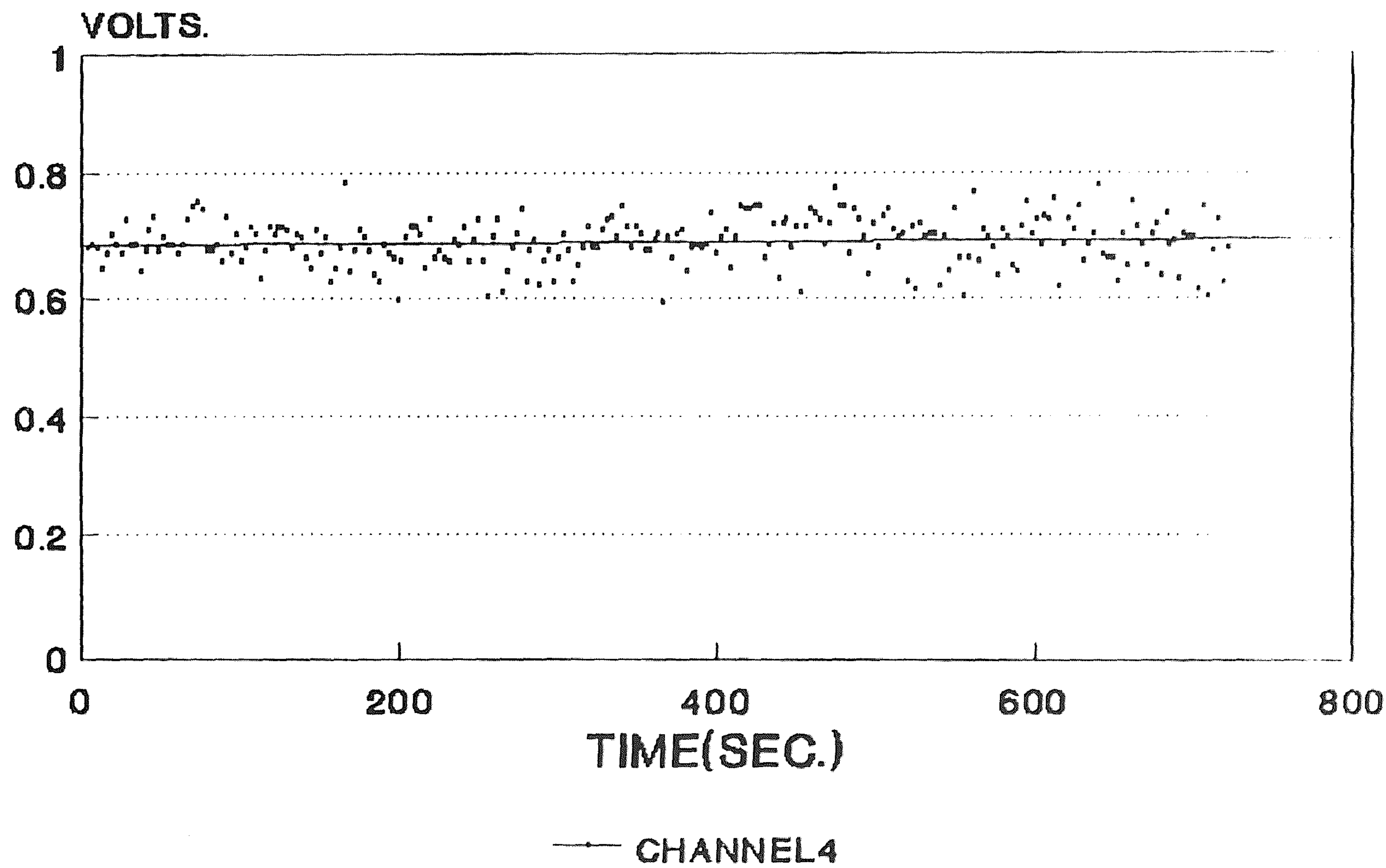

Fig.47 Internal deformation data for F11

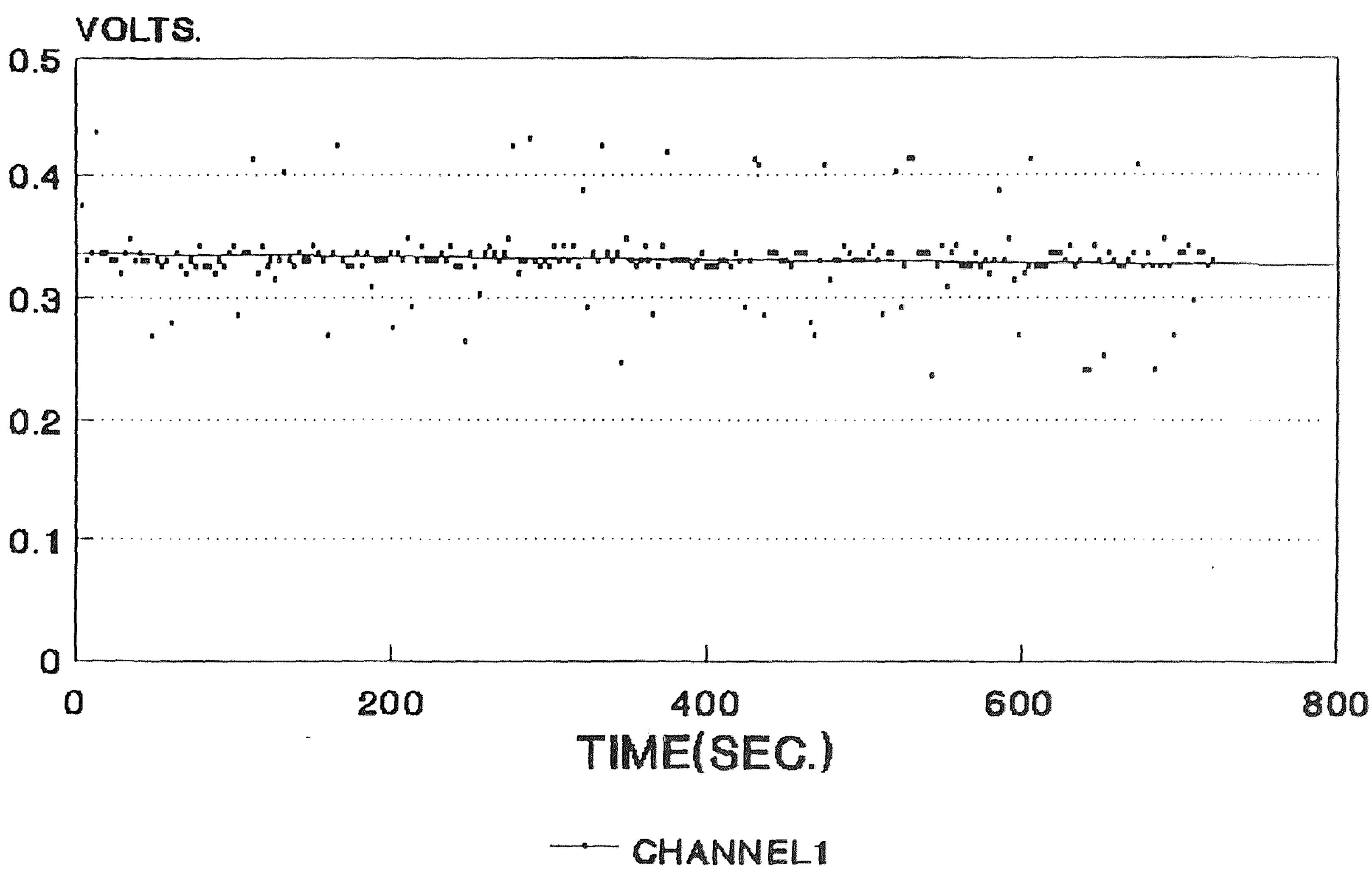

Fig.48 Internal deformation data for F12

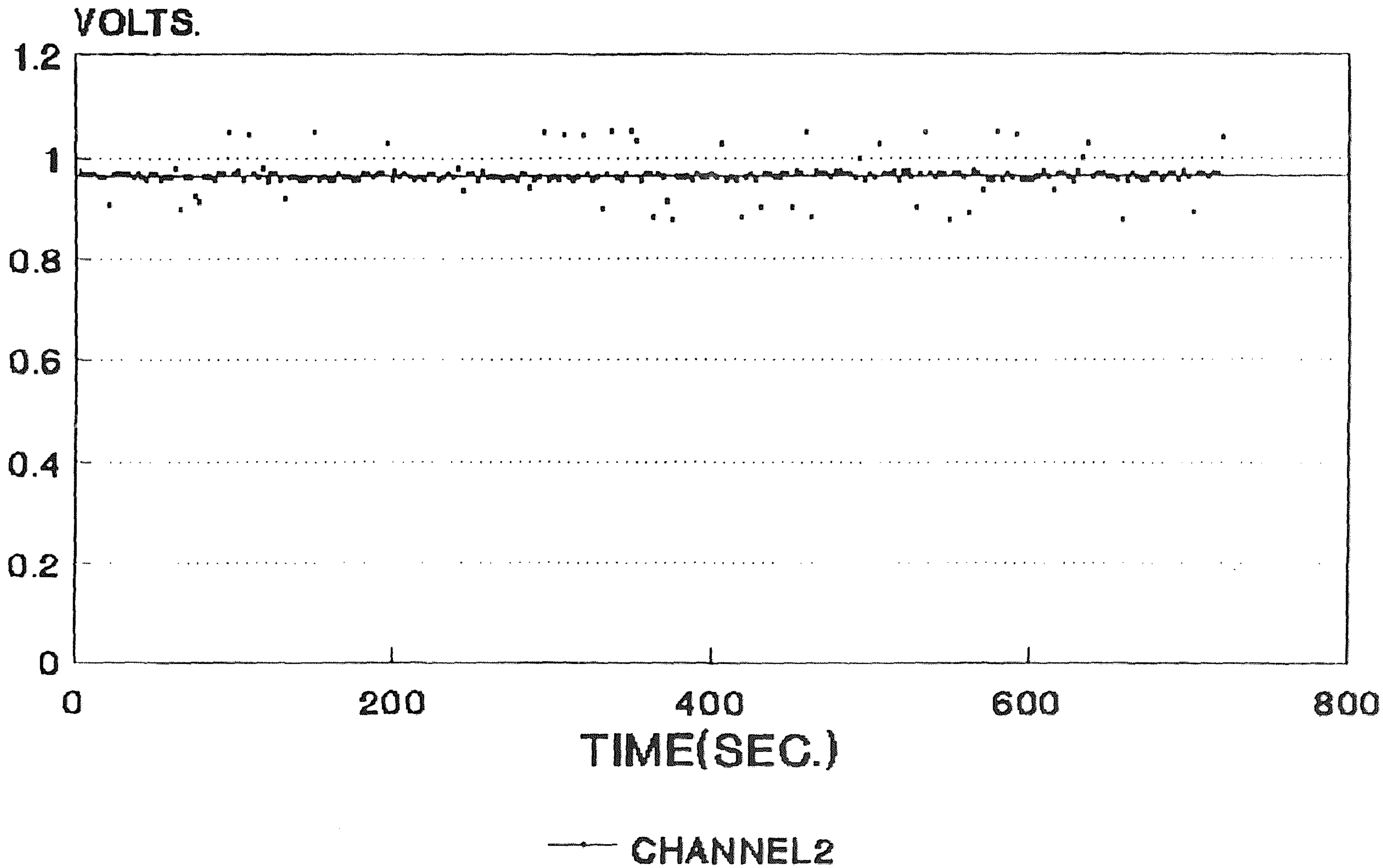

Fig.49 Internal deformation data for F12

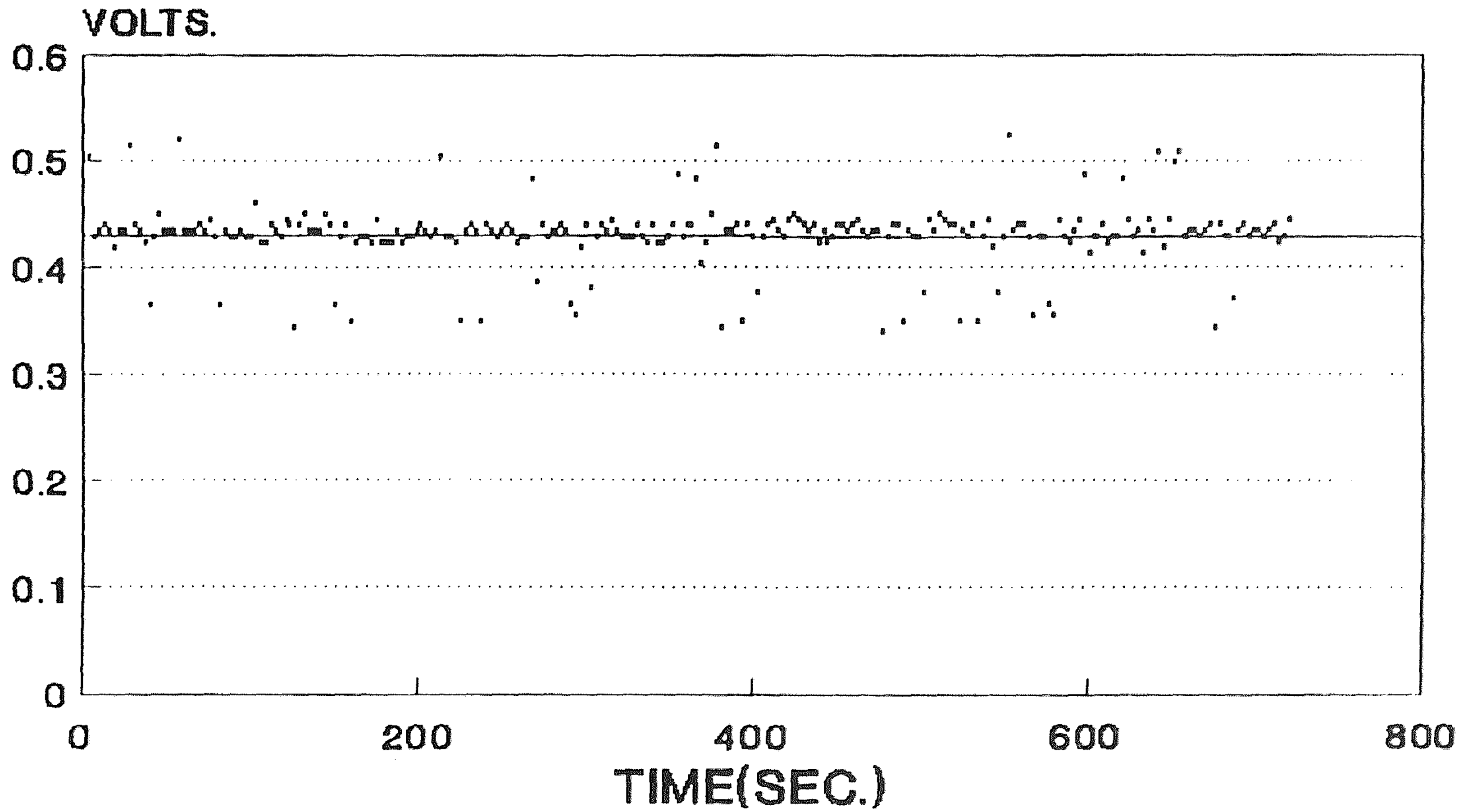

Fig.50 Internal deformation data for F12

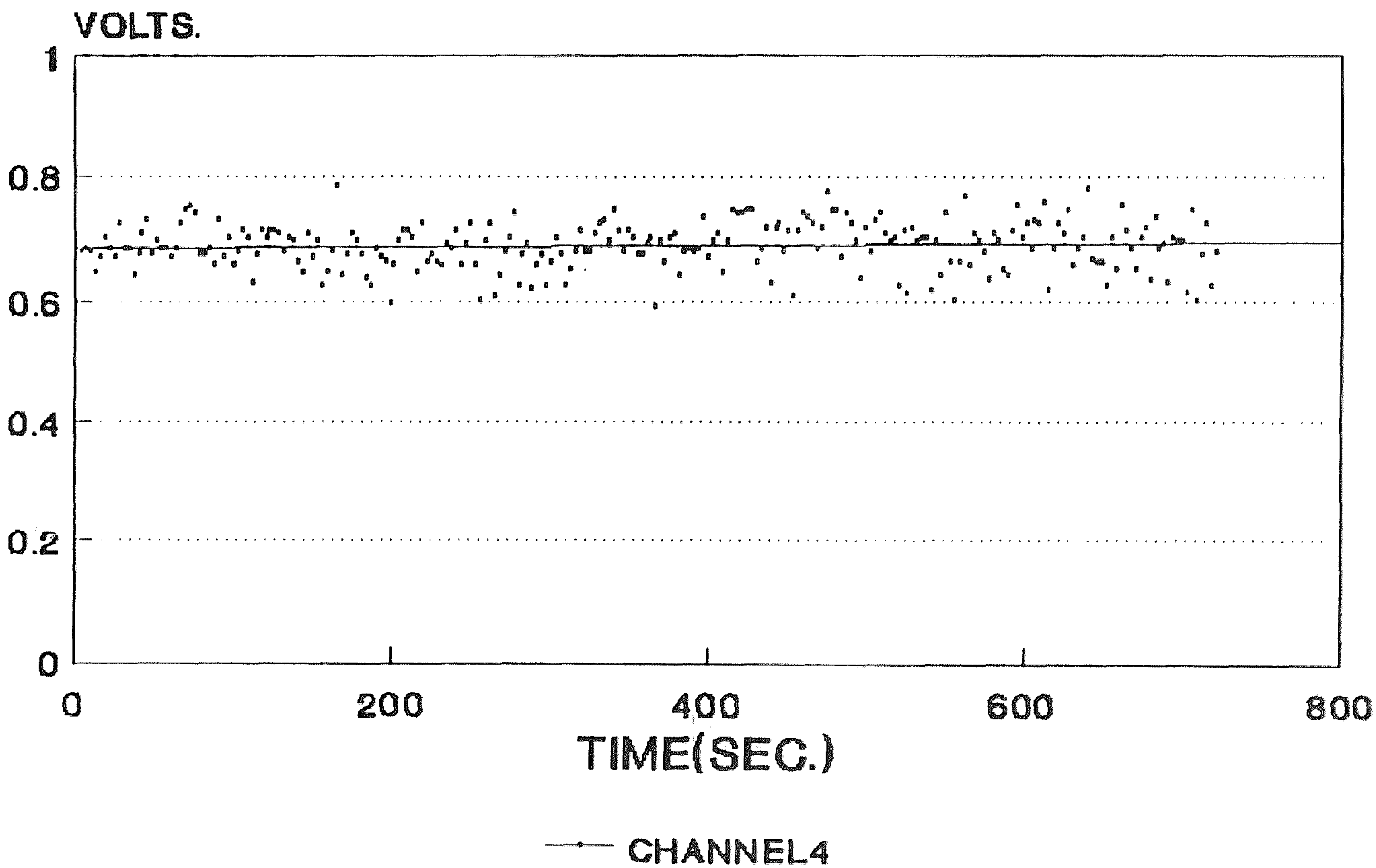

Fig.51 Internal deformation data for F12

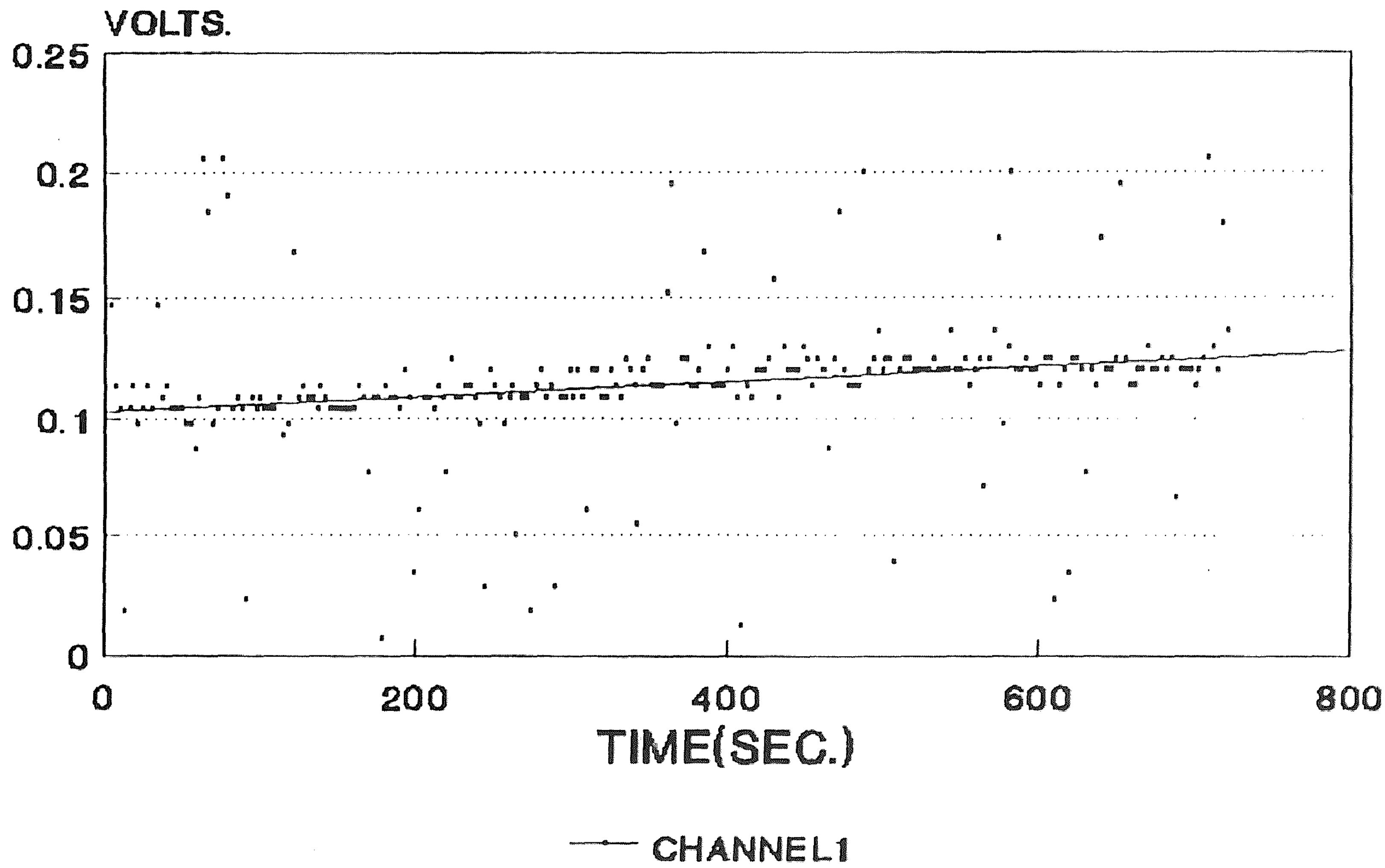

Fig.52 Internal deformation data forF19A

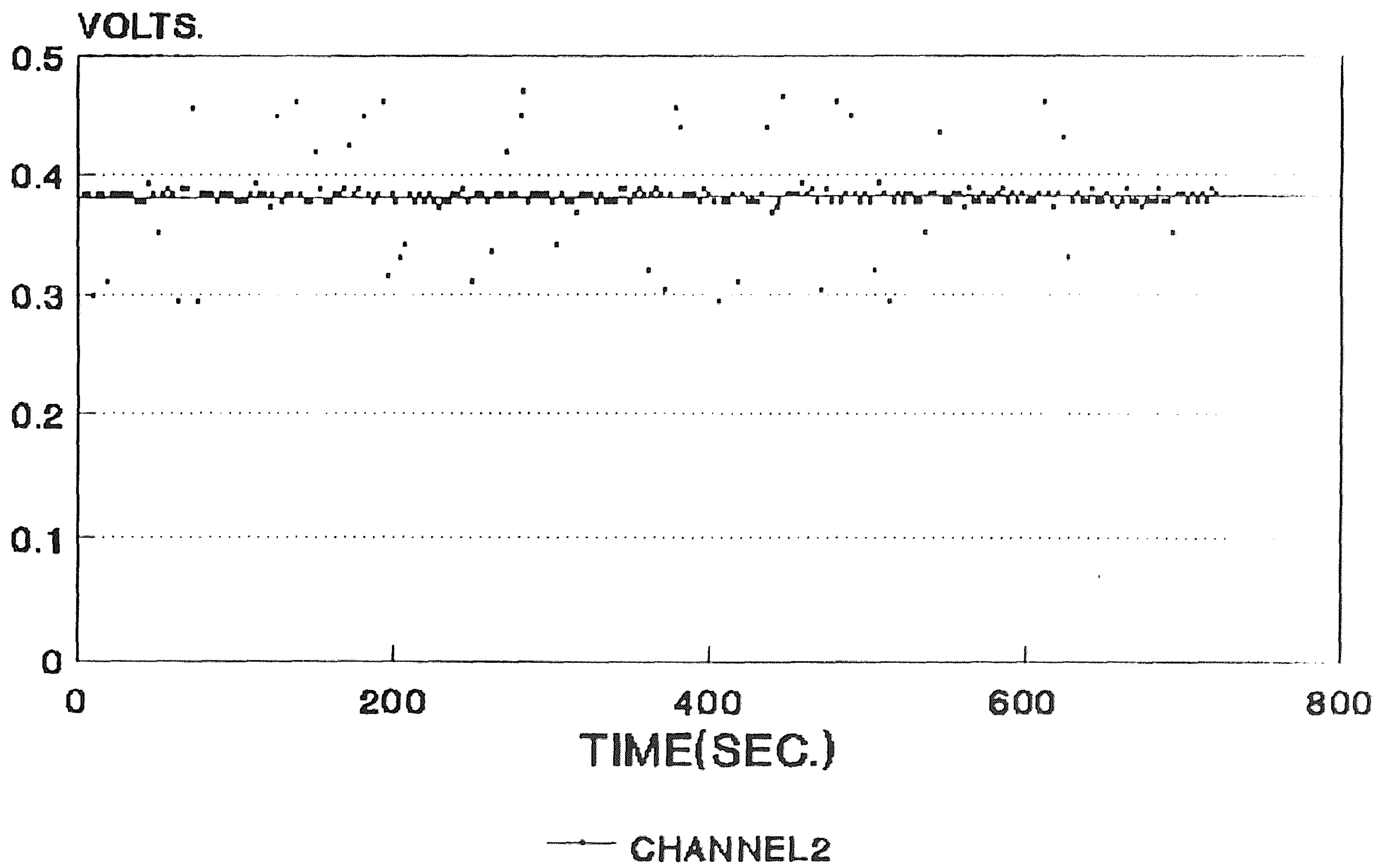

Fig.53 Internal deformation data forF19A

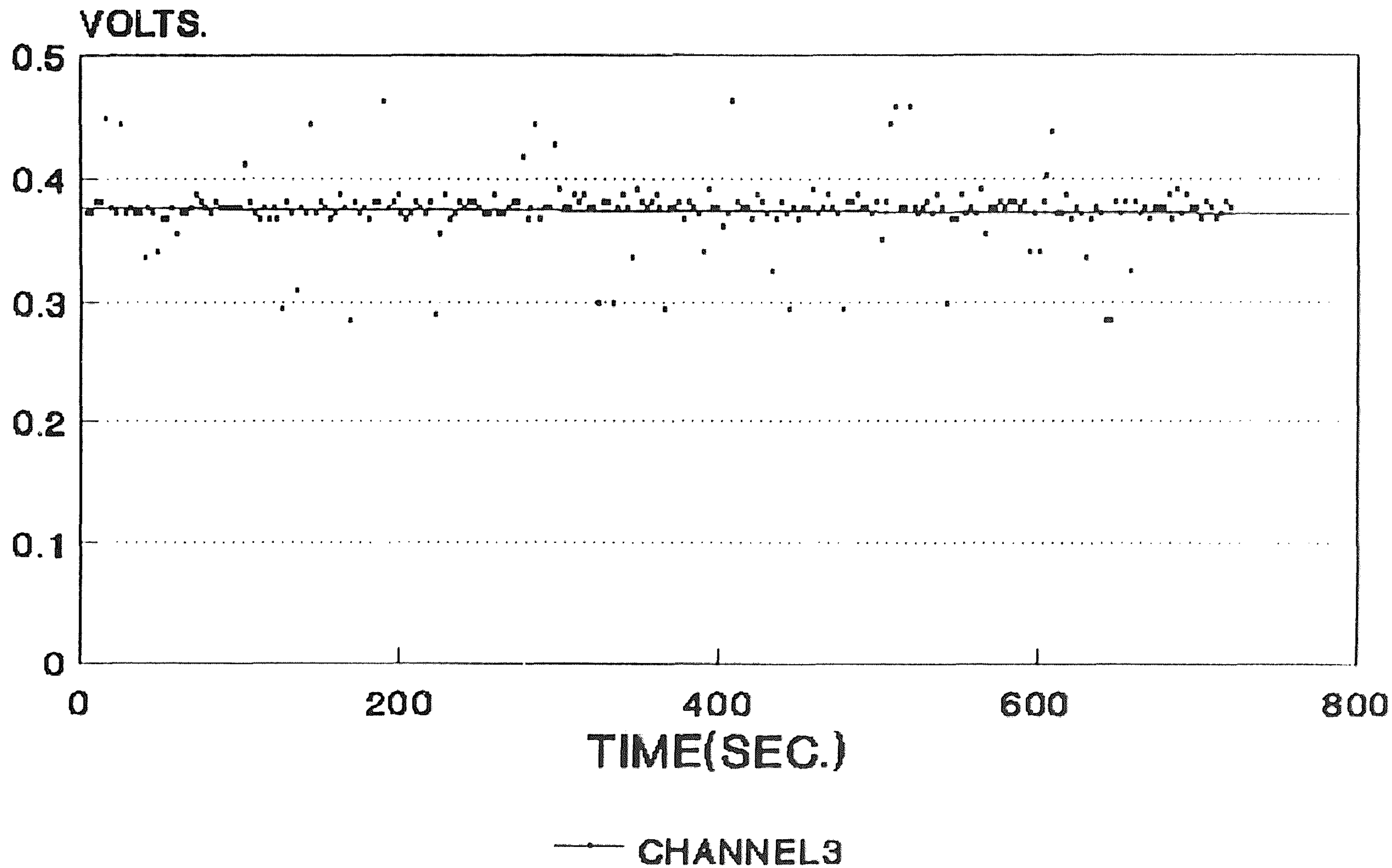

Fig.54 Internal deformation data forF

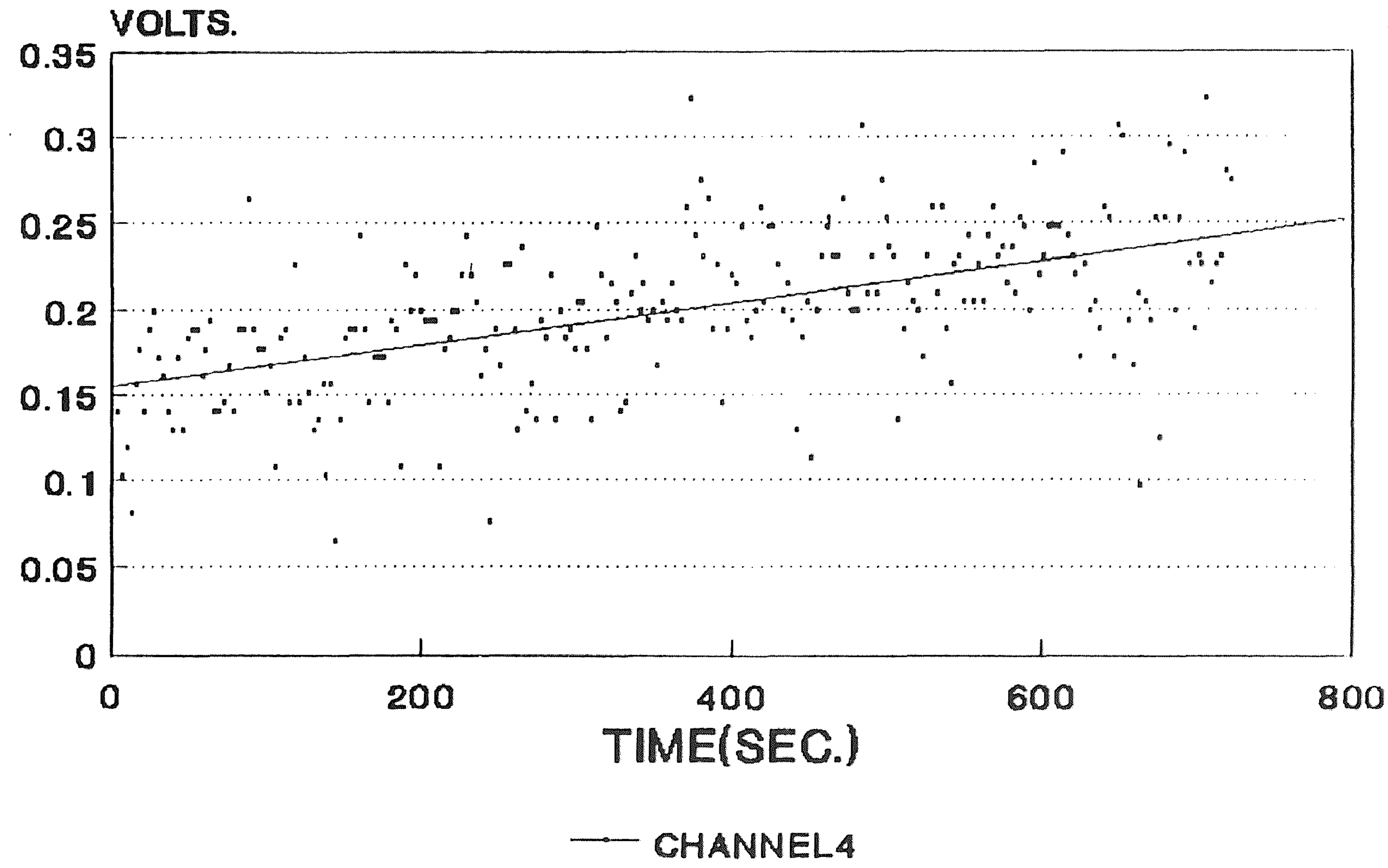

Fig.55 Internal deformation data forF19A

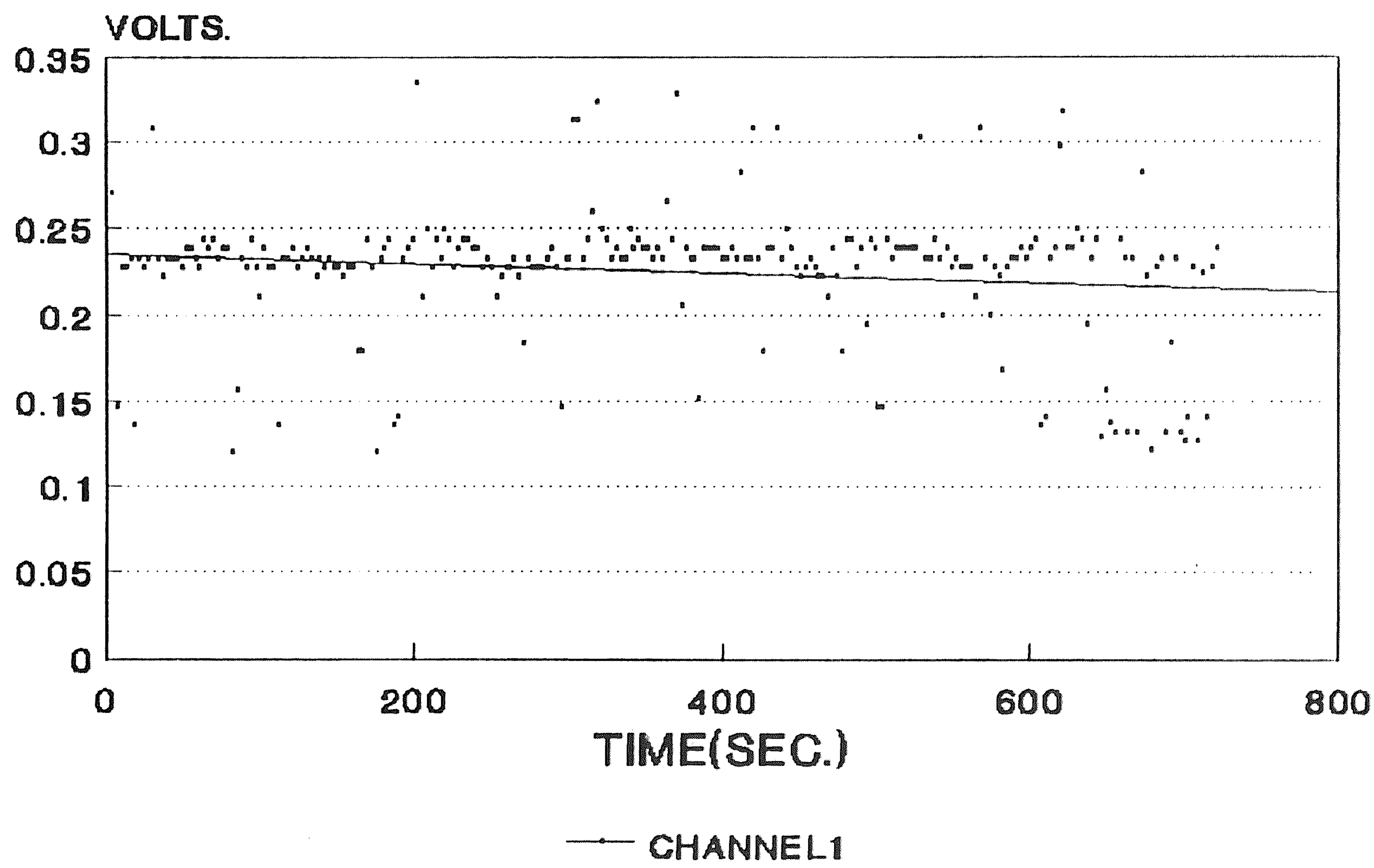

Fig.56 Internal deformation data for19B

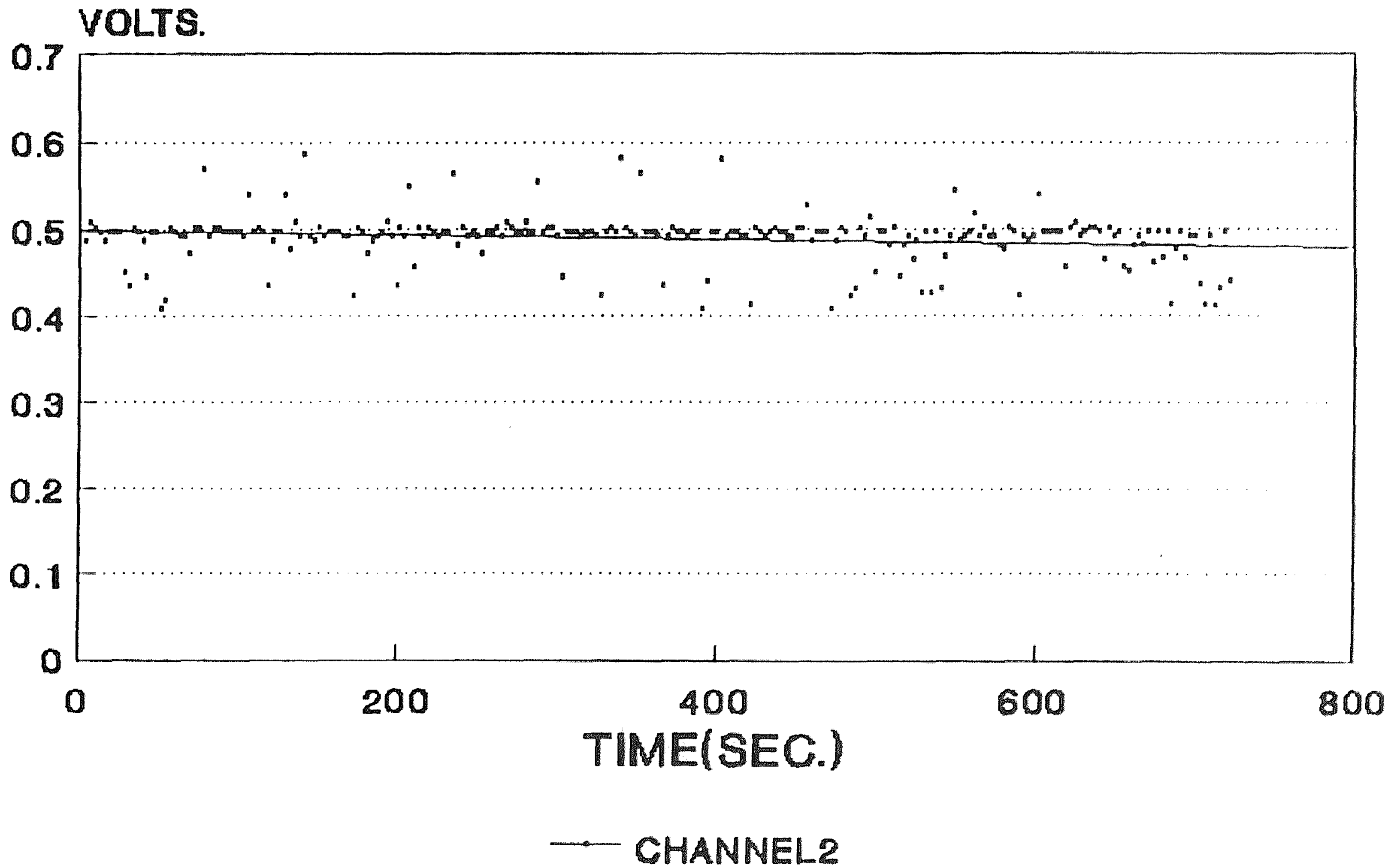

Fig.57 Internal deformation data forF19B

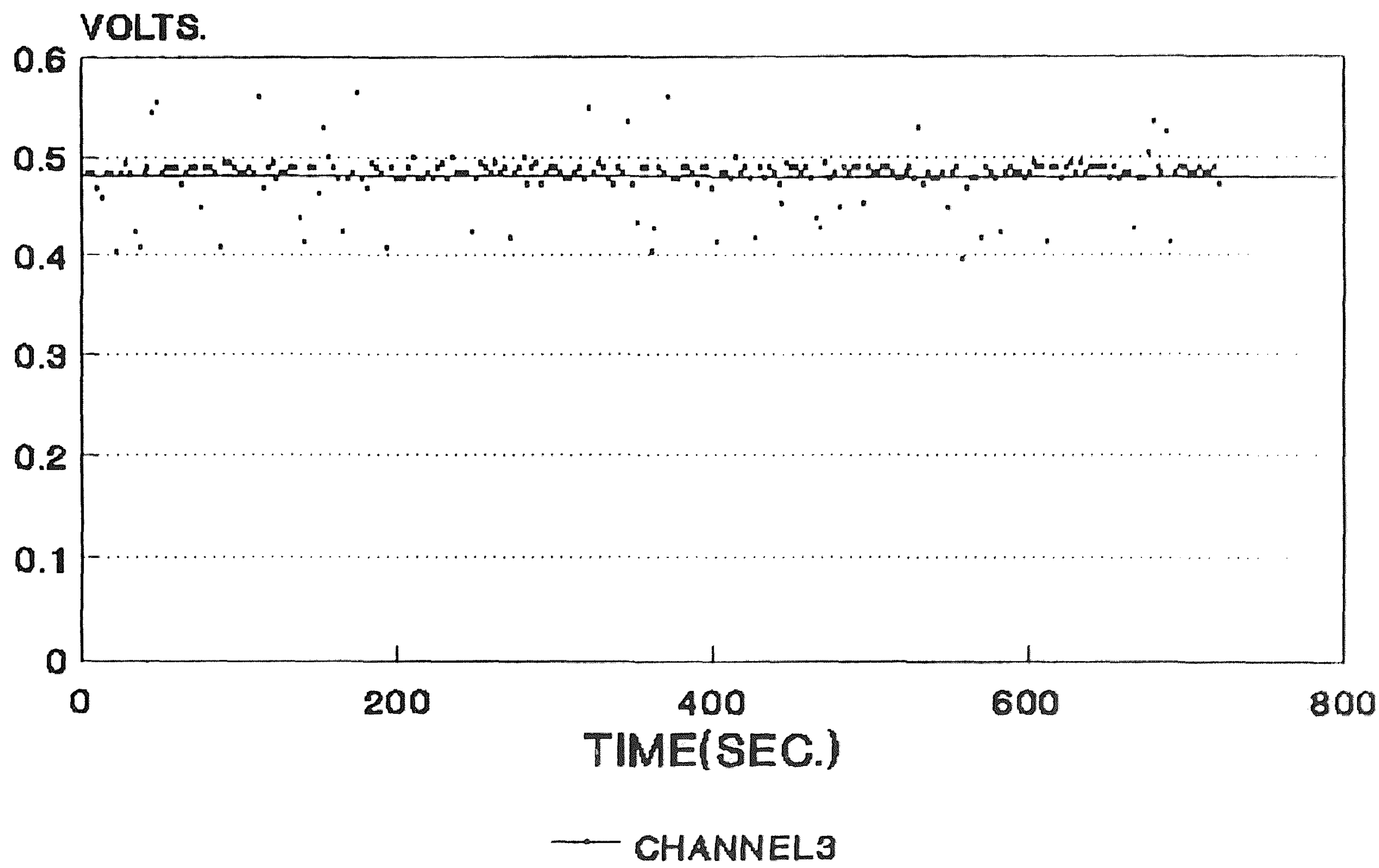

Fig.58 Internal deformation data forF19B

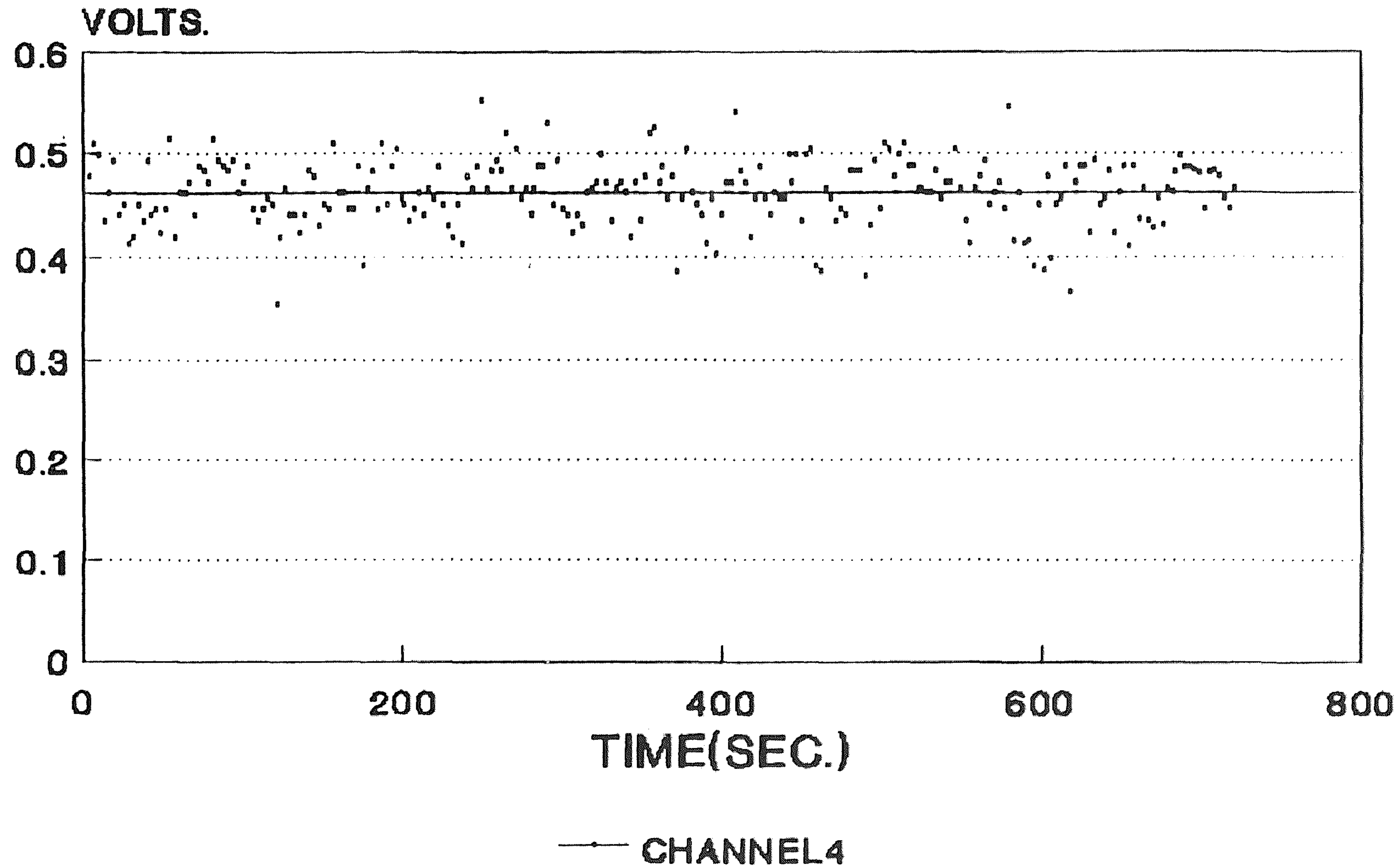

Fig.59 Internal deformation data forF1

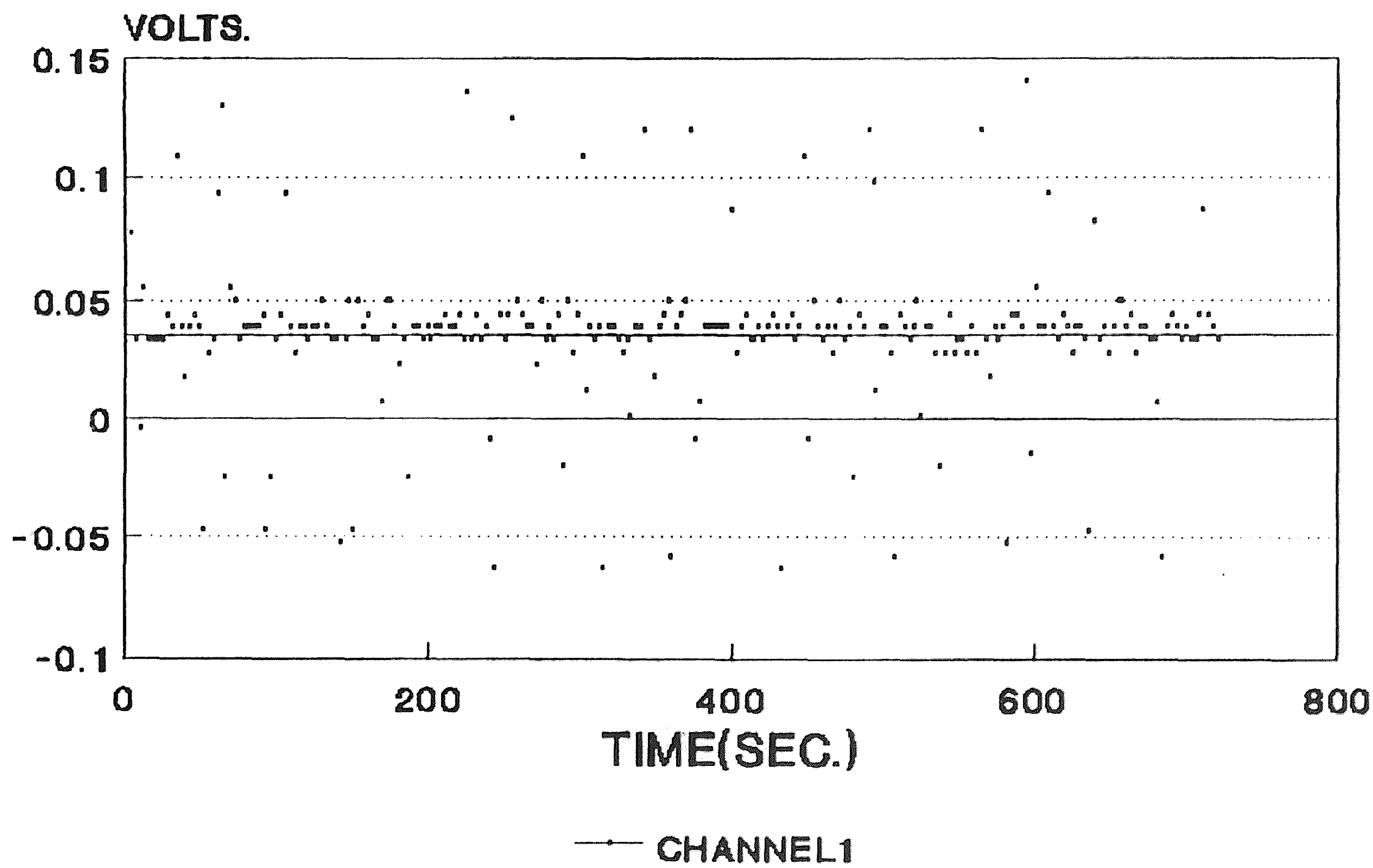

Fig.60 Internal deformation data forF19C

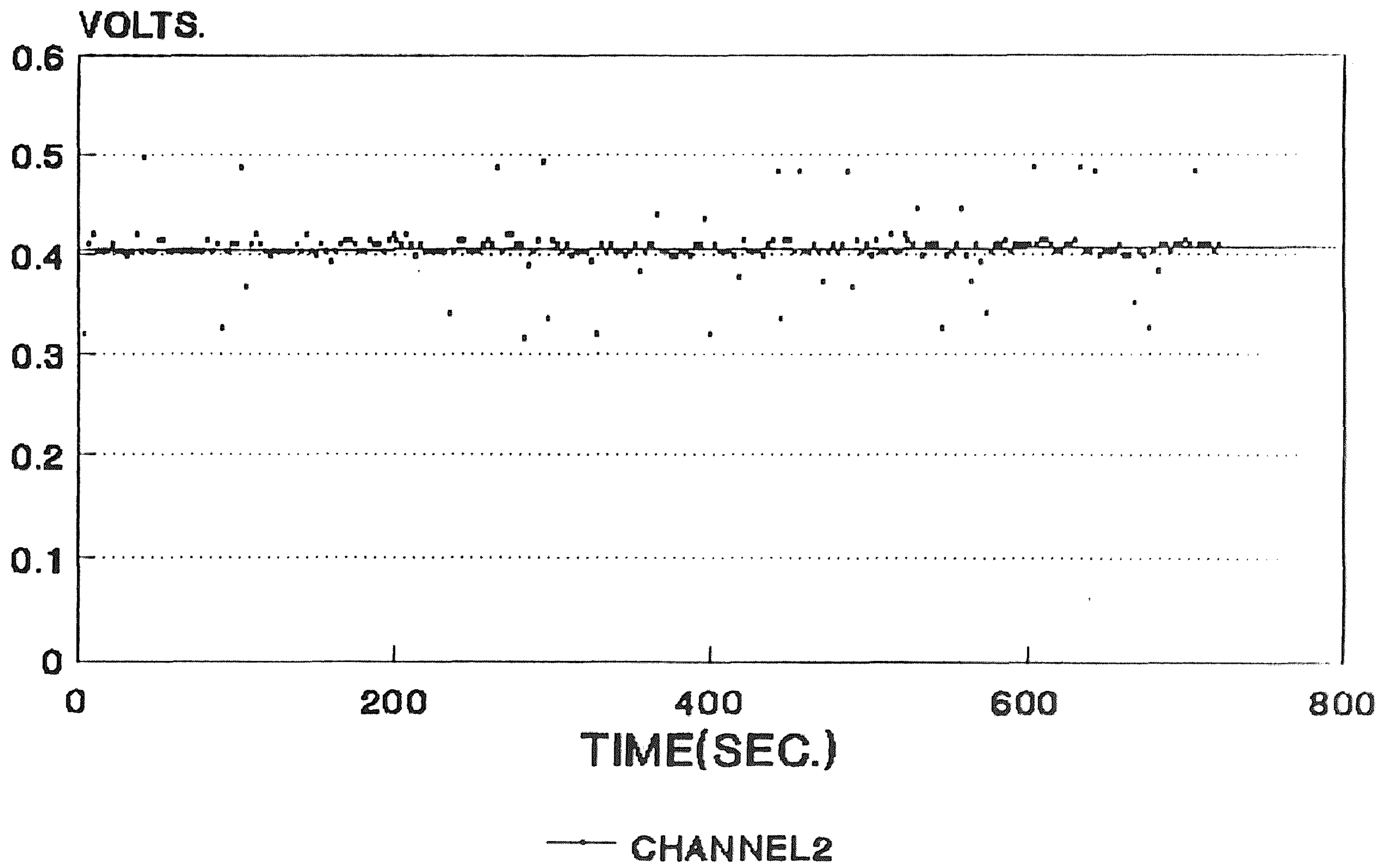

Fig.61 Internal deformation data forF19C

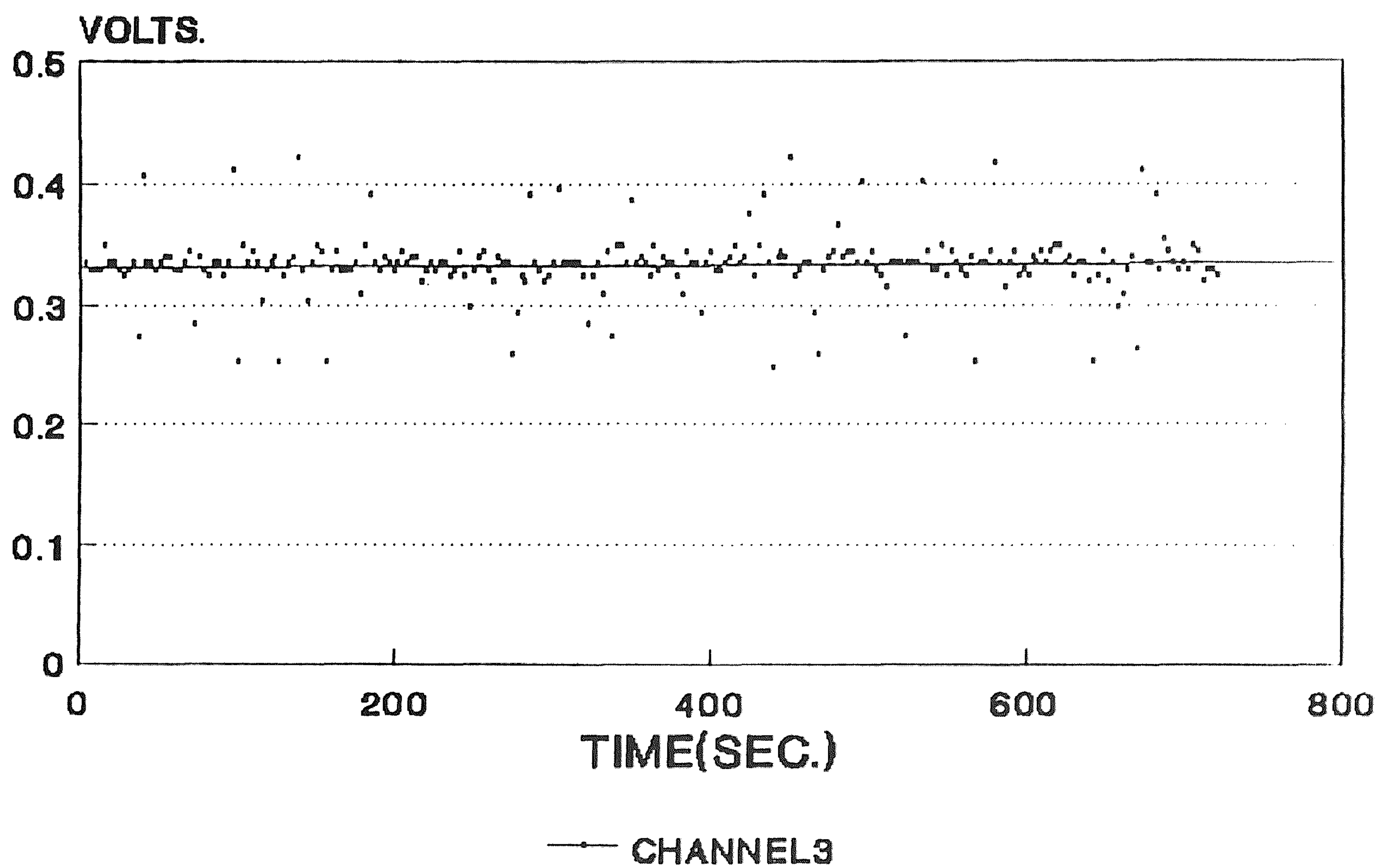

Fig.62 Internal deformation data F19C

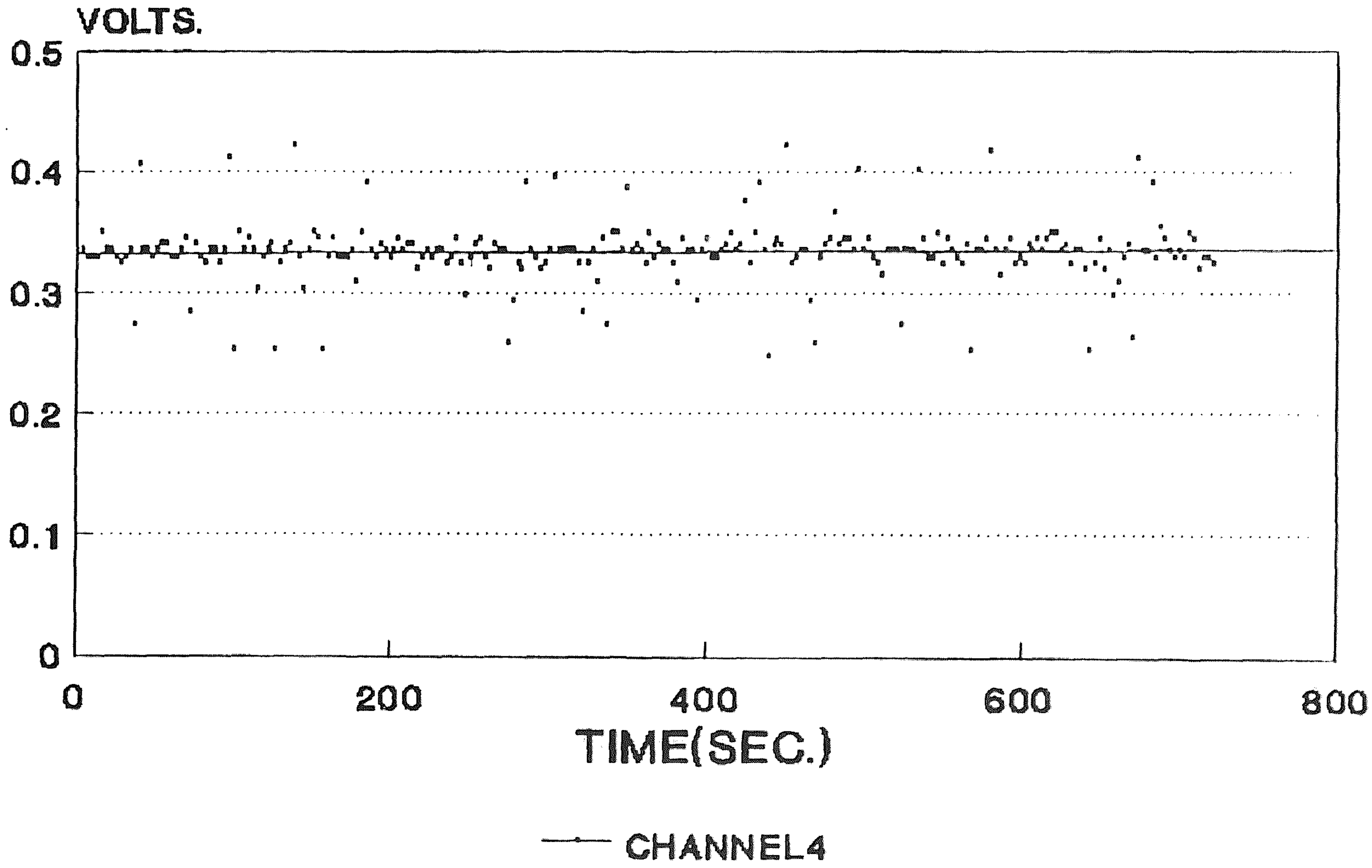

Fig.63 Internal deformation data for [illegible]9C

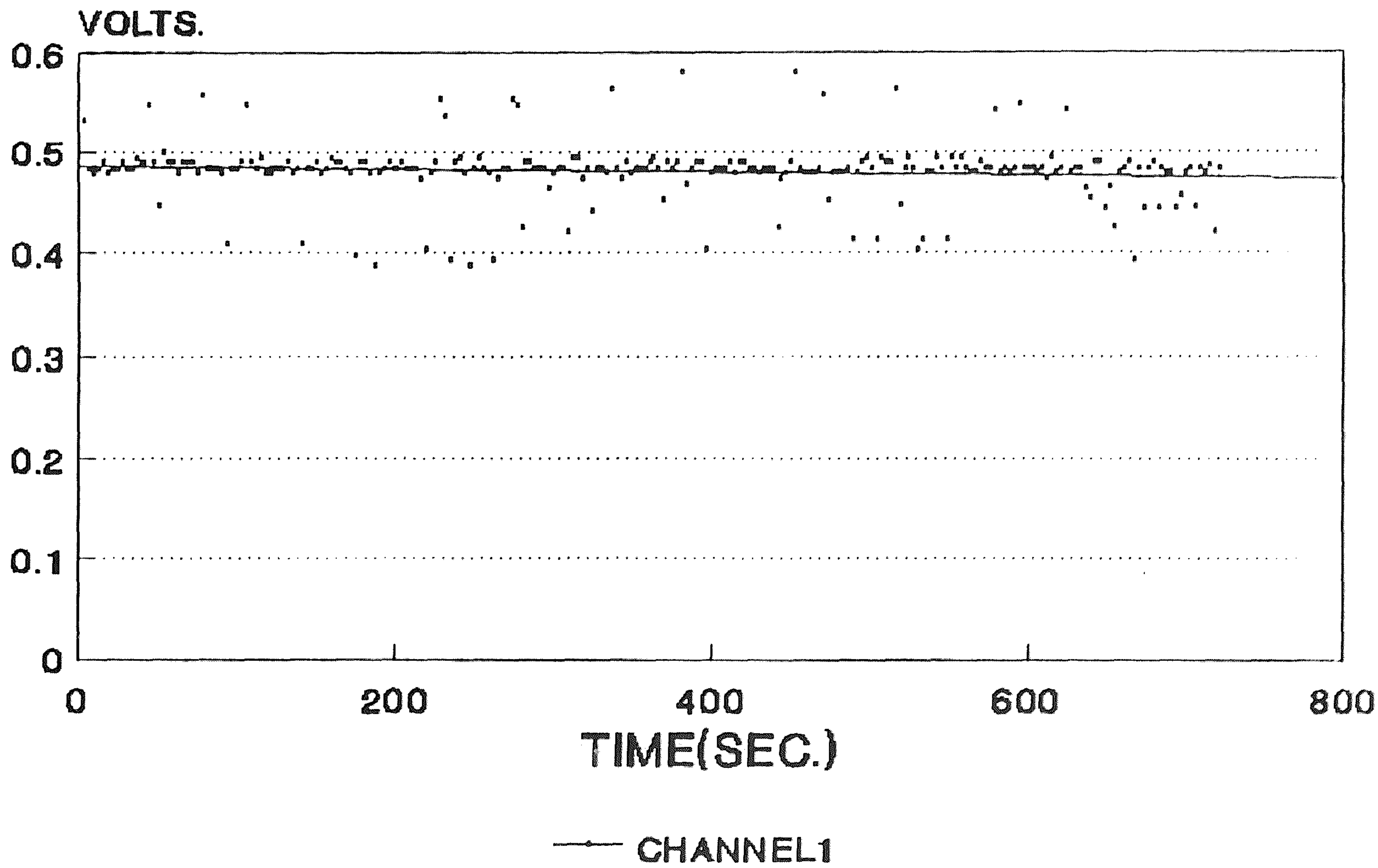

Fig.64 Internal deformation data forF19D

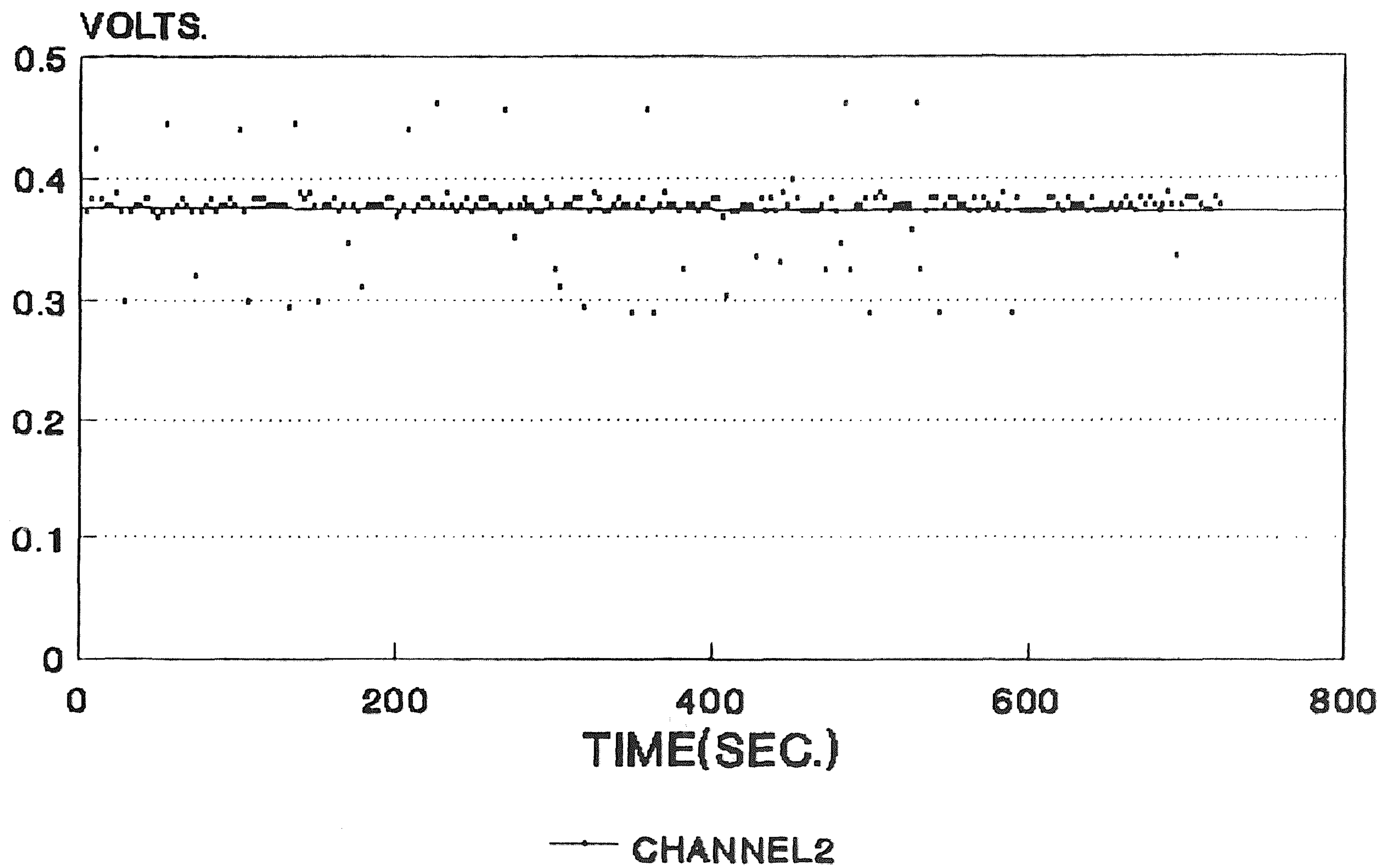

Fig.65 Internal deformation data forF19I

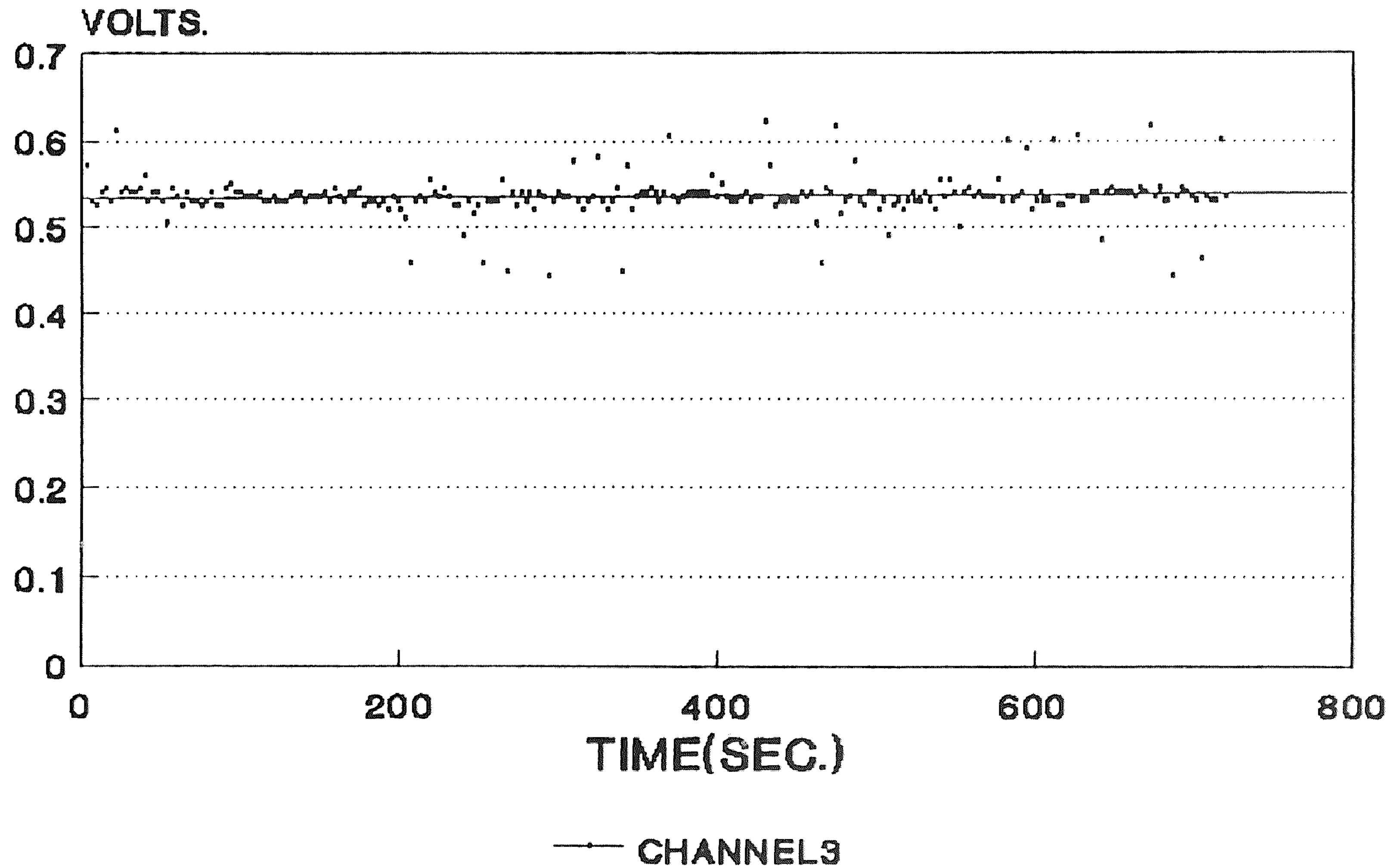

Fig.66 Internal deformation data forF19D

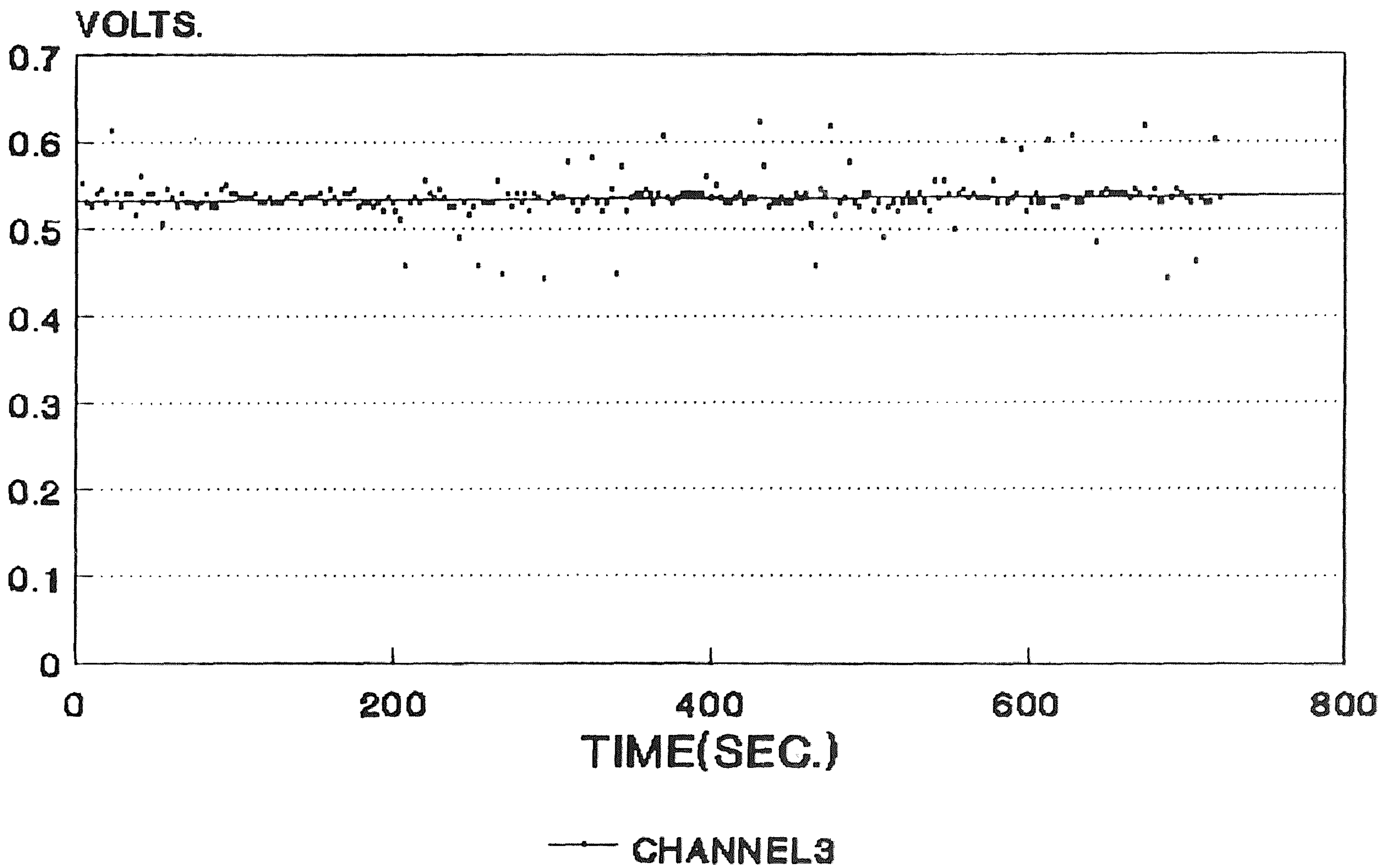

Fig.67 Internal deformation data forF19D

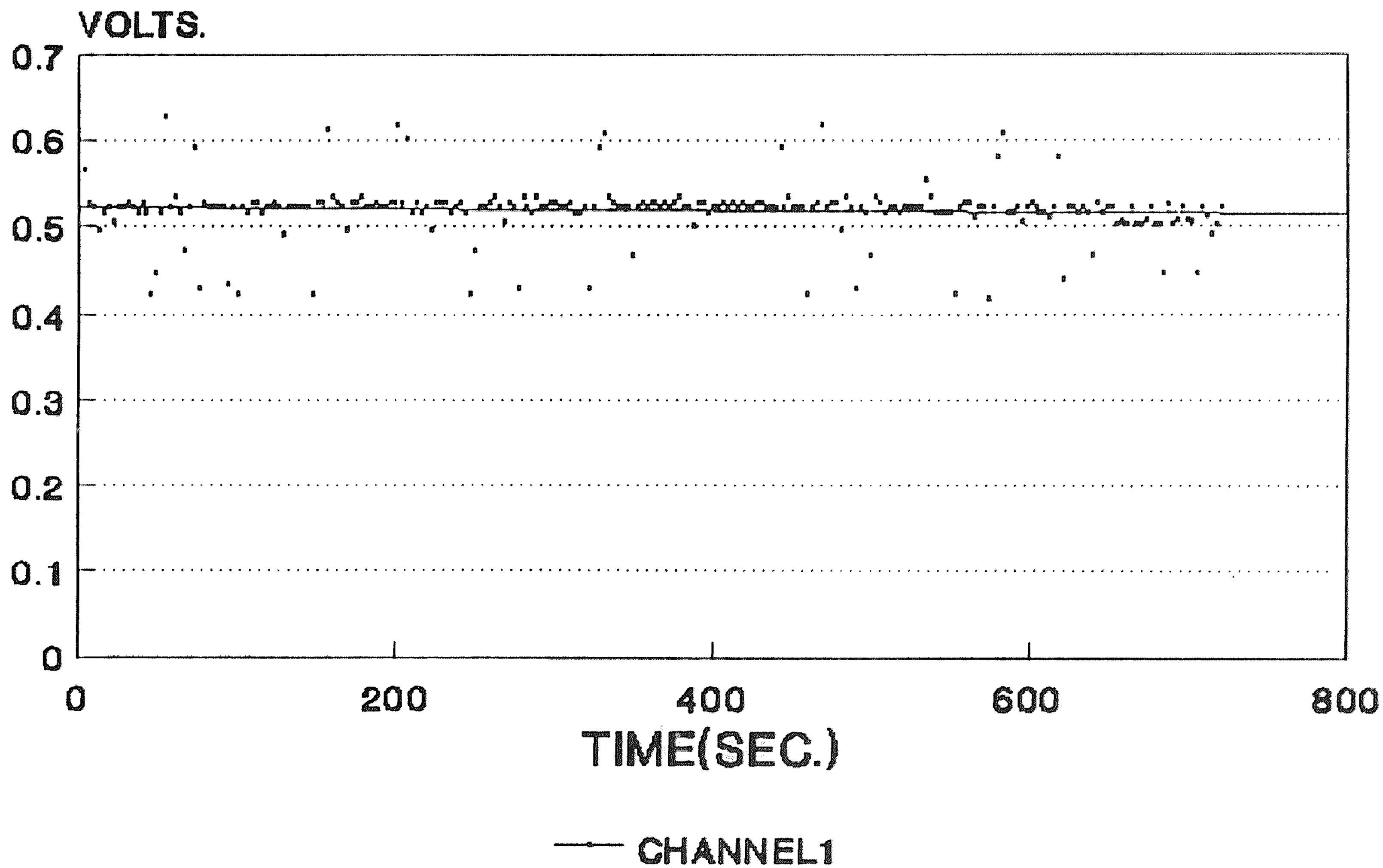

Fig.68 Internal deformation data forF28A

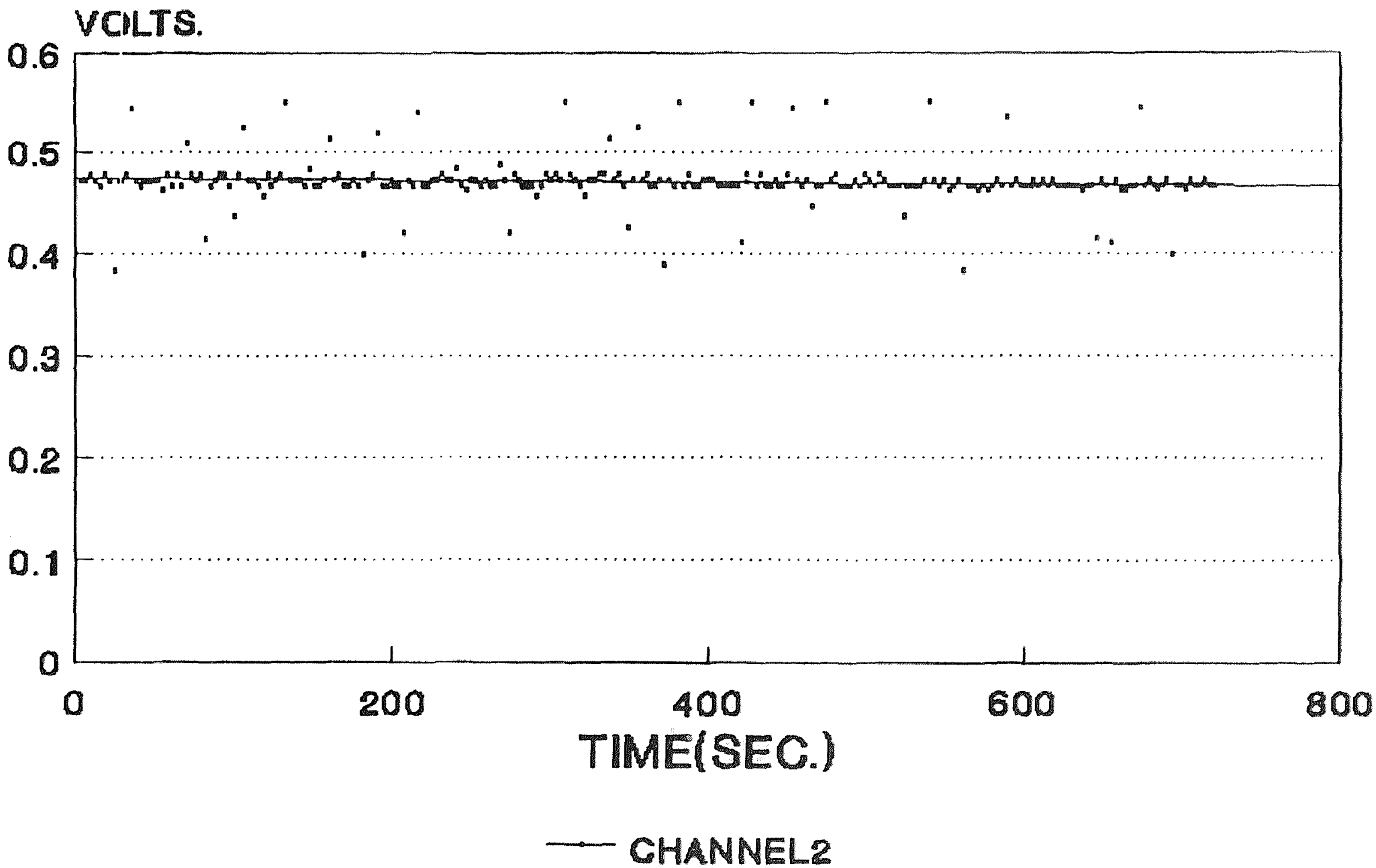

Fig.69 Internal deformation data forF2.

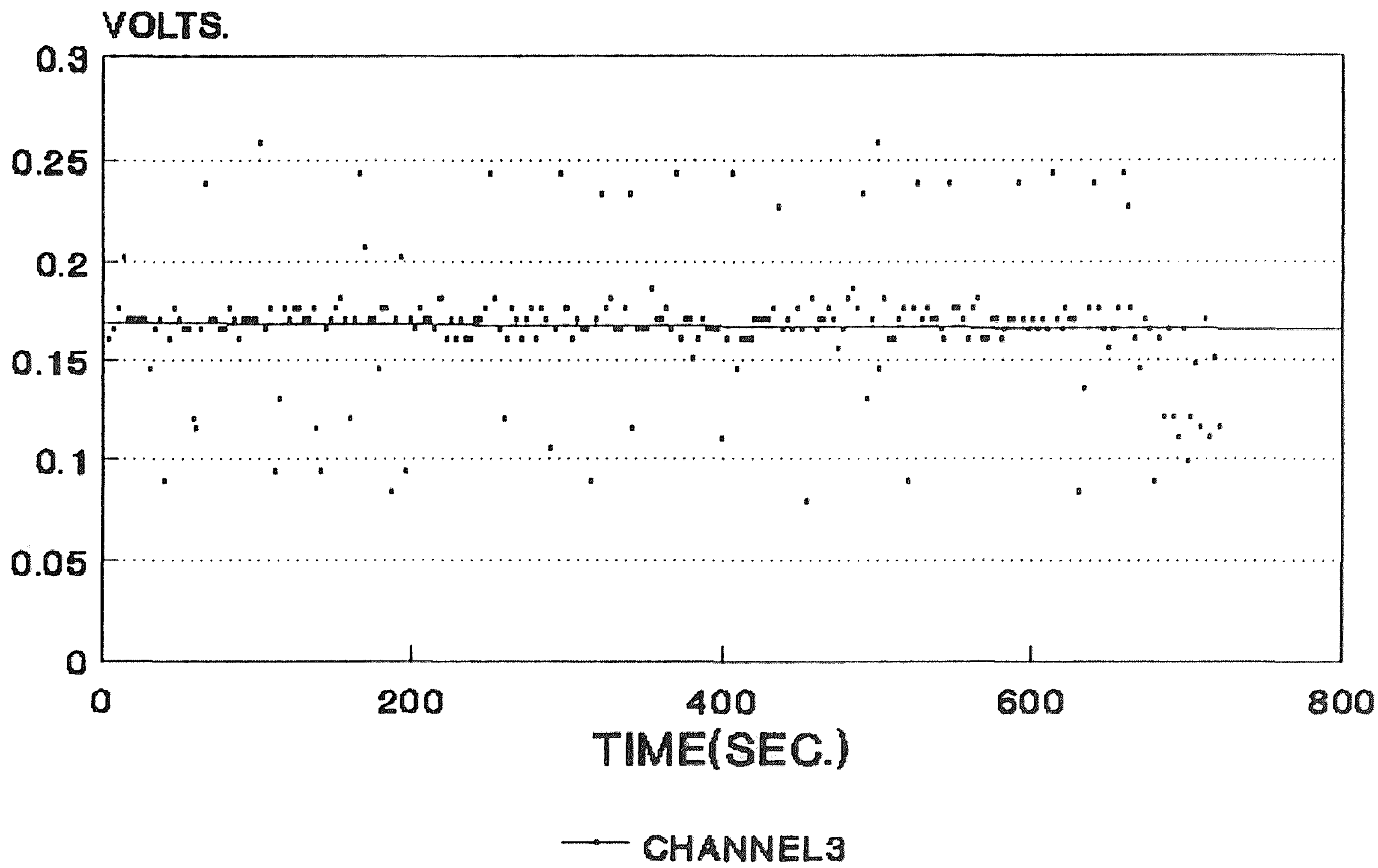

Fig.70 Internal deformation data forF28

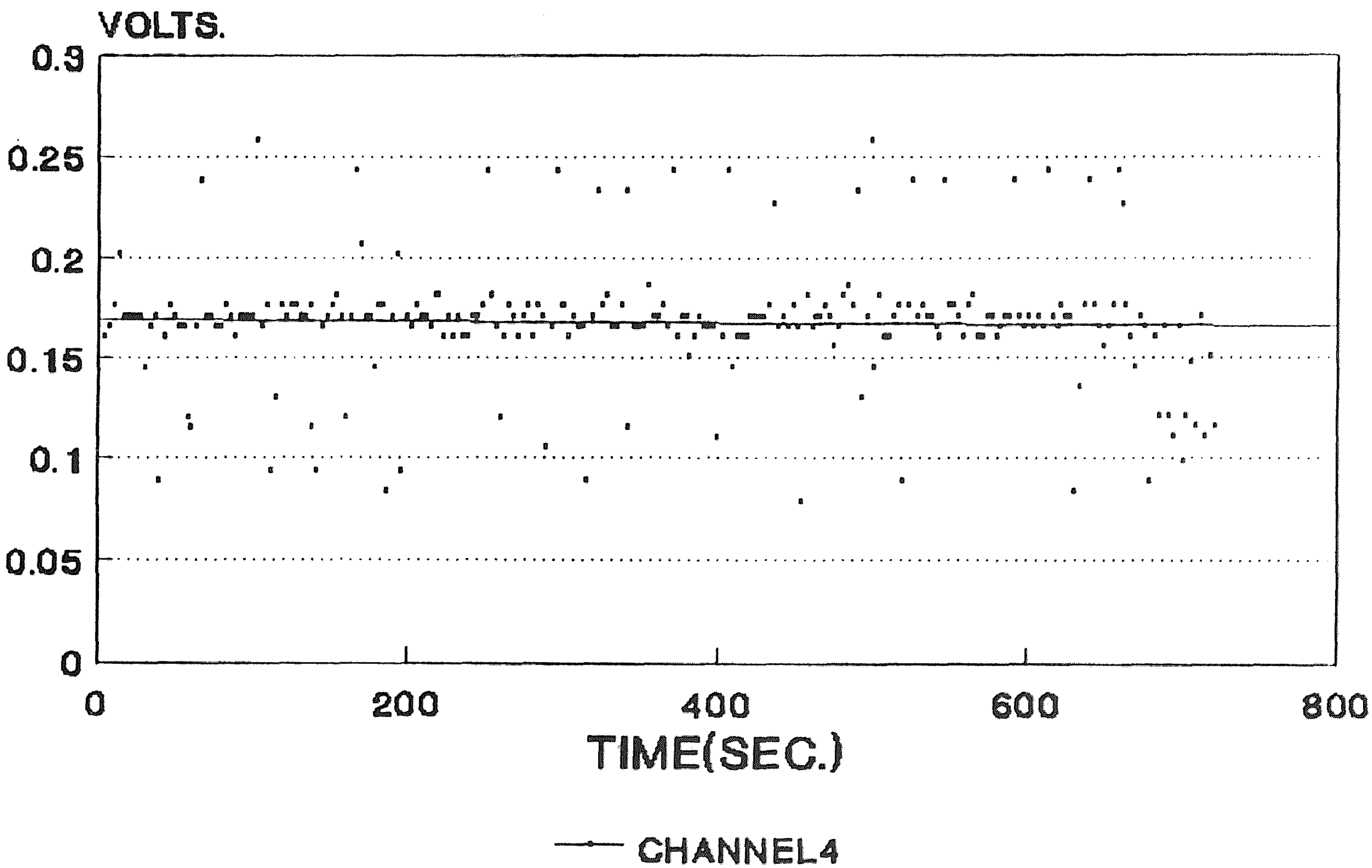

Fig.71 Internal deformation data for i 3A

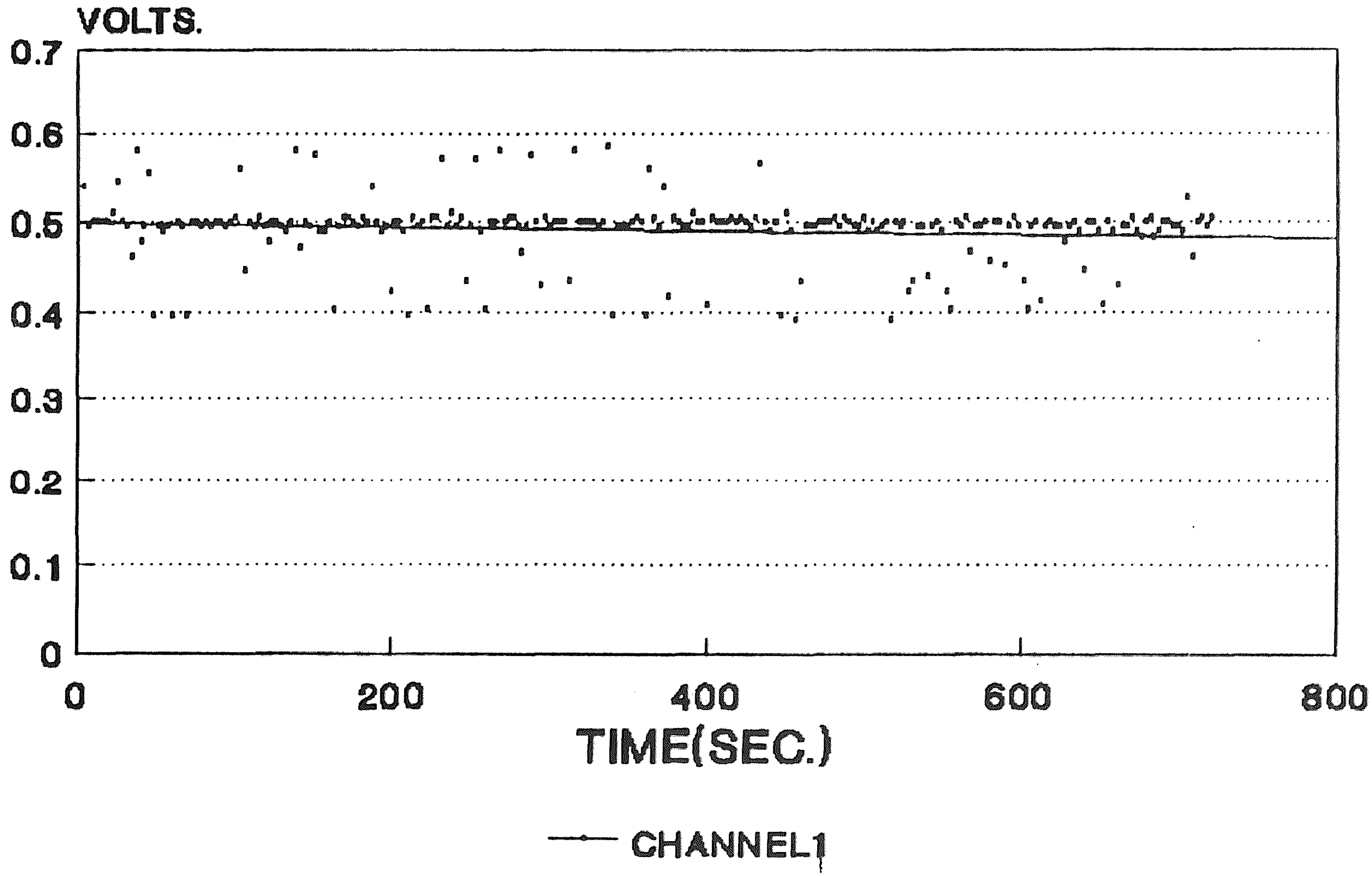

Fig.72 Internal deformation data forF

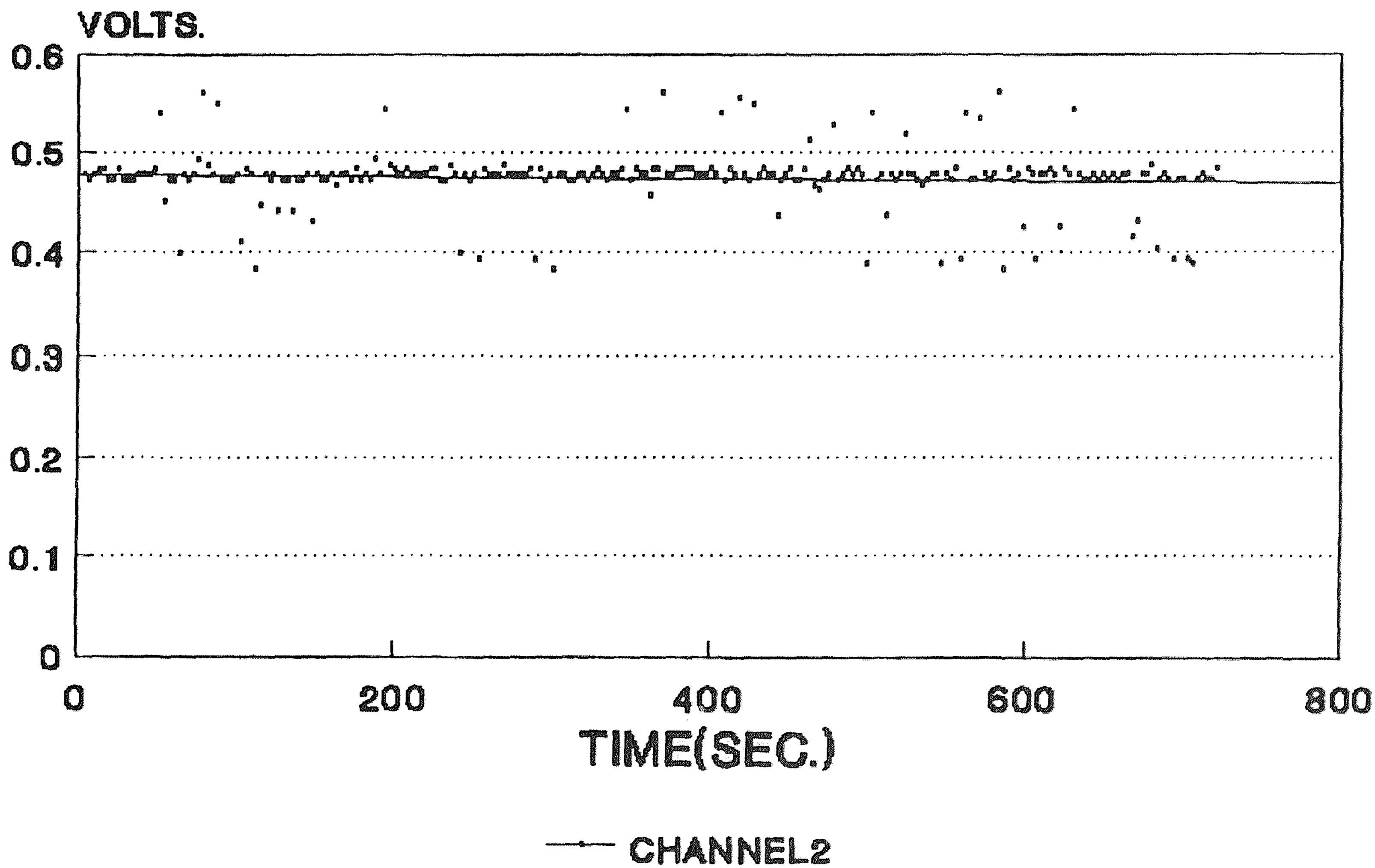

Fig.73 Internal deformation data forF28B

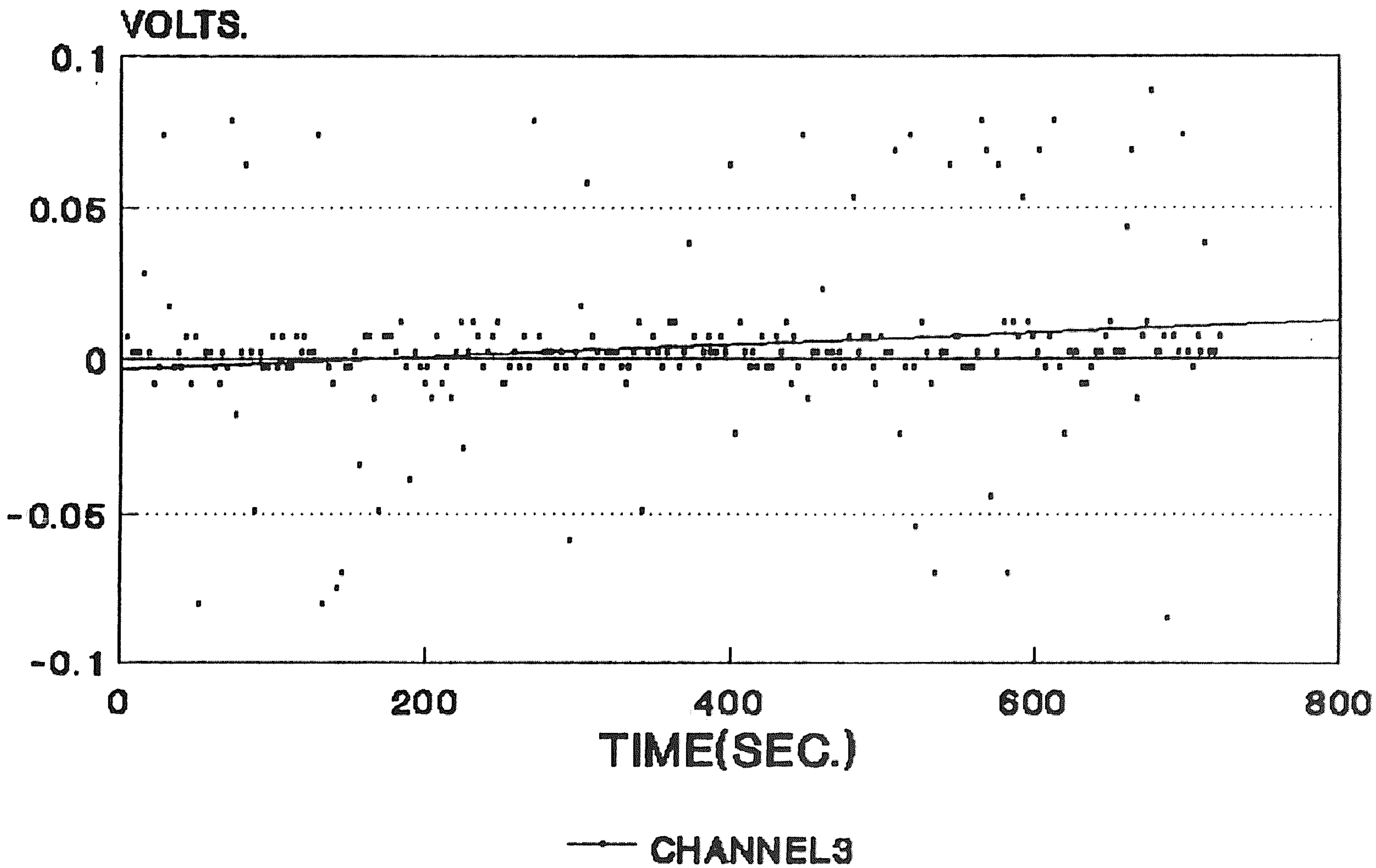

Fig.74 Internal deformation data for F28B

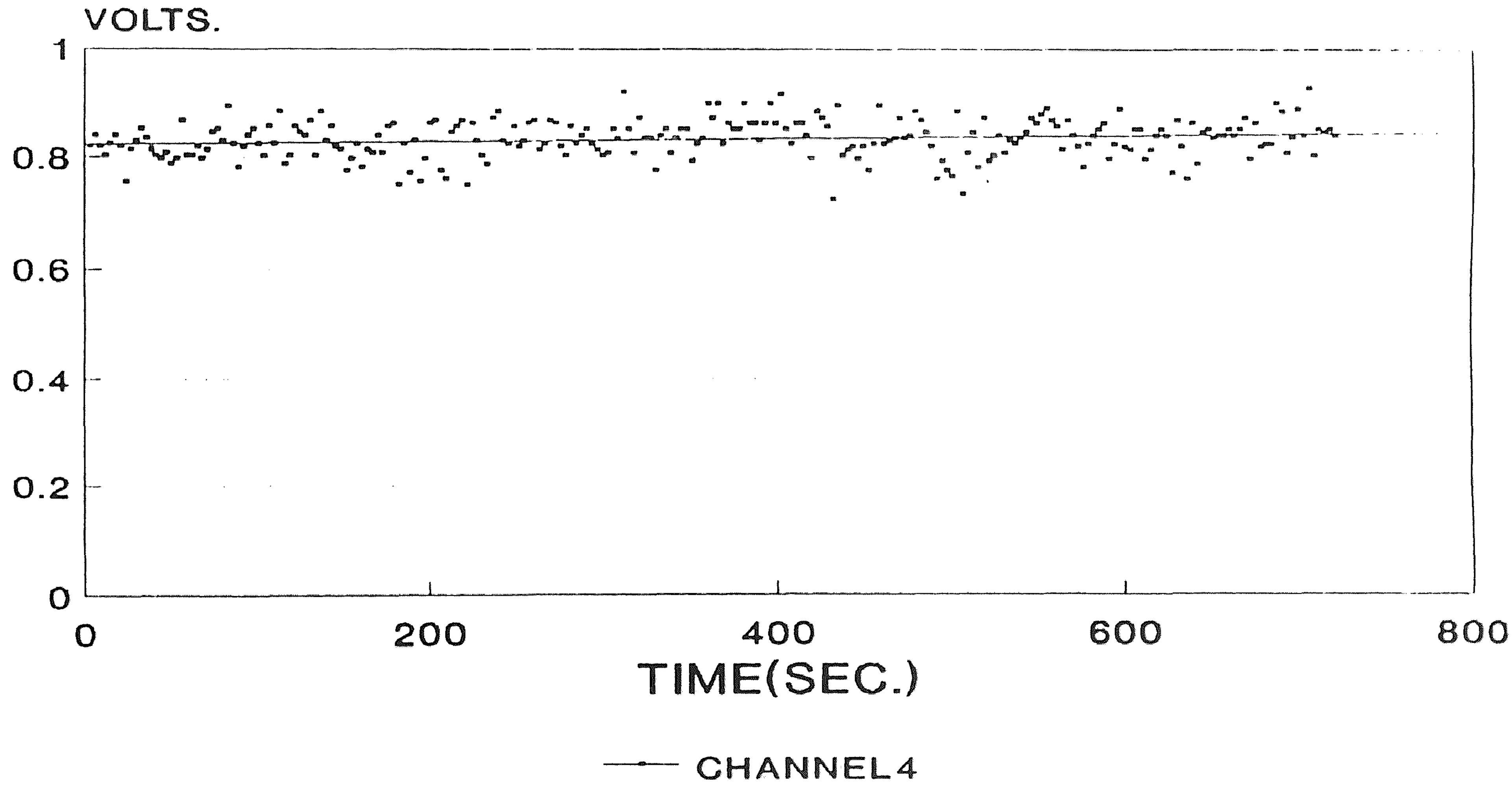

Fig.75 Internal deformation data forF28B

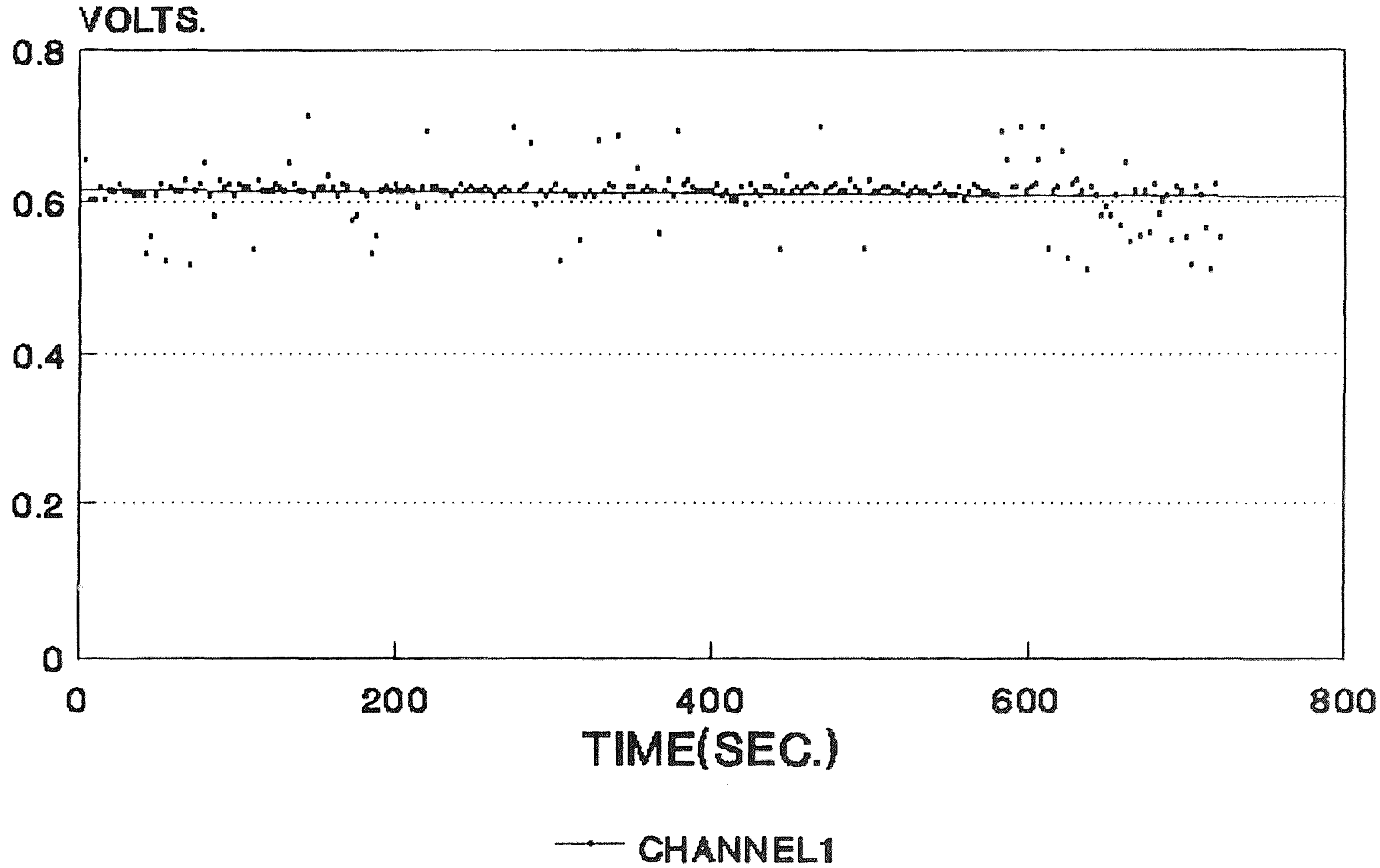

Fig.76 Internal deformation data ForF28C

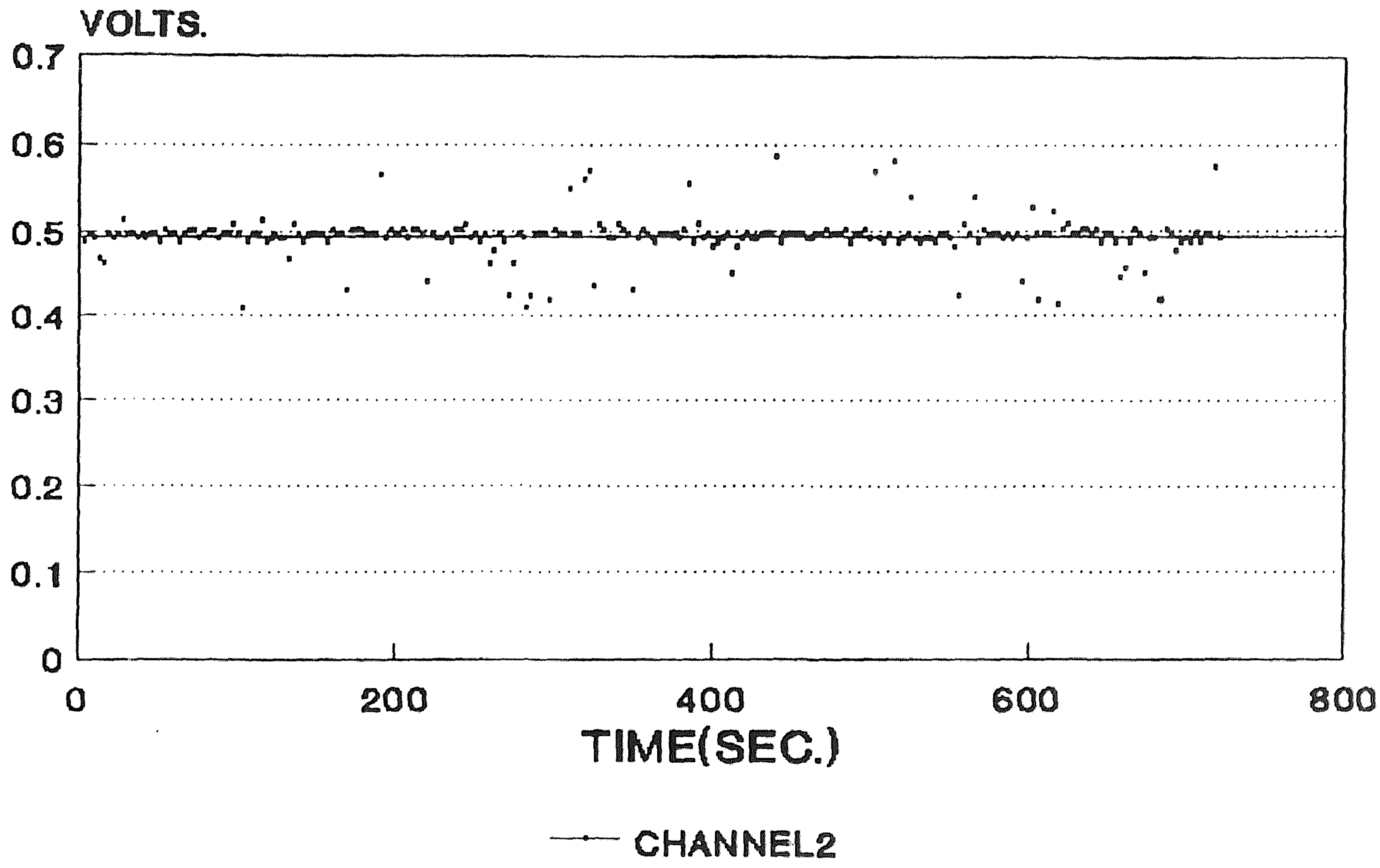

Fig.77 Internal deformation data forF28C

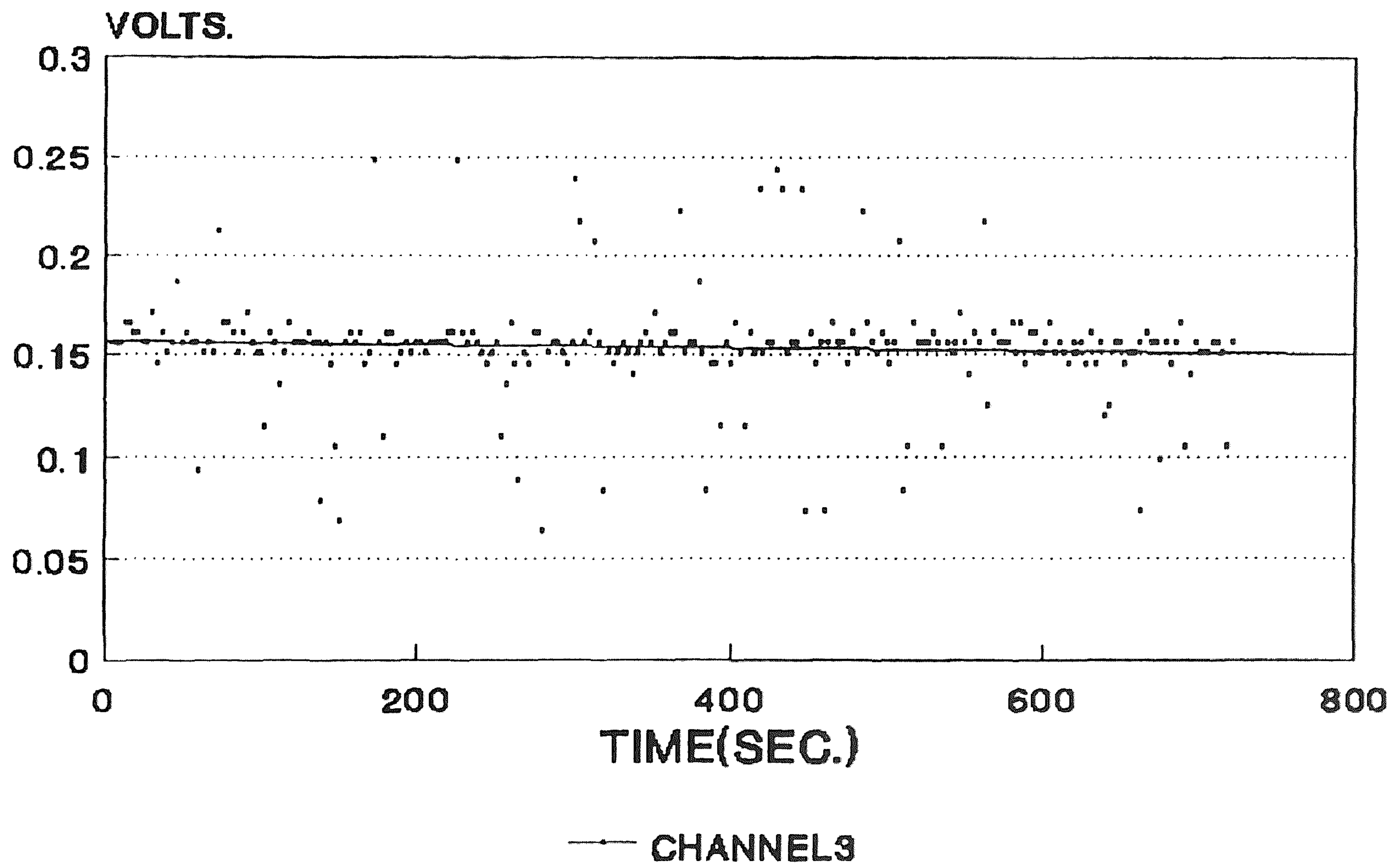

Fig.78 Internal deformation data forF28C

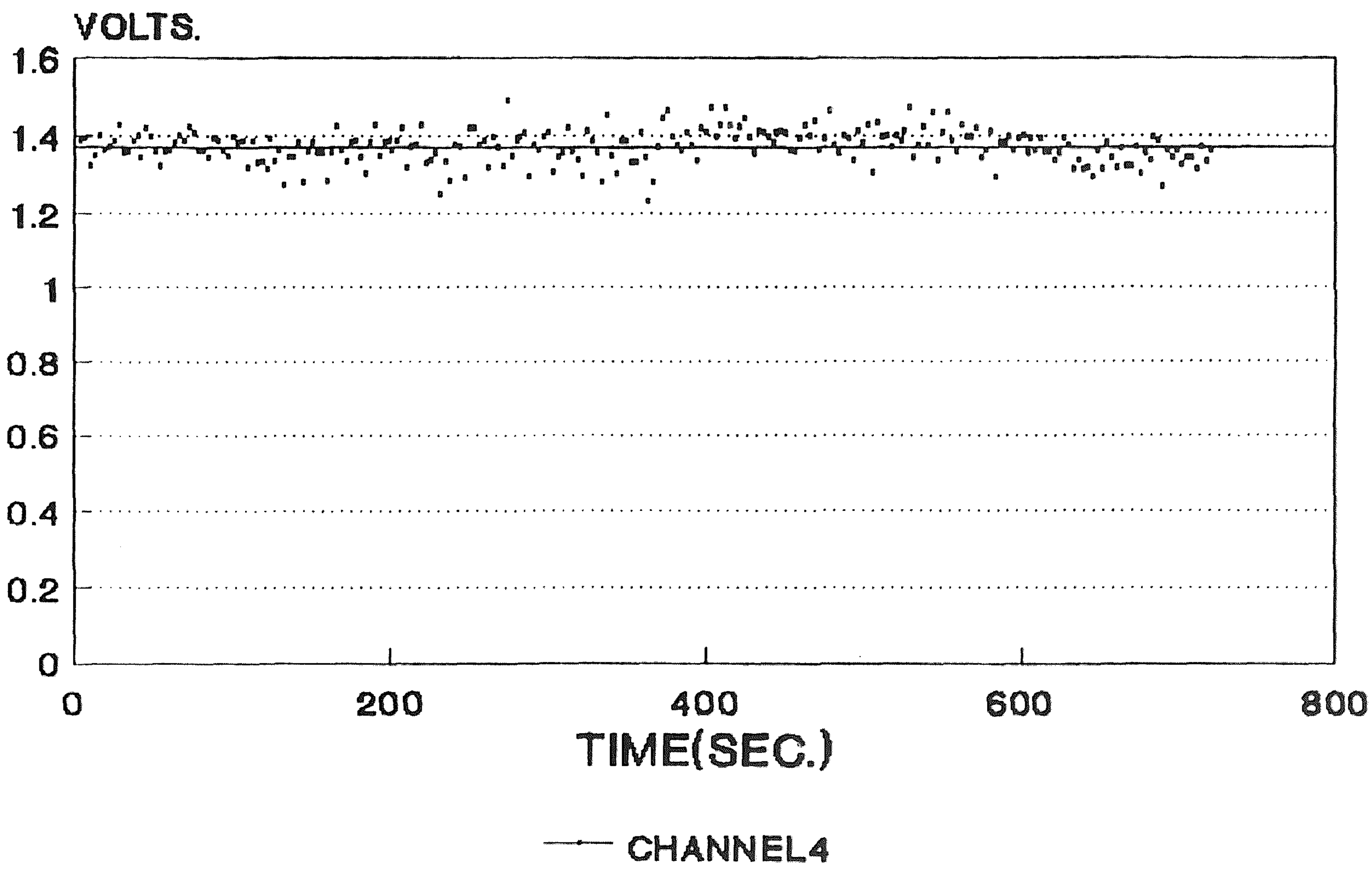

Fig.79 Internal deformation data forF28C

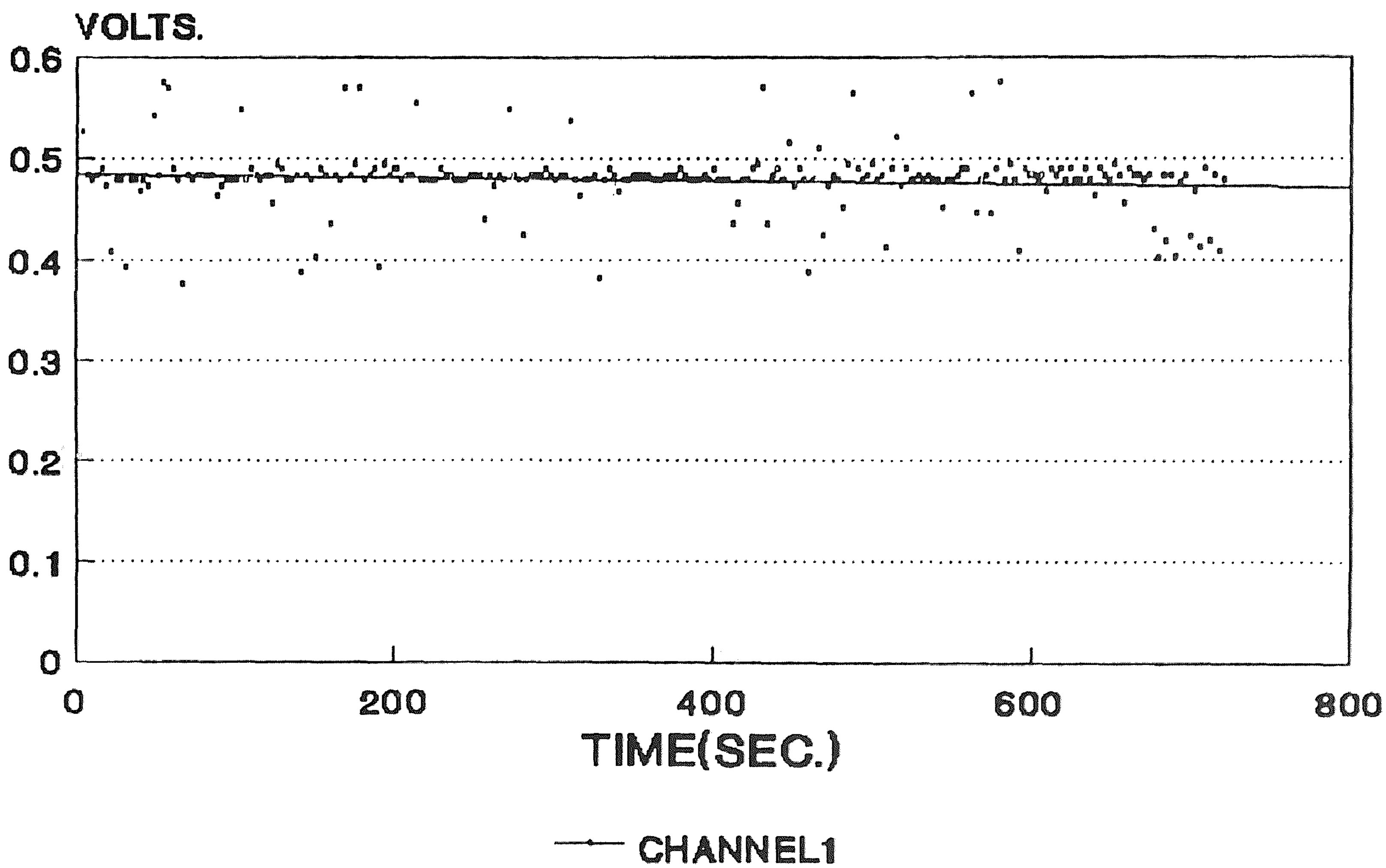

Fig.80 Internal deformation data for M1A

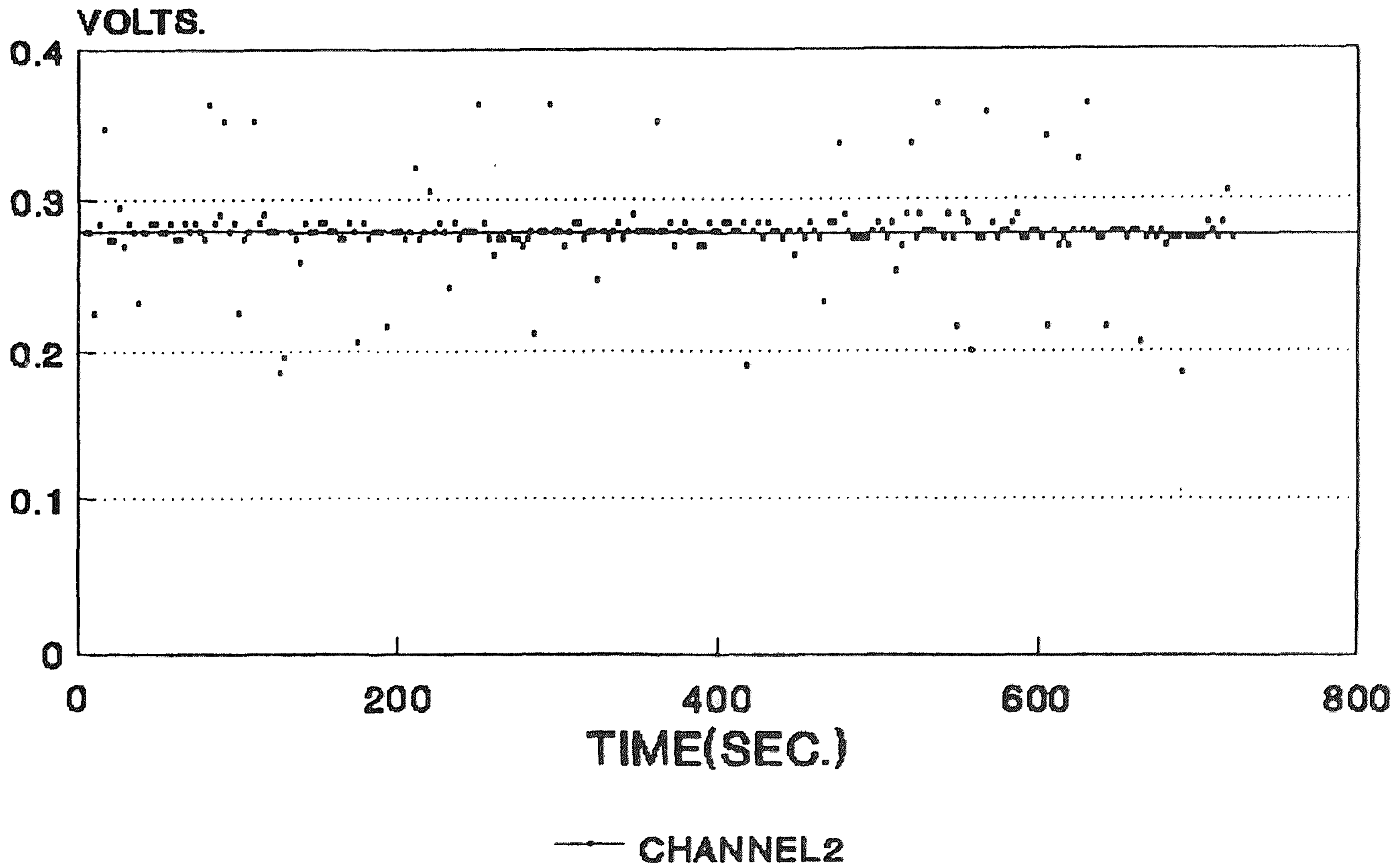

Fig.81 Internal deformation data fc.

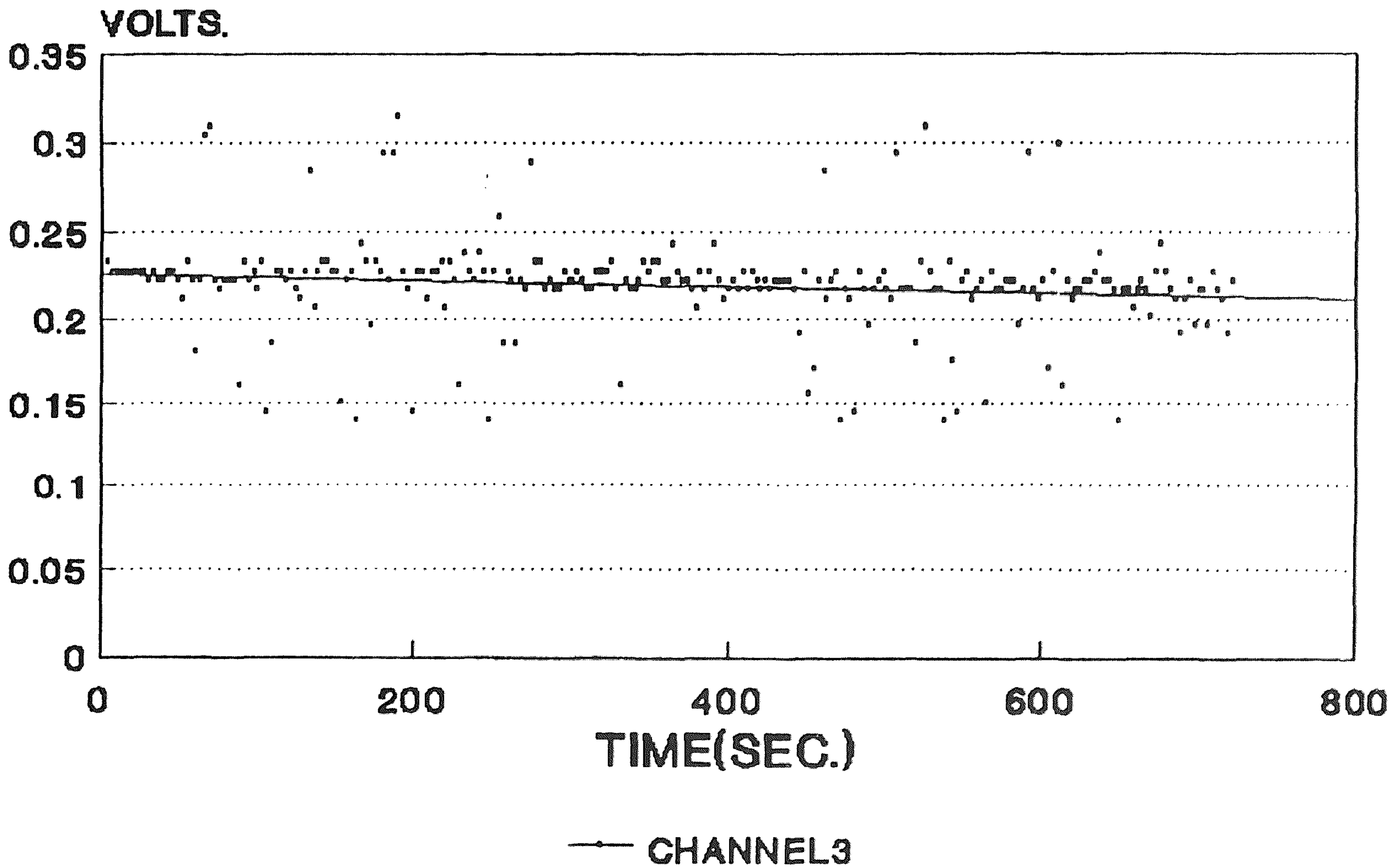

Fig.82 Internal deformation data fo

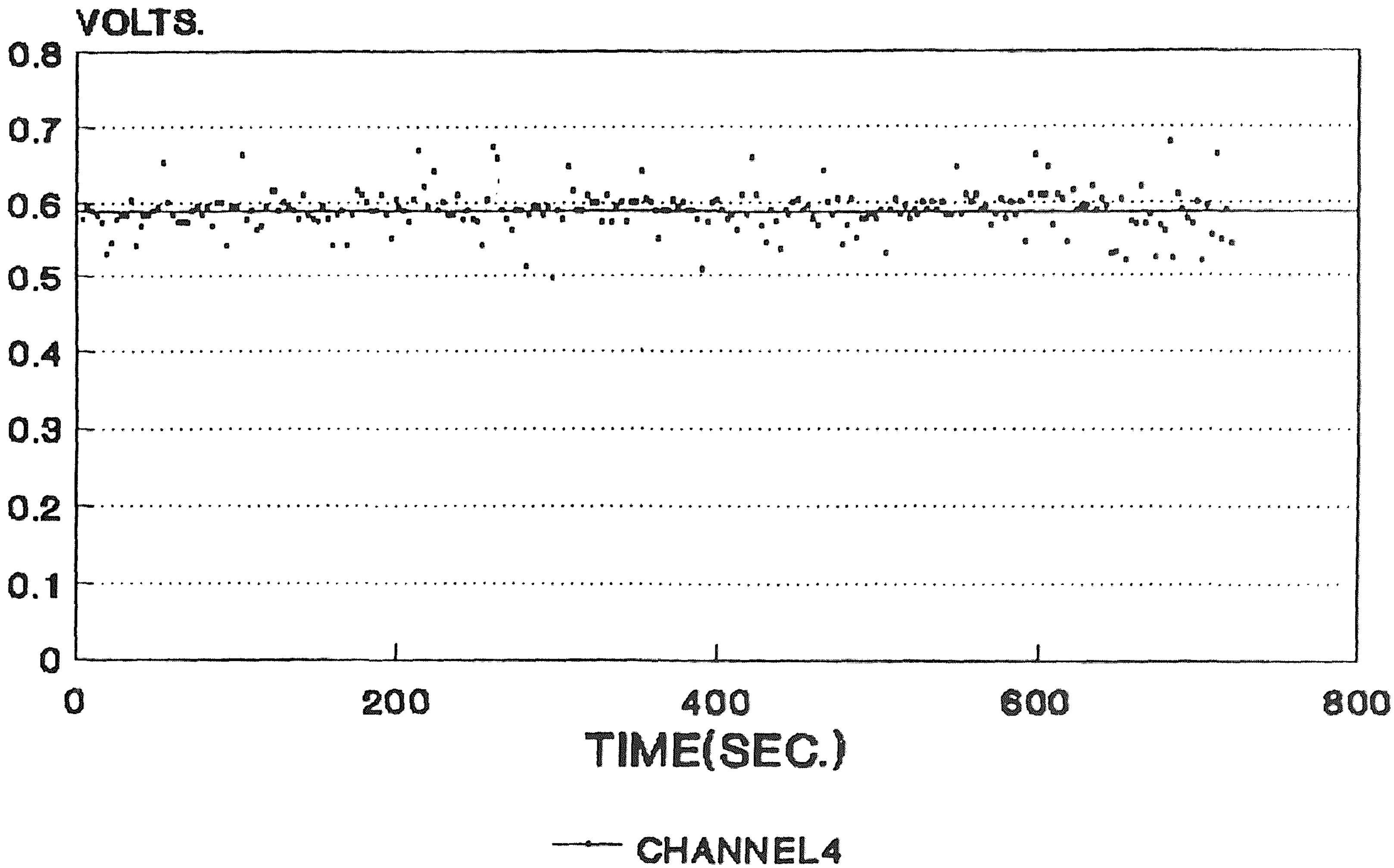

Fig.83 Internal deformation data for M1A

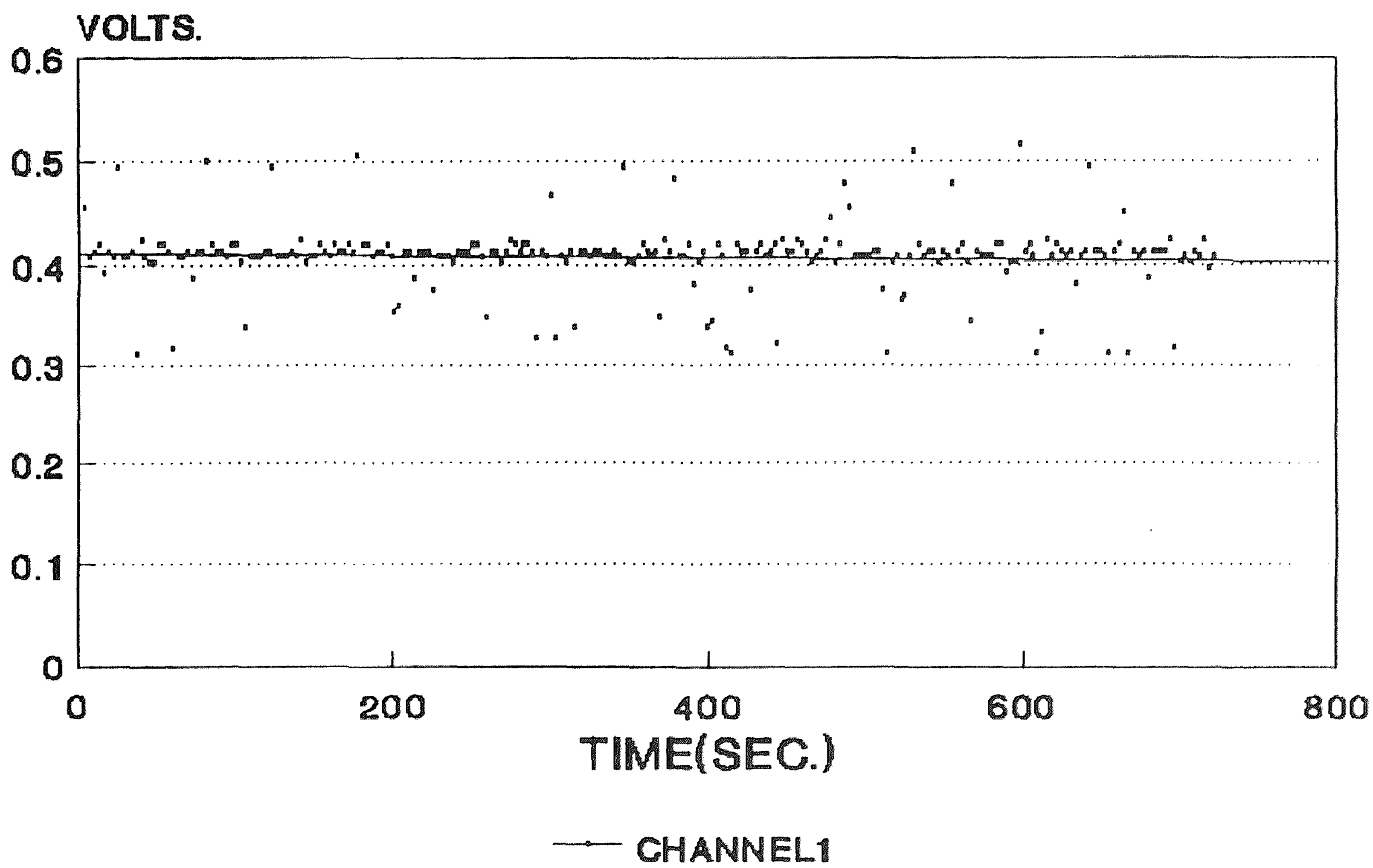

Fig.84 Internal deformation data for M1B

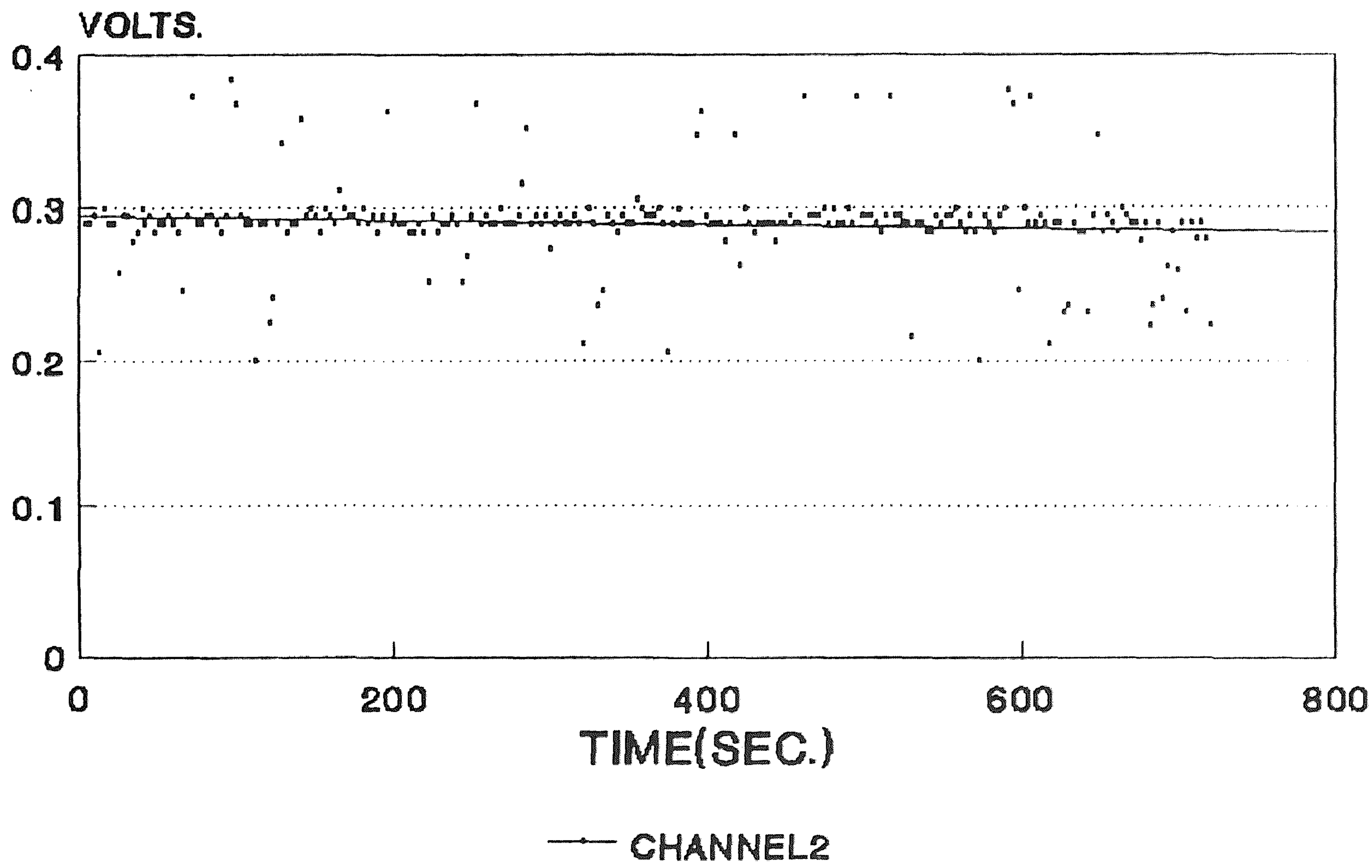

Fig.85 Internal deformation data M1B

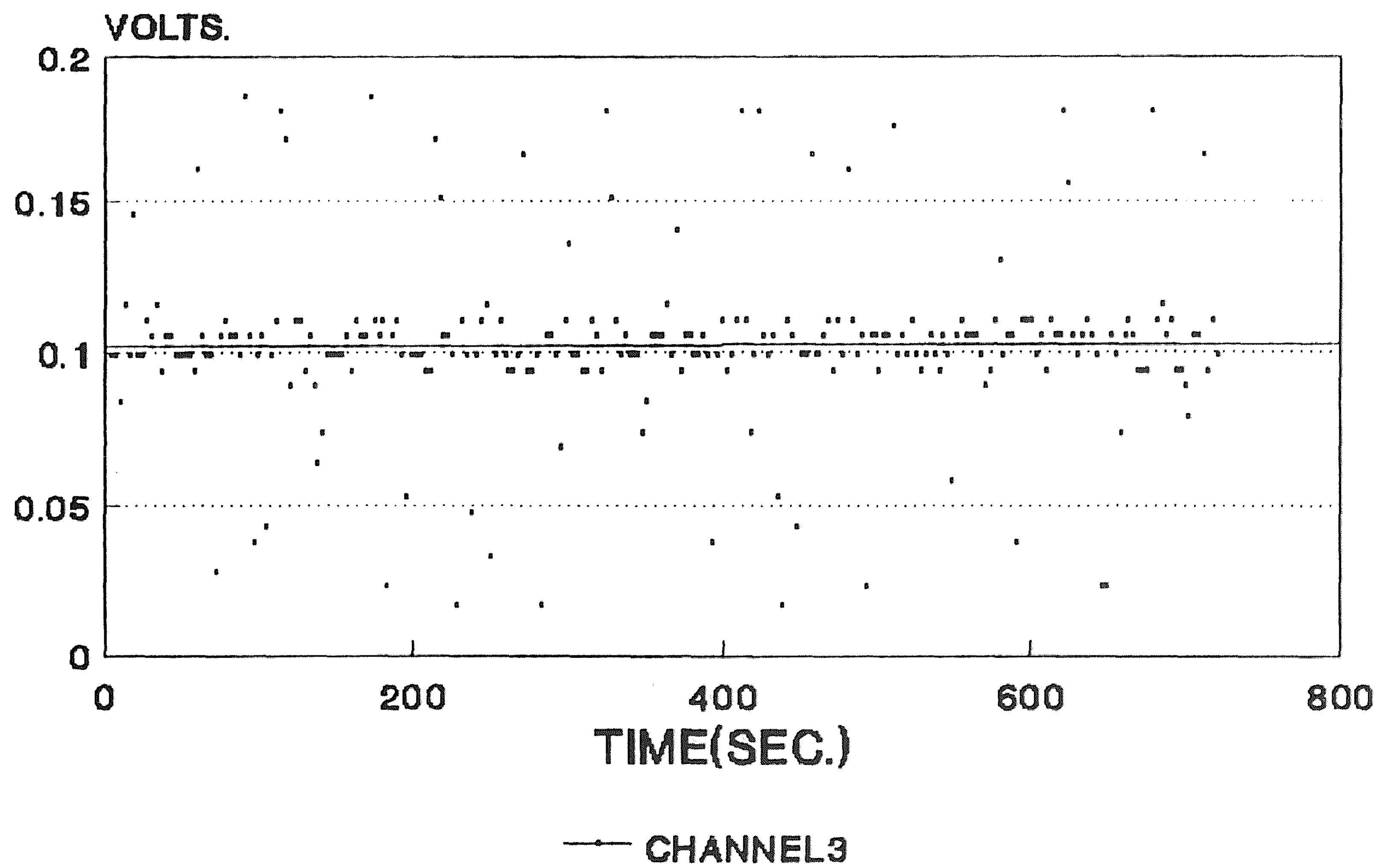

Fig.86 Internal deformation data .1B

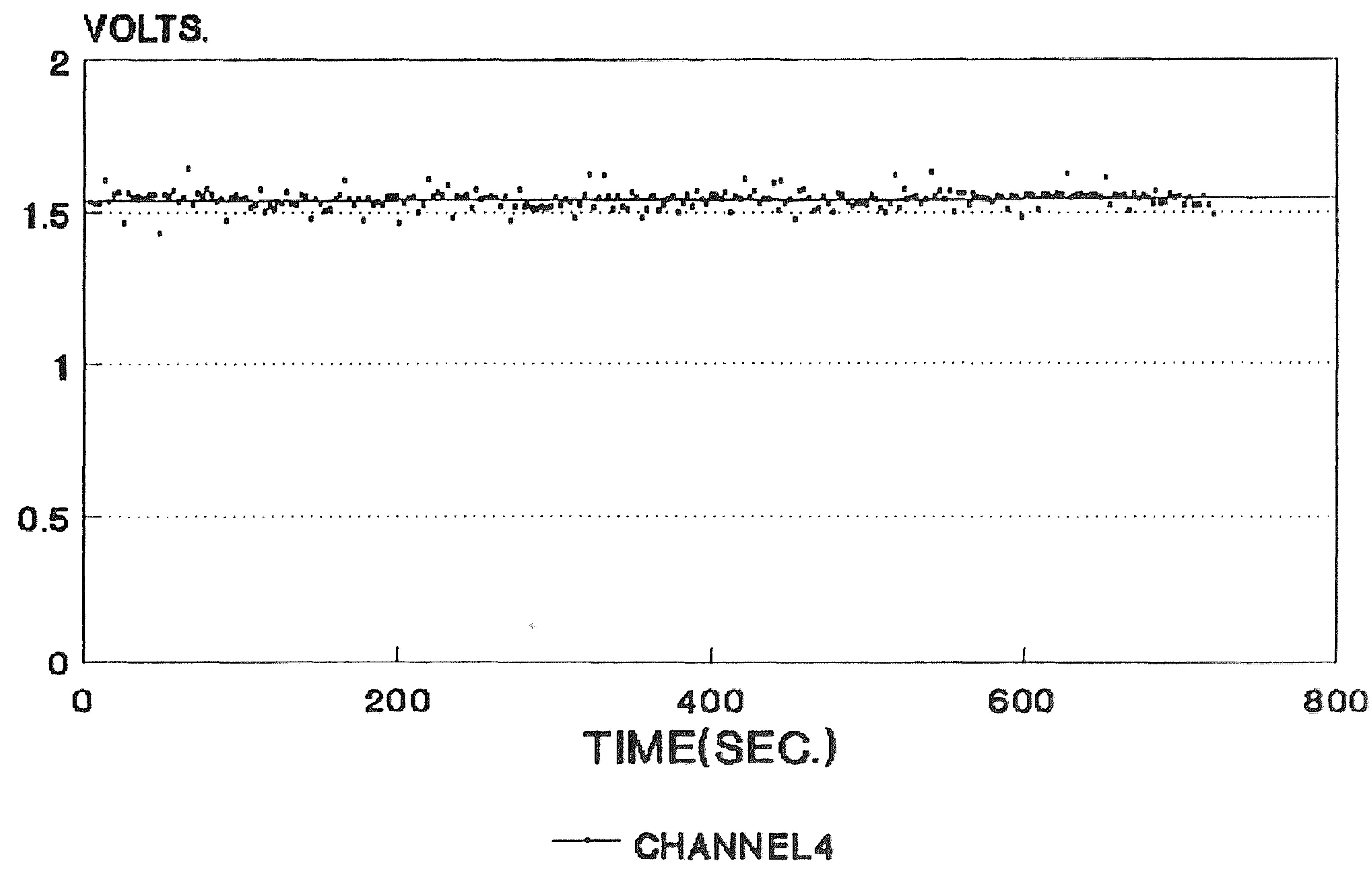

Fig.87 Internal deformation data for M1B

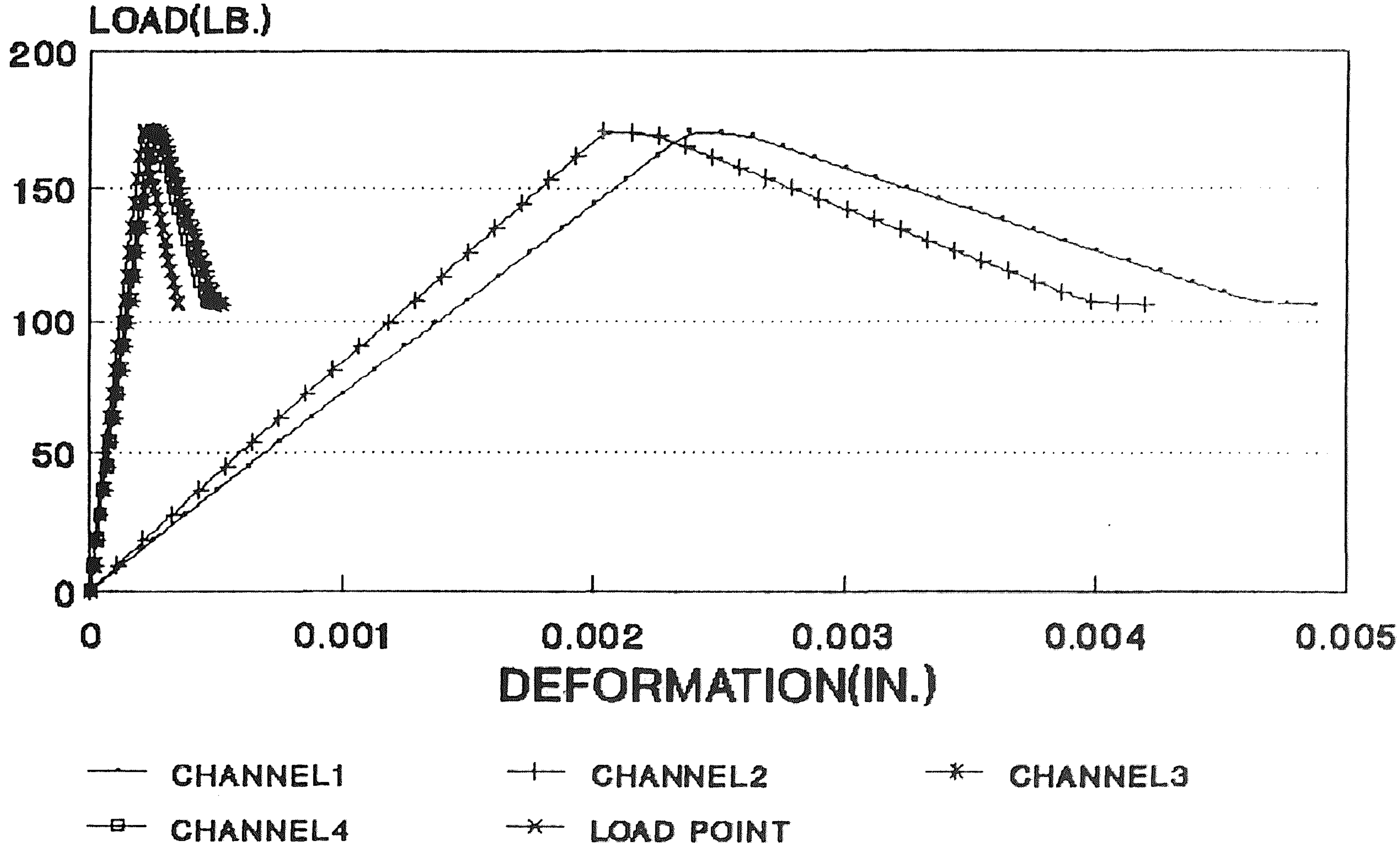

Fig.88 Internal deformation for J31

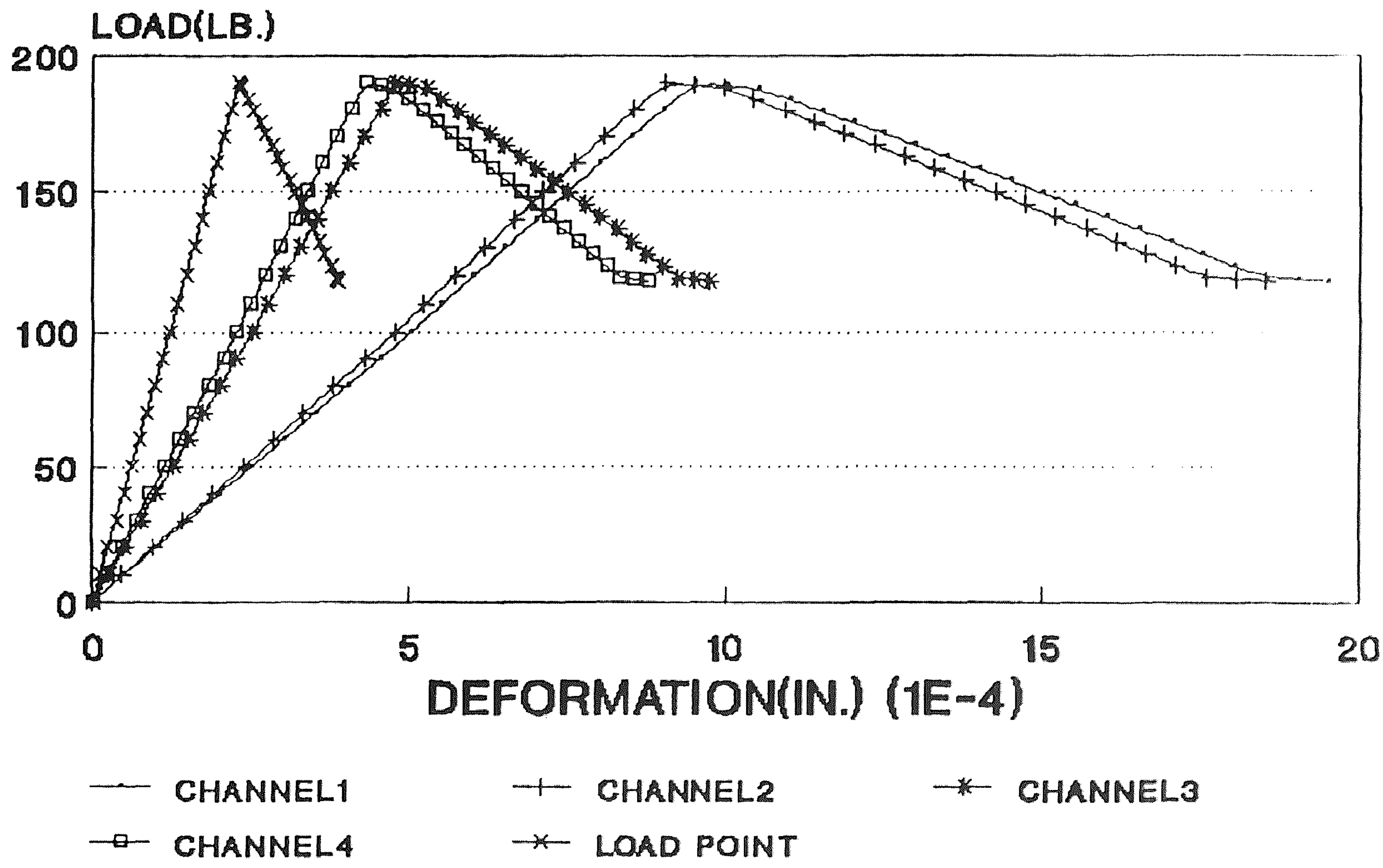

Fig.89 Internal deformation for F2

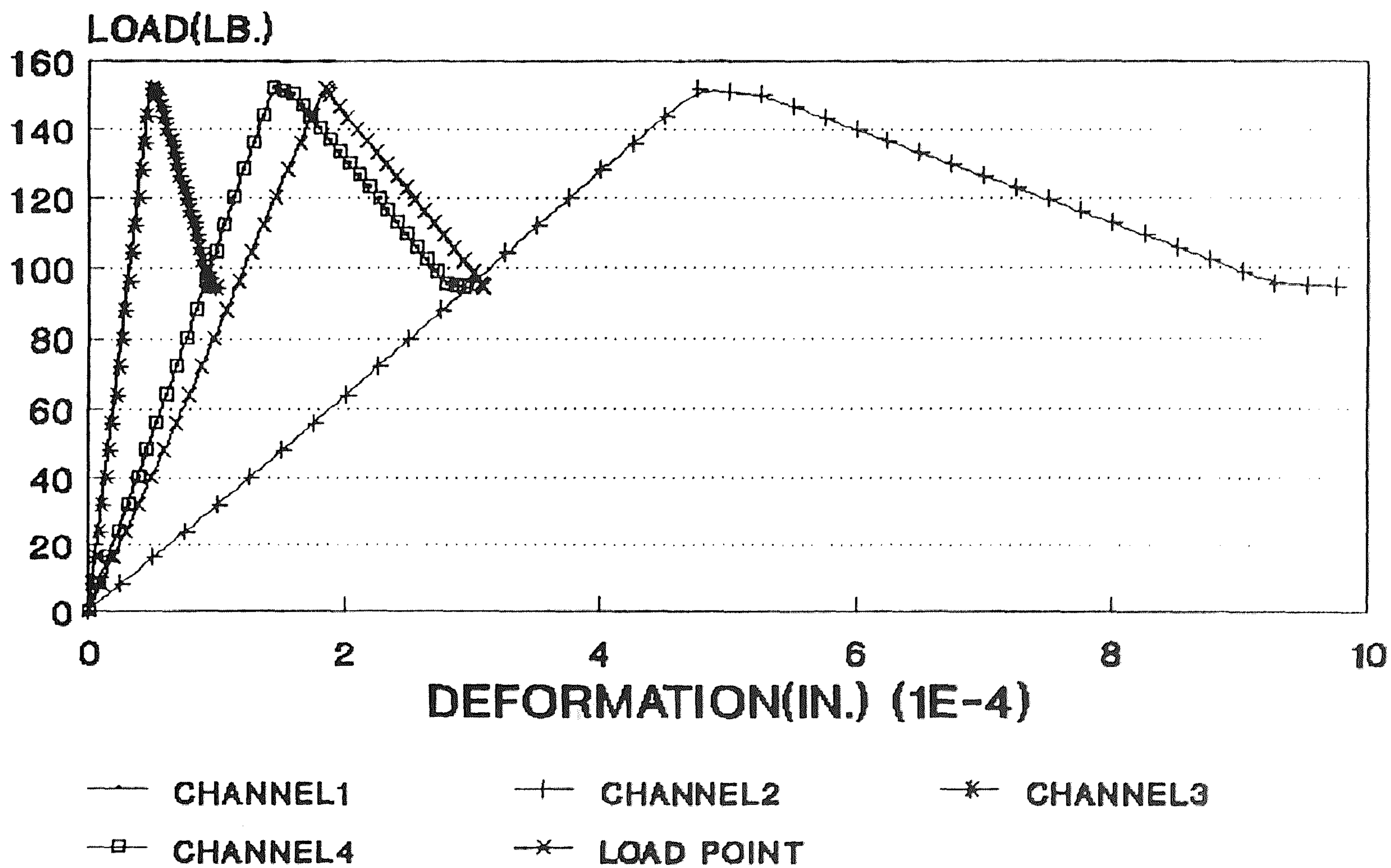

Fig.90 Internal deformation for F[illegible]2

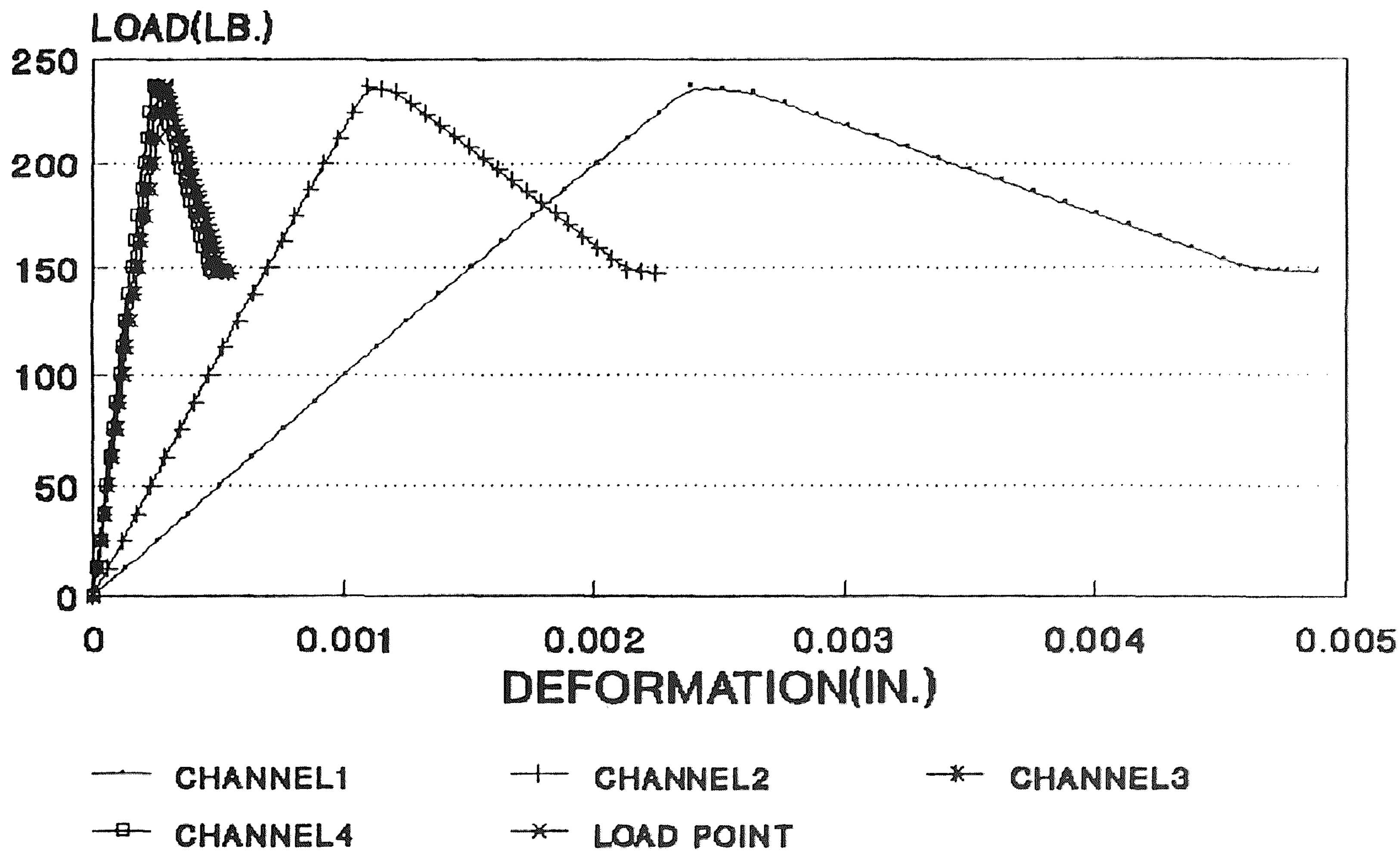

Fig.91 Internal deformation for F

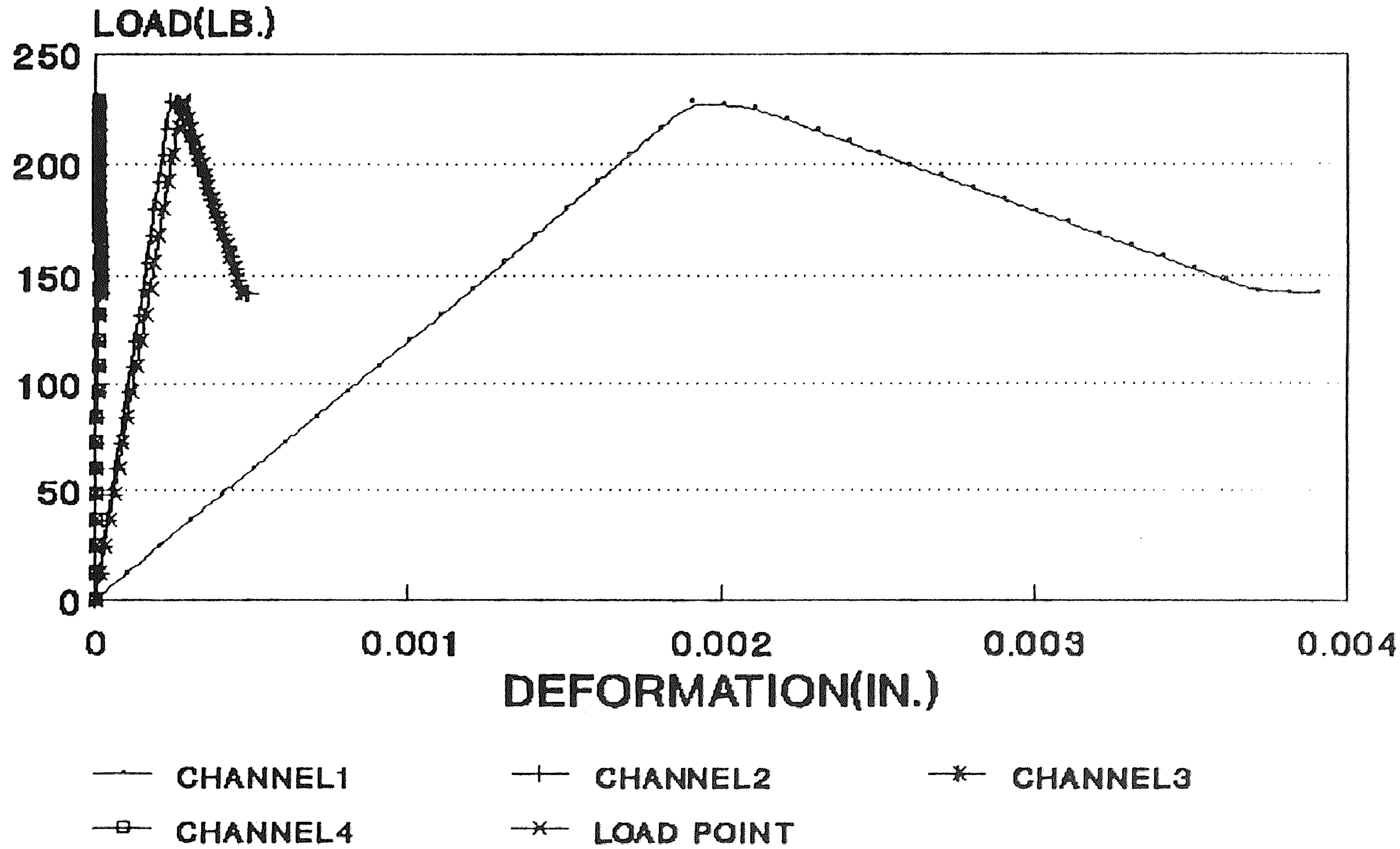

Fig.92 Internal deformation for F11

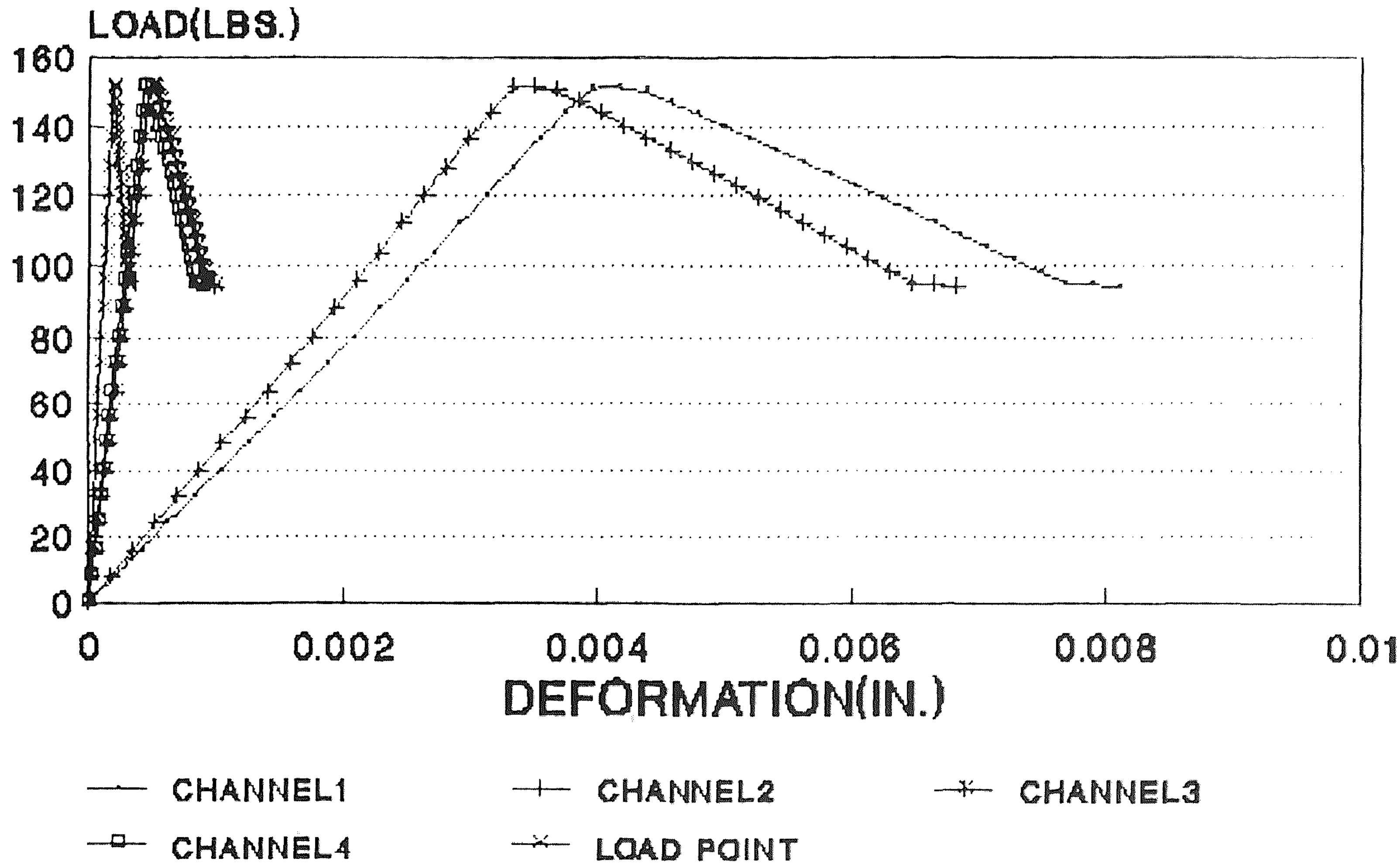

Fig.93 Internal deformation for F12

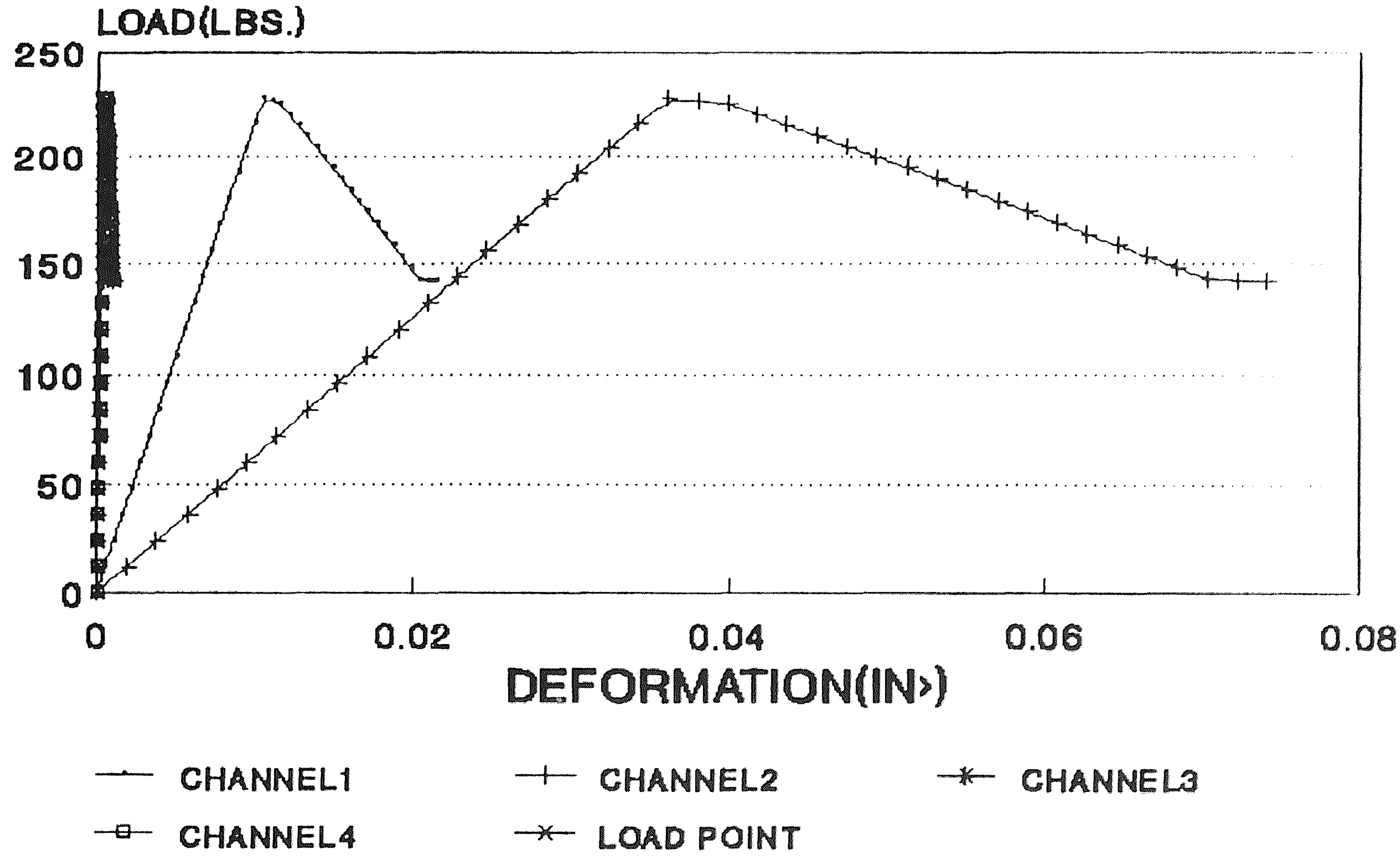

Fig.94 Internal deformation .9B

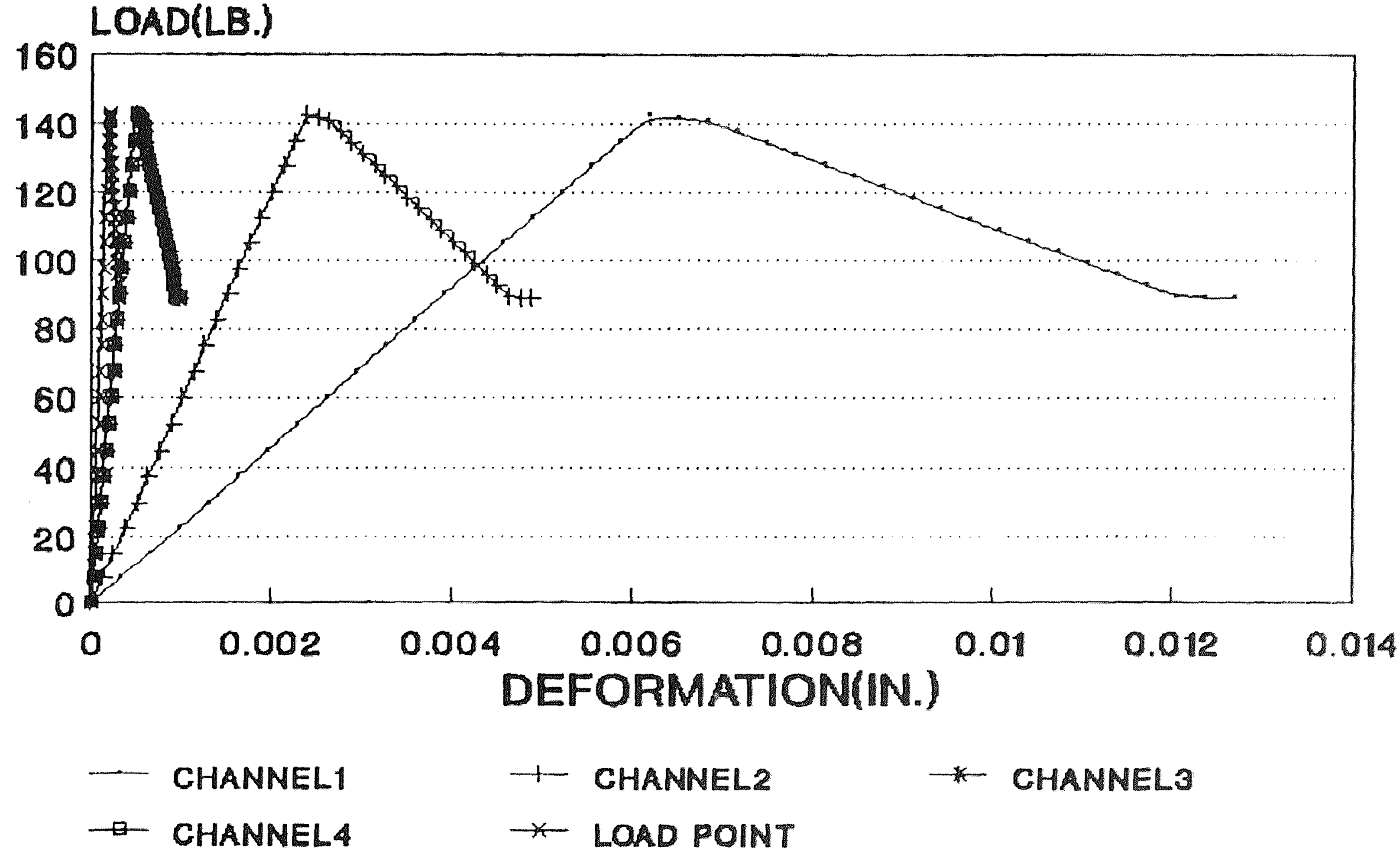

Fig.95 Internal deformation for F19D

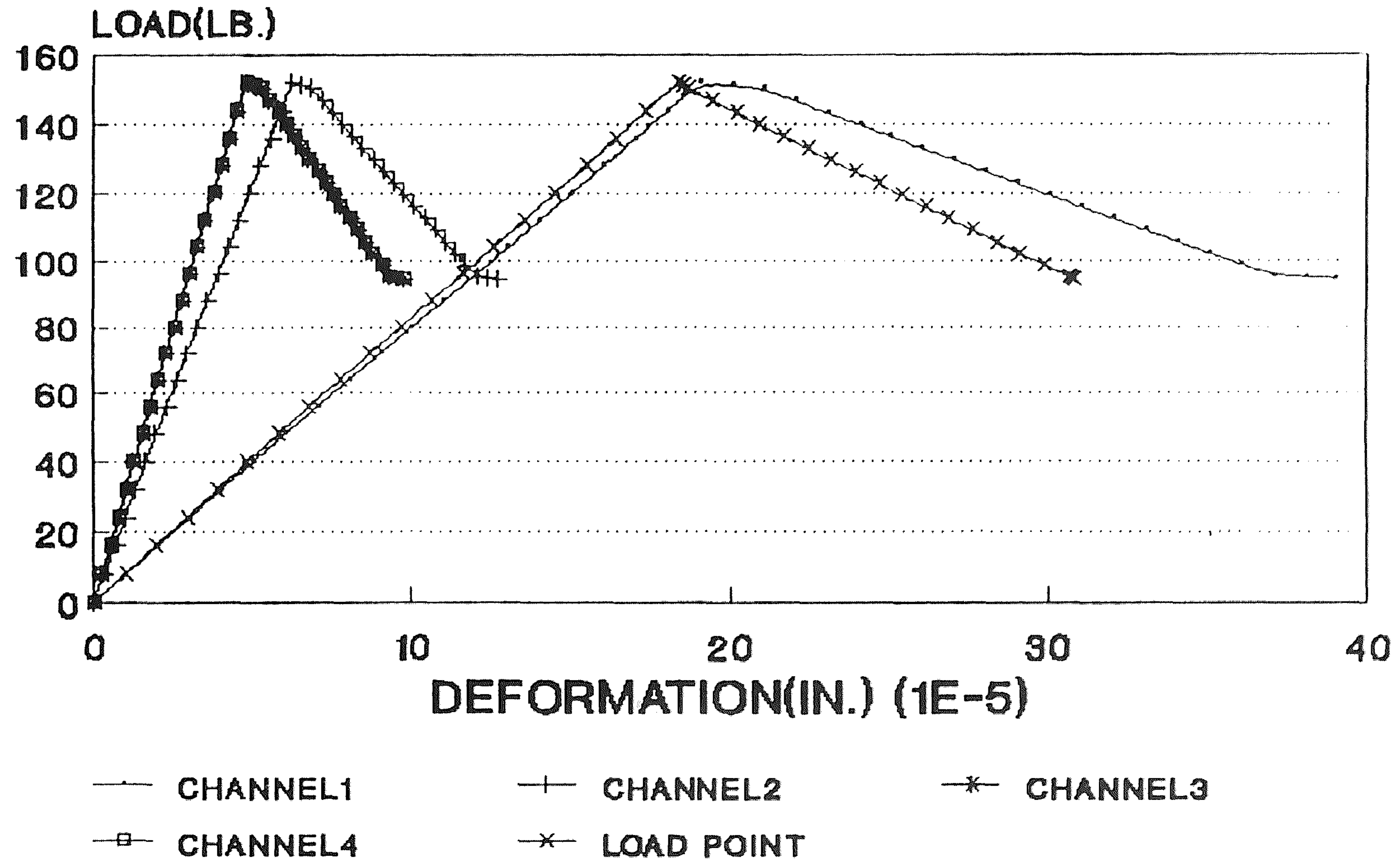

Fig.96 Internal deformation for F28a

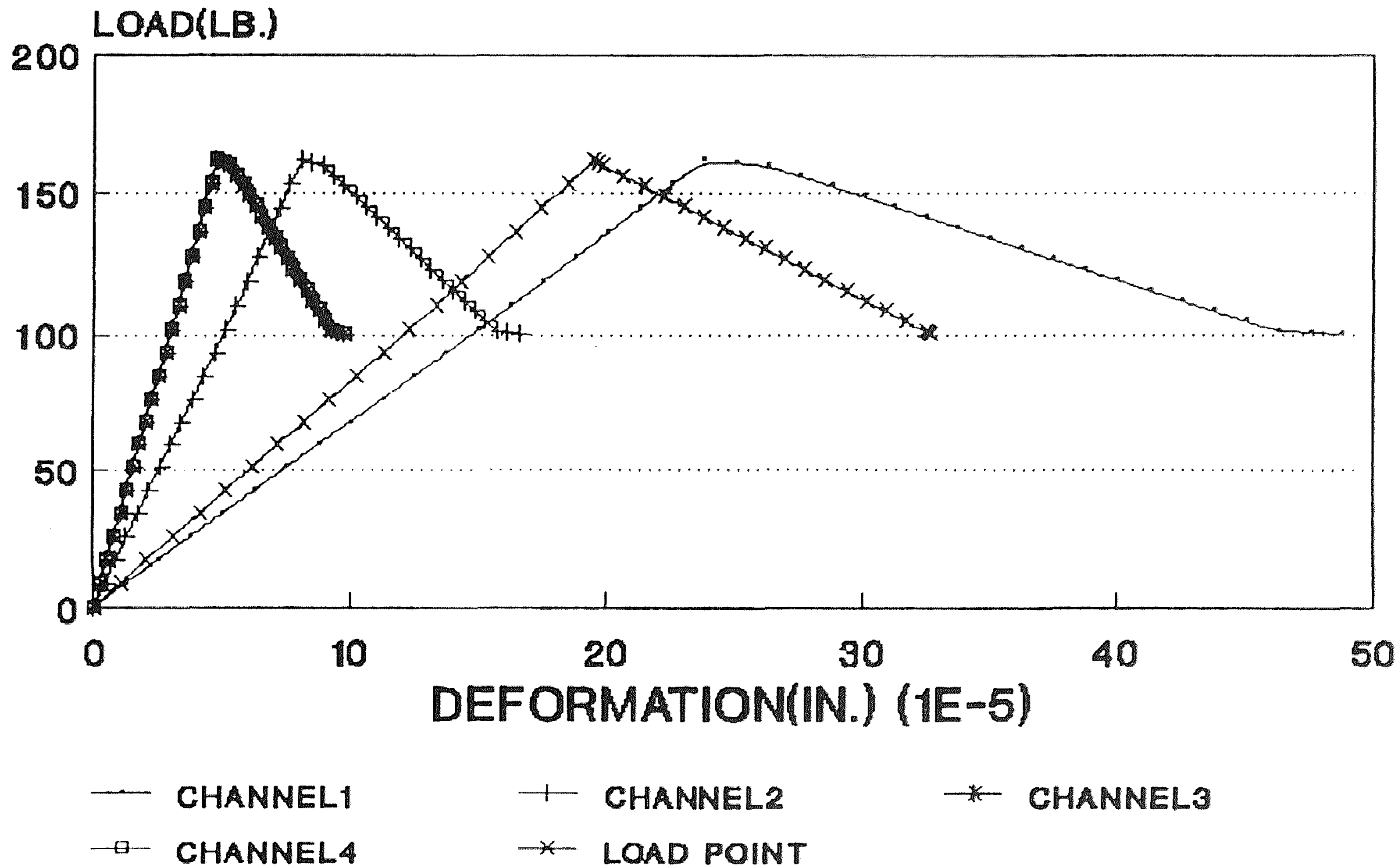

Fig.97 Internal deformation for F28C

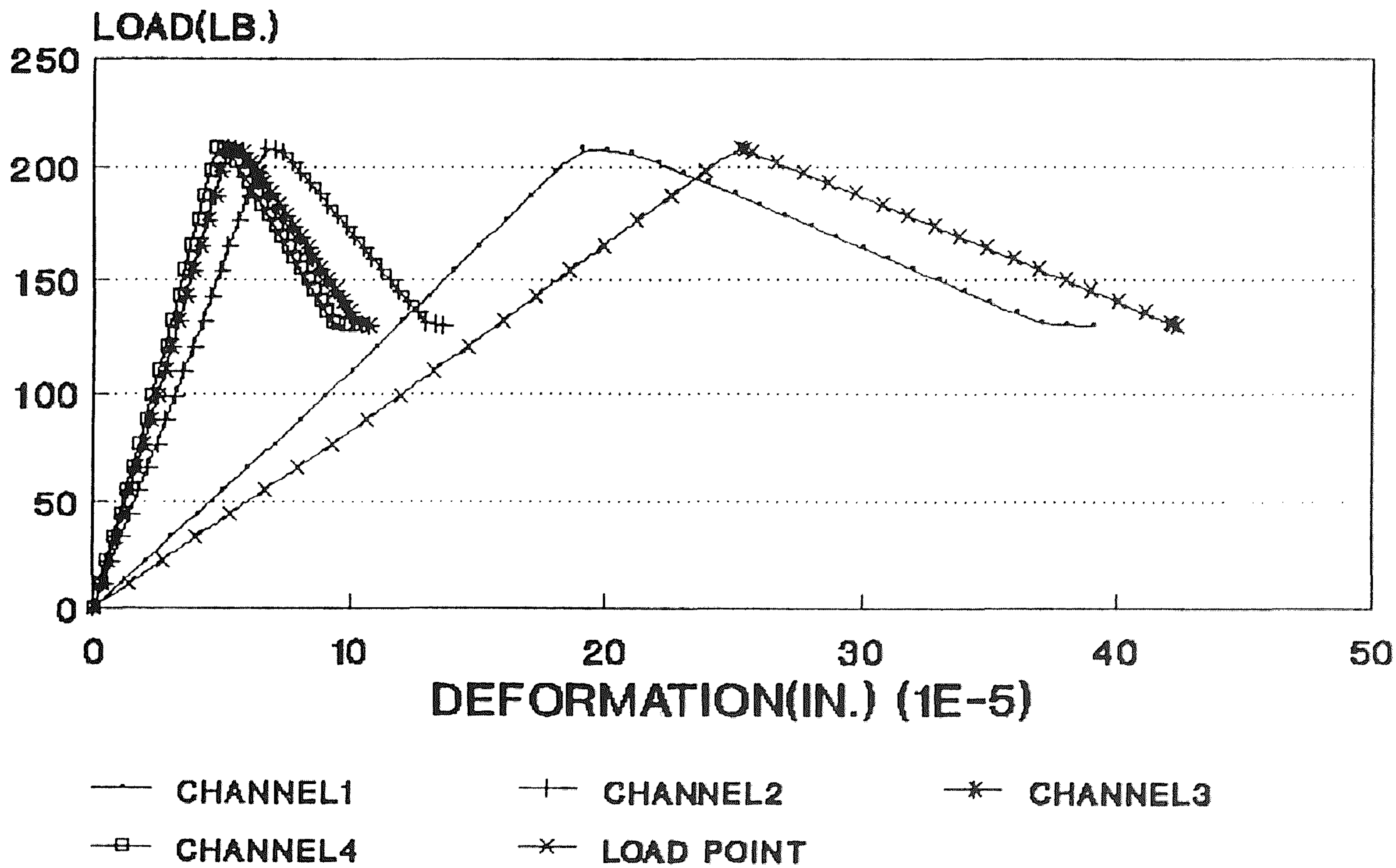

Fig.98 Internal deformation for M1A

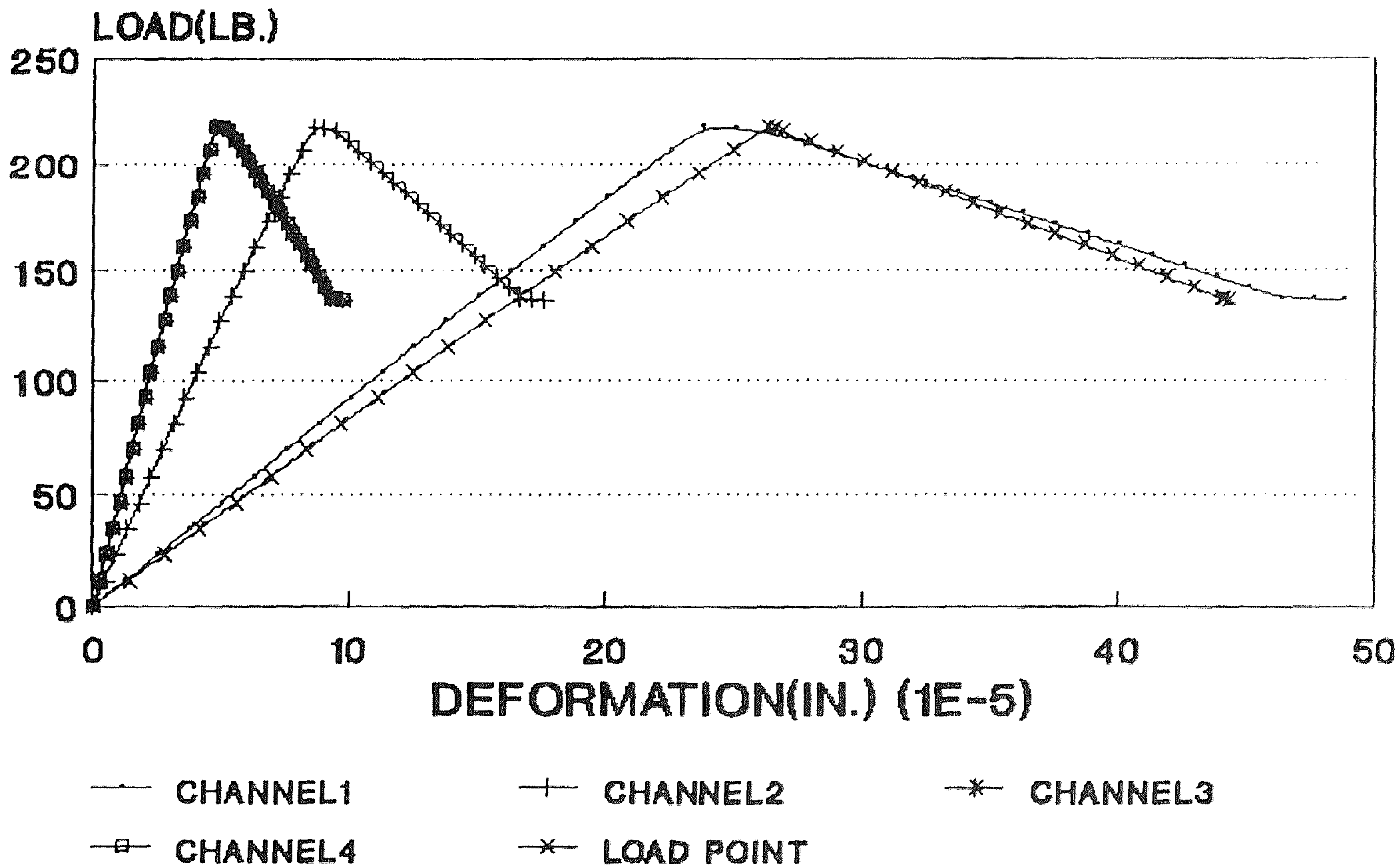

Fig.99 Internal deformation for MB

some of the specimen cracks did not propagate in a straight manner , and therefore did not stretch the fibers.

Fig.100 thru 109 illustrate the deformation pattern at different load intervals for each one of the specimen tested. As indicated in these figures , COD values in almost all cases were considerably much larger than all the other deformations. For this reason , in another set of figures (110 thru 119) ,internal deformation patterns are compared separately. Results shown in Fig.110 thru 119 indicate that the critical cracking zone in compact tension is approximately 1.7 inchs , whereas in the three point bend specimen is about 1.2 inchs.

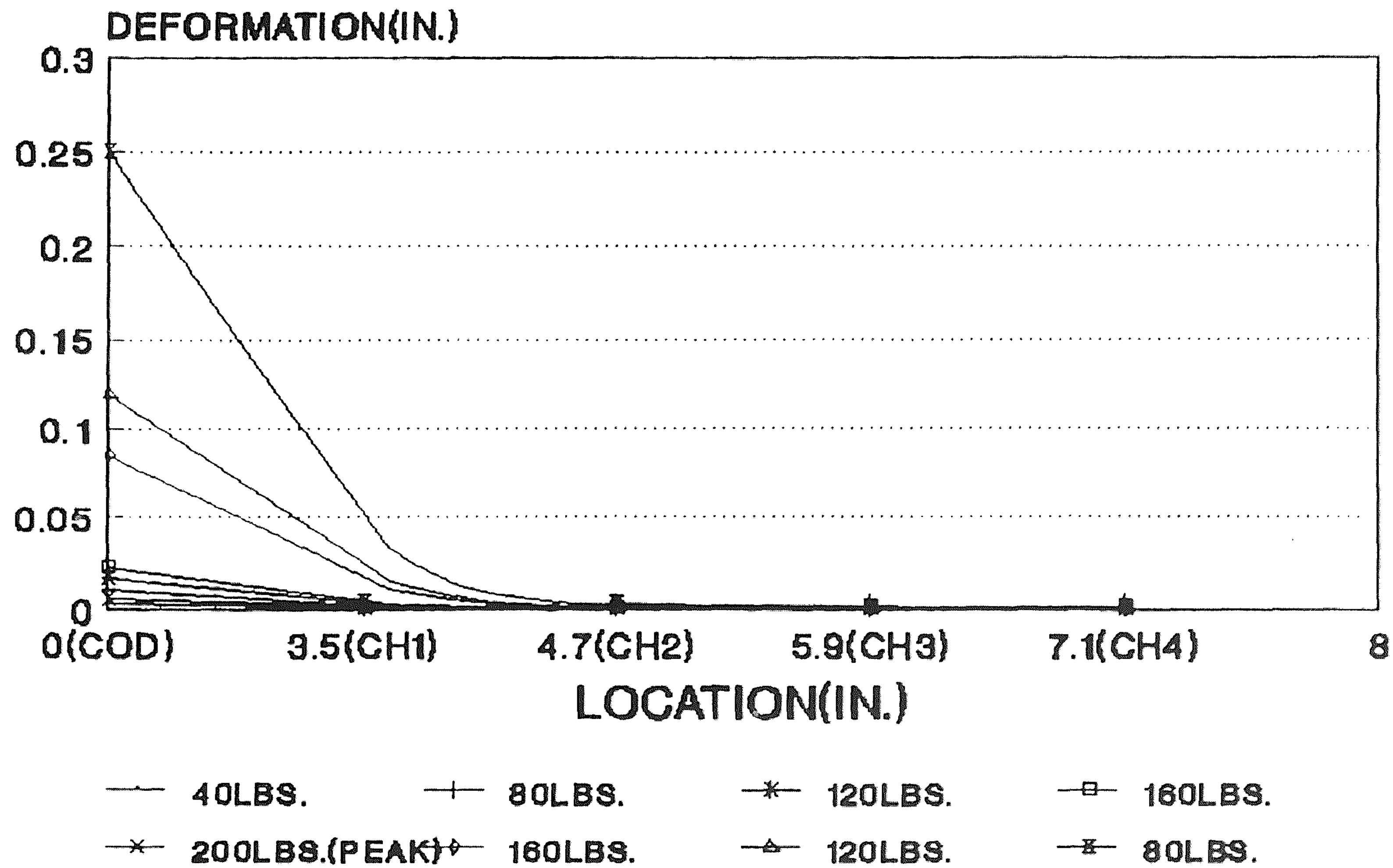

Fig.100 Defor. pattern at diff. load F2

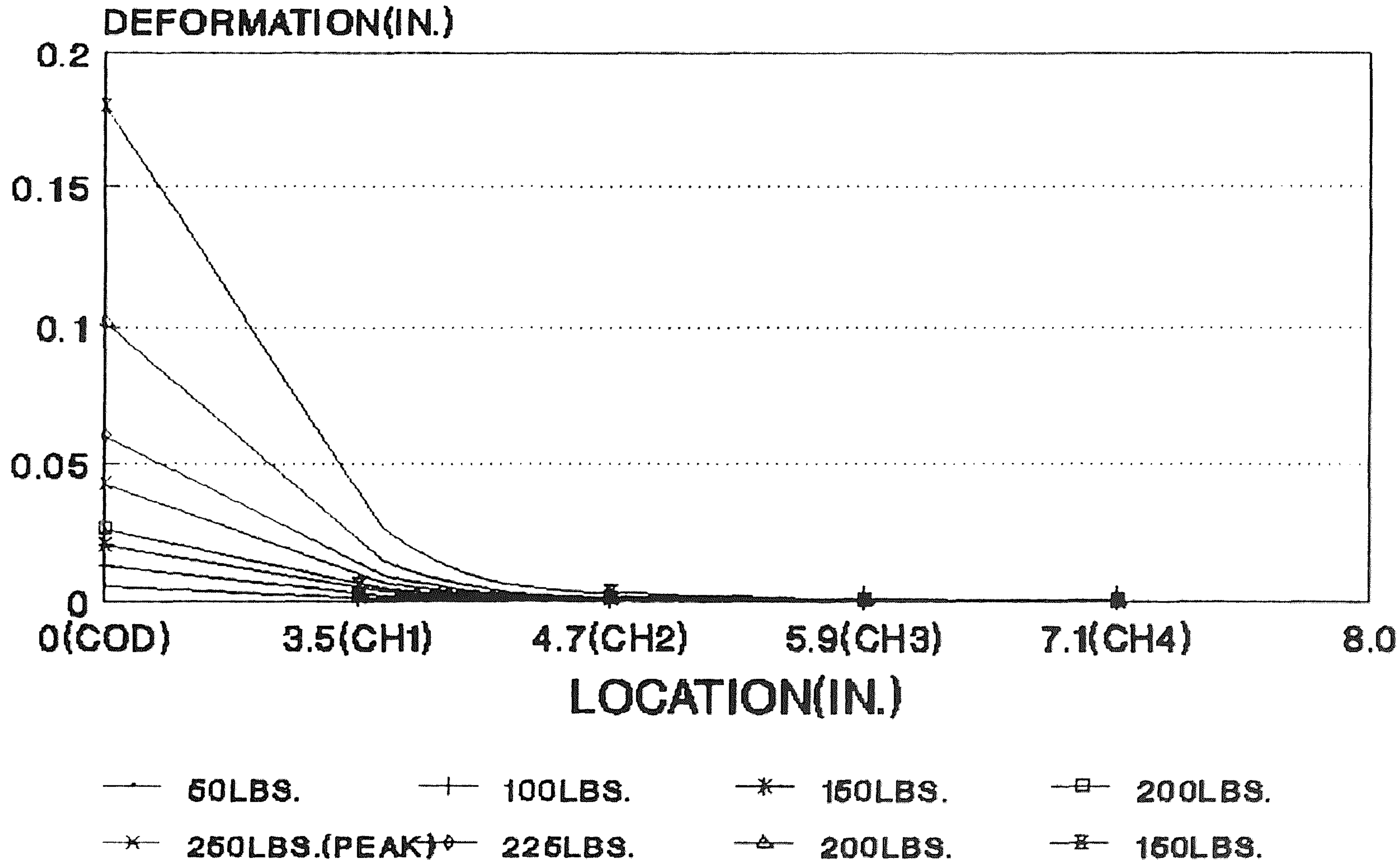

Fig.101 Defor. pattern at diff. load F8

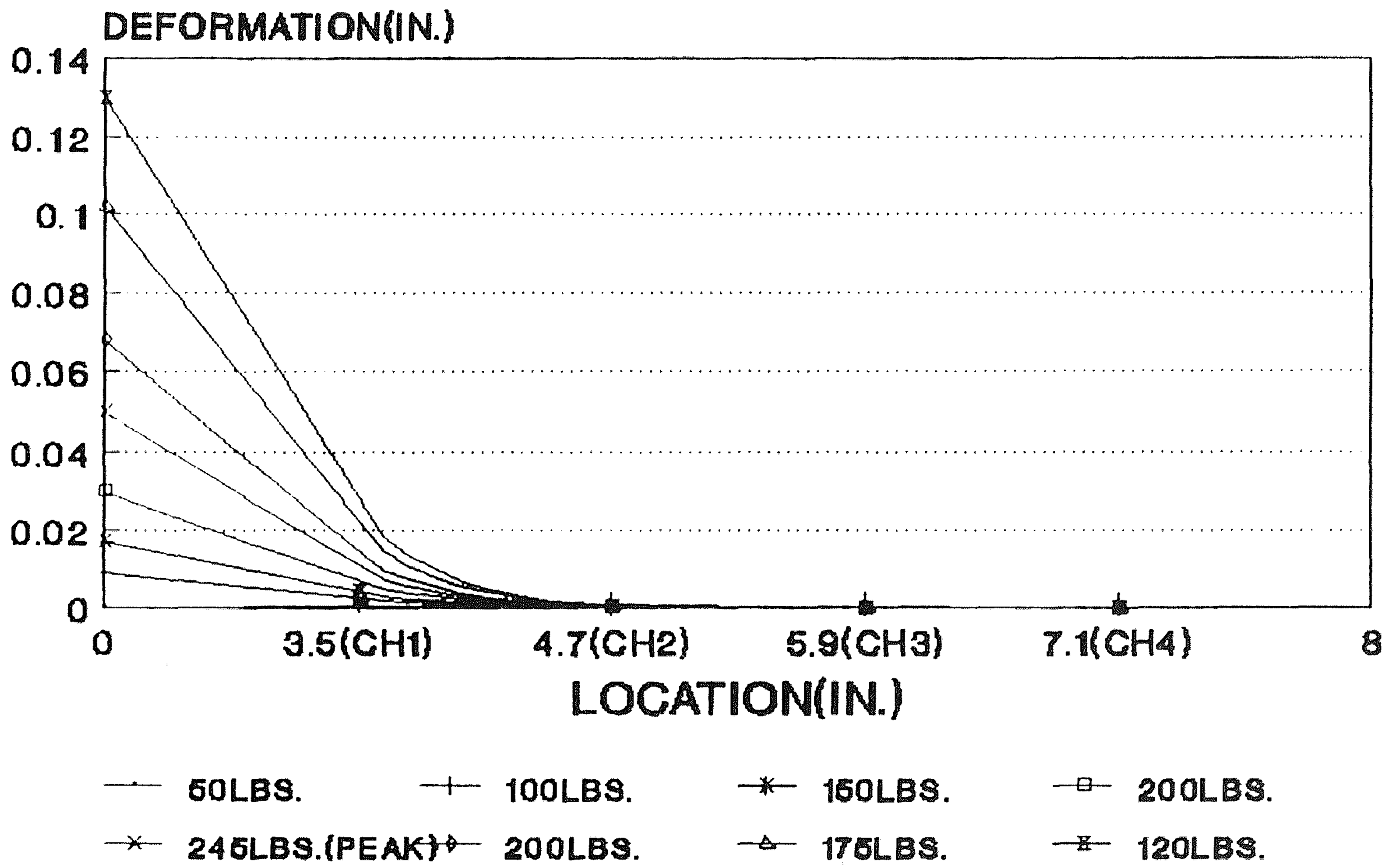

Fig.102 Defor. pattern at diff. load F11

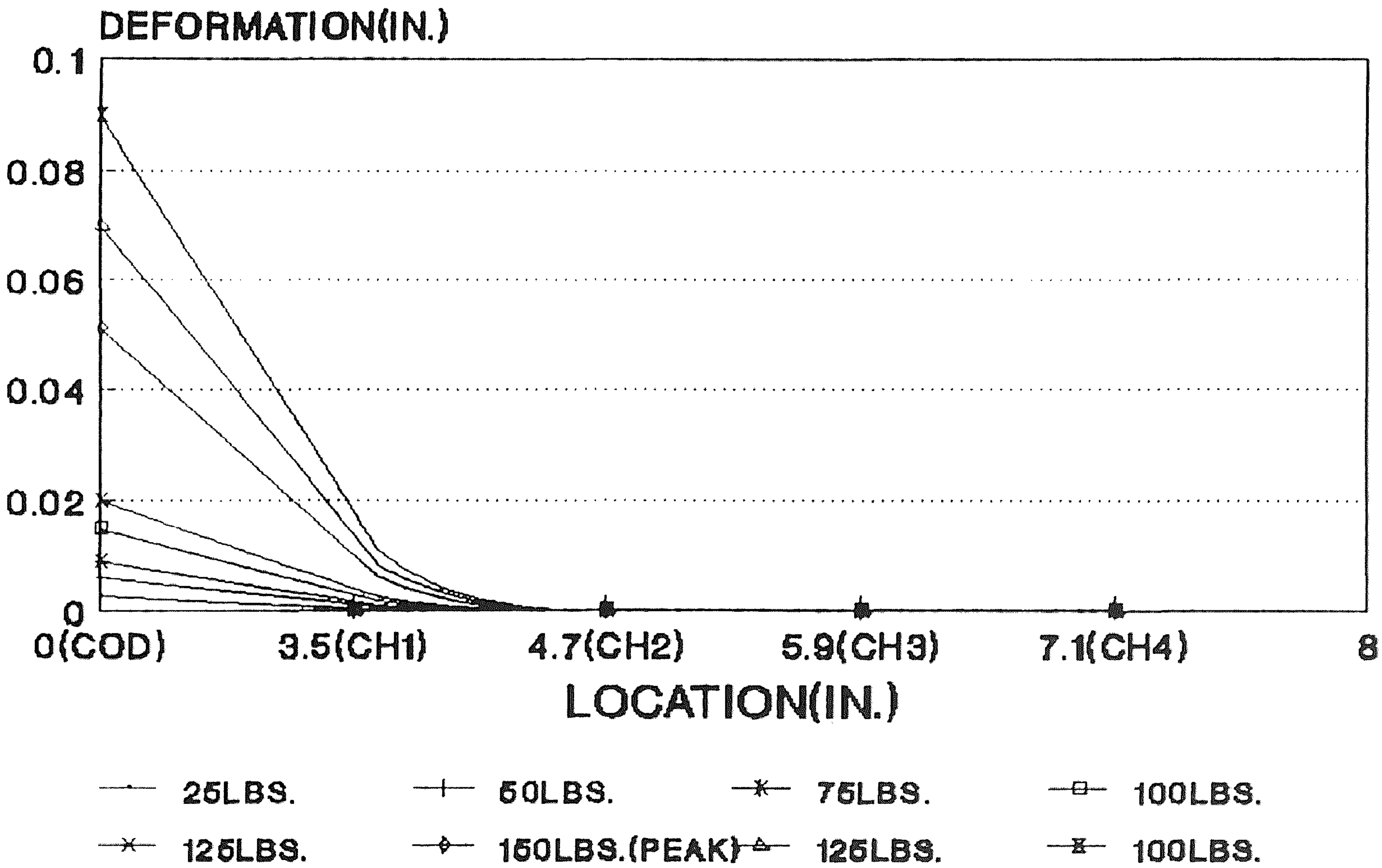

Fig.103 Defor. pattern at diff. load F12

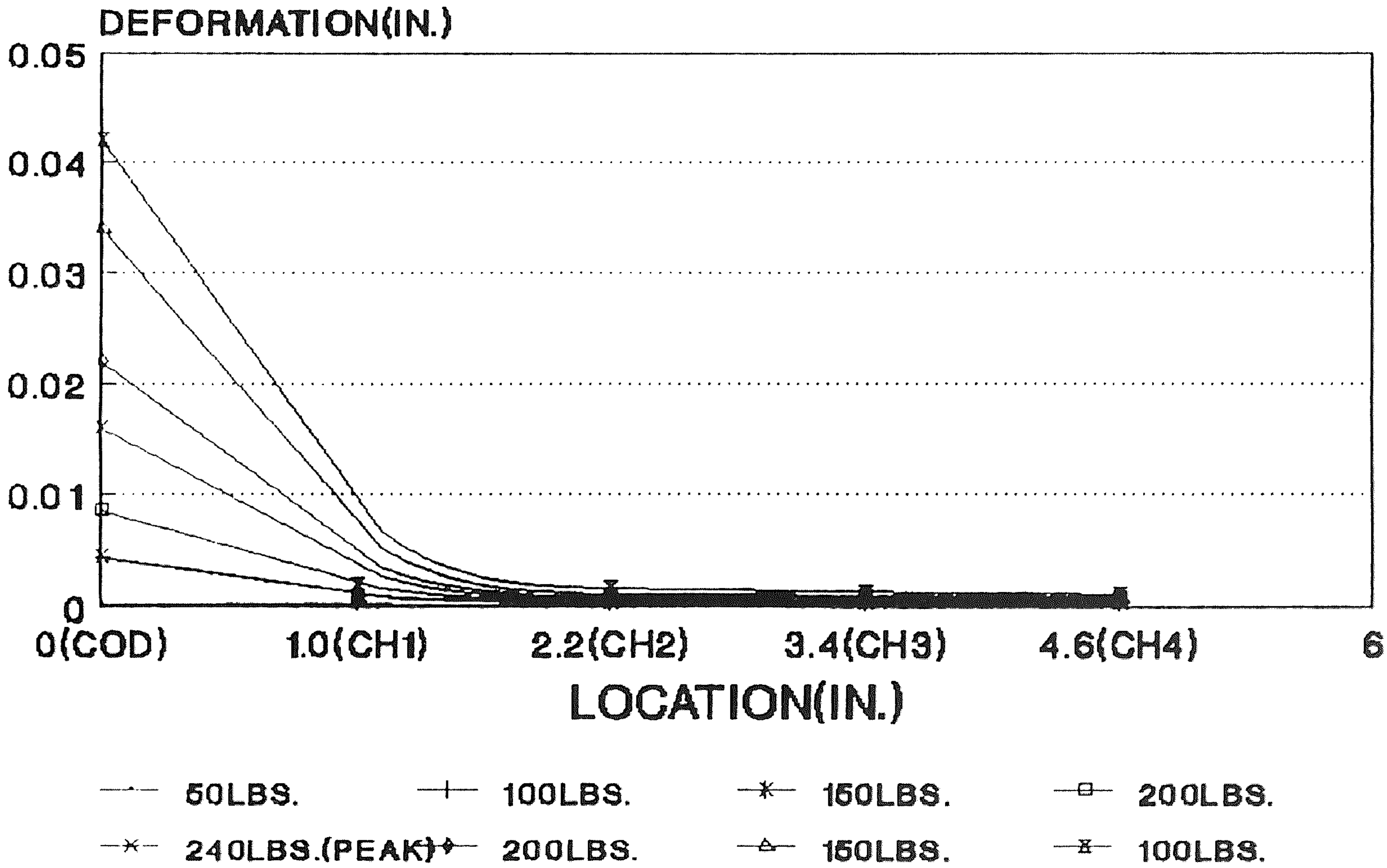

Fig.104 Defor. pattern at diff. loadF19B

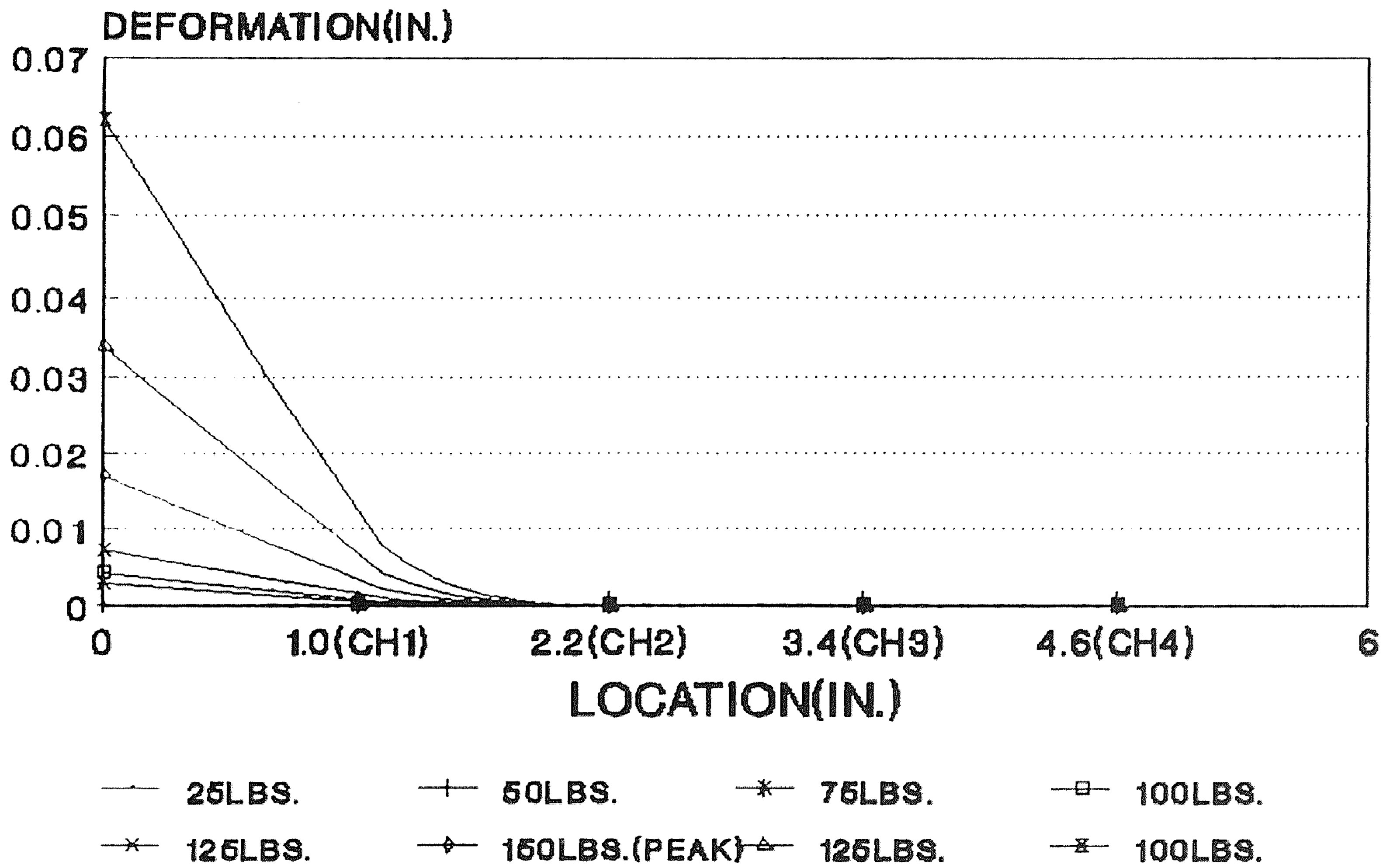

Fig.105 Defor. pattern at diff. loadF19D

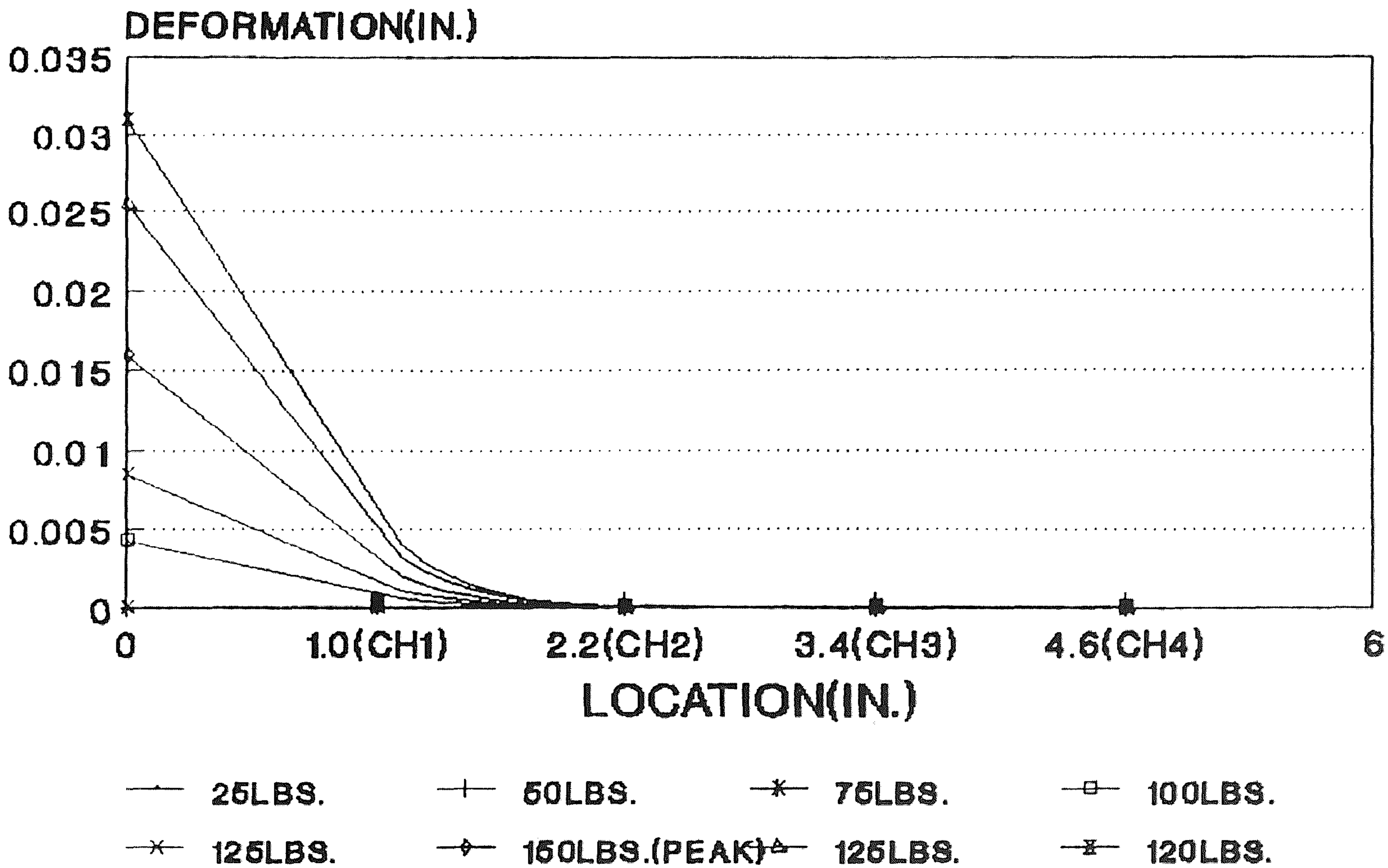

Fig.106 Defor. pattern at diff. loadF28A

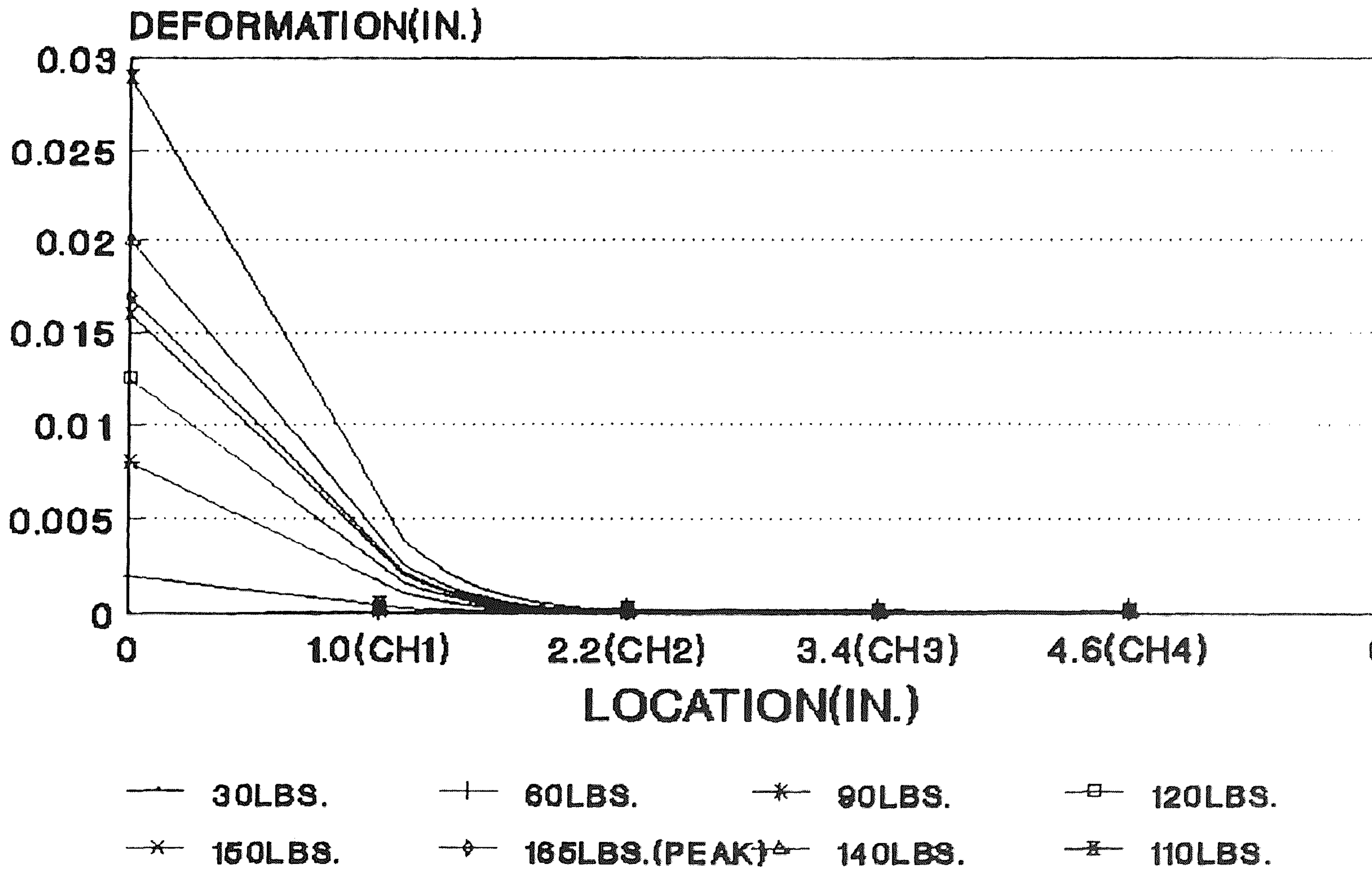

Fig.107 Defor. pattern at diff. loadF28C

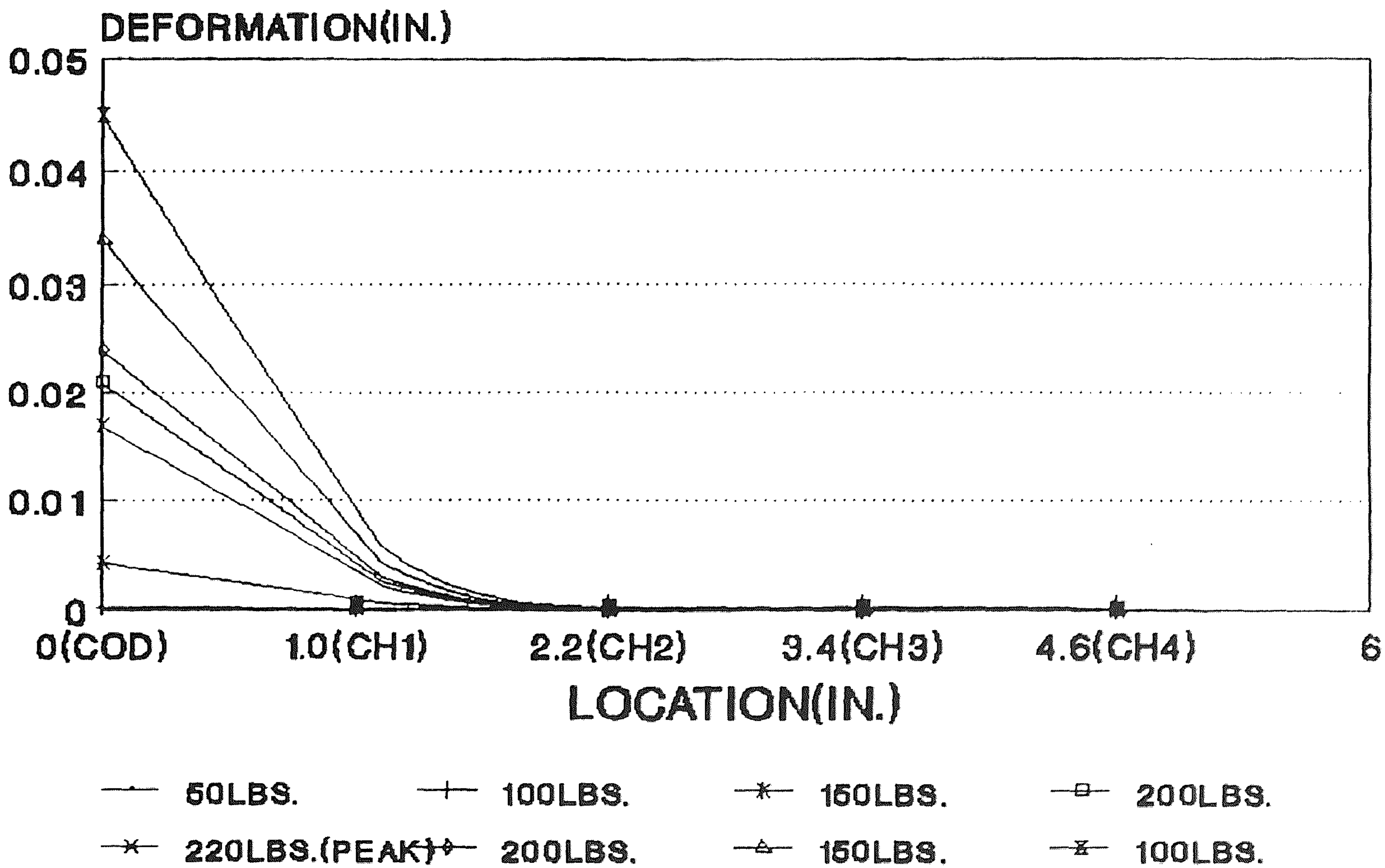

Fig.108 Defor. pattern at diff load M1A

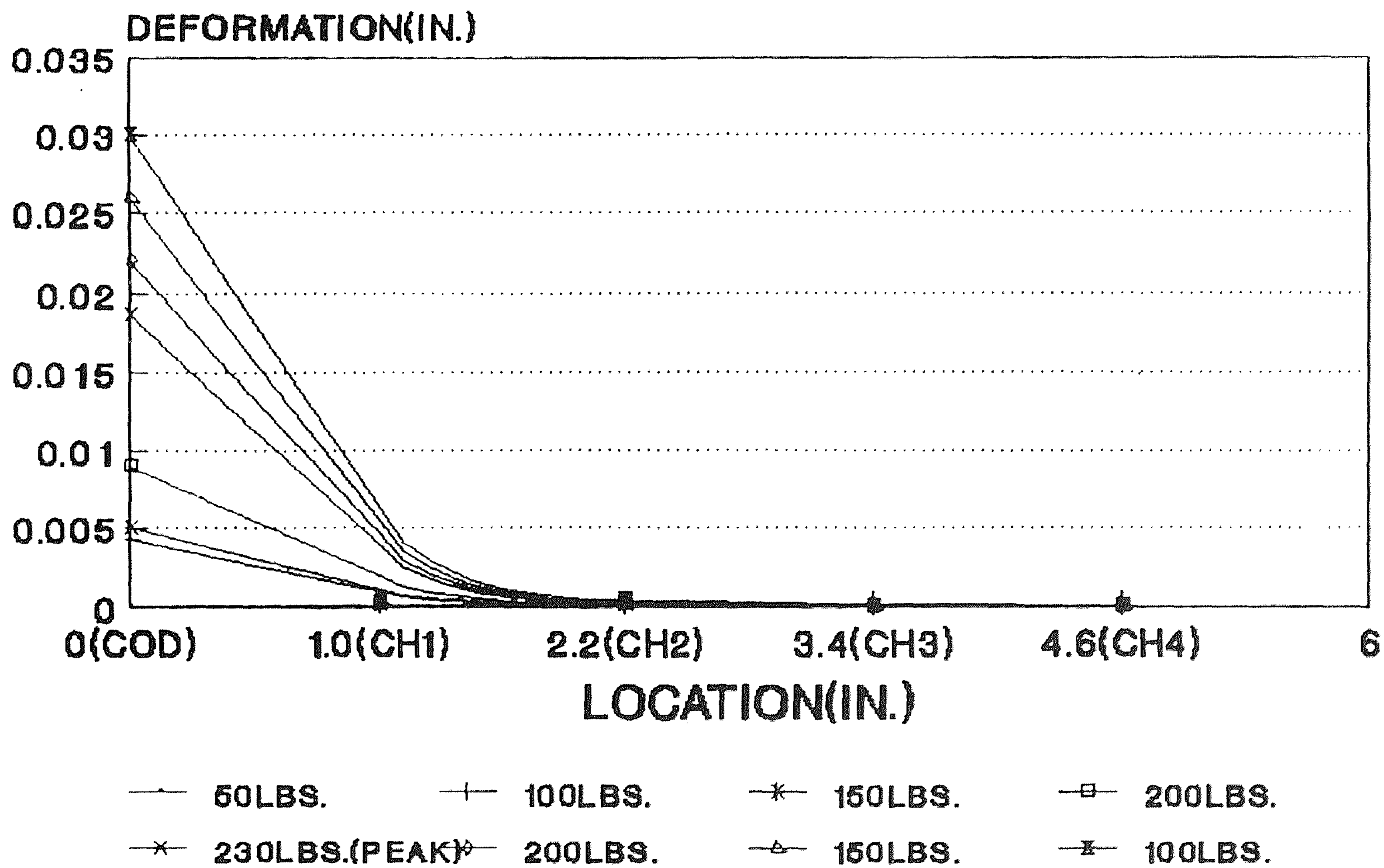

Fig.109 Defor. pattern at diff. load

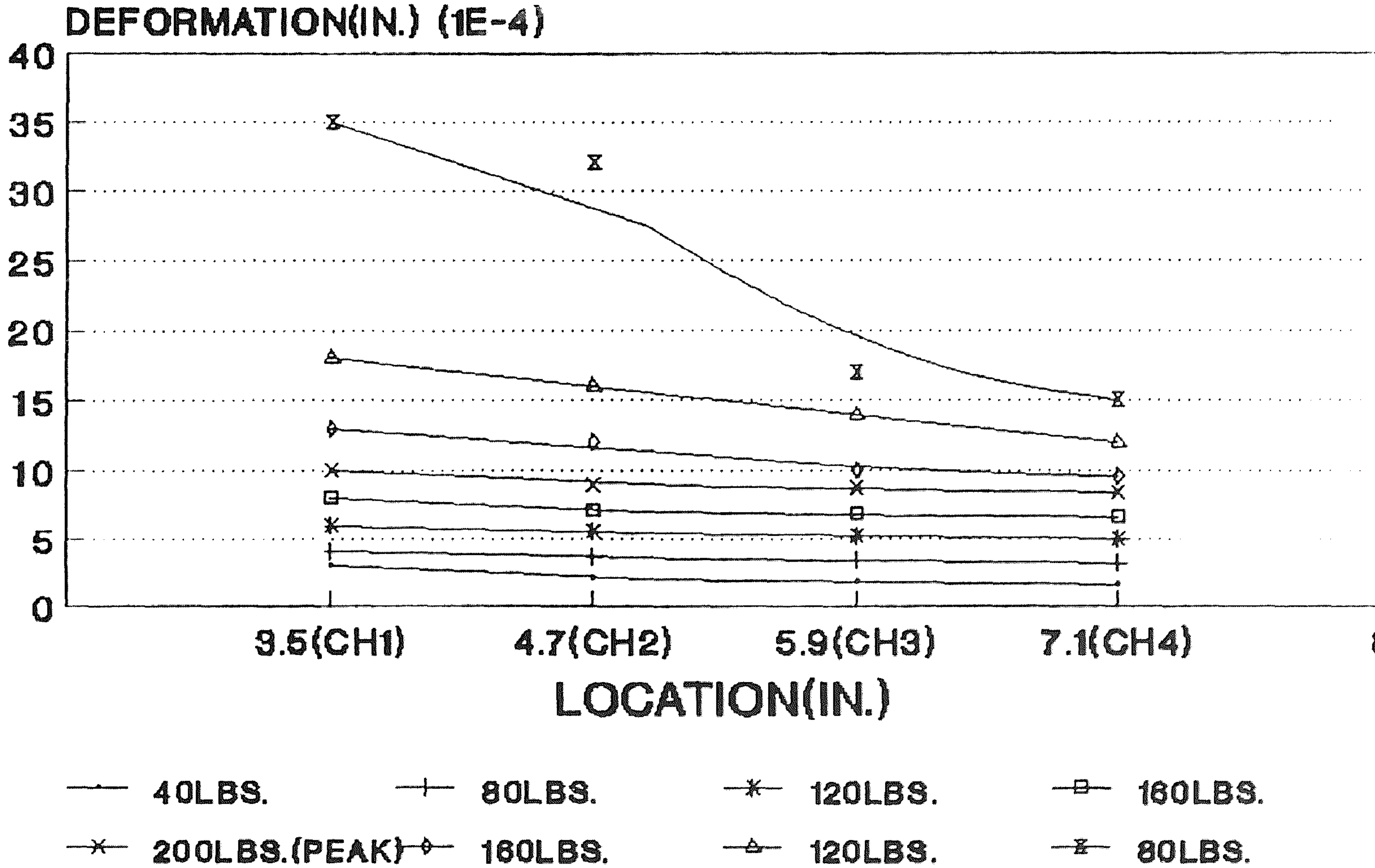

Fig.110 Defor. pattern without C 2

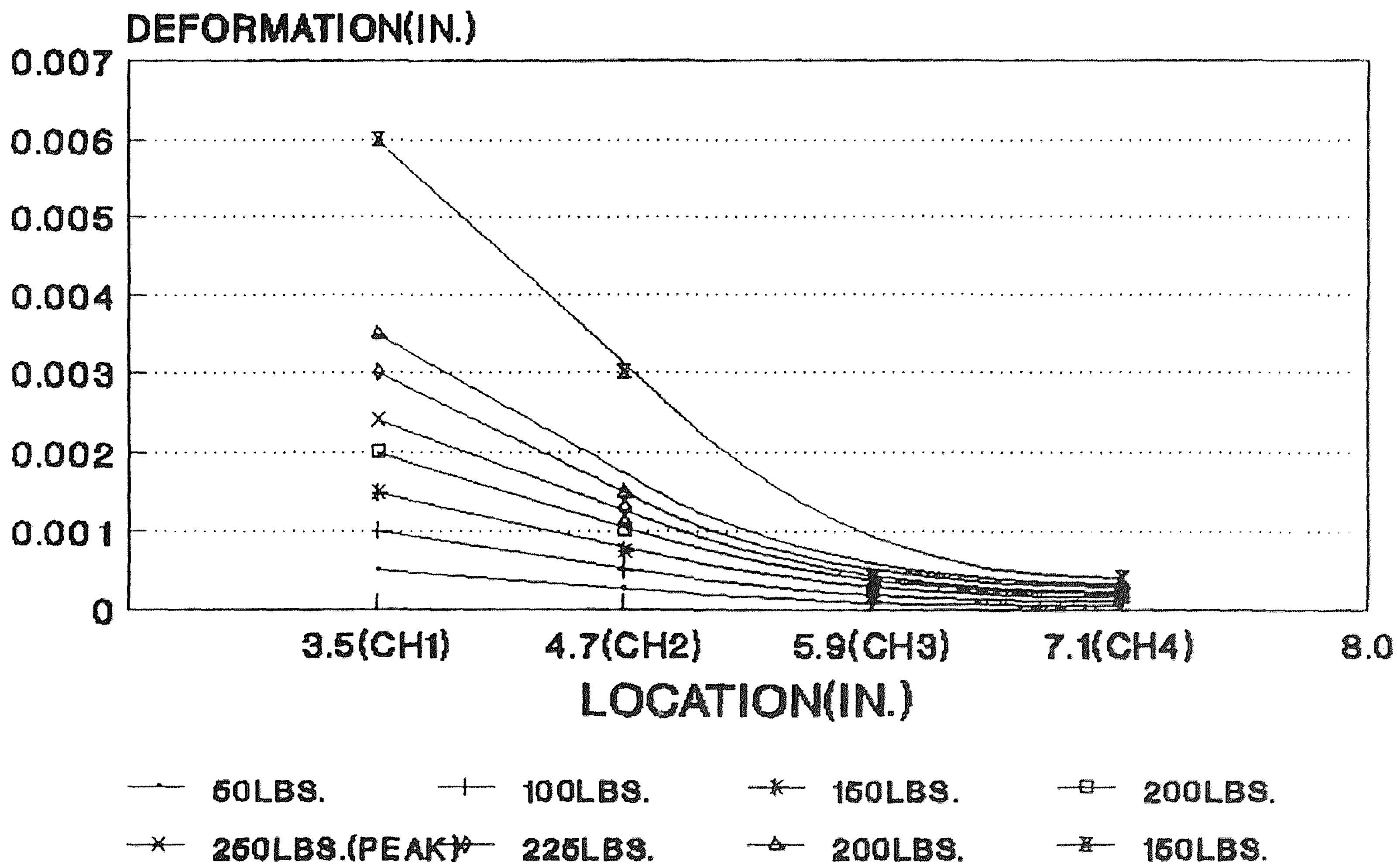

Fig.111 Defor.pattern without COL

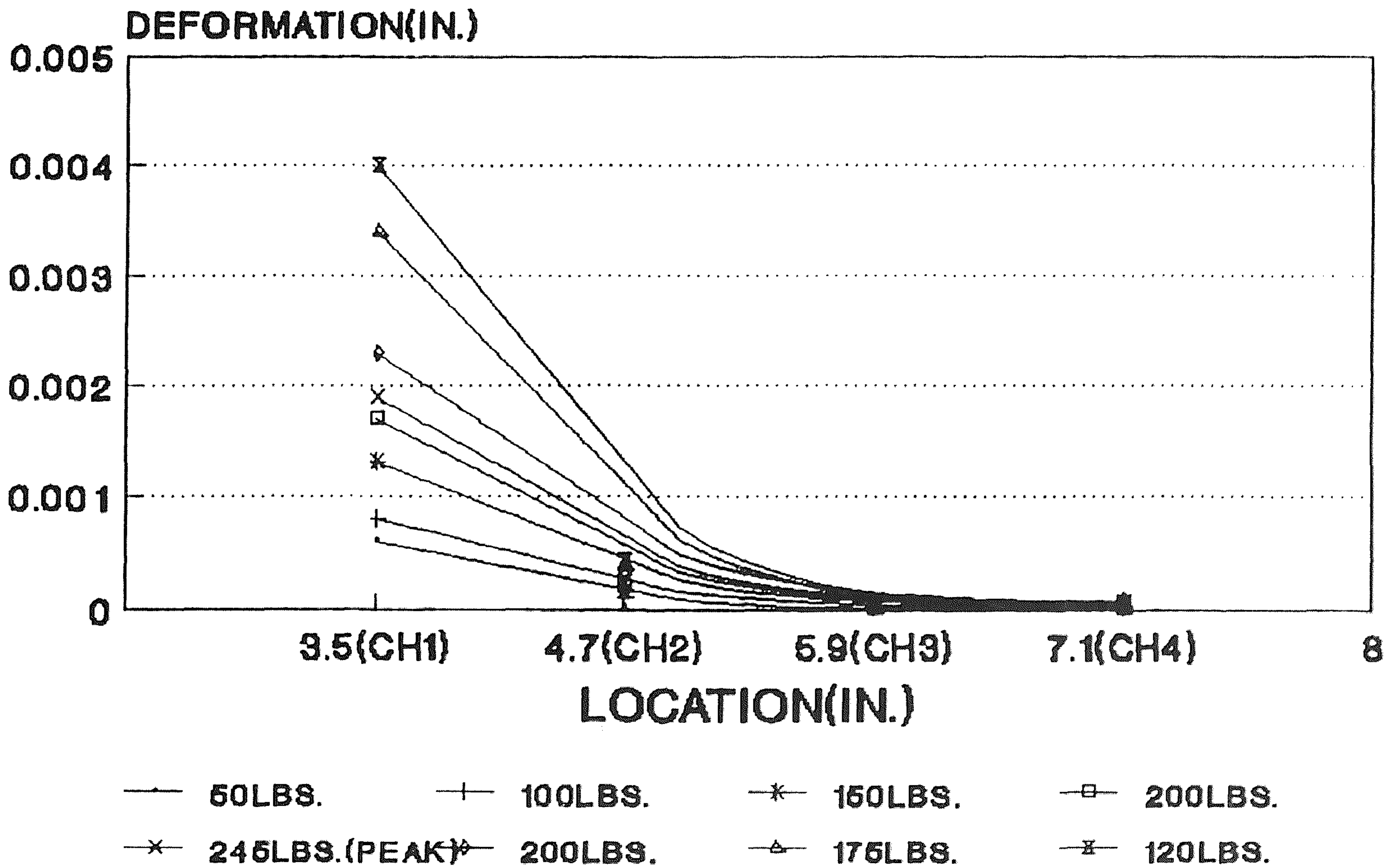

Fig.112 Defor. pattern without COD F11

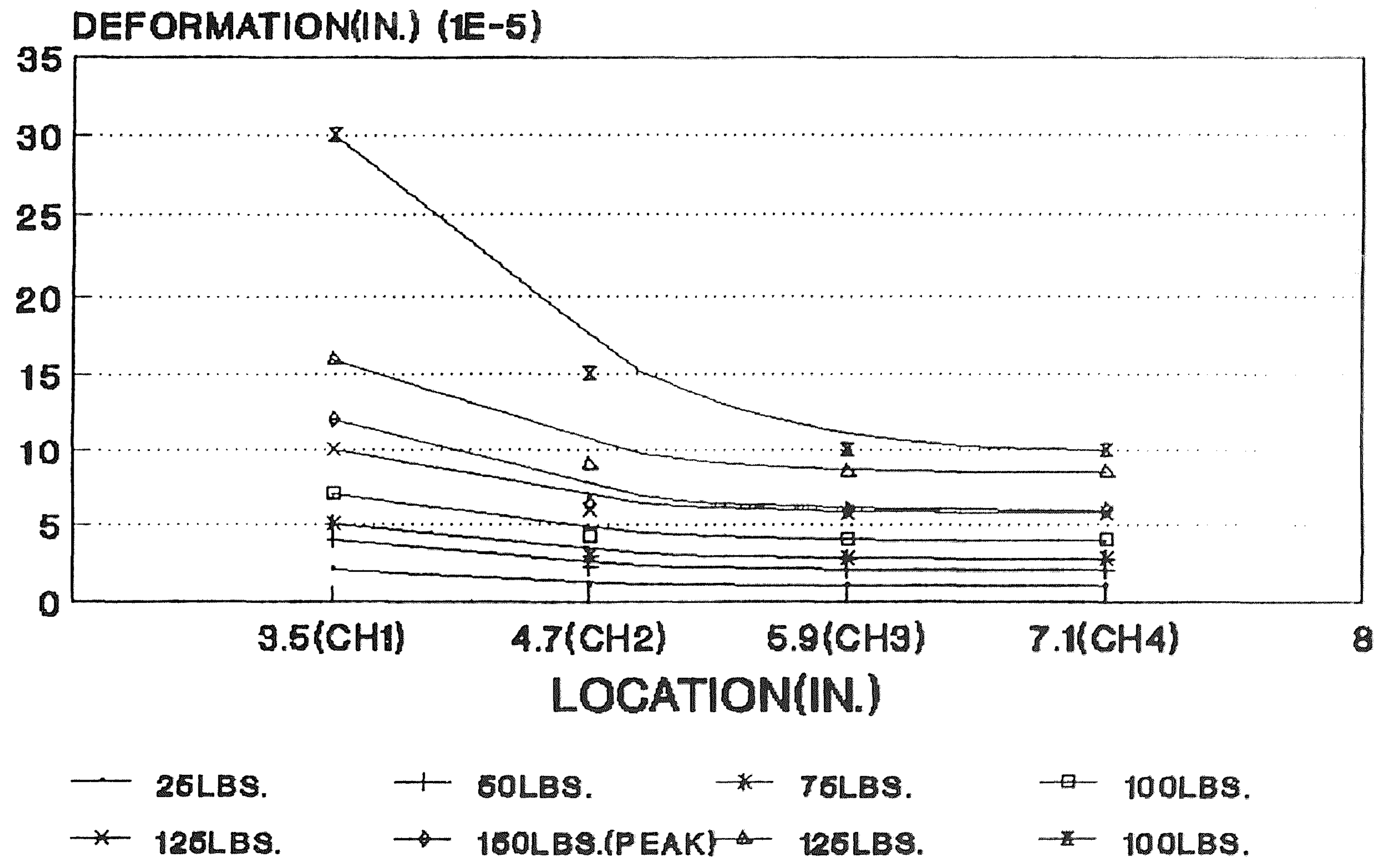

Fig.113 Defor. pattern w COD F12

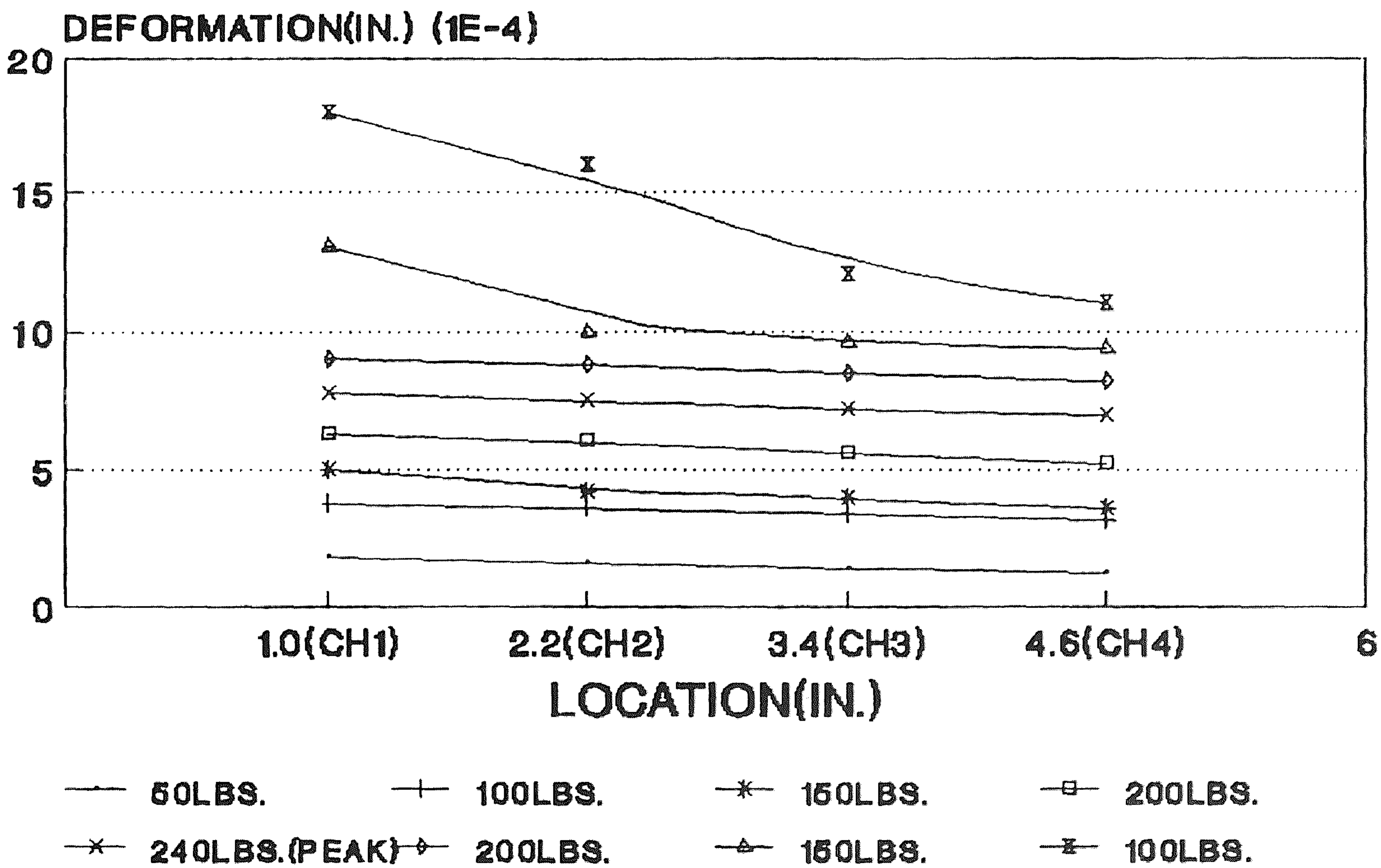

Fig.114 Defor. pattern without CO

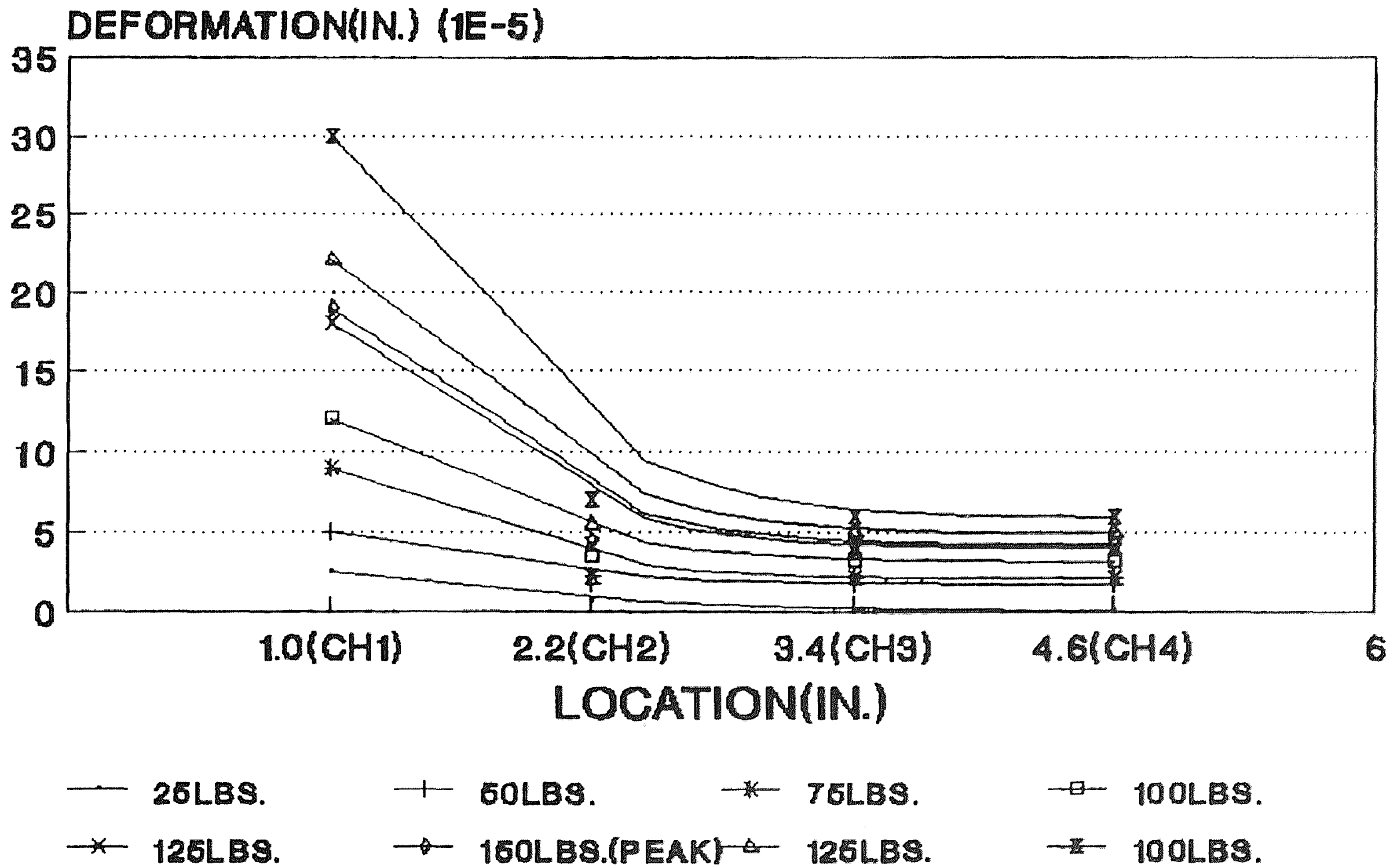

Fig.115 Defor. pattern without CC

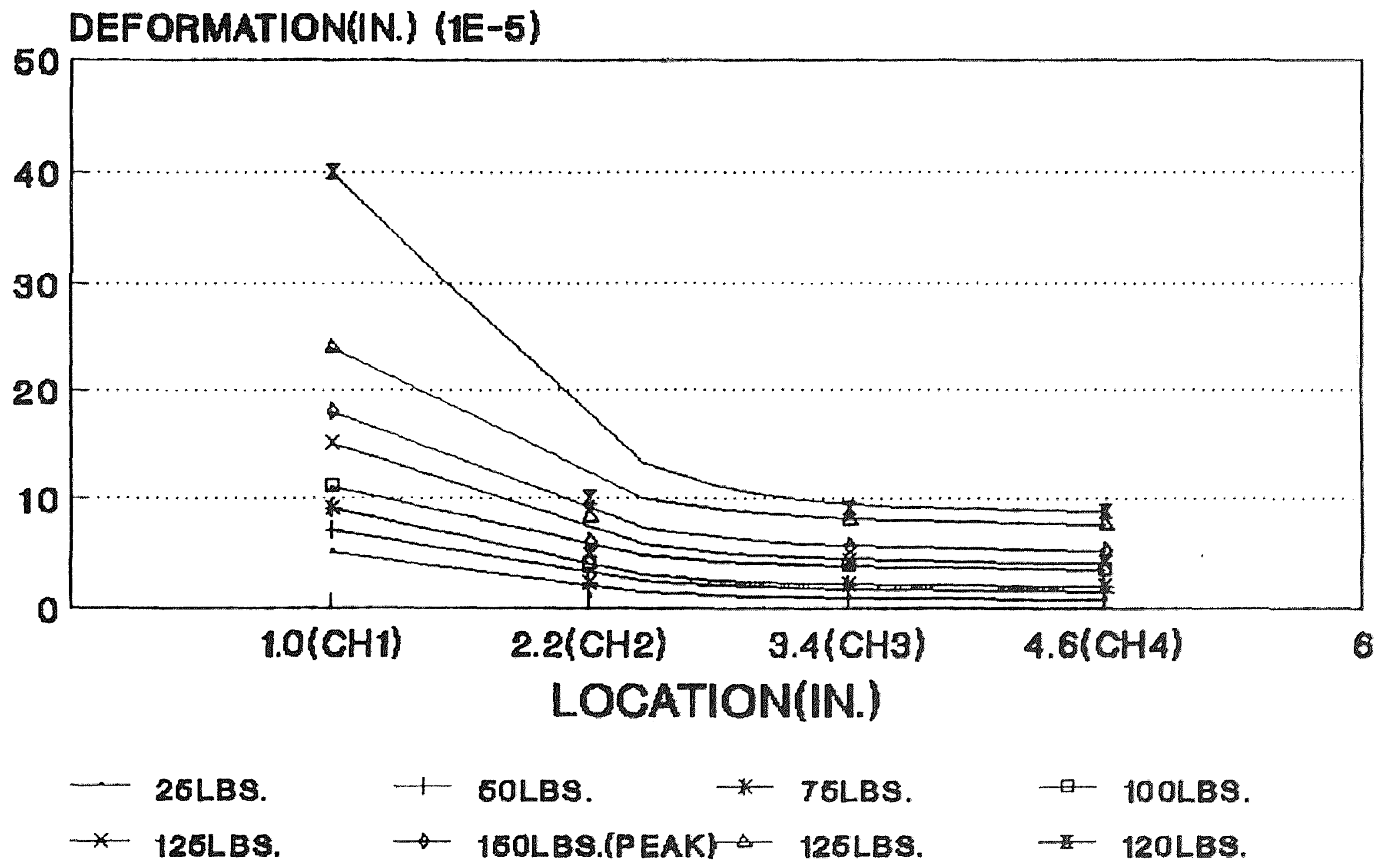

Fig.116 Defor. pattern without COI

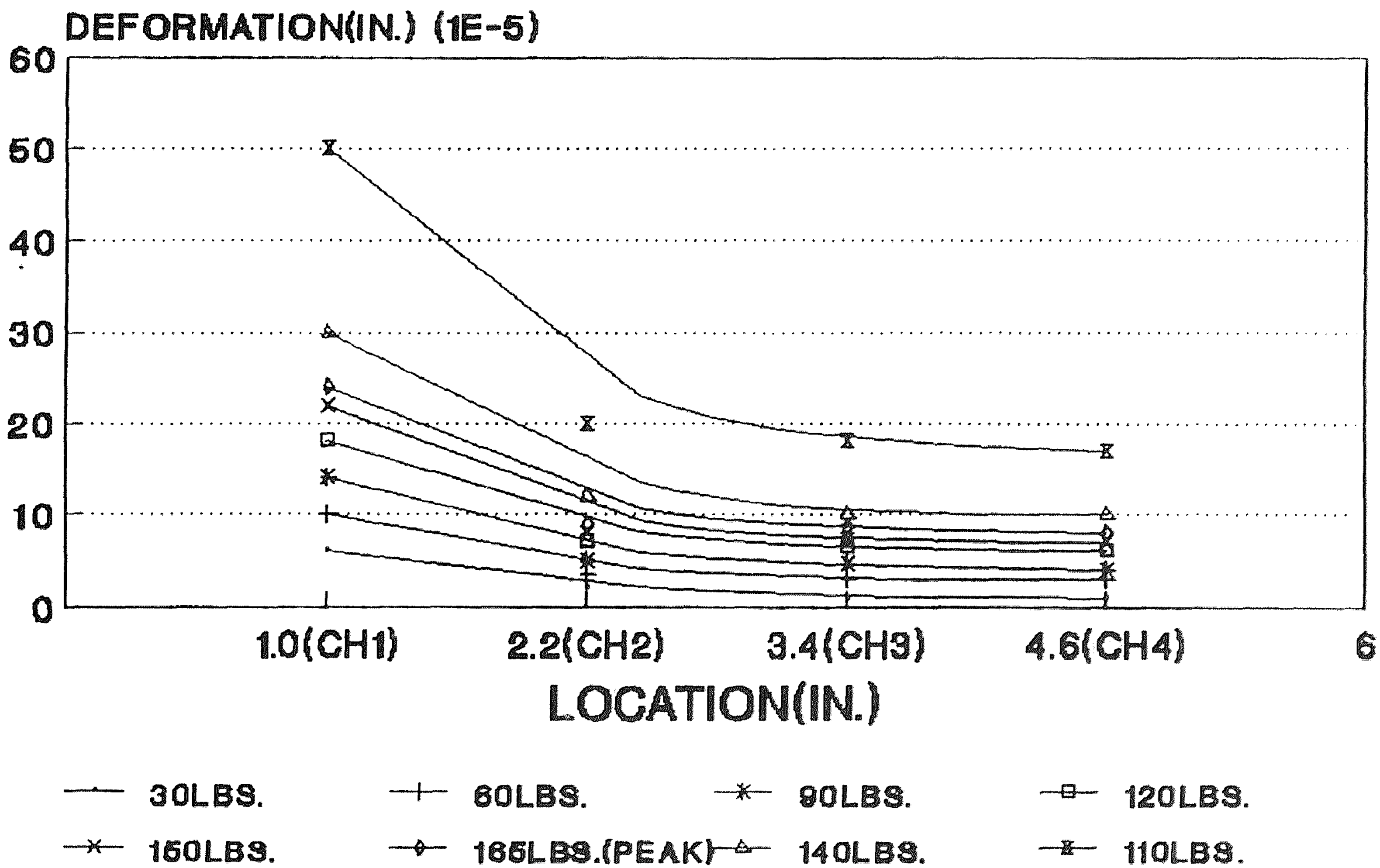

Fig.117 Defor. pattern without) F28C

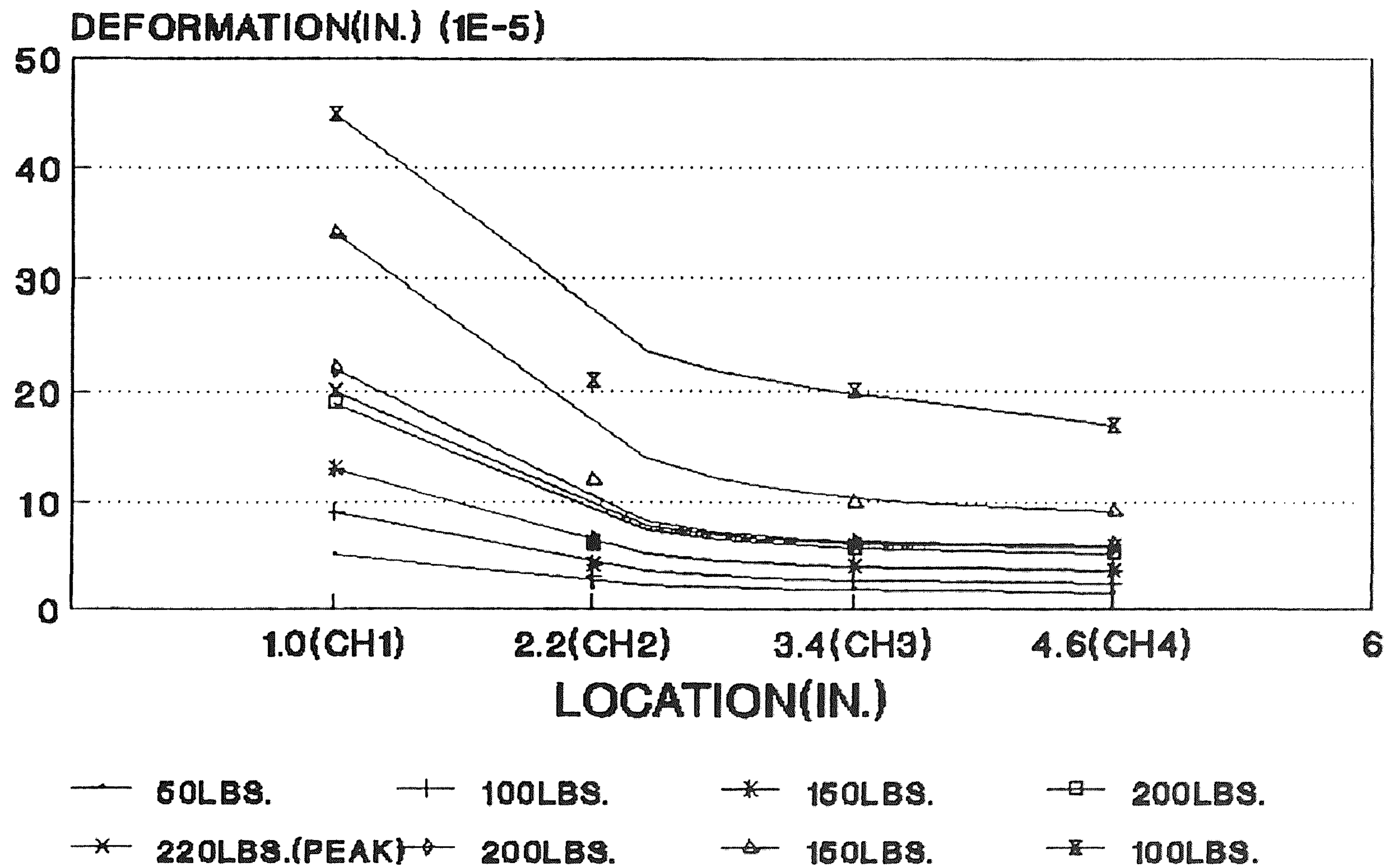

Fig.118 Defor. pattern without COD

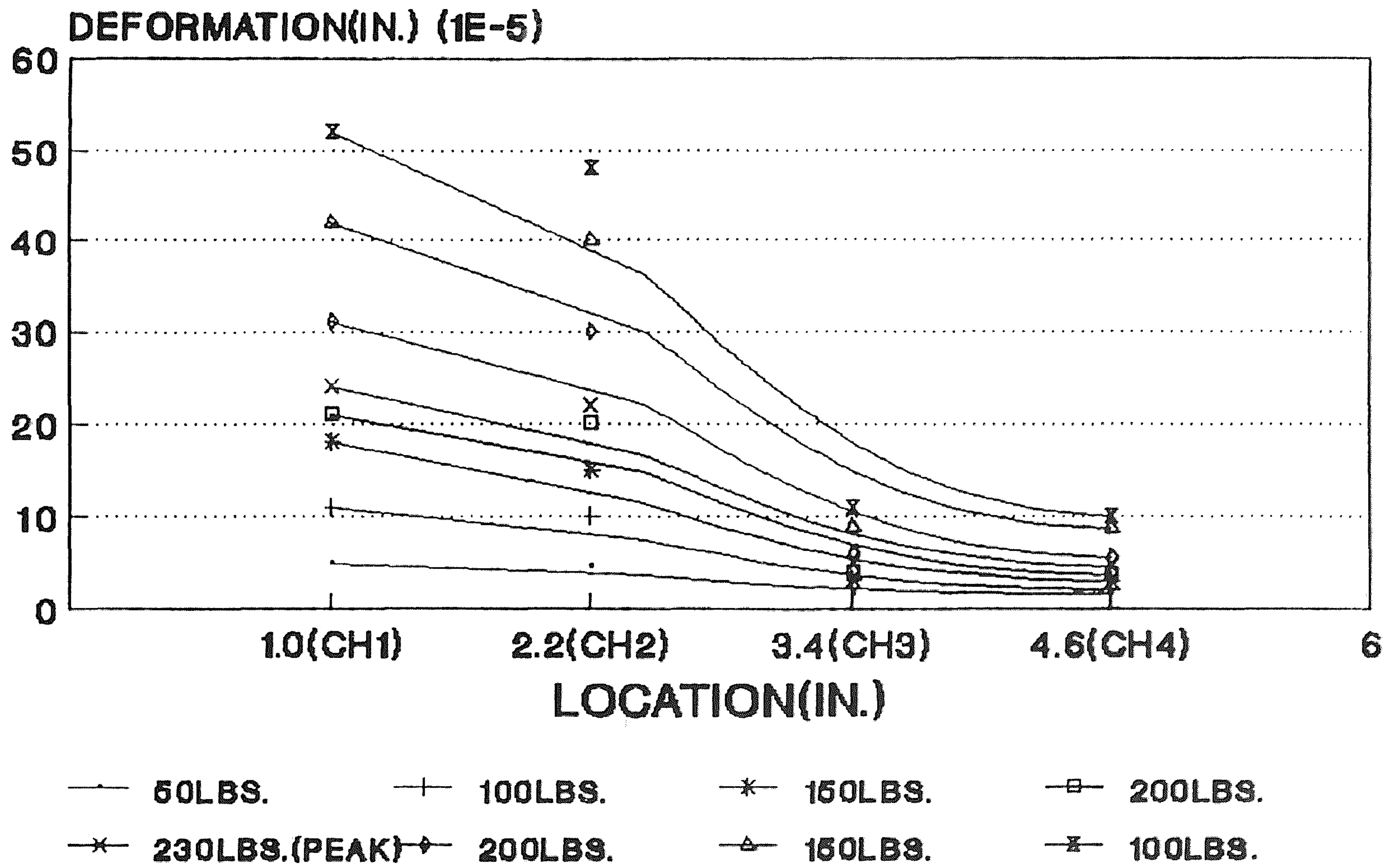

Fig.119 Defor. pattern without CO

CHAPTER IV Conclusion

IV.1 Conclusion

Based on the results obtained in this research , the following conclusions can be drawn :

1. The experimental techniques which were used in this study are reliable and worth further usage.
2. The critical load for CT specimen (tension test) is about 170LBS.
3. The critical load for three point bend specimen is about 220LBS.
4. The average critical COD of CT specimen (tension test) is about 0.048 inch.
5. The average critical COD of three point bend specimen is about 0.016 inch.
6. The average critical internal deformation of CT specimen for CH1 , CH2 , CH3 & CH4 is about 0.0018 , 0.0013 , 0.0004 & 0.0003 inch respectively.
7. The average critical internal deformation of BEAM specimen for CH1 , CH2 , CH3 & CH4 is about 0.0002 , 0.00016 , 0.00005 & 0.00003 respectively.

IV.2 Future Research

The experimental method presented in this study for internal deformation measurement is new and requires further research for improvements.

Possible future research might be the following :

1. Place more than four fiber optic sensors in the process zone for deformation measurements.
2. Use this technique for concrete specimen subjected to impact load for detection of cracking.

REFERENCES

1. Hillerborg,A., Modeer,M., and Petersson,P.E.,"Analysis of Crack Formation and Crack Growth in Concrete by Means of Fracture Mechanics and Finit Elements,"Cement and Concrete Research,Vol. 6,1976, pp. 773-782.
2. Ingraffea,A.R.,Henze,F.E.,"Finite Element Models for Rock Fracture Mechanics,"International Journal for Numerical and Analytical Methods in Geomechanics, Vol. 4,1980, pp.25-43.
3. Brown,J.H.,"Measuring The Fracture Toughness of Cement Paste and Mortar,"Magnize of Concrete Research, Vol. 24, No.81,1972,pp.185-196.
4. Petersson,P.E.,"Crack Growth and Development of Fracture Zones in Plain Concrete and Similar Materials,"Report No.TVBM-1006, Lund Institute of Technology, Dec. 1981 174 pages.
5. Visalvanich,K,Naaman,A.E.,"Fracture Methods in Cement Composites, "ASCE-EMD, Vol.107 No. EM6 , Dec. 1981, pp. 1155-1171.
6. Li,V.C.,"Fracture Resistance Parameters For Cementitious Materials and Their Experimental Determinations," Applications of Fracture Mechanics to Cementitious Composites,NATO-ARW, Sept. 1984,Northwestern Unversity , S.P. Shah,Editor.
7. Dugdale ,D.S., "Yielding of Steel Sheets Containing Slits ," Journal of Mechanics, Physics and Solids, Vol.8 ,1960

, pp. 100-104.

8. Barrenblatt,G.J.,"The Mathemathical Theory of Equilibrium Crack in The Brittle Fracture,"Advances in Applied Mechanics,Vol. 7,1962, pp. 55-125.

9. Wecharatana,M.,Shah,S.P.,"Predictions of Nonlinear Fracture Process Zone in Concrete, "ASCE -EMD , Vol. 109 No. 5, October 1983, pp. 1231-1246.

10. Cho,K.Z., Kobayashi,A.S., Hawkins,N.M., Barker,D.B., Jeang,F.L., "Fracture Process Zone of Concrete Cracks," ASCE-EMD, Vol.110, No. 8, August 1984, pp.1174-1184.

11. Kaplan,M.F.,"Crack Propagation and The Fracture of Concrete," ACI Journal, Vol. 58, No. 5, November 1961, pp.591-610.

12. Walsh,P.F.,"Fracture of Plain Concrete," Indian Concrete Institute, Vol. 46, No. 11, Nov. 72.

13. Mindess,S., Nadeau,J.S.,"Effect of Notch Width on K for Mortar and Concrete,"Cement and Concrete Research, Vol. 6,1967 , pp.529-534.

14. Ansari,F. , Yang,S.X. , "Microcomputer Controlled Closed-Loop Testing System in a Vibration Isolated Environment." Experimental Techniques (SEM) , Vol.12 , No.2 , Feb. 1988 , PP. 25-27

APPENDIX A

```
100 '*******************************************************************
110 '*                                                                 *
120 '*             MENG.BAS - DATA ACQUISTION PROGRAM                  *
130 '*  MetraByte Corporation                    Rev. 1.10   8-27-84   *
140 '*******************************************************************
150 '
160 '--------------- STEP 1 ----------------------------------------
170 'Load DASH16.BIN by contracting workspace  & initialize
180 CLEAR, 49152!        'Contract BASIC's workspace to 48K
190 DEF SEG = 0          'Get BASIC's segment in memory
200 SG = 256 * PEEK(&H511) + PEEK(&H510)
210 SG = SG + 49152!/16
220 DEF SEG = SG         'Load segment for CALL routine
230 BLOAD "DASH16.BIN", 0         'Load it
240 DIM DIO%(8),A%(18000)
250 DIO%(0) = &H300 'DASH-16 board base address
260 DIO%(1) = 2      'Selected interrupt level for DASH-16
270 DIO%(2) = 3      'Selected DMA level for DASH-16
280 DASH16 = 0       'Declare & initialize other CALL parameters
290 FLAG% = 0
300 MD% = 0          'Select Mode 0 - initialize driver

310 CALL DASH16 (MD%, DIO%(0),FLAG%)    'do it
320 IF FLAG%<>0 THEN PRINT "INITIALIZATION ERROR":STOP   'any error?
330 '
340 '--------------- STEP 2 ----------------------------------------
350 'Prompt user for multiplexer scan limits
360 '(this step can be omitted if default limits o.k.)
370 'Set up multiplexer scanning limits
380 MD%=1             'Mode 1 - set scan limits
390 INPUT "Lower multiplexer scanning limit (0-7 or 15)? : ",DIO%(0)
400 INPUT "Upper multiplexer scanning limit (0-7 or 15)? : ",DIO%(1)
410 CALL DASH16 (MD%, DIO%(0),FLAG%)
420 IF FLAG%<>0 THEN PRINT "Error in scan limits # ";FLAG% : STOP
430 '
440 '--------------- STEP 3 ----------------------------------------
450 'SET UP SCANNING RATE (20HZ)
460 MD% = 17
470 DIO%(0) = 50 : DIO%(1) = 1000
480 CALL DASH16 (MD%, DIO%(0),FLAG%)
490 IF FLAG%<>0 THEN PRINT"Error in scan rate set up # ";FLAG% : STOP
500 '
510 '--------------- STEP 4 ----------------------------------------
530 DIO%(0) = 18000
540 DIO%(1) = VARPTR(A%(0))    'Array locator
550 DIO%(2) = 1                'Trigger source - programmable timer
560 MD%=4
570 CALL DASH16 (MD%, DIO%(0),FLAG%)
580 IF FLAG%<>0 THEN PRINT "Error in mode 4 # ";FLAG% : STOP
590 '
600 '--------------- STEP 5 ----------------------------------------
610 'Display converted data
616 OPEN "C:DATA.DAT" FOR OUTPUT AS #1
620 FOR I=0 TO 18000
630 WRITE #1, A%(I)
640 NEXT I
650 END
```

```
      PROGRAM   CHAN.FOR
      DIMENSION D1(300),D2(300),D3(300),D4(300),D5(300)
     *,D6(300),L1(300),L2(300),L3(300),L4(300),L5(300)
     *,L6(300)
      N=300
      OPEN(1,FILE='DATA.DAT',STATUS='OLD')
      OPEN(2,FILE='CH1.DAT',STATUS='NEW')
      OPEN(3,FILE='CH2.DAT',STATUS='NEW')
      OPEN(4,FILE='CH3.DAT',STATUS='NEW')
      OPEN(5,FILE='CH4.DAT',STATUS='NEW')
      DO 10 I=1,N
      READ(1,15)L1(I)
      READ(1,15)L2(I)
      READ(1,15)L3(I)
      READ(1,15)L4(I)
      READ(1,15)L5(I)
      READ(1,15)L6(I)
   15 FORMAT(I5)
   10 CONTINUE
      DO 20 J=1,N
      D1(J)=((L1(J)-351.4)/182.11-1.2)*1000.0
      D2(J)=(L2(J)/198.98-2.8)*1000.0
      D3(J)=(L3(J)/192.23-2.6)*1000.0
      D4(J)=(L4(J)/189.97-2.18)*1000.0
   20 CONTINUE
      JJ=0
      DO 30 K=1,N
      JJ=JJ+3
      WRITE(2,25)JJ,D1(K)
      WRITE(3,25)JJ,D2(K)
      WRITE(4,25)JJ,D3(K)
      WRITE(5,25)JJ,D4(K)
   25 FORMAT(5X,I3,10X,F10.3)
   30 CONTINUE
      STOP
      END
```

Name	Type	Offset	P	Class
D1	REAL	16		
D2	REAL	1216		
D3	REAL	2416		
D4	REAL	3616		
D5	REAL	4816		
D6	REAL	6016		
I	INTEGER*4	14420		
J	INTEGER*4	14432		
JJ	INTEGER*4	14440		
K	INTEGER*4	14444		
L1	INTEGER*4	7216		
L2	INTEGER*4	8416		
L3	INTEGER*4	9616		
L4	INTEGER*4	10816		
L5	INTEGER*4	[illegible]		

```
      PROGRAM   TOT.FOR
      DIMENSION B1(40),B2(40),B3(40),B4(40),B5(40)
     *           ,AC1(39),AC2(39),AC3(39),AC4(39)
      DIMENSION F(40),G(40),A(39)
      DATA D1,D2,D3,D4,P/0.00035,0.0004,0.000133,
     *0.00034,198.0/
      OPEN(1,FILE='CD1.DAT',STATUS='NEW')
      OPEN(2,FILE='CD2.DAT',STATUS='NEW')
      OPEN(3,FILE='CD3.DAT',STATUS='NEW')
      OPEN(4,FILE='CD4.DAT',STATUS='NEW')
      OPEN(5,FILE='CD5.DAT',STATUS='NEW')
      OPEN(6,FILE='A1.OUT',STATUS='NEW')
      OPEN(7,FILE='A2.OUT',STATUS='NEW')
      OPEN(8,FILE='TT.DAT',STATUS='NEW')
      AD1=D1/40.0
      AD2=D2/40.0
      AD3=D3/40.0
      AD4=D4/40.0
      AP=P/20.0
      B1(1)=0.0
      B2(1)=0.0
      B3(1)=0.0
      B4(1)=0.0
      B5(1)=0.0
      WRITE(1,33)B1(1),B5(1)
      WRITE(2,33)B2(1),B5(1)
      WRITE(3,33)B3(1),B5(1)
      WRITE(4,33)B4(1),B5(1)
      DO 10 I=1,19
      B1(I+1)=B1(I)+AD1
      B2(I+1)=B2(I)+AD2
      B3(I+1)=B3(I)+AD3
      B4(I+1)=B4(I)+AD4
      B5(I+1)=B5(I)+AP
      WRITE(1,33)B1(I+1),B5(I+1)
      WRITE(2,33)B2(I+1),B5(I+1)
      WRITE(3,33)B3(I+1),B5(I+1)
      WRITE(4,33)B4(I+1),B5(I+1)
   10 CONTINUE
      DO 88 K=20,21
      B1(K+1)=B1(K)+AD1
      B2(K+1)=B2(K)+AD2
      B3(K+1)=B3(K)+AD3
      B4(K+1)=B4(K)+AD4
      B5(K+1)=B5(K)-AP*0.1
      WRITE(1,33)B1(K+1),B5(K+1)
      WRITE(2,33)B2(K+1),B5(K+1)
      WRITE(3,33)B3(K+1),B5(K+1)
      WRITE(4,33)B4(K+1),B5(K+1)
   33 FORMAT(5X,F15.13,10X,F8.4)
   88 CONTINUE
      DO 82 IJ=22,37
      B1(IJ+1)=B1(IJ)+AD1
      B2(IJ+1)=B2(IJ)+AD2
      B3(IJ+1)=B3(IJ)+AD3
      B4(IJ+1)=B4(IJ)+AD4
      B5(IJ+1)=B5(IJ)-AP*1.2
```

```
      WRITE(1,33)B1(IJ+1),B5(IJ+1)
      WRITE(2,33)B2(IJ+1),B5(IJ+1)
      WRITE(3,33)B3(IJ+1),B5(IJ+1)
      WRITE(4,33)B4(IJ+1),B5(IJ+1)
   82 CONTINUE
      DO 67 IK=38,39
      B1(IK+1)=B1(IK)+AD1
      B2(IK+1)=B2(IK)+AD2
      B3(IK+1)=B3(IK)+AD3
      B4(IK+1)=B4(IK)+AD4
      B5(IK+1)=B5(IK)-AP*0.05
      WRITE(1,33)B1(IK+1),B5(IK+1)
      WRITE(2,33)B2(IK+1),B5(IK+1)
      WRITE(3,33)B3(IK+1),B5(IK+1)
      WRITE(4,33)B4(IK+1),B5(IK+1)
   67 CONTINUE
      AC1(1)=0.0
      AC2(1)=0.0
      AC3(1)=0.0
      AC4(1)=0.0
      DO 37 I=1,39
      J=I+1
      AC1(J)=AC1(I)+(B1(J)-B1(I))*((B5(I)+B5(J))/2.0)
      AC2(J)=AC2(I)+(B2(J)-B2(I))*((B5(I)+B5(J))/2.0)
      AC3(J)=AC3(I)+(B3(J)-B3(I))*((B5(I)+B5(J))/2.0)
      AC4(J)=AC4(I)+(B4(J)-B4(I))*((B5(I)+B5(J))/2.0)
   37 CONTINUE
      WRITE(6,66)AC1(19)
      WRITE(6,66)AC2(19)
      WRITE(6,66)AC3(19)
      WRITE(6,66)AC4(19)
   66 FORMAT(10X,'AREA=',F9.3)
      F(1)=0.0
      G(1)=0.0
      WRITE(5,22)F(1),G(1)
      DO 25 I=1,19
      G(I+1)=G(I)+AP
      F(I+1)=(G(I+1)*0.043)/1000*0.02801
      WRITE(5,22)F(I+1),G(I+1)
   25 CONTINUE
      DO 91 J=20,21
      G(J+1)=G(J)-AP*0.1
      F(J+1)=((G(J)-G(J+1))*0.043/1000)*0.02801
   91 WRITE(5,22)F(J+1),G(J+1)
      DO 92 K=22,37
      G(K+1)=G(K)-AP*1.2
      F(K+1)=((G(K)-G(K+1))*0.043/1000)*0.02801
   92 WRITE(5,22)F(K+1),G(K+1)
      DO 93 L=38,39
      G(L+1)=G(L)-AP*0.05
      F(L+1)=((G(L)-G(L+1))*0.043/1000)*0.02801
   93 WRITE(5,22)F(L+1),G(L+1)
      TA=0.0
      DO 94 M=1,39
      N=M+1
      [illegible]=F(N)-F(M)
```

```
D Line# 1       7
1              A(M)=X*G(N)
1              TA=TA+A(M)
1           94 CONTINUE
               WRITE(7,14)TA
            22 FORMAT(5X,F15.13,10X,F8.4)
            14 FORMAT(10X,'AREA=',F9.3)
               DO 75 MN=1,40
1           73 FORMAT(F8.4,5X,F8.6,5X,F8.6,5X,F8.6,5X,F8.6,5X,F8.6)
1           75 WRITE(8,73)B5(MN),B1(MN),B2(MN),B3(MN),B4(MN),F(MN)
               STOP
               END
```

Name	Type	Offset	P	Class
A	REAL	1756		
AC1	REAL	1132		
AC2	REAL	1288		
AC3	REAL	1444		
AC4	REAL	1600		
AD1	REAL	1932		
AD2	REAL	1936		
AD3	REAL	1940		
AD4	REAL	1944		
AP	REAL	1948		
B1	REAL	12		
B2	REAL	172		
B3	REAL	332		
B4	REAL	492		
B5	REAL	652		
D1	REAL	1912		
D2	REAL	1916		
D3	REAL	1920		
D4	REAL	1924		
F	REAL	812		
G	REAL	972		
I	INTEGER*4	1952		
IJ	INTEGER*4	1980		
IK	INTEGER*4	1984		
J	INTEGER*4	1988		
K	INTEGER*4	1956		
L	INTEGER*4	2012		
M	INTEGER*4	2020		
MN	INTEGER*4	2072		
N	INTEGER*4	2024		
P	REAL	1928		
TA	REAL	2016		
X	REAL	2028		

Name	Type	Size	Class
MAIN			PROGRAM

```
D-Line# 1       7
         PROGRAM    DEF.FOR
         DIMENSION B1(40),B2(40),B3(40),B4(40),B5(40)
        *               ,AC1(39),AC2(39),AC3(39),AC4(39)
         DATA D1,D2,D3,D4,P/0.00035,0.0004,0.000133,
        *0.00034,198.0/
         OPEN(1,FILE='CD1.DAT',STATUS='NEW')
         OPEN(2,FILE='CD2.DAT',STATUS='NEW')
         OPEN(3,FILE='CD3.DAT',STATUS='NEW')
         OPEN(4,FILE='CD4.DAT',STATUS='NEW')
         AD1=D1/40.0
         AD2=D2/40.0
         AD3=D3/40.0
         AD4=D4/40.0
         AP=P/20.0
         B1(1)=0.0
         B2(1)=0.0
         B3(1)=0.0
         B4(1)=0.0
         B5(1)=0.0
         WRITE(1,33)B1(1),B5(1)
         WRITE(2,33)B2(1),B5(1)
         WRITE(3,33)B3(1),B5(1)
         WRITE(4,33)B4(1),B5(1)
         DO 10 I=1,19
         B1(I+1)=B1(I)+AD1
         B2(I+1)=B2(I)+AD2
         B3(I+1)=B3(I)+AD3
         B4(I+1)=B4(I)+AD4
         B5(I+1)=B5(I)+AP
         WRITE(1,33)B1(I+1),B5(I+1)
         WRITE(2,33)B2(I+1),B5(I+1)
         WRITE(3,33)B3(I+1),B5(I+1)
         WRITE(4,33)B4(I+1),B5(I+1)
      10 CONTINUE
         DO 88 K=20,21
         B1(K+1)=B1(K)+AD1
         B2(K+1)=B2(K)+AD2
         B3(K+1)=B3(K)+AD3
         B4(K+1)=B4(K)+AD4
         B5(K+1)=B5(K)-AP*0.1
         WRITE(1,33)B1(K+1),B5(K+1)
         WRITE(2,33)B2(K+1),B5(K+1)
         WRITE(3,33)B3(K+1),B5(K+1)
         WRITE(4,33)B4(K+1),B5(K+1)
      33 FORMAT(5X,F10.7,10X,'1',10X,F8.4)
      88 CONTINUE
         DO 82 IJ=22,37
         B1(IJ+1)=B1(IJ)+AD1
         B2(IJ+1)=B2(IJ)+AD2
         B3(IJ+1)=B3(IJ)+AD3
         B4(IJ+1)=B4(IJ)+AD4
         B5(IJ+1)=B5(IJ)-AP*0.43
         WRITE(1,33)B1(IJ+1),B5(IJ+1)
         WRITE(2,33)B2(IJ+1),B5(IJ+1)
         WRITE(3,33)B3(IJ+1),B5(IJ+1)
```

```
D Line# 1         7
                  DO 67 IK=38,39
1                 B1(IK+1)=B1(IK)+AD1
1                 B2(IK+1)=B2(IK)+AD2
1                 B3(IK+1)=B3(IK)+AD3
1                 B4(IK+1)=B4(IK)+AD4
1                 B5(IK+1)=B5(IK)-AP*0.05
1                 WRITE(1,33)B1(IK+1),B5(IK+1)
1                 WRITE(2,33)B2(IK+1),B5(IK+1)
1                 WRITE(3,33)B3(IK+1),B5(IK+1)
1                 WRITE(4,33)B4(IK+1),B5(IK+1)
1              67 CONTINUE
                  AC1(1)=0.0
                  AC2(1)=0.0
                  AC3(1)=0.0
                  AC4(1)=0.0
                  DO 37 I=1,39
1                 J=I+1
1                 AC1(J)=AC1(I)+(B1(J)-B1(I))*((B5(I)+B5(J))/2.0)
1                 AC2(J)=AC2(I)+(B2(J)-B2(I))*((B5(I)+B5(J))/2.0)
1                 AC3(J)=AC3(I)+(B3(J)-B3(I))*((B5(I)+B5(J))/2.0)
1                 AC4(J)=AC4(I)+(B4(J)-B4(I))*((B5(I)+B5(J))/2.0)
1              37 CONTINUE
                  WRITE(6,66)AC1(19)
                  WRITE(6,66)AC2(19)
                  WRITE(6,66)AC3(19)
                  WRITE(6,66)AC4(19)
               66 FORMAT(10X,'AREA=',F9.3)
                  STOP
                  END
```

Name	Type	Offset	P	Class
AC1	REAL	812		
AC2	REAL	968		
AC3	REAL	1124		
AC4	REAL	1280		
AD1	REAL	1456		
AD2	REAL	1460		
AD3	REAL	1464		
AD4	REAL	1468		
AP	REAL	1472		
B1	REAL	12		
B2	REAL	172		
B3	REAL	332		
B4	REAL	492		
B5	REAL	652		
D1	REAL	1436		
D2	REAL	1440		
D3	REAL	1444		
D4	REAL	1448		
I	INTEGER*4	1476		
IJ	INTEGER*4	1512		
IK	INTEGER*4	1516		
J	INTEGER*4	1520		
[illegible]	INTEGER*4	1480		